공학박사 학위논문

Deformation and Stiffness Characteristics during Creep of Weathered Residual Soil in Korea

국내 풍화토의 크리프 변형 및 강성 특성

2015년 8월

서울대학교 대학원

건설환경공학부

박 가 현

Abstract

Deformation and Stiffness Characteristics during Creep of Weathered Residual Soil in Korea

Park, Kahyun

Department of Civil and Environmental Engineering

The Graduate School

Seoul National University

Granular materials are prevalent sub-soils in which many geotechnical structures are constructed. Recent studies have revealed the importance of certain time-dependent behaviors, including time-dependent deformations and changes of the engineering properties of granular materials. The deformation of granular materials under constant loading influences geotechnical structures such as buildings, bridge abutments, earth-retaining structures, and earth slopes. Moreover, excessive deformations over time under a constant load can cause serviceability issues. However, time-dependent deformation, which may result in unexpected deformations of the ground or structural failures, has not been properly considered in geotechnical designs. Therefore, to solve existing problems in geotechnical engineering, it is important to investigate deformation behavior in detail as it occurs with time.

Despite its geological predominance and the fact that it is the most common type of soil used as a construction material in South Korea, the long-

term behavior of weathered residual soil has yet to be clearly investigated. The time-dependent behavior of a granular material depends on the material properties, confining pressure, and relative density. Weathered residual soils are used as construction materials with various degrees of field compaction, which are closely linked to the relative density. Thus, analyzing the effects of the relative density and stress conditions on the time-dependent behavior of soil is crucial for a proper investigation of the long-term behavior of weathered residual soil.

The aims of this research are to investigate the influences of the relative density, stress ratio and effective stress on the creep behaviors of weathered residual soil and to study the effects of time on the variations of the elastic shear stiffness. To achieve these goals, a series of laboratory tests were designed such that the effects of the relative density, stress ratio, and effective stress on the creep/aging behaviors of weathered residual soil in Korea could be explored.

Observations and evaluations of creep deformation under a constant load with various relative densities are discussed in detail. By performing a series of stress path triaxial creep tests under both isotropic and anisotropic conditions under every vertical effective stress level (100, 200, and 400 kPa) for 48 hours, creep strains were analyzed. For a comparison with triaxial test results, creep deformations were also evaluated under laterally constrained conditions using a one-dimensional consolidation testing apparatus. In addition, based on these experimental observations, the creep parameters for numerical modelling are provided to predict creep deformation in the field.

The developed creep strains depend strongly on the initial relative density, current stress state, and stress ratio. Specimens with low and medium relative density levels showed contractive creep behavior, whereas specimens with high densities showed dilative creep behavior. The effects of the effective stress on the creep behavior also depend on the initial relative density. In

specimens with low and medium relative density levels, high effective stress stimulates the development of creep strain. However, in specimens with high relative densities, high effective stress inhibits the development of creep strain. A high stress ratio promotes creep strain in axial direction, but impedes volumetric creep strain.

The aging effects on elastic shear stiffness due to creep are also evaluated under various sample conditions with different relative density and shearing conditions and with different confining stresses. The elastic shear moduli during the creep period were measured using orthogonal bi-directional bender elements. By evaluating the aging effects on the directional stiffness as obtained from bender element tests, changes in the soil structure could be inferred during creep. Moreover, the relationship between the developing creep strain and the measured soil stiffness could be determined. Variations of the stiffness anisotropy during creep, an important factor in various problems related to ground deformation, are also investigated.

Variations of the elastic shear stiffness and deformation during creep depend on the stress ratio and the initial relative density. The continuous change in the stiffness anisotropy during creep was found to be closely related to the patterns in creep deformation. In addition, the increase in the elastic stiffness is more sensitive to the direction of the major principal stress than it is to the direction of the minor principal stress during creep.

Keywords: Creep, Aging, Triaxial test, Weathered residual soil in Korea, Granular soil, Time-dependent behavior, Anisotropy

Student Number: 2010-30238

Contents

List of Tables

List of Figures

Chapter 1. Introduction

1.1 General

The engineering properties of soil change with time (Schmertmann, 1991). These time-dependent behaviors can influence buildings, bridge abutments, earth-retaining structures, and earth slopes. Excessive deformation with time under a constant load may lead to serviceability problems. However, time-dependent deformation, which may result in structural failures or unexpected deformations of the ground, is not properly considered in geotechnical designs. Therefore, to solve the actual problems with regrad to geotechnical engineering, it is important to investigate the detailed deformation behaviors over time.

Recent studies have revealed that with regrad to the development of creep deformation, an increase in the stiffness or strength of granular materials under constant loading cannot be ignored, thus motivating more intensive investigations of the time-dependent behaviors of granular materials. Mitchell and Solymar (1984), Charlie et al. (1992), and Thomann and Hryciw (1992) showed increases in the strength and stiffness via the cone penetration of sands. York (1994), Chow et al. (1998), and Axelsson (2002) presented the set-up effects of driven or displacement piles in sands. More recently, Kuwano and Jardine (2002), Bowman and Soga (2003), Wang et al. (2008), and Wang and Gao (2013) experimentally showed that the creep and subsequent stiffness gains in sands over time are not negligible.

Despite its geological prevalence and the fact that it is the most common type of soil used as a construction material in the country, the long-term behavior of weathered residual soil in South Korea has yet to be studied rigorously. The time-dependent behavior of granular materials depends on the material properties, confining pressure and relative density. Weathered residual soils have been widely used as construction materials with various degrees of field compaction which are closely linked to the relative density. Therefore, analyzing the effects of the relative density and stress conditions on the time-dependent behavior of soil is crucial in detailed investigations of the long-term behavior of weathered residual soil.

1.2 Purpose and scope of the study

The objectives of this study are as follows. The first is to investigate the effects of the relative density, stress ratio, and effective stress on the creep behavior of weathered residual soil. The second is to study variations in the elastic shear stiffness during creep. To achieve these goals, a series of laboratory tests were designed such that the effects of the relative density, stress ratio, and effective stress on the creep/aging behaviors of weathered residual soil in Korea could be explored. The time-dependent behaviors are analyzed in three parts. The first part is an assessment of the deformation characteristics, the second is an evaluation of the elastic shear stiffness characteristics, and the third is an estimation of the creep parameters for numerical modeling.

In the section describing the assessment of the deformation characteristics, first, the overall stress-strain behavior is briefly introduced. Secondly, the procedures specifying the time origin of the creep phase are examined, after which creep strains in terms of axial, radial, volumetric, and shear deformations are evaluated. Based on the volumetric creep responses, the concept of state-dependent volumetric creep behavior is also suggested.

In the second section of the evaluation of the elastic shear stiffness characteristics, at first, the stiffness after creep is compared with the stiffness before creep obtained from overall stress-strain curves. Secondly, variations in the elastic shear stiffness during creep with time are presented. And then, the time-dependent increase in the elastic shear stiffness is quantified using

existing equations. Finally, the evolution of stiffness anisotropy is investigated.

Based on the experimental results, in the third part, each volumetric and shear creep strain curve, which is defined as a form of equation for the different relative density using basic creep parameters, is provided for numerical modelling predictions.

1.3 Organization of the thesis

This thesis is divided into seven chapters. This chapter introduces the background, the necessity, objectives and the scope of this research.

Chapter two is a literature review of previous studies which investigated the time-dependent behaviors of granular materials. Previous works on the effects of creep or aging on granular materials are explained with examples. In addition, existing research on the effects of fine contents on the time-dependent behavior of granular soils and on the anisotropy effects on creep/aging are introduced.

In chapter three, the testing materials, testing apparatus, and testing program are described. A triaxial testing apparatus with a small-strain measurement system and combined bender element tests are explained in detail. The procedures and conditions of stress path creep tests are also described.

Chapter four presents the first part of the results: the deformation characteristics. Non-linear creep strains are evaluated for various samples of weathered residual soil with different relative density and stress conditions. The patterns of developing creep strains are obtained according to the initial relative density and stress conditions. Moreover, based on experimental observations, the concept of state-dependent volumetric creep behavior is

suggested.

Chapter five shows the second part of the results: the stiffness characteristics obtained from the bender element tests. The variations in the elastic shear stiffness as measured by the bender element tests and the axial and radial directions of the specimens during creep are experimentally investigated. The evolution of the stiffness anisotropy of weathered residual soil during creep is also described.

Chapter six gives the creep parameters of the numerical modelling. The volumetric and shear creep strain curves obtained from Chapter 4 are defined in the form of an equation using two basic parameters.

Finally, the conclusions of the research and recommendations based on the results are presented in Chapter seven together with applications of this work for geotechnical practices.

Chapter 2. Time-dependent Behavior of Granular Material

2.1 Introduction

The time-dependent behaviors of clay such as the time-dependent deformations or aging effects have been widely reported for decades by several researchers. Since the 1980s, the observations of the time-dependent behavior of granular materials have been increased. Early studies of the time-dependent effects on granular materials that are field observations of the increase in cone penetration resistance or liquefaction resistance stimulated more intensive research on the time-dependent behavior of granular materials. Then, the creep deformations of granular materials have been of interest. In the beginning of the research, the contractive creep deformations and short-term creep test results were reported. Recently, however, the dilative creep deformations and long-term creep test results have been addressed. More recently, anisotropy during creep is one of the emerging issues in the research of the time-dependent behaviors.

In this chapter, the previous researches dealing with the time-dependent behaviors in the granular materials are introduced with general characteristics of the time-dependent behaviors and existing mechanisms of creep/aging. In addition, literatures discussing effects of fine contents on creep behaviors and effects of creep or aging on anisotropy of soils are introduced.

The main topics of chapter 2 are:

(1) Experimental findings and mechanisms of creep/aging,

(2) Effects of fine contents on the time-dependent behavior of granular materials,

(3) Effects of creep/aging on anisotropy, and

(4) General creep behavior.

2.2 Experimental findings and mechanism of creep/aging

2.2.1 Literature review of creep in sand

Generally, creep refers to the time-dependent deformation at constant effective stress. Whereas relatively abundant researches have been conducted on the time-dependent deformations of clayey soils, relatively little researches have been performed on the time-dependent deformations of granular materials. That is because clay shows significantly more pronounced time effects than most sands. However, recent studies have revealed that the time-dependent behaviors of granular materials cannot be ignored.

In this chapter, a review of creep in sand of the literatures is presented. Firstly, the experimental observations of laboratory tests are introduced. And then, existing proposed mechanisms of creep are summarized.

Experimental observations on creep in sand

The deformations under constant loading, is referred as creep, depends on the number of parameters, including relative density, confining stress, stress increment size, stress ratio(q/p'), condition of drainage, and time. Murayama et al. (1984) showed that the creep test results for loose Toyoura sands are consistent with those predicted by the equations based upon the rheological model proposed by Murayama (1983).

Mejia et al. (1988) demonstrated that volumetric and shear creep strains

increase as the stress ratio, confining pressure, stress increment size and grain angularity increase in the drained triaxial creep tests.

Yamamuro and Lade (1993) found that contractive creep deformation increases as the confining pressure increases, and creep deformation resulting from particle breakage is more predominant at high stress level.

Kuwano and Jardine (2002) also conducted triaxial tests to investigate the creep behavior of granular materials. Saturated Toyora sands and Ballotini glass beads were used in this experiment for different relative density (28-63%). Creep tests (multiple constant stress stages) had lasted for 3 hours under both isotropic and anisotropic stress conditions. To precisely measure the strain, local LVDTs were used, directly attached to the specimens.

The tested granular materials showed significant time-dependent behavior. The volumetric creep deformations developing within 2 hours of the end of loading amounted to 20-50% of the deformation observed during the previous fully drained loading stages under isotropic stress conditions. The creep strain-time relationships did not follow the classical semi-logarithmic pattern having been expected for clays. Plots of creep rate against time appeared to follow power-low trends. Also, the creep behavior depends on the effective stress level and the imposed stress condition. Lastly, the very significant creep straining was observed at stress levels (30-400kPa) where particle crushing is unlikely to have played a major role. They introduced more satisfactory explanations for the creep of granular material that dynamic

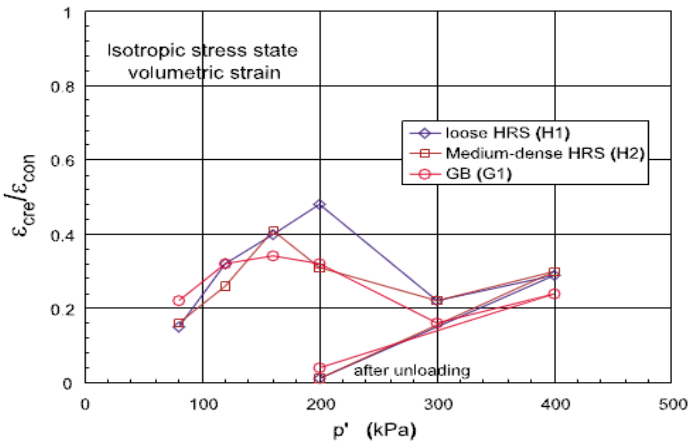

Figure 2.1 The ratio of creep strain and instantaneous strain under isotropic stress ($\Delta\varepsilon_{cre}$ / $\Delta\varepsilon_{con}$) (Kuwano and Jardine, 2002)

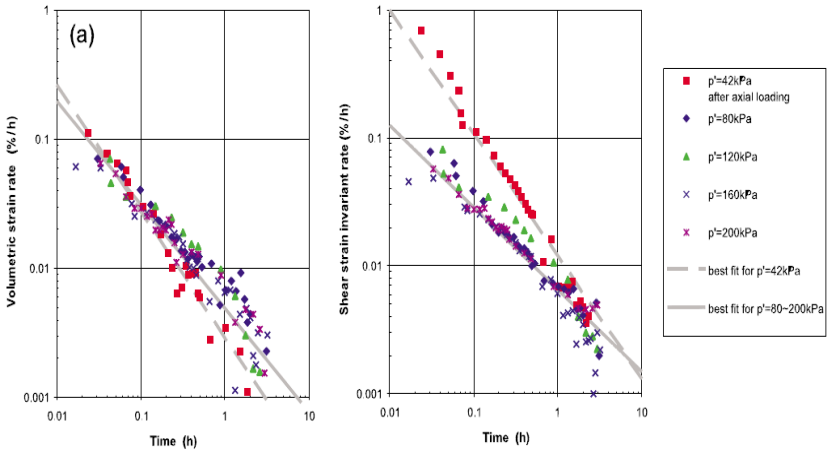

Figure 2.2 Relationship between time and creep strain rate (Kuwano and Jardine, 2002)

breaking and reforming of strong force chains took place. They also pointed out that contractive volumetric creep strains are higher in the loose specimens than those in the dense specimens.

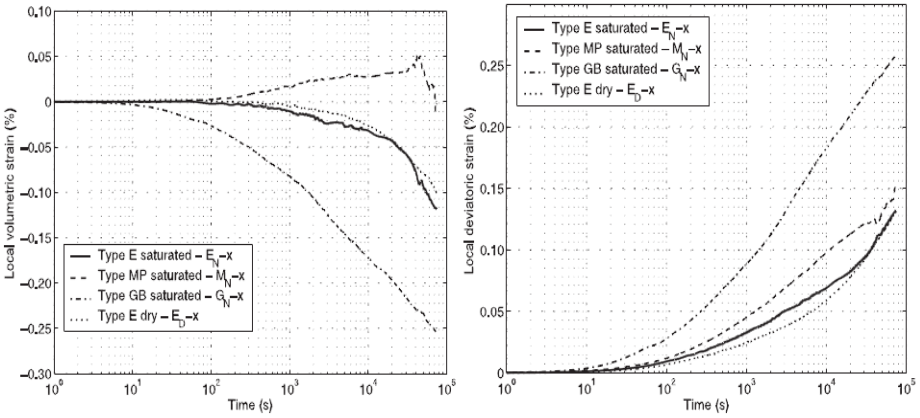

(a) (b)

Figure 2.3 (a) Volumetric and (b) deviatoric strain development with log time for series X compression creep (Bowman and Soga, 2005)

More recently, dilative volumetric creep behaviors of granular materials have been partially reported by some researchers. Bowman and Soga (2005) postulating the set-up effect of displacement piles in dense granular materials (D_r of approximately 71%) described the volumetric dilatation during creep of medium dense sands, especially under high stress ratio (q/p'=1.33) condition. Volumetric response involved contraction, followed by dilation associated with a high degree of shearing during creep.

Rimoy and Jardine (2011) observed dilative creep deformation for the specimens of Thames Valley sands with very low relative density (D_r of approximately 21%) under high stress ratio (q/p'=0.87) condition. Creep stages were imposed on triaxial specimens at constant stress state after K_0 compression. Their results showed a changing pattern of volumetric strains

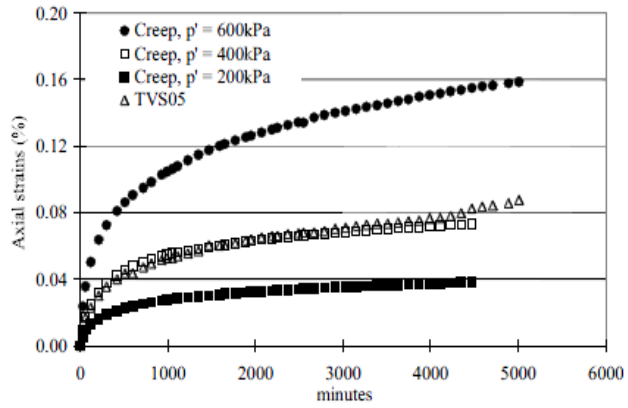

Figure 2.4 Axial strain-time trends during creep (Rimoy and Jardine, 2011)

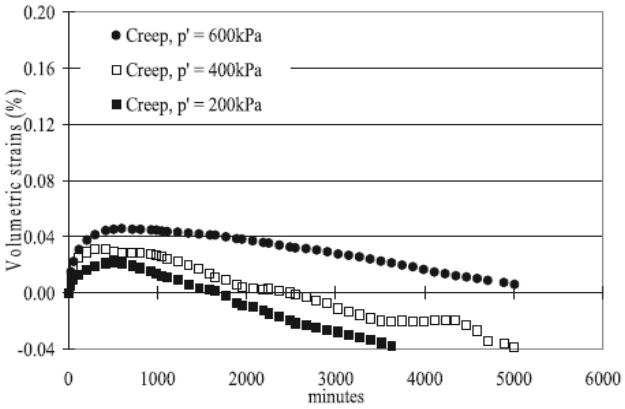

Figure 2.5 Volume strain-time trends followed in creep stages of stress path triaxial tests on TVS specimens (Rimoy and Jardine, 2011)

with time while axial creep strains showed monotonic contractive behavior. The volumetric response was initially contractive at the beginning, after which it became dilative. The higher pressure tests show related trends but with delayed start of dilation and lower rates and falling degrees of dilation.

Similar dilative creep behavior in sands was also noted by Karimpour and Lade (2013). The specimens were loaded up to a deviator stress level of 70%-75% of their deviator strength under confining pressures of 250 and 8000kPa. The specimens underwent dilation during creep at low confining pressures. According to Karimpour and Lade (2013), rotation and rearrangement of particles, which may result in dilation, are governing mechanisms of creep behavior at low confining stresses, where breakage of asperities may trigger the rotation and rearrangement of grains. Most previous studies, however, dealing with volumetric dilation during creep of granular materials have been limited to the high stress ratio (q/p'=0.87~1.33) conditions.

Table 2.1 presents the summarized previous literatures of creep in sands.

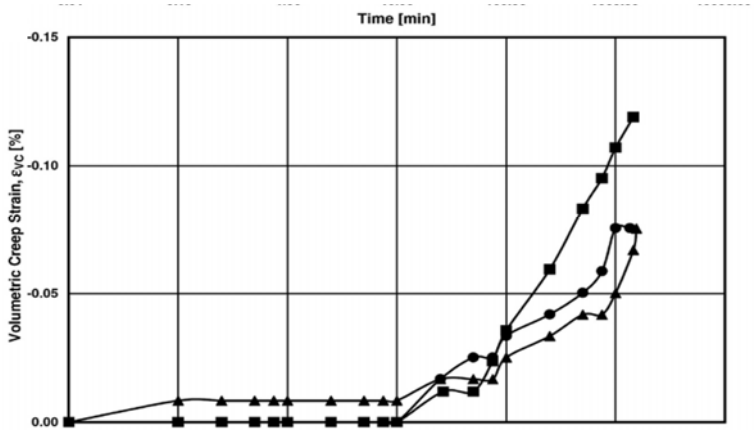

Figure 2.6 Volumetric creep strain with time (Karimpour and Lade, 2013)

Table 2.1 Summary of creep in sand reported in the previous works (continued)

Reference	Material	D_r (%)	σ'_v (kPa)	Methodology	Measured time period	Creep behavior with time
Murayama et al. (1984)	Toyora sands	loose sand	88-167	TX	20 min	The creep test results are consistent with those predicted by the equations based upon the rheological model (Murayama 1983).
Mejia et al. (1988)	Taillings sand			oedometer & TX		Volumetric and shear creep strains increases as the stress ratio, confining pressure, stress increment size and grain angularity increase.

Table 2.1 Summary of creep in sand reported in the previous works (continued)

Reference	Material	D_r (%)	σ'_v (kPa)	Methodology	Measured time period	Creep behavior with time
Kuwano and Jardine (2002)	Toyora sands and Ballotini glass beads	28-63	30-400	TX	3 hours	Volumetric creep deformations developed within 2 hours of the end of loading amounted to 20-50% of the deformation of loading.
Bowman and Soga (2003, 2005)	Leighton Buzzard clean silica sand (Type E), unwashed silica beach sand (Type MP), glass beads (Type GB)	71	50-600	TX	21.6 hours	Volumetric response involved contraction, followed by dilation.

Table 2.1 Summary of creep in sand reported in the previous works

Reference	Material	D_r (%)	σ'_v (kPa)	Methodology	Measured time period	Creep behavior with time
Rimoy and Jardine (2011)	Thames Valley sand	21	200-600	TX	3days	Initially contractive then, dilative
Karimpour and Lade (2013)	Virginia beach sand	98	250, 8000	TX	1day, 2 month	volumetric dilation at low confining pressure

Mechanism of creep

There are some hypotheses describing the mechanism of creep in granular materials. The proposed mechanism can be categorized as follows:

(1) Particle crushing

(2) Particle rearrangement, sliding, and rolling

Under very high stress conditions, particle crushing is considered as main mechanism of creep in granular materials. Leung et al. (1997) conducted 1-D compression tests with aerial pluviated sands. Duration of each loading step was 5 days. 25mm-diameter and 20-mm height specimens were prepared with 38% and 75% relative density for both dry and saturated sands. The confining pressure ranged from 4.1 MPa to 37.4 MPa. Because this research was conducted under very high confining pressure, the particle breakage played the important role in thee creep. Gradual particle breakage increases the contact between the particles, and causes settlement, soil resistance and stiffness gains with time. Karimpour and Lade (2013) also detected the particle crushing during creep under high confining pressure (8000 kPa). The results of sieve analysis supported this hypothesis both before and after creep tests.

The time-dependent behaviors in granular material also can be attributed to the rearrangement of grains with time due to particle slippage or rolling. Lade and Liu (1998) described the data of a series of isotropic compression triaxial tests. They concluded that the viscous characteristics of granular

media result from slippage between particles. According to Bowman and Soga (2003), volumetric creep response of sand is very complex. For loose sand, the creep strain is generally contractive. The main mechanisms of contractive behavior are void flattening, asperity yield and particle breakage. Void flattening may initially occur as voids perpendicular to the applied load tend to flatten (Kuhn, 1999). This would lead to contraction. Contrast to the loose sand, dense sand shows the dilatant behavior. In contrast to contractive behavior, dilatant mechanisms of creep are void elongation and growth, particle sliding and rolling. These occur as contact forces continue to redistribute towards producing a more stable fabric. Void elongation becomes dominant with increasing deviator strain with time, as elongated voids tend to grow in the direction of the applied major principal stress (Kuhn, 1999 and Oda et al., 1985). The redistribution of contact forces can only occur due to particle rearrangement, therefore, rolling and sliding of particles lead to dilation early.

2.2.2 Literature review of aging in sand

Recent studies have revealed that the increase of stiffness or strength of granular materials under constant loading cannot be ignored, which stimulates more intensive investigation on the time-dependent behavior of granular materials. Engineering properties of soils change with time which is called aging. Penetration resistance, liquefaction resistance, soil stiffness or strength, capacity of driven piles are included in these engineering properties. Mitchell

and Solymar (1984), Charlie et al. (1992a and b), and Thomann and Hryciw (1992) showed the increase in the strength and stiffness via cone penetration of sands. York (1994), Chow et al. (1998), and Axelsson (2002) presented set-up effects of driven or displacement piles in sands.

A review of aging in granular materials is presented in this chapter. A review of aging in granular materials include:

(1) Field evidences of aging in sand

(2) Laboratory testing results of aging in sand

(3) Mechanism of aging in sand

Field evidences of aging in sand

There are many examples in the literatures showing the time effects on stiffness or strength characteristics in sands via field tests. These literatures described gains in cone penetration resistance or set-up effects of piles in sands.

Mitchell and Solymar (1984) discussed that time-dependent strength gain in freshly deposited or densified sands is due to formation of silica gel films as a cementing agent at the grain contact creating a cohesive strength (c') in aged sands. Mitchell and Solymar (1984) noticed that strength and modulus of reconstituted samples may give significantly lower values that exist for the undisturbed sand deposit. Subsequent cone penetration test results showed an increase in the magnitude of the penetration resistance over a period of months after densification by blasting or vibrocompaction (Figure 2.7).

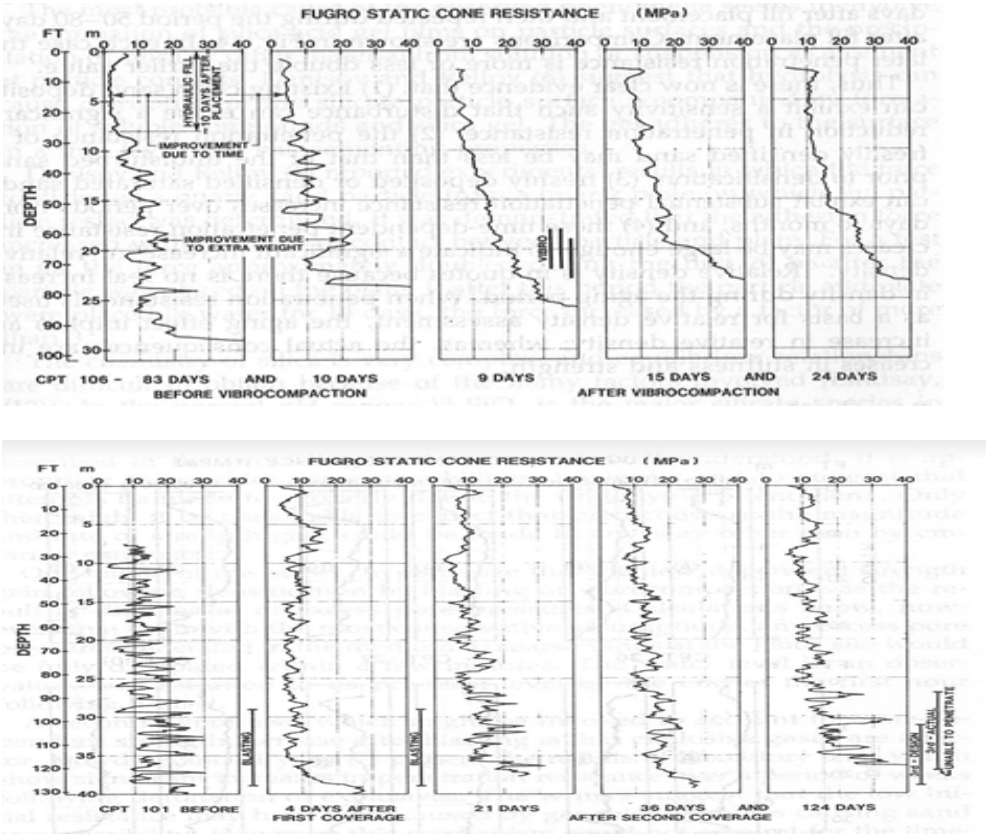

Figure 2.7 Effect of time after (a) blasting and (b) vibrocompaction on penetration resistance (Mitchell and Solymar, 1984)

Thomann and Hryciw (1992) investigated time effects on stiffness and strength changes in cohesionless soils (Agsco and Ottawa sands) via field tests. Both sands are uniform with subrounded, fine particles. In field tests, decreases in soil strength and stiffness were observed following an explosion in medium-dense sand. Thomann and Hryciw (1992) found that after disturbance, time-dependent increases in penetration resistance were observed. Figure 2.8 shows the change in tip resistance after disturbance. Time-

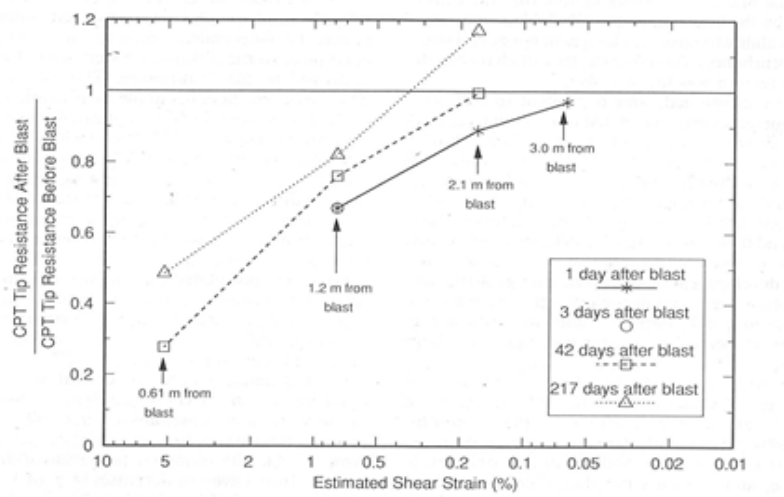

Figure 2.8 Change in tip resistance after disturbance as a function of estimated shear strain (Thomann and Hryciw, 1992)

dependent tip resistance increases up to 28% depending on the shear strain levels were observed after 217 days.

York (1994) postulated that setup and relaxation effects during testing and subsequent installation of piled foundations in a glacial deposit of clean sand. Displacement piles driven into medium dense sand deposit show time-dependent increases. As shown in Figure 2.9, for the glacial sands, the pile capacity increased as 40-80% because of set up effect. This figure shows very similar trends with the results of Tavenas and Audy (1972).

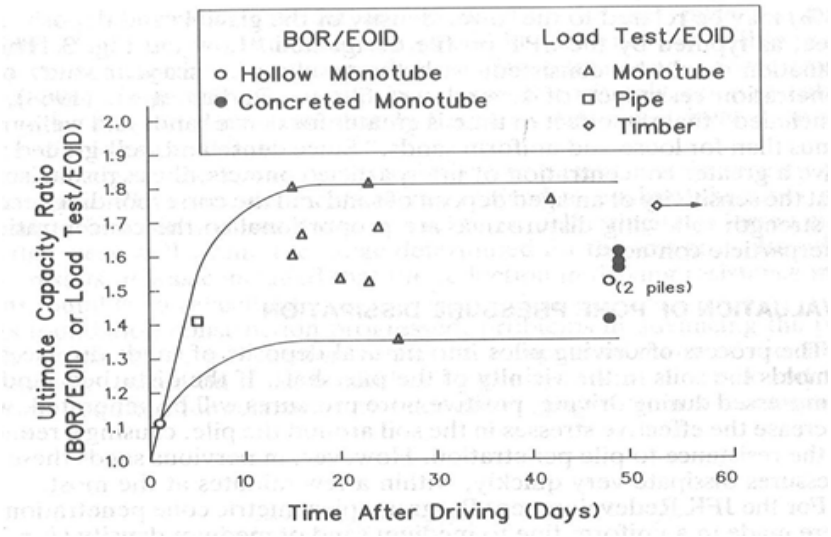

Figure 2.9 Evaluation of setup (York, 1994)

Chow et al. (1998) illustrated that the shaft capacities of displacement piles driven into dense marine sand at Dunkerque had increased by 85% over five years after installation as in Figure 2.10. The available evidence suggests that a circumferential arching mechanism develops during pile driving that limits the radial stresses acting on the pile shaft. It was concluded that creep leads to a breakdown of these arching stresses, allowing increases in radial stress and hence gains in shaft capacity.

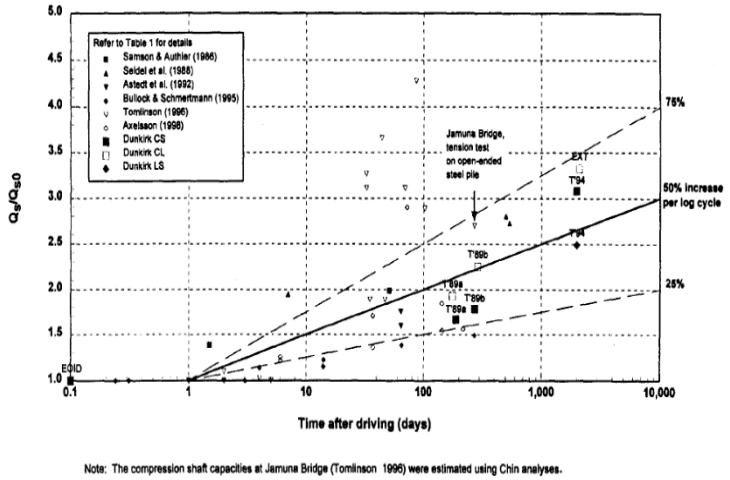

Note: The compression shaft capacities at Jamuna Bridge (Tomlinson 1996) were estimated using Chin analyses.

Figure 2.10 Increase in shaft capacity with time (Chow et al., 1998)

Troncoso and Garces (2000) postulated the results of in-situ tests of shear wave propagation to investigate the effects of geologic process, stress history and aging on the shear modulus of soils. Shear wave velocities were measured in downhole wave propagation tests in the sandy silts of the abandoned deposits of tailings. As in Figure 2.11, the increase in stiffness of soil deposits with age is obviously shown and expressed as a curve in relation with time. The results showed that soil structures get stiffer after aging or surcharging to high stress levels.

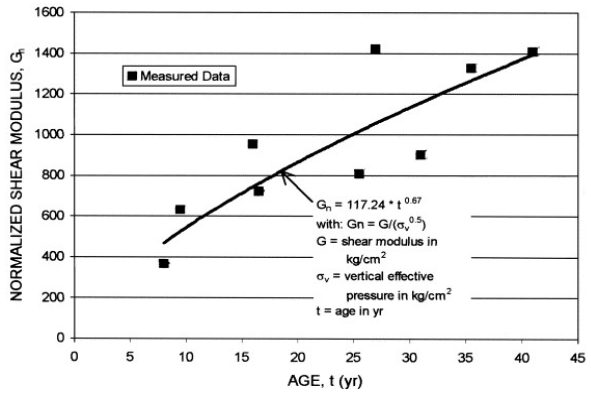

Figure 2.11 Normalized shear modulus of age for tailings (Troncoso and Garces, 2000)

Axelsson (2002) investigated long-term setup effect for driven piles in non-cohesive soils. The main observation of this research is a distinct increase in capacity over time and further as in Figure 2.12. It was interesting that the large increase in horizontal stress took place which reveals dilation effects at the pile-soil interface. Furthermore, these effects increased over time.

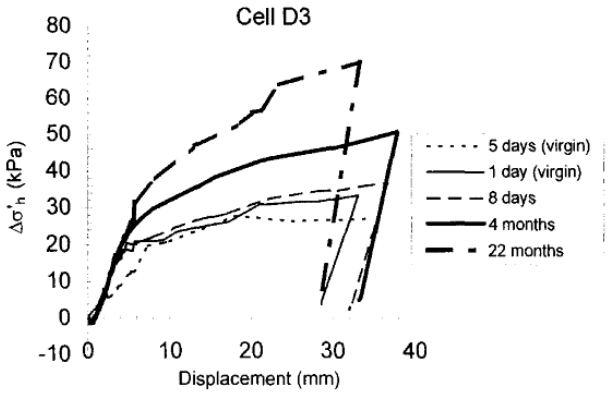

Figure 2.12 Increase in σ'_h during loading versus pile head displacement (Axelsson, 2002)

Laboratory testing results of aging in sand

Daramola (1980) showed that increased modulus occurred in saturated Ham river sands as well as clays. The secant modulus of the freshly prepared sample was designated E_0. The secant modulus of three sample left under sustained pressure for ten days was found to be $1.033E_0$. The corresponding values for samples of consolidation age of 30 days and of 152 days were found to be $1.583E_0$ and $1.992E_0$, respectively (Figure 2.13).

Joshi et al. (1995) studied the effects of aging on the penetration resistance of freshly deposited sands for local river sand and Beaufort Sea sand. The sands were aged under constant stress of 100 kPa for a period of up

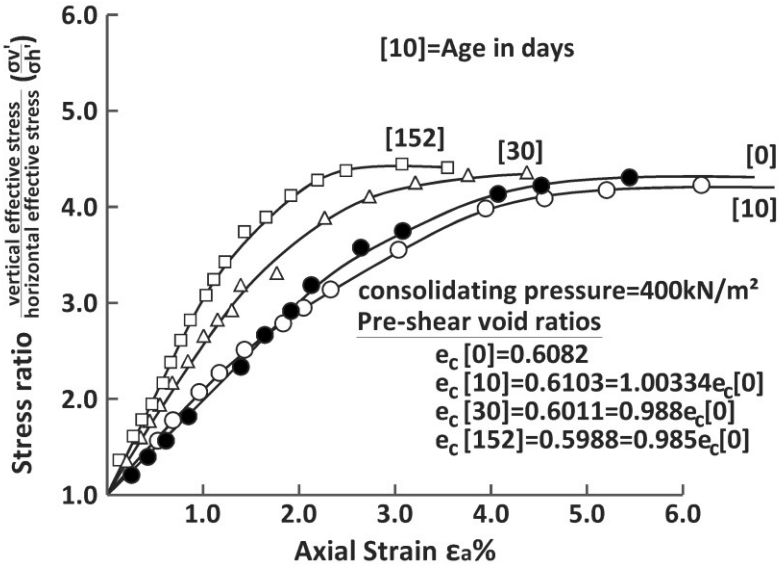

Figure 2.13 Effect of age of consolidation on stress-strain characteristics of Ham River Sand (Daramola, 1980)

to 2 years. As can be seen in Figure 2.14, the results suggested that aging significantly increases the penetration resistance of sands. In the case of the rate of the increase in penetration resistance, the submerged sand was higher than the dry sand. Joshi et al. (1995) explained that the increase in penetration resistance of sand of submerged in water is not only due to particle rearrangement, as in the case of dry sand, but is also due to dissolution and precipitation of salts and other impurities and possibly silica at the particle contacts and in the interspaces as Mitchell and solymar (1984).

Howie et al. (2002) explored effects of aging on stiffness of very loose Fraser River sands, a uniform fine clean sand, via laboratory triaxial compression tests. They showed that high stress ratio resulted in very low initial moduli with no aging but the moduli increased by several hundred

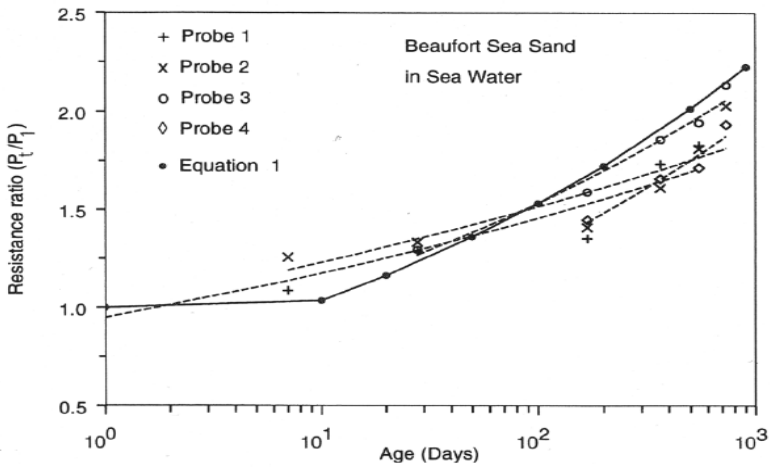

Figure 2.14 Resistance ratio, P_t/P_1, versus age for river sand in sea water (Joshi et al., 1995)

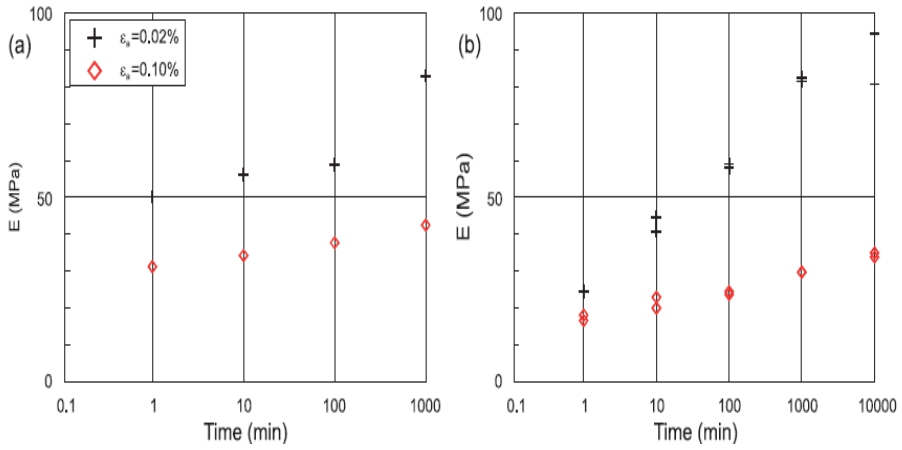

Figure 2.15 Variation in secant modulus with time at 0.02% and 0.1% strain for (a) R=1.0 and (b) R=2.0 (Howie et al., 2002)

percent during the first 1000 min (≈17 hr) of aging. Also, the initial moduli of aging at isotropic stress conditions were higher than those of aging at high stress ratio (Figure 2.15). These results well described that the stiffness of very loose sand depends on the time of confinement prior to shearing and the stress ratio where the sample is aged.

Baxter and Mitchell (2004) performed a series of laboratory tests to study mechanisms of aging effects under controlled conditions (relative density, different pore fluids, and different temperatures). Two different sands were tested and different periods of aging were adopted. However, no increase in the minicone penetration resistance was observed over time. These results showed contrasting behavior to those performed by Dowding and Hryciw (1986) and Joshi et al. (1995) and several evidences of aging effects on sand.

Wang et al. (2008) performed laboratory experiments and DEM simulation to figure out the aging mechanisms of sand. Leighton Buzzrard sand was used with 78% relative density. True triaxial tests with 3-directional bender elements were performed. Each aging stage lasted 3 days under isotropic and anisotropic stress conditions. Wang et al. (2008) explained that aging rate decreases because particle rearrangement which is the main mechanism of aging, is hard to occur under the high isotropic confining pressure.

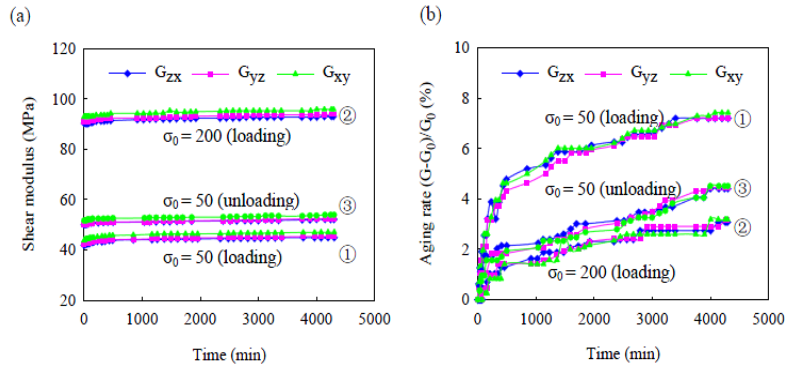

Figure 2.16 Isotropic stress condition (Wang et al., 2008)

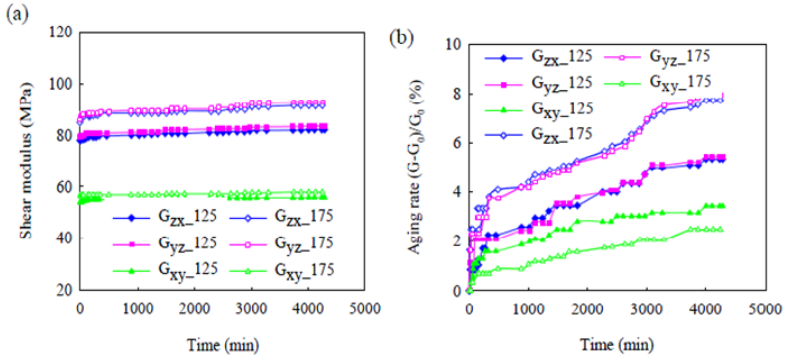

Figure 2.17 Anisotropic stress condition (Wang et al., 2008)

As can be seen in Figure 2.16, for the isotropic stress condition, the shear moduli increase as the normal stress increases (50 kPa → 200 kPa). The aging rate decreases as the normal stress increases (50 kPa → 200kPa). On the other hand, the shear moduli decrease and the aging rate increases as the stress decreases (200 kPa → 50kPa). As shown in Figure 2.17, under the anisotropic condition, z-direction becomes the principal direction, and the aging rate of G_{yz} (or G_{zx}) is higher than that of G_{xy}.

Wang and Gao (2013) showed that a lower aging rate was measured because when a higher confining pressure is applied, the soil sample should be slightly more densified so the particle rearrangement is minimized in response to aging. More homogenized contact forces are anticipated among soil particles; therefore, less contact forces change during aging.

Table 2.2 summarizes the aging effects in sand reported in the previous works.

Table 2.2 Summary of aging effects in sand reported in the previous works (continued)

Reference	Material	D_r (%)	σ'_v (kPa)	Densification method	Measured time period	Improvement with time	Notes
Daramola (1980)	Ham River sand	dense state	400	-	10-152 days	Secant modulus increases 1.583 times after 30 days, 1.992 times after 152 days	
Mitchell and Solymar (1984)	Alluvial sand	40-70	100-460	Vibrocompaction	24 days	Variable increase in q_c.	
Mitchell and Solymar (1984)	Alluvial sand	40-70	360-610	Blasting	124 days	50-100% increase in q_c.	
Schmertmann (1986)	Sand from Florida coastline	20-60	0-100	Dynamic compaction	80 days	240% increase in q_c.	

Table 2.2 Summary of aging effects in sand reported in the previous works (continued)

Reference	Material	D_r (%)	σ'_v (kPa)	Densification method	Measured time period	Improvement with time	Notes
Charlie et al. (1992)	Sand in the south Platte River, northwest Colorado	70-85	30-90	Blasting	5.5 years	q_c increased 18% after 18 weeks (211% after 5 years), q_l decreased 39% after 18 weeks (42% after 5.5 years)	
Joshi et al. (1995)	locally available river sand, and Beaufort Sea sand	87-95	100	-	1 day-2 years	90% increase in penetration resistance in 1 year for sand submerged sea water, 80% increase (distilled water) 30% increase (air dried)	Lab. tests
Chow et al. (1998)	Dense marine sand at Dunkirk, northern France	75					

Table 2.2 Summary of aging effects in sand reported in the previous works

Reference	Material	D_r (%)	σ'_v (kPa)	Densification method	Measured time period	Improvement with time	Notes
Howie et al. (2002)	Fraser River sand	13-17	20-280		1000 minutes		
Baxter and Mitchell (2004)	Evanston beach sand	40, 80	100	-	30-118 days	No increase in minicone q_c.	PS tests. lab tests.
Baxter and Mitchell (2004)	Density sand	40, 80	100	-	30-118 days	No increase in minicone q_c.	PS tests. lab tests.
Wang and Gao (2013)	Toyora sand	~80	50-175	-	3 days	~4.8% increase in G_{hv}, ~ 5.1 % in G_{hh}	True TX tests. Lab tests

Mechanism of aging in sand

Several explanations have been proposed to illustrate the phenomenon of aging in the granular materials. The proposed mechanisms can be categorized as follows:

(1) chemical bonding

(2) mechanical process

(3) other mechanisms

The hypothesis proposed by Mitchell and Solymar (1984) was also reported by Joshi et al. (1995). The proposed main mechanism of the increase in the penetration resistance of freshly deposited or densified sands is formation of silica gel films as a cementing agent at the grain contact creating a cohesive strength (c') in aged sands. According to Joshi et al. (1995), the rate of gains in the penetration resistance of the submerged specimens in sea water was higher than that of the submerged specimens in distilled water or dry samples. From the results of SEM of the specimens, the formation of cementing bonds at the grain particles or interspaces was observed.

According to Mesri et al. (1990) and Schmertmann (1991), particle movements are the major mechanism of aging in granular materials. Mesri et al. (1990) concluded that engineering time aging effects in sand seems to require some movement of the particles. Also, they pointed out that less restriction like low viscosity of pore fluid or low density conditions of particle movements promotes the aging effects. Schmertmann (1991) proposed that the changes in engineering properties of soils during creep/aging were mainly

resulted from particle slippage resulting in particle interlocking or internal stress redistribution.

Although the mechanisms of aging provided by Schmertmann, Mesri, Mitchell and Solymar are frequently cited ones, other hypotheses also exist including blast gas dissipation (Dowding and Hryciw, 1986) and static fatigue at grain contacts (Michalowski and Nadukuru. 2012).

Dowding and Hryciw (1986) postulated that the increases in penetration resistance after blast densification is possibly due to the dissipation of blast gases into solution leading to aging effects in sands.

Michalowski and Nadukuru (2012) pointed out that the increase in the horizontal stress in a sand bed can be resulted from an increase in the intergranular contact stiffness. This increase in contact stiffness is owing to the delayed process of stress corrosion cracking of the micromorphologic features on grain surfaces at the contacts, which brings grains closer together (grain convergence). Consequently, the macroscopic stiffness of sand increases, and under 1D strain conditions, the horizontal stress in the sand bed increases. This hypothesis gives more plausible explanation for time-delayed increases in cone penetration resistance following dynamic compaction.

2.3 Effects of fine-contents on the time-dependent behavior of granular materials

In the field, granular materials often contain different amount of fines. Uniformly graded sands have been frequently used to investigate the behavior of granular materials in the laboratory. Therefore, the behaviors of granular material containing fines can be quite different from that of uniformly graded sand. Hence, in this chapter, a review of literatures for fine contents effects on the time-dependent behavior of granular material is presented.

Wang and Tsui (2009) investigated the effect of aging on dynamic properties of sands. In this research, the kaolinite powder was added to the sand in order to study the influence of fines on the aging effects. Dry kaolinite powder was mixed with Toyoura sand samples with 3 and 15% of fine content. The variations of the shear-modulus increase and the damping ratio of these samples over 2 days of aging at 100 kPa are presented in Figures 2.18~2.19, respectively. Wang and Tsui concluded that with an addition of kaolinite powder, the stiffness of the specimen increases and contact property between sand particles also changed. As can be seen in Figure 2.18, the aging effects of the specimens to which powder was added are higher than those of the specimens with the clean sand. The results also suggested that the contact properties vary from time to time. As shown in Figure 2.19, kaolinite powder has a larger small-strain damping ratio (1%) than Toyoura sand does (0.28%). Based on the test results, Wang and Tsui concluded that an addition of fines in

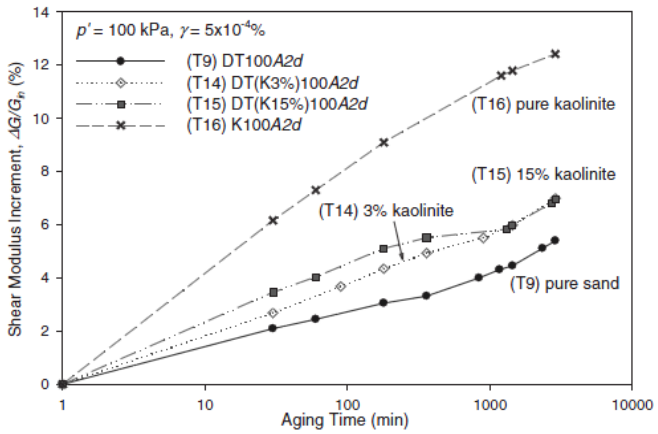

Figure 2.18 Comparison of the shear modulus increment $\Delta G_{2d} / G_{in}$ in samples with different fines (kaolinite) contents (Wang and Tsui, 2009)

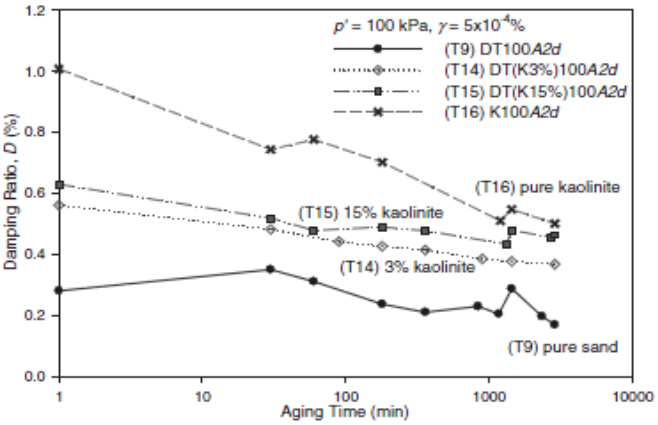

Figure 2.19 Comparison of the small-strain damping ratio in samples with different fines (kaolinite) contents during 2 days of aging (Wang and Tsui, 2009)

the sand samples can raise the aging rate because of more significant creep and aging rate made by the kaolinite.

Karimpour and Lade (2013) conducted a series of triaxial creep tests for specimens with different gradation curves. Figure 2.20 shows the effect of grain distribution curve on the axial and volumetric creep strains. Type 1 with higher uniformly graded soil shows lower axial and volumetric creep strains. Karimpour and Lade (2013) explained that creep deformation increases with the fine contents because adding fines results in more contact points between the particles and asperities.

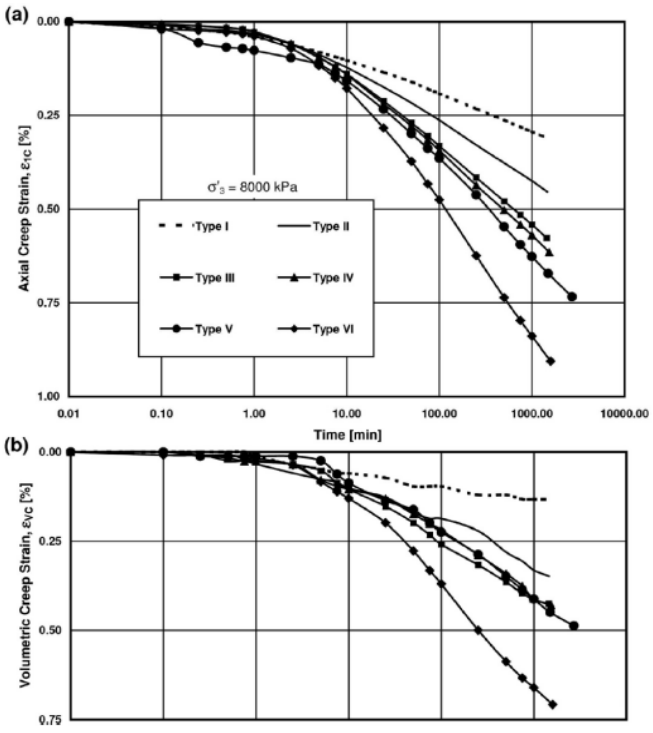

Figure 2.20 Effect of grain distribution curve on variation of (a) axial and (b) volumetric creep strains with time (Karimpour and Lade, 2013)

From these researches, we can expect that the effect of creep/aging on weathered residual soil containing fine contents is greater than that on uniformly graded sand.

2.4 Effects of creep/aging on anisotropy

The anisotropy of soil in stiffness is also an important factor in various problems relating to ground deformation. Previous researchers such as Ochiai and Lade (1983) and Kirkgard and Lade (1991 and 1993) experimentally investigated the influence of initial fabric anisotropy on the failure of soils. Herein, a research dealing with effects of creep/aging on anisotropy of granular materials is reviewed.

Wang and Gao (2013) conducted experiments and discrete element method (DEM) simulations in order to investigate aging effects on the stiffness changes of sand with inherent anisotropy. The true triaxial apparatus with multi-directional bender element systems was used to evaluate the evolution of the small strain shear moduli of sand samples with relative density of 80% during aging. As can be seen in Figure 2.21, with increasing applied confining pressure on the loading path, the stiffness anisotropy decreases. On the unloading path, the stiffness increases as the confining stress decreases. In comparison with the specimens before and after aging, it was found that the stiffness anisotropy is more remarkable for the specimens after 3 days of aging.

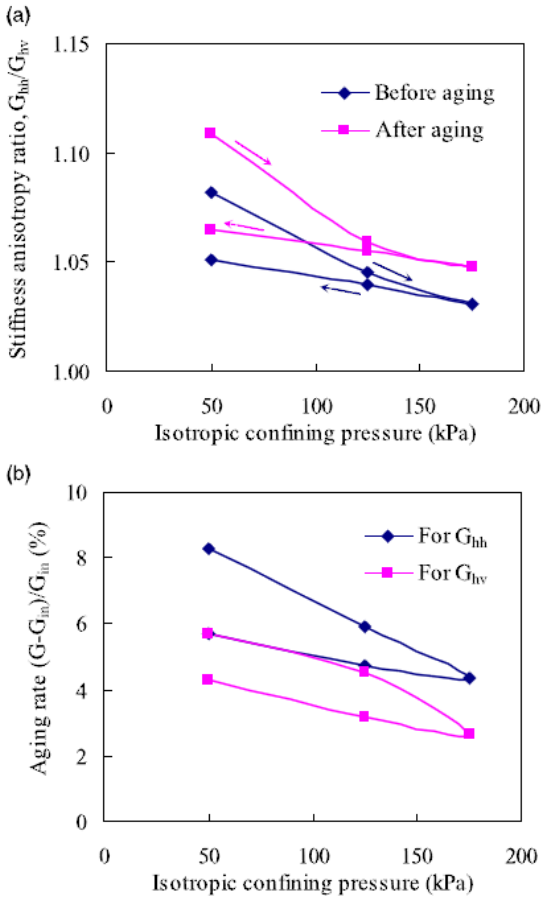

Figure 2.21 Summary of (a) stiffness anisotropy and (b) anisotropic aging rate of Toyoura sand samples before and after 3 days of aging (Wang and Gao, 2013)

Therefore, it is important to evaluate the effects of creep/aging on anisotropy to solve the actual geotechnical deformation problems.

2.5 General creep behavior

Typical strain-time curves obtained from creep tests under constant loading over sufficiently long periods of time can be categorized into three stages. As in Figure 2.22, there is first a period of transient creep during which the strain rate decreases with time, followed by creep at nearly a constant rate for some period. For materials susceptible to creep rupture, the creep rate then accelerates leading to failure. These three stages are termed primary, secondary, and tertiary creep. Generally, primary and secondary creep curve are the area of engineering interest, where the creep rate is almost constant. The primary and secondary creep can be predictable.

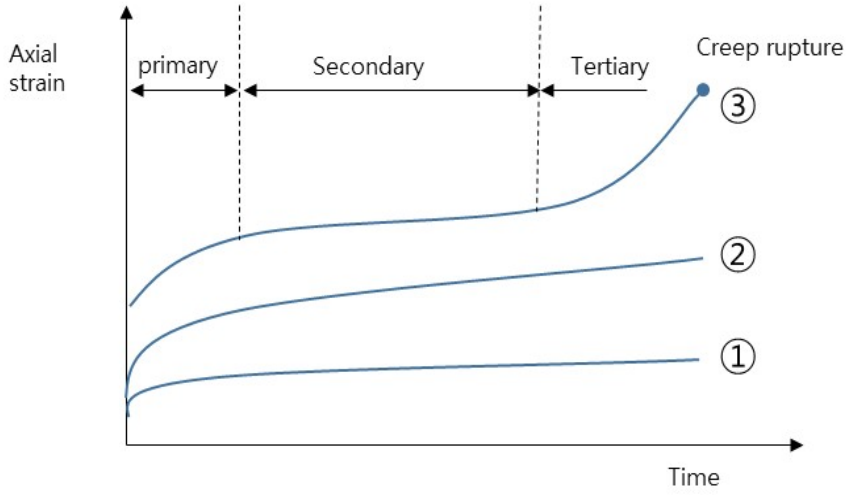

Figure 2.22 Creep under constant stress (Mitchell and Soga, 2005)

2.6 Summary

The time-dependent behaviors of granular materials have been reported by several researchers. In this chapter, the previous researches dealing with the creep deformations or increases in stiffness or strength with time in the granular materials have been presented.

From the previous sections, it was revealed that the time-dependent behavior in granular materials cannot be ignored and behaviors of granular materials containing fines is quite different from pure sands.

The creep deformations of sands in the literatures showed both contractive and dilative behavior. However, the questions, occurring conditions or mechanisms of contractive or dilative deformations, still remain unsolved. There have been numerous evidences of aging effects on granular materials, but there are few studies dealing with the evolution of anisotropy of granular materials during creep. Despite geological prevalence and most common type soil as construction materials in South Korea, the time effects on creep or aging behavior of Korean weathered residual soil have not been intensely investigated yet. Therefore, the aims of my dissertation are to investigate the overall time-dependent deformation behaviors and to study the directional shear moduli evolution during creep of weathered residual soil in Korea.

Chapter 3. Test Materials and Apparatus

3.1 Introduction

In this paper, triaxial tests and one-dimensional compression tests were performed to investigate creep/aging behavior of weathered residual soil. Also, bender elements were attached to the sample to obtain stiffness characteristics at very small strain region.

A testing program was specially designed to illustrate stress conditions of the backfill materials of earth-retaining walls. Different densities of the specimens crept under different effective stresses and stress ratio. With local LVDTs directly attached to the specimens, deformations under constant loading were continuously obtained. Also, orthogonal bi-directional bender elements evaluate the time effect on the directional stiffness at regular intervals.

This chapter mainly discusses the tested material, testing apparatus, and testing program.

3.2 Testing materials

Weathered residual soil was manually sampled near the Mt. Cheonggye, Seoul, Korea. The grain size distribution curve and physical properties of sampled soil are shown in Figure 3.1, and Table 3.1, respectively. Weathered residual soil is classified as well-graded silty sand (SM) and contains 17% fines. The minimum and maximum void ratios of the soil were 0.53 and 1.27, respectively. To prepare specimens for the triaxial tests, particles larger than the opening size of No.20 sieve, i.e. 0.850 mm, were removed from original samples. 70 mm-diameter and 155 mm-high triaxial specimens were prepared by compacting sieved soils mixed with water to have the initial moisture content of 15%. To consider the variation in the field density of compacted soils, three different groups of the specimens with the relative density of 73, 85, and 96% were prepared.

In the one-dimensional compression tests, both Jumunjin sands and weathered residual soil were chosen to compare the creep behaviors. The grain size distribution curve and physical properties of Jumunjin sand are also shown in Figure 3.1, and Table 3.1, respectively. Jumunjin sand represents poor-graded uniform distribution. The minimum and maximum void ratios of the Jumunjin sand were 0.60 and 0.99, respectively. 60 mm-diameter and 20 mm-high oedometer specimens were prepared by compacting soils mixed with water to have the initial moisture content of 15% as well as the triaxial tests. Three different groups of weathered residual soil specimens with the relative density of 73, 85, and 96% (termed here low, medium, and very dense

sand, respectively) were prepared. For the comparative study, Jumunjin sand specimens with the relative density of 96% were prepared.

The SEM microphotographs of soils of Jumunjin sand and weathered residual soil are shown in Figure 3.2, respectively. As can be seen, the particle shape of weathered residual soil is angular in comparison with round shape of Jumunjin sand particles.

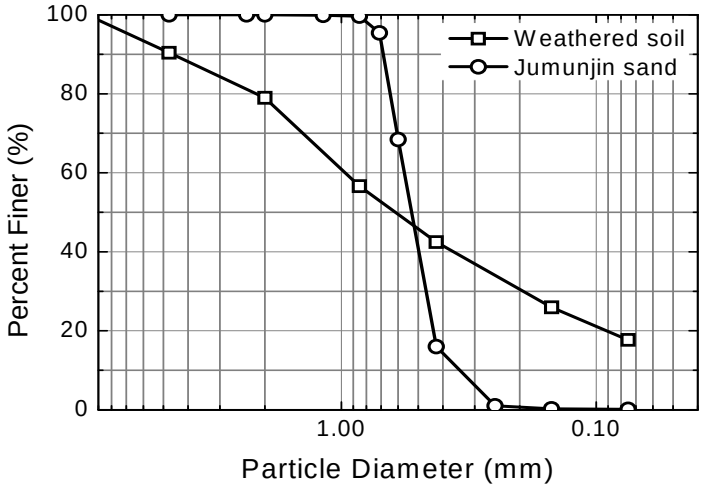

Figure 3.1 Particle size distribution of tested material

Table 3.1 Physical properties of tested materials

Tested material	G_s	e_{max}	e_{min}	Percent finer than #200 sieve (%)	C_c	C_u	USCS
Jumunjin Sand	2.65	0.99	0.60	0	1.5	0.9	SP
Korean Weathered Residual Soil	2.67	1.27	0.53	17	33	1.3	SM

(a) Jumunjin Sand

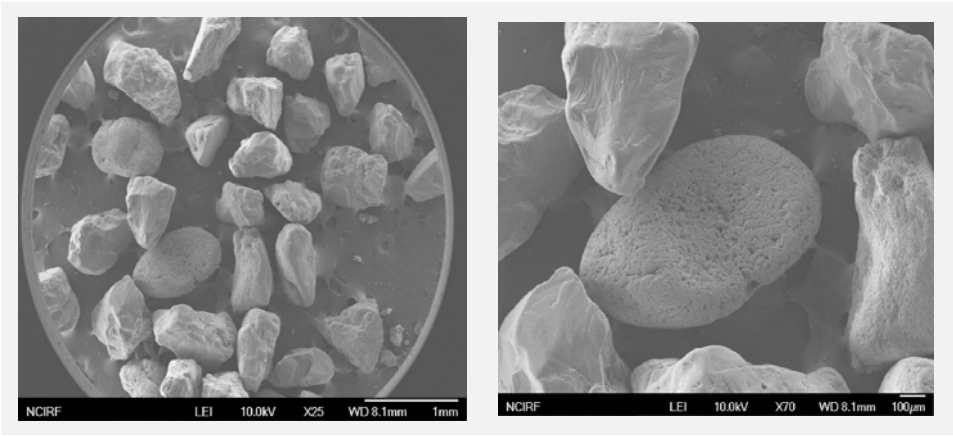

(b) Weathered Residual soil

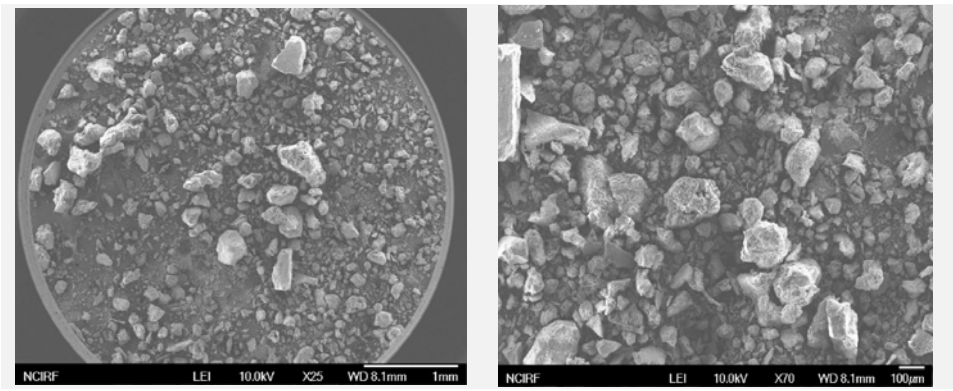

Figure 3.2 SEM microphotographs of soils used in the tests (a) Jumunjin sand (b) weathered residual soil

3.3 Testing apparatus

3.3.1 Triaxial testing apparatus

Figure 3.3 illustrates the schematic diagram of the GDS triaxial testing equipment that consists of the loading-frame, 4-channel dynamic data logger for the 4-kN capacity submersible load cell, 8-channel data logger for miniature LVDTs mounted directly into the specimen, and two controllers to control cell and back pressures. To measure the shear wave velocities in the different directions, two pairs of locally designed and manufactured bender elements were used. Following the suggestion of Kuwano and Jardine (2002), specially designed lubricated ends at both sides of the specimen were employed.

Shear wave velocities in two different horizontal directions were measured via two pairs of bender elements during creep. A single-pulse sinusoidal input signal of 10-volt amplitude was shot for each measurement using bender elements.

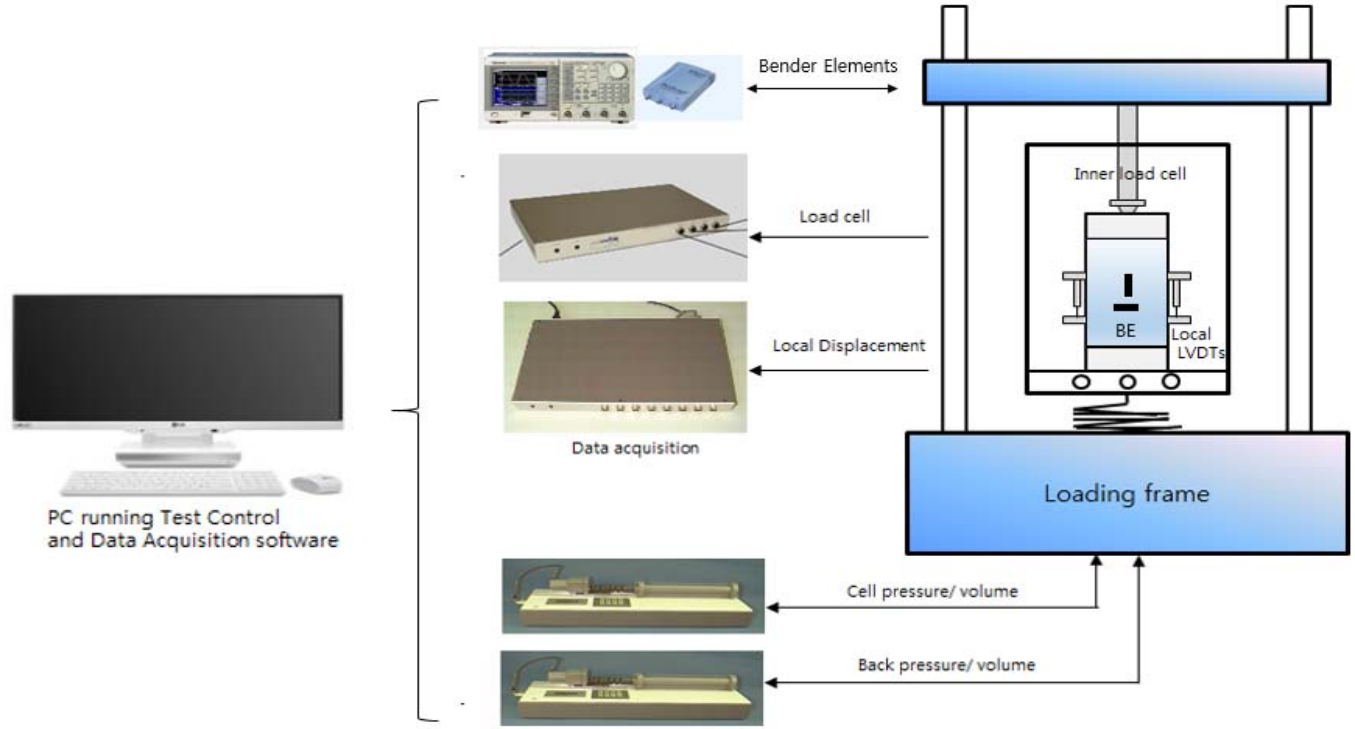

Figure 3.3 Schematic diagram of triaxial testing system

Small strain measurement system

Creep deformation is very small compared to consolidation or shear deformations. Therefore, precise measurement is very important. However, in conventional triaxial testing apparatus, devices for displacement or load measurement are installed outside of triaxial cell resulting in several types of errors such as seating error, bedding error, alignment error and compliance error as in Figure 3.4 (Baldi et al., 1988).

In this study, as in Figure 3.5, in order to measure creep deformations precisely, high resolution (precision of 10-4mm) of local LVDTs manufactured by GDS instruments were mounted directly into the specimens and 4-kN capacity submersible inner load cell was used. Figure 3.6 shows the way to attach the local LVDTs into the specimens.

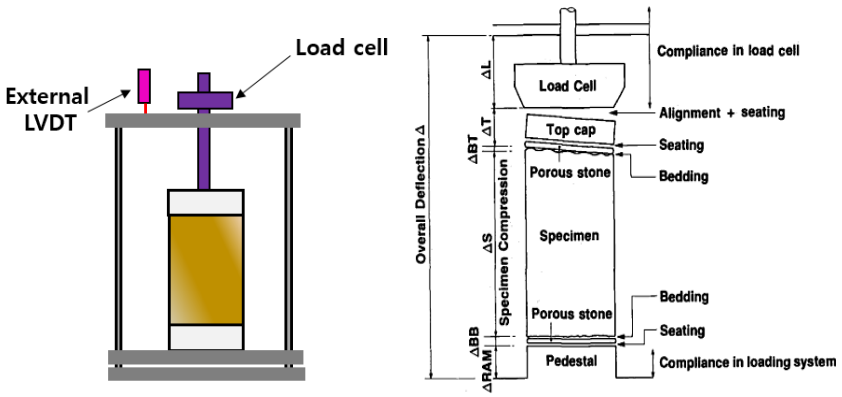

Figure 3.4 Sources of error in external axial deformation measurements (Baldi et al., 1988)

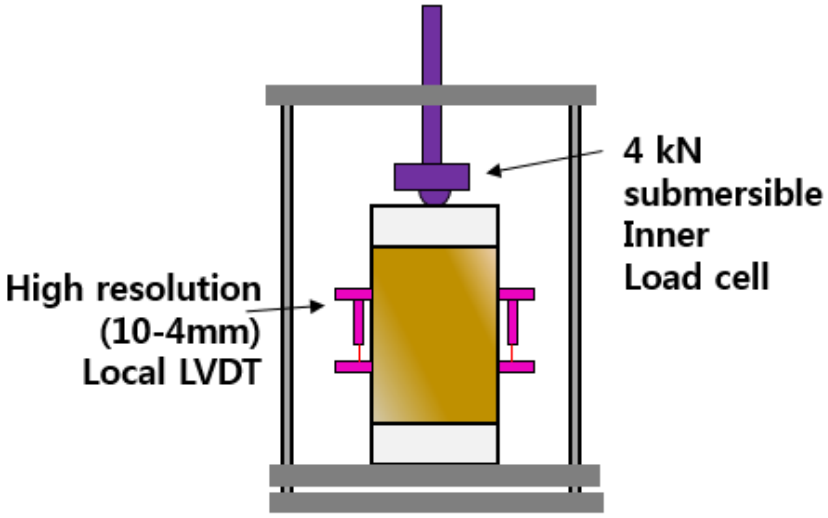

Figure 3.5 Triaxial testing devices for small strain measurement

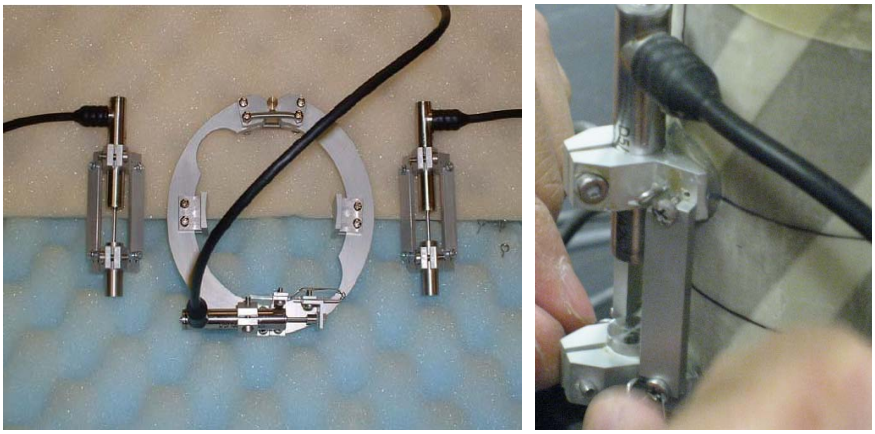

Figure 3.6 Local LVDTs manufactured by GDS instruments

Combined Bender Element tests

To measure variations in the directional soil stiffness during creep, bi-directional bender elements tests were performed. Bender element is a two-layer piezoelectric transducer which consists of two-layer piezoelectric ceramic and one-layer copper shim at the center. Bender elements are commonly used in pairs to obtain the shear wave velocity in a soil specimen.

Figure 3.7 shows the schematic diagram of bender elements test. First of all, a transmitter bender sends a signal from a function generator through a specimen to a receiver bender element on the opposite side. A propagated signal is delivered through an oscilloscope to the computer for data processing. Knowing the distance between two bender elements, shear wave velocity can be calculated by measuring the traveling time. With a bulk density of specimen, a shear modulus can be easily calculated.

Figure 3.8 shows illustration of multi directional bender elements. As in Figure 3.8, three-directional bender elements tests were performed to measure the directional soil stiffness. However, the values of G_{vh} could not be obtained because of limitation of energy transportation. According to Gao and Wang (2011), the values of G_{vh} and those of G_{hv} are very similar in the granular materials. Hence, it is considered that this study to investigate the directional stiffness of weathered residual soil in Korea might be moderate. The detailed basis of evaluation of anisotropy is given in Appendix A.1.

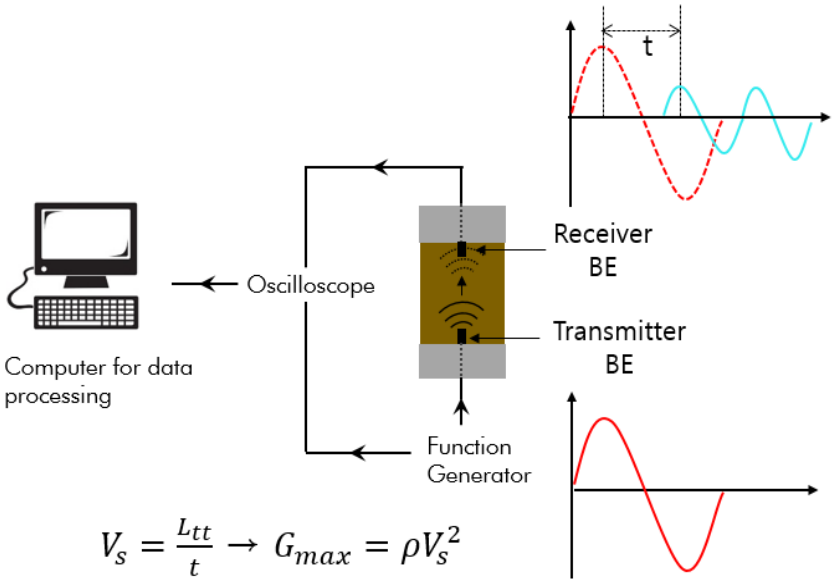

Figure 3.7 Schematic diagram of bender elements test

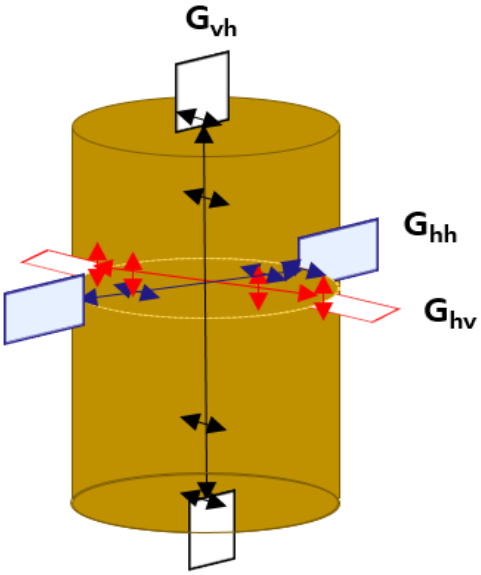

Figure 3.8 Illustration of multi directional bender elements

Figure 3.9 Preparation of the specimen with local LVDTs and multi directional bender elements

Figure 3.10 Bender elements and their sockets used in this study

Figure 3.9 shows the picture of the specimen with local LVDTs and multi directional bender elements and Figure 3.10 shows bender elements and their sockets used in this study. Top and bottom caps were produced with light material to change the sockets and benders and move the triaxial cell easily. To find out an optimal combination of a pair of bender elements, several preliminary bender elements tests had been performed. From the preliminary bender elements tests, it was found that a combination of parallel (input) to series (output) with shielding and grounding is the most suitable to measure the shear wave velocity because output signal of series type of bender elements is larger than that of parallel type of bender elements. Manufacturing the bender elements in the laboratory, size and length of benders can be adjusted. The original size of bender used in this study is 15 X 6.4 X 0.66 (length X width X thickness in millimeters) and the size of bender after insertion to the socket is 4 X 6.4 X 0.66 (length X width X thickness in millimeters).

AFG 3021B Function generator of Tektronix Instruments was used to generate the input signal for bender element tests. A single-pulse sinusoidal input signal, peak to peak input amplitude is 20V, was selected to obtain clear and unbiased data. When a receive bender receive a transmitted wave from transmitter bender, a wave is visualized by ADC-212 oscilloscope of Pico technology through a computer. Then, arrival time can be measured by a computer program, Picoscope.

Because the bender element response is promoted when the frequency of the input sine signal approaches the resonant frequency of the bender element-

soil system (Coop et al. 1996 and Lee and Santamarina 2005), the preliminary study was performed to find out the resonant frequency. As a result, the frequency of 5 kHz was selected for the bender element tests.

In order to determine the arrival time, point C in Figure 3.11, zero after first bump, was selected (Lee and Santamarina, 2005). A typical output signal gathered from a step input signal is presented in Figure 3.11. Figure 3.12 shows an example for raw data of shear wave signals.

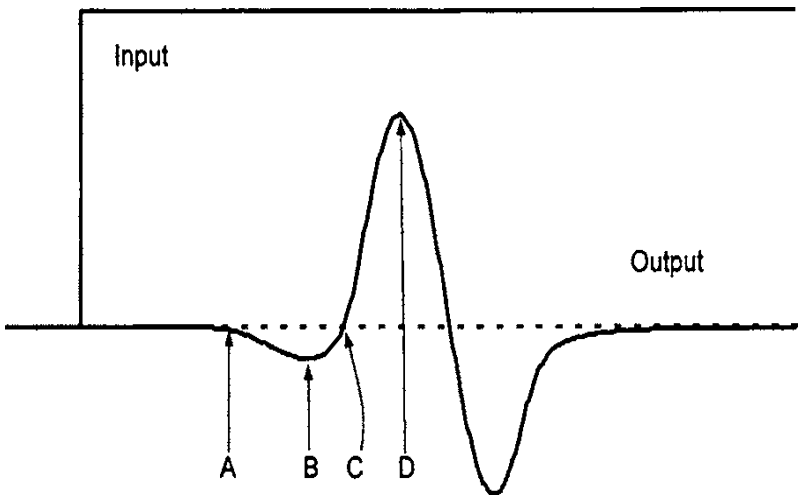

Figure 3.11 Typical shear wave signal within near field: (A) first deflection, (B) first bump maximum, (C) zero after first bump, and (D) major first peak (Lee and Santamarina, 2005)

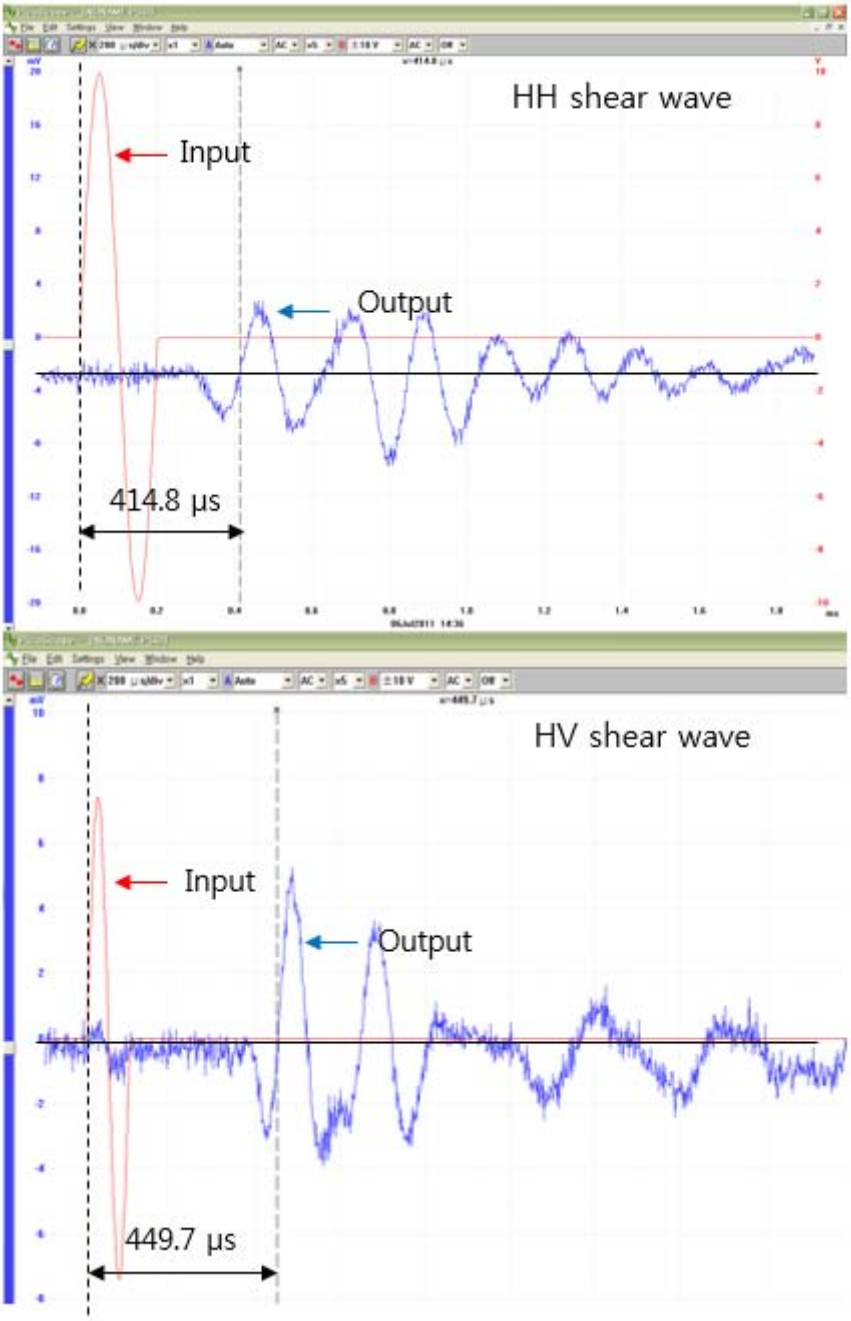

Figure 3.12 Raw data of shear wave signals

3.3.2 One-dimensional compression testing apparatus

In the one-dimensional creep tests, conventional one-dimensional compression testing apparatus was employed as in Figure 3.13. In order to measure the creep deformation precisely, high resolution (resolution of 10-4mm) of local LVDTs manufactured by GDS instruments were installed. The axial deformations are automatically acquired by GDSLAB with time at regular intervals.

Figure 3.13 One-dimensional compression testing apparatus

3.4 Testing program

3.4.1 Triaxial tests

After flushed by CO_2 gas, the specimen was saturated by applying back pressure of 200 kPa. Subsequently, the specimens were consolidated with isotropic or anisotropic stresses depending on the testing program. To minimize excess pore water pressure, the specimen was slowly consolidated by applying σ'a at the rate not exceeding ~ 1.73 kPa/min. For the anisotropic consolidation, two stress ratios were chosen, q/p', of 0.2 and 0.4, where $p'=(\sigma'_a+2\sigma'_r)/3$ is the mean normal effective stress, $q=\sigma'_a-\sigma'_r$ is the deviator stress, and σ'_a and σ'_r axial and radial effective stresses, respectively.

Figure 3.14 shows the stress paths with the stress ratio of 0, 0.2, and 0.4. When the stress path reached the axial effective stresses of 100, 200, and 400 kPa, the creep tests were conducted while the stress was held constant under load controlled system and this continued for 48 hours. The marks along the stress paths in Figure 3.14 indicated the stresses at each creep stage. The points of each creep stages are determined based on Figure 3.15. Figure 3.15 illustrates the stress conditions of the sub-soil under a retaining wall. As shown in Figure 3.15, the vertical stresses of elements for the same depths are constant, whereas the radial stress decreases as the position of the element is more outwardly located.

The increment of radial stress for the elements at the same depth can be expressed by:

$$\delta\sigma_r = -\delta q \tag{3.1}$$

where the deviator stress is $q = \sigma_a - \sigma_r$ and $\delta\sigma_a = 0$

The mean normal effective stress is given by:

$$p' = \frac{\sigma_a + 2\sigma_r}{3} \tag{3.2}$$

Substituting equation (3.1) into (3.2), the incremental mean normal effective stress can be derived as:

$$\delta p = \frac{2\delta\sigma_r}{3} = -\frac{2\delta q}{3} \tag{3.3}$$

Thus, the stress conditions of elements at the same depth is located along the line of $\delta p = -\frac{2\delta q}{3}$ as indicated in Figure 3.14. In this study, assuming that the unit weight density of soil is $2t/m^3$, creep test conditions are determined as in Figure 3.15 to illustrate the stress conditions of the elements at depths of 5 m, 10 m, and 20 m from the ground surface.

In the early stages of creep researches on granular materials had been conducted for short periods of time due to experimental difficulties like a temperature maintenance problem or apparatus limitations (Kuwano and Jardine 2002). Herein, to investigate the creep behavior for longer periods of time, 48 hours creep tests were performed under constant stress conditions.

To investigate the evolution of anisotropy during creep, using two pairs of bender elements installed horizontally on the specimen with the different polarization directions, elastic shear moduli, G_{hv} and G_{hh}, were measured at a given interval during creep stage.

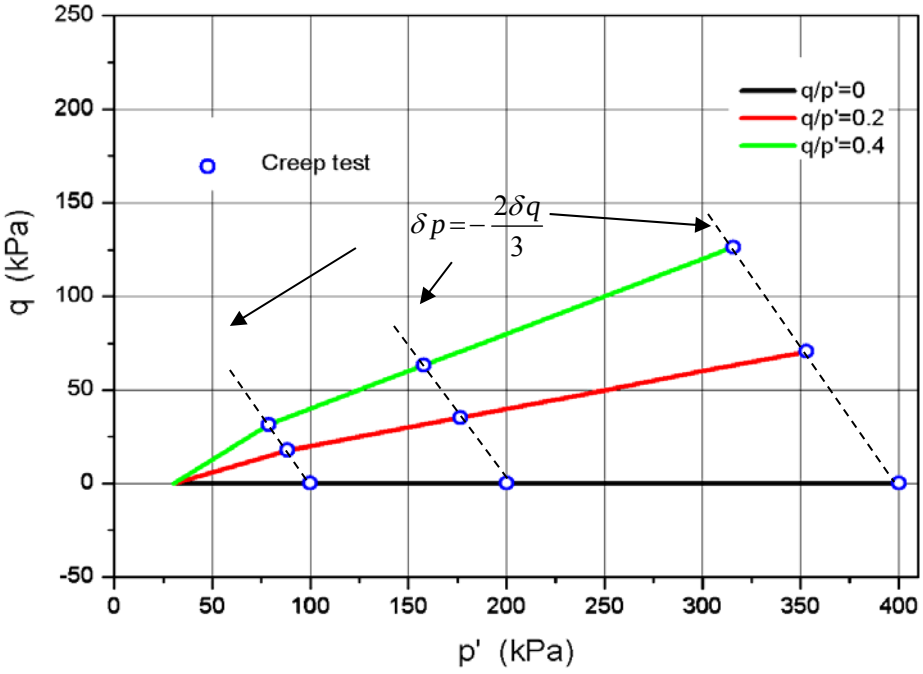

Figure 3.14 Applied stress paths for consolidation and creep

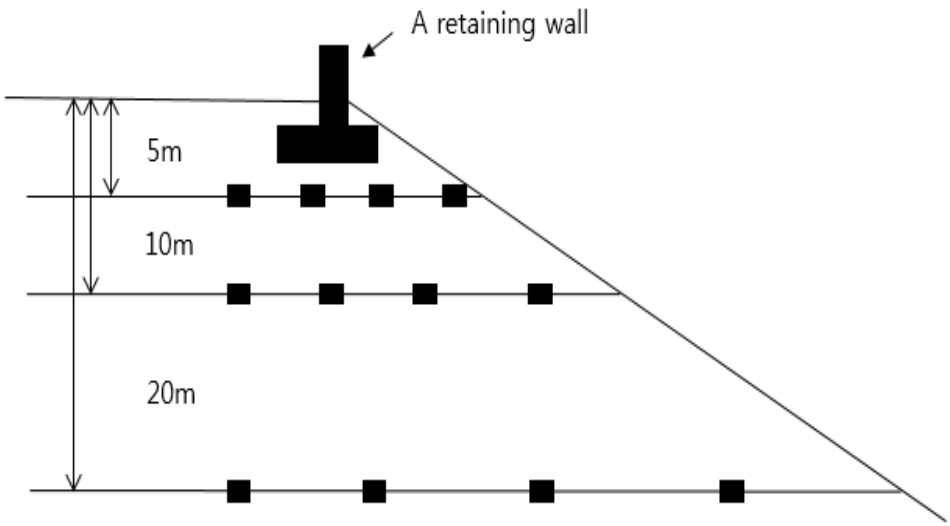

Figure 3.15 Illustration of the stress conditions of sub-soil elements under a retaining wall

3.4.2 One-dimensional compression tests

60 mm-diameter and 20 mm-high oedometer specimens were prepared by compacting soils mixed with water to have the initial moisture content of 15% as well as the triaxial tests. As the conventional consolidation test, double loading method was employed. The loading was applied immediately from 10 to 640kPa, in multiple stages. At each loading stage, it was considered to reach the final and stable deformation when the rate of deformation was no greater than 0.005mm/day. Then the next-step loading was applied. The elapsed time for each loading stage was about 7 days.

Chapter 4. Experimental Results and Analysis: Deformation Characteristics

4.1 Introduction

The deformation characteristics of weathered residual soils in Korea are discussed in this chapter. A series of triaxial creep tests were conducted to investigate the overall creep deformations. To explore different stress conditions, a number of the triaxial specimens were prepared.

Time-dependent deformations, especially for the granular material, are very small in comparison with the consolidation or shearing deformations. Therefore, for precise measurement of creep deformations, high accuracy of local LVDTs and submersible inner load cells were used as described in Chapter 3.

The main topics of chapter 4 are:

(1) Creep strains of triaxial compression tests and

(2) State-dependent volumetric creep behavior.

4.2 Creep strains of triaxial compression tests

4.2.1 Stress-strain curves of triaxial compression tests

In this chapter, overall stress strain behavior of triaxial compression tests were presented, in terms of axial stress-strain behavior and volumetric stress-strain behavior.

Figure 4.1 shows the relationships between the axial effective stress and axial strains during consolidation and creep for the specimens subjected to the stress ratio of 0, 0.2, and 0.4, respectively. Figure 4.2 shows the relationships between the mean normal effective stress and volumetric strains during consolidation and creep for the specimens subjected to the stress ratio of 0, 0.2, and 0.4, respectively. The patterns of stress-strain curves depend on the initial relative density. It is clearly observed that a specimen with higher relative density exhibits stiffer response than others. It is also interesting that specimens with a high relative density shows dilative behavior under constant stress state as in Figure 4.2(c). Based on these volumetric strains, the changes of relative density are calculated and the results are summarized in Appendix A.2.

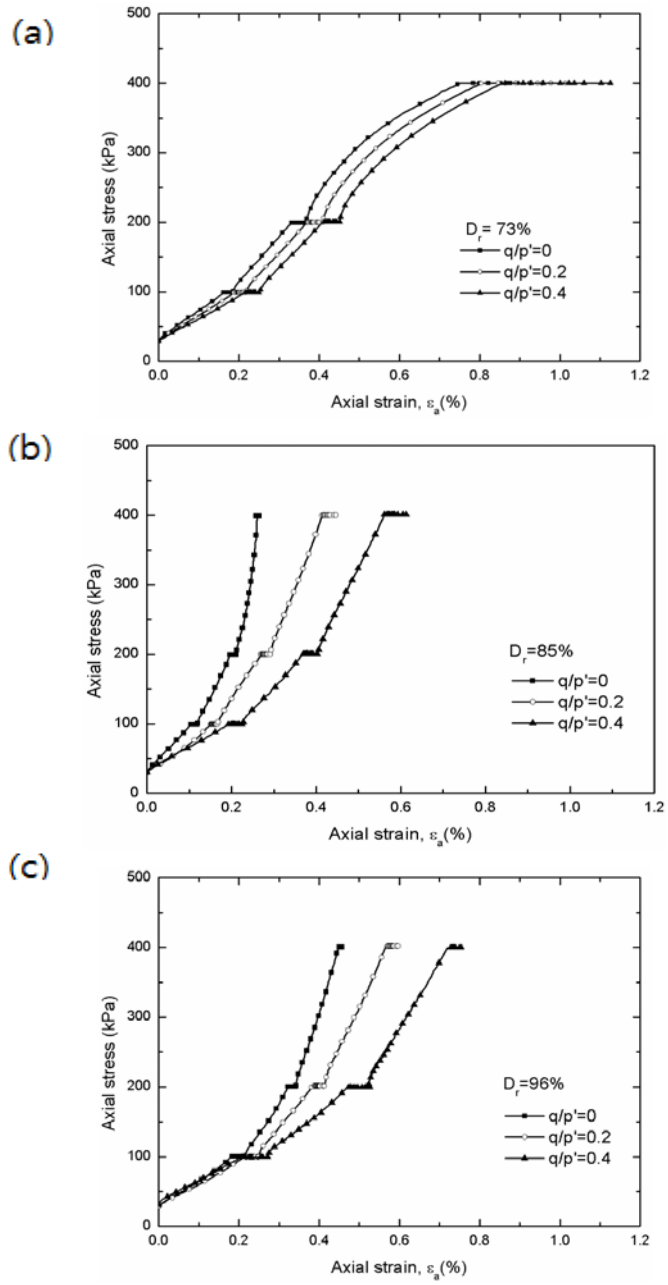

Figure 4.1 Axial stress strain curves of initial relative density of (a) 73%, (b) 85%, and (c) 96%, respectively

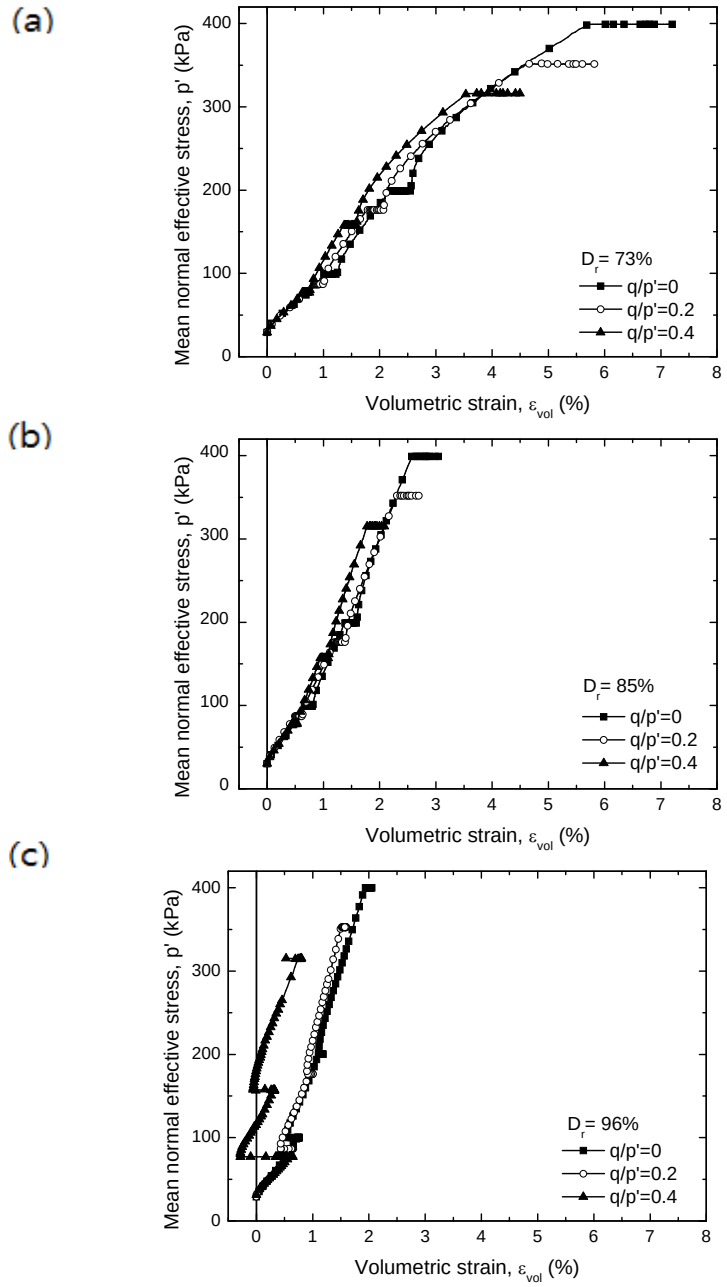

Figure 4.2 Volumetric stress strain curves of initial relative density of (a) 73%, (b) 85%, and (c) 96%, respectively

4.2.2 Specifying the time origin of the creep phase

To estimate the creep deformation, it is important to define the initiation of creep stage. Figures 4.3~4.5 show the observed volumetric strains with time. As in Figures 4.3~4.5, the ends of each loading are indicated by arrows. The rate of volumetric strain decreases rapidly at the end of loading leading to initiation of creep. In other words, the excess pore water pressure is rapidly dissipated. It is assumed that there is no volumetric strain due to dissipation of excess pore water pressure (consolidation) under constant loading. As a results, the strain observed during loading can be classified as consolidation and the strain observed under constant loading can be classified as creep.

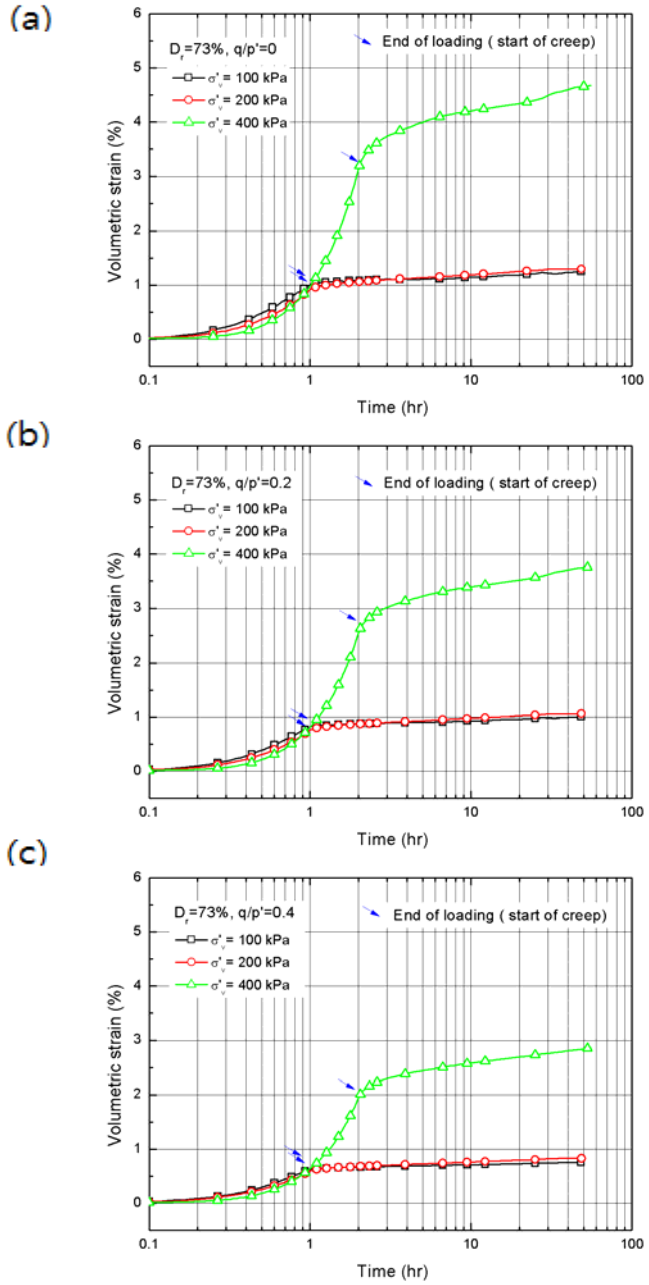

Figure 4.3 Specifying the time origin of the creep phase of (a) q/p'=0, (b) q/p'=0.2, and (c) q/p'=0.4, respectively (D_r=73%)

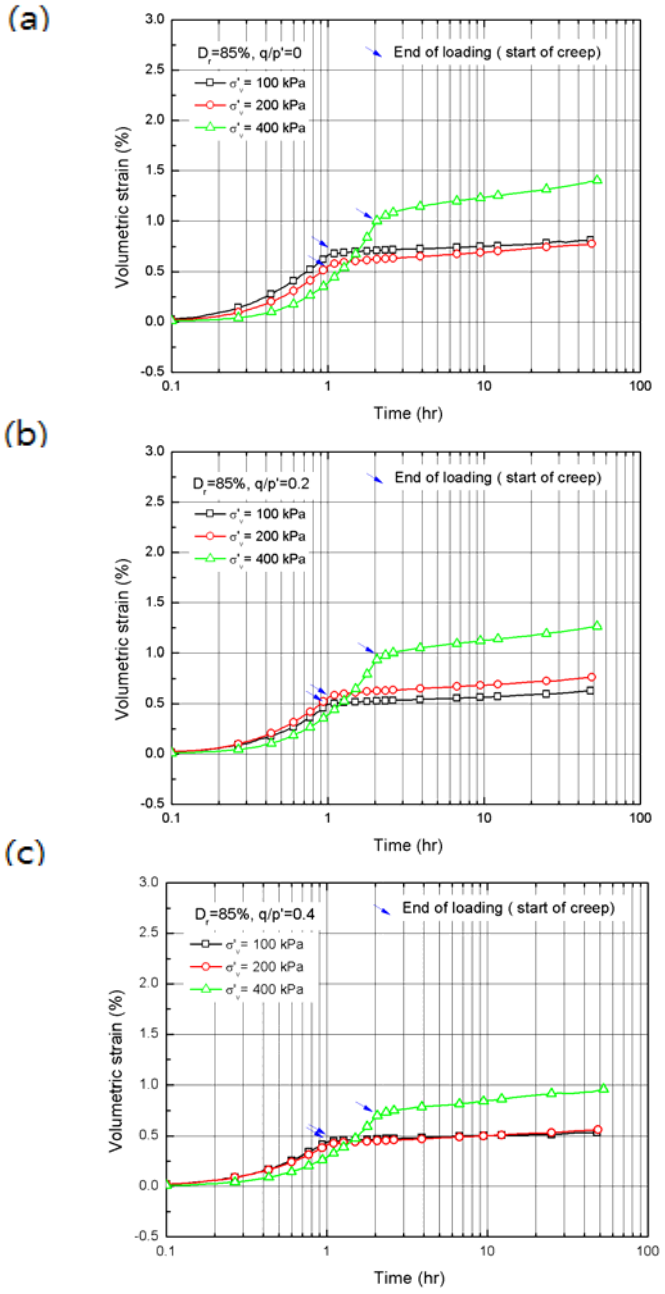

Figure 4.4 Specifying the time origin of the creep phase of (a) q/p'=0, (b) q/p'=0.2, and (c) q/p'=0.4, respectively (D_r=85%)

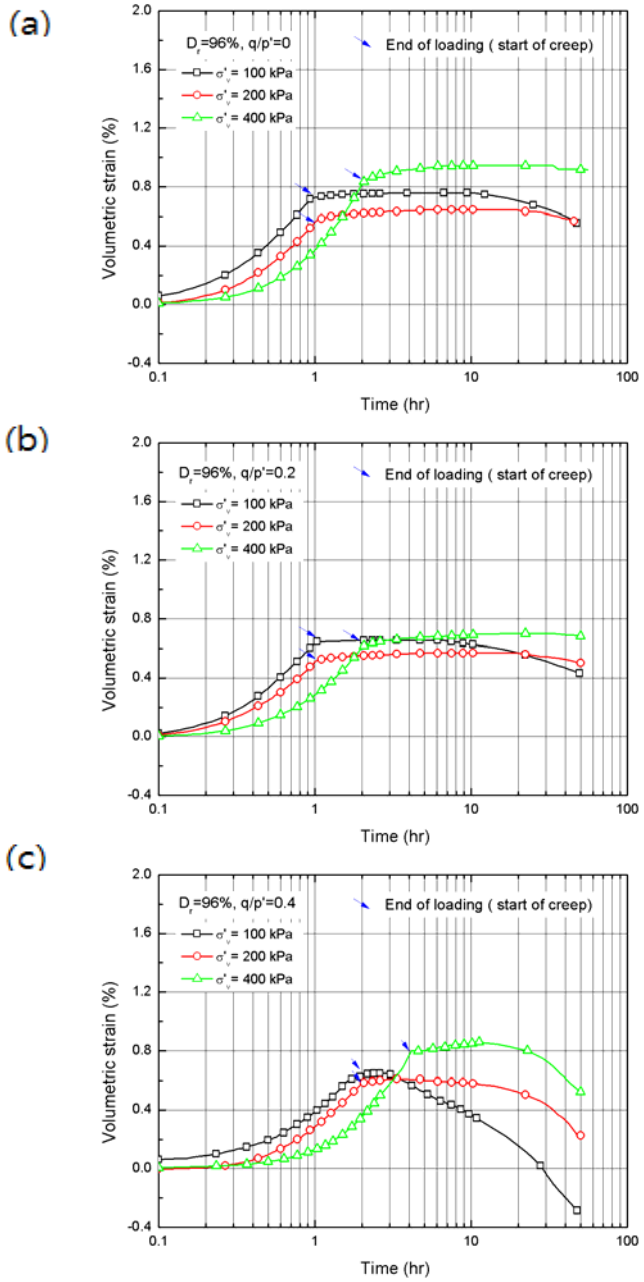

Figure 4.5 Specifying the time origin of the creep phase of (a) q/p'=0, (b) q/p'=0.2, and (c) q/p'=0.4, respectively (D_r=96%)

4.2.3 Creep response

Axial creep strain

After isotropic (q/p'=0) and anisotropic (q/p'=0.2, 0.4) consolidation, the creep deformations were evaluated for the specimens with the initial relative density of 73%, 85%, and 96%. Each drained triaxial tests were performed under the saturated condition. Minimum B-value of 0.9 was achieved by applying a back pressure of 200kPa after CO_2 flushing.

Based on Figures 4.3~4.5, the axial creep deformations were estimated. Figures 4.6~4.8 illustrate the observed axial creep strain for the specimens with the initial relative density of 73%, 85%, and 96%, respectively. The contractive axial creep strains developed for all cases.

Regardless of initial relative density, as the stress ratio increases (i.e., horizontal confining stress decreases), the axial creep strain increases for the same vertical effective stress condition as in Figures 4.6~4.8. However, occurring axial creep strains in accordance with the vertical effective stress highly depend on the initial relative density. As can be seen in Figure 4.6, for the same stress ratio condition, the more axial creep strains developed as the confining pressure increases in the specimens with low relative density.

As shown in Figure 4.7, for the specimens of medium relative density, patterns of occurring axial creep strains are more complex. Axial creep strains depend on the stress ratio. The tendency of observed creep strains of anisotropically consolidated (q/p'=0.2 and 0.4) medium dense specimens was similar with that of the specimens with low relative density. On the other hand,

axial creep strains of the isotropically consolidated medium dense specimens show the similar tendency with the results of the specimens with high relative density. High mean normal effective stresses of isotropic consolidation condition seem to result in increasing of confining resistance. In the case of very dense specimens as in Figure 4.8, in contrast to the results of low relative density, axial creep strains decrease as the vertical effective stress increases. The development of axial creep strains within 3 hours, 40 hours, and their ratios are summarized in Appendix A.3.

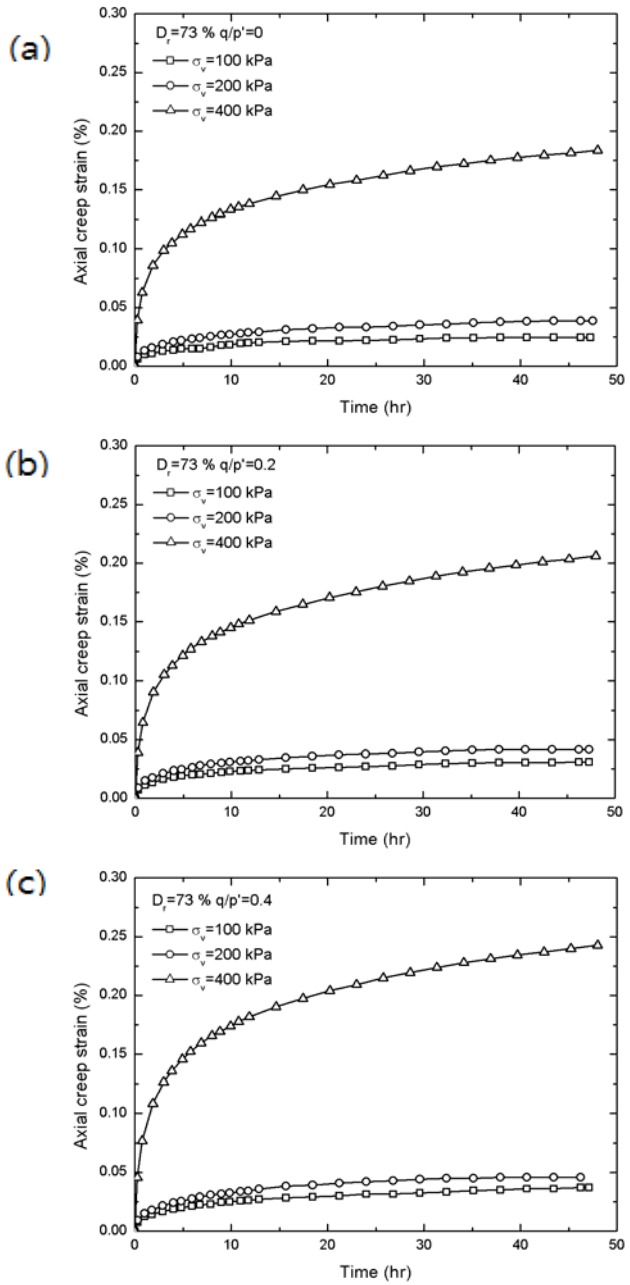

Figure 4.6 Axial creep strains for the specimens with D_r=73% of (a) q/p'=0, (b) q/p'=0.2, and (c) q/p'=0.4, respectively

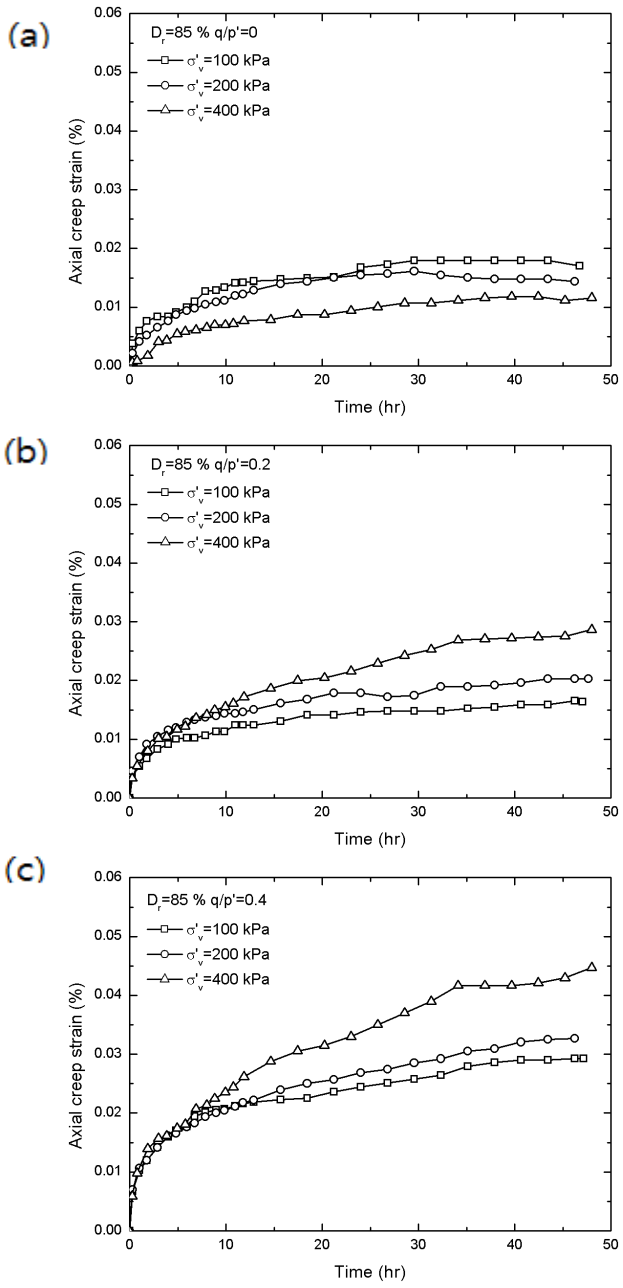

Figure 4.7 Axial creep strains for the specimens with D_r=85% of (a) q/p'=0, (b) q/p'=0.2, and (c) q/p'=0.4, respectively

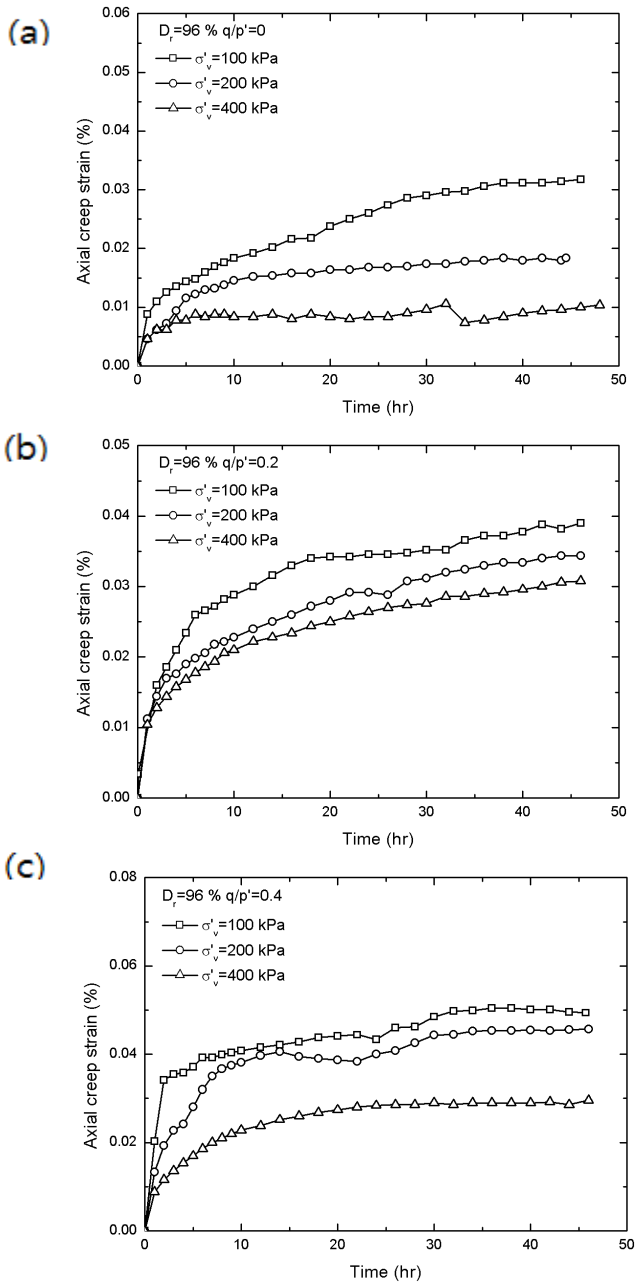

Figure 4.8 Axial creep strains for the specimens with D_r=96% of (a) q/p'=0, (b) q/p'=0.2, and (c) q/p'=0.4, respectively

Volumetric creep strain

Volumetric creep strains were evaluated based on Figures 4.3~4.5. Volumetric creep strains were plotted against time depending on the stress conditions for the different initial relative densities as in Figures 4.9~4.11. In contrast to the axial creep strains, volumetric creep strains showed both contractive and dilative behavior depending on the initial relative density.

Contractive volumetric creep strains were observed in the specimens with low and medium initial densities. As can be seen in Figures 4.9~4.10, the greater volumetric creep strains developed with increasing the vertical effective stress for the same stress ratio condition. In addition, the greater volumetric creep strains were produced as the stress ratio decreased (i.e., mean normal effective stress increases) under the same vertical effective stress ratio conditions.

In the case of the specimens with high density, however, more complex responses during creep were observed as shown in Figure 4.8. Volumetric creep strains were initially contractive, and then they became dilative after certain time. Contraction was observed in the beginning because of plasticity of soil. It is considered that the soil structure reaches the limit state to be compressed, and then the specimens show expansive behavior. The specimens applied high confining stress and low stress ratio show the delayed dilation trends. Similar results that the specimens contract in the beginning of creep, then dilate had been reported by Rimoy and Jardine (2011). Lower p' and higher q/p' condition stimulates dilative behavior of dense specimen. Contrast to results of the specimens with low and medium relative density, high

confining pressure inhibits the expansion of specimens with high density. The development volumetric creep strains within 3 hours, 40 hours, and their ratios are summarized in Appendix A.3. To compare the creep rate of weathered residual soil in Korea to that of other materials in the literatures, volumetric creep strain rate was plotted against time as in Appendix A.4.

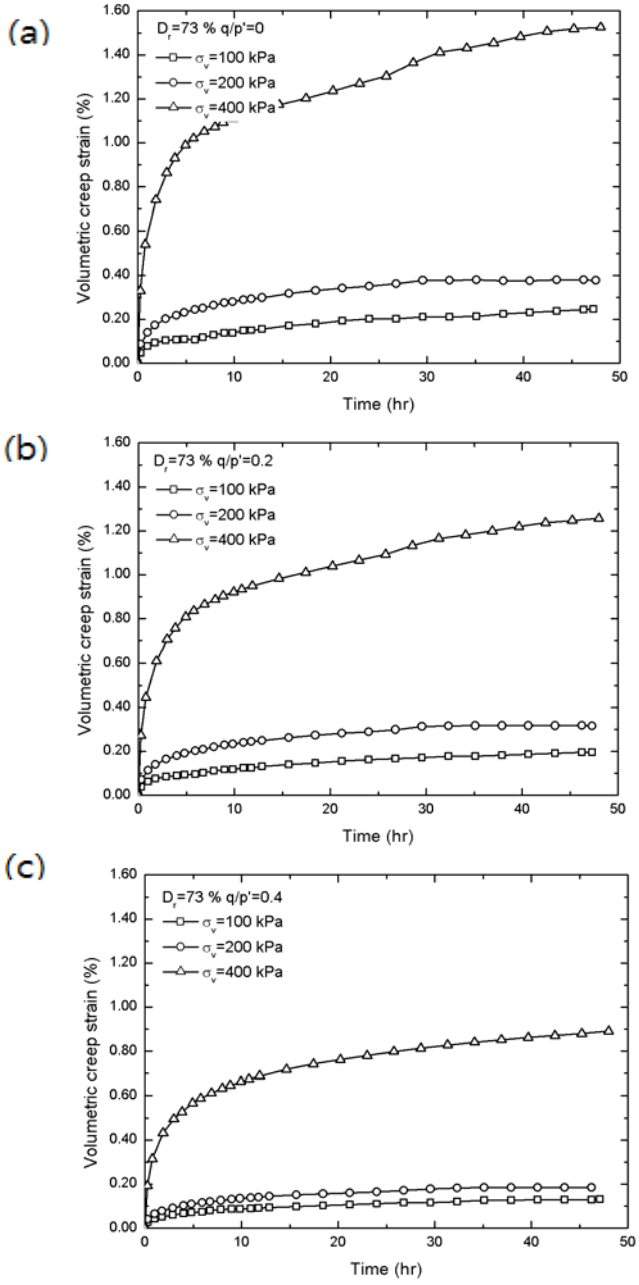

Figure 4.9 Volumetric creep strains for the specimens with D_r=73% of (a) q/p'=0, (b) q/p'=0.2, and (c) q/p'=0.4, respectively

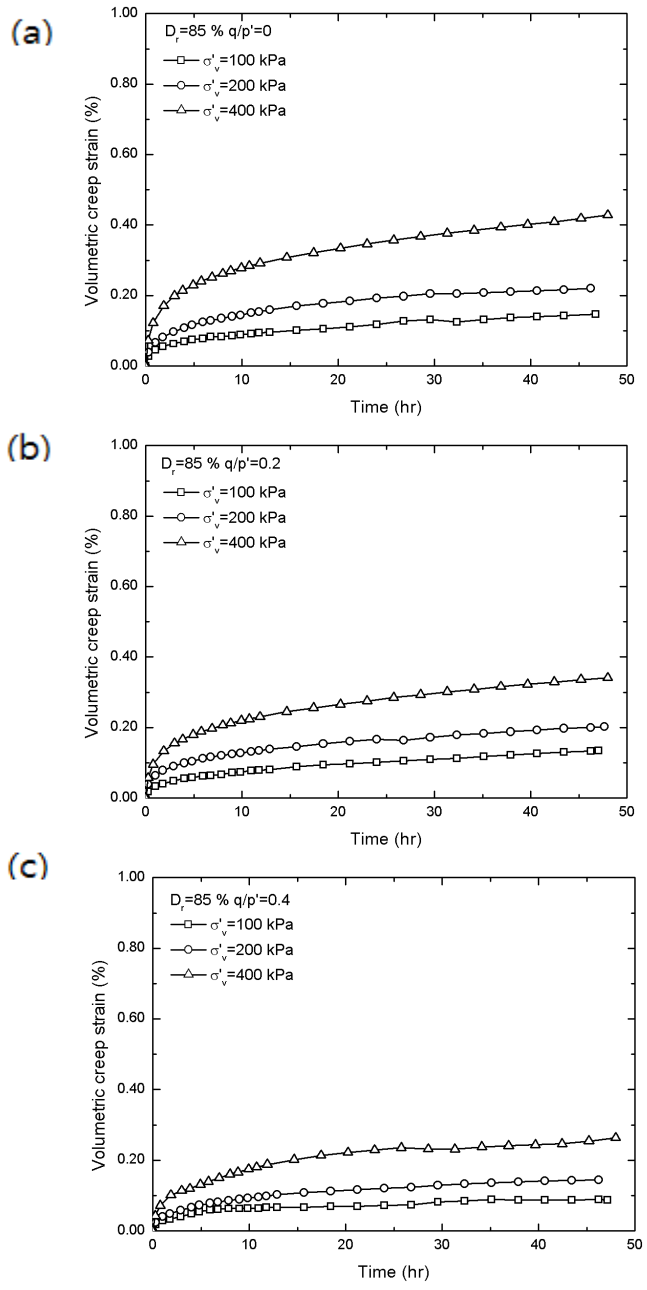

Figure 4.10 Volumetric creep strains for the specimens with D_r=85% of (a) q/p'=0, (b) q/p'=0.2, and (c) q/p'=0.4, respectively

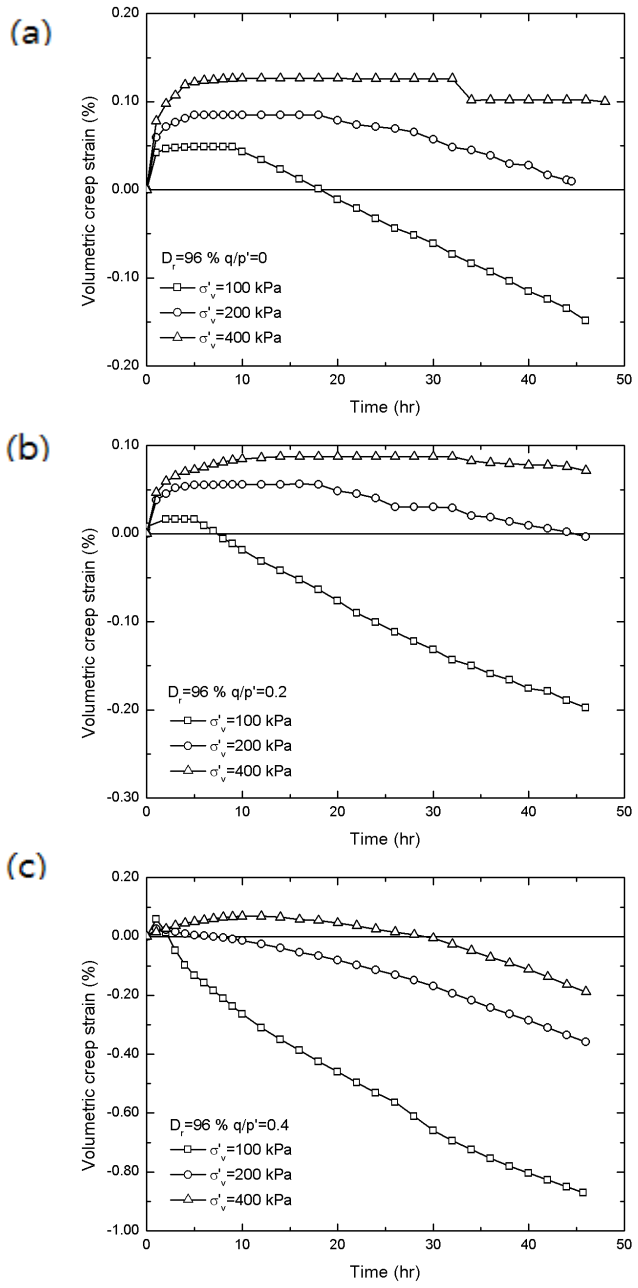

Figure 4.11 Volumetric creep strains for the specimens with D_r=96% of (a) q/p'=0, (b) q/p'=0.2, and (c) q/p'=0.4, respectively

Radial creep strain

Radial strains, ε_{rad} $(=1/2(\varepsilon_{vol}-\varepsilon_a))$, were calculated indirectly from the direct measurement of volumetric strain and the axial strain. Radial creep strains were also evaluated based on Figures 4.3~4.5.

Figures 4.12~4.14 present the occurring radial creep strain with time of the specimens with the initial relative density of 73%, 85%, and 96%, respectively.

As can be seen in Figures 4.12~4.13, the greater radial creep strains were observed with high radial confining pressure in the specimens with low and medium initial density. That is, the high stress in radial direction stimulates the rearrangement of particles in the radial direction which results in greater radial creep deformations because the initial structure of the specimens in the horizontal direction is relatively weaker than that in the vertical direction.

The specimens of high initial density (D_r=96%), however, show the complex behavior in the radial creep strain. Radial creep strains were initially contractive, and then they became dilative after certain time. When reminding Bowman and Soga (2005) and Michalowski and Nadukuru (2012) postulating that the radial stress of laterally restrained conditions increases with time in the dense sand, the observation of expansive horizontal creep strains with time can be expected under the triaxial creep test conditions rather than the increase of radial stress. It can be concluded that complex volumetric responses in very dense specimens result from the radial responses because of the initial structures of the specimens, possibly due to the effect of the compaction for preparing relatively dense samples used in this study.

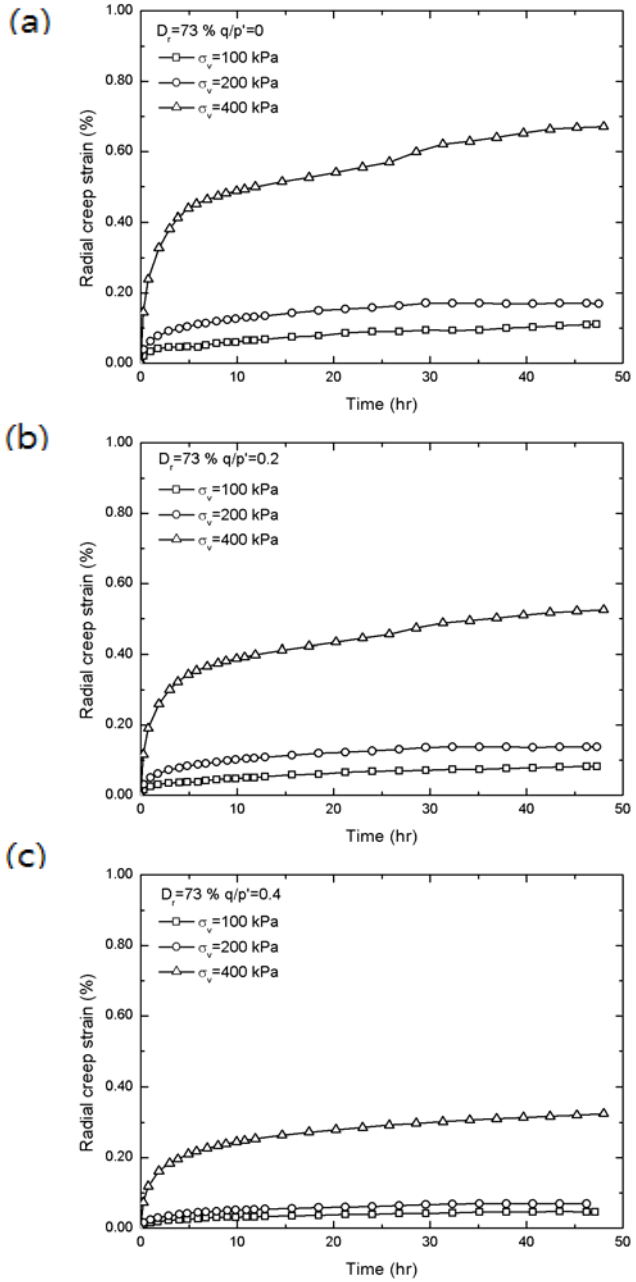

Figure 4.12 Radial creep strains for the specimens with D_r=73% of (a) q/p'=0, (b) q/p'=0.2, and (c) q/p'=0.4, respectively

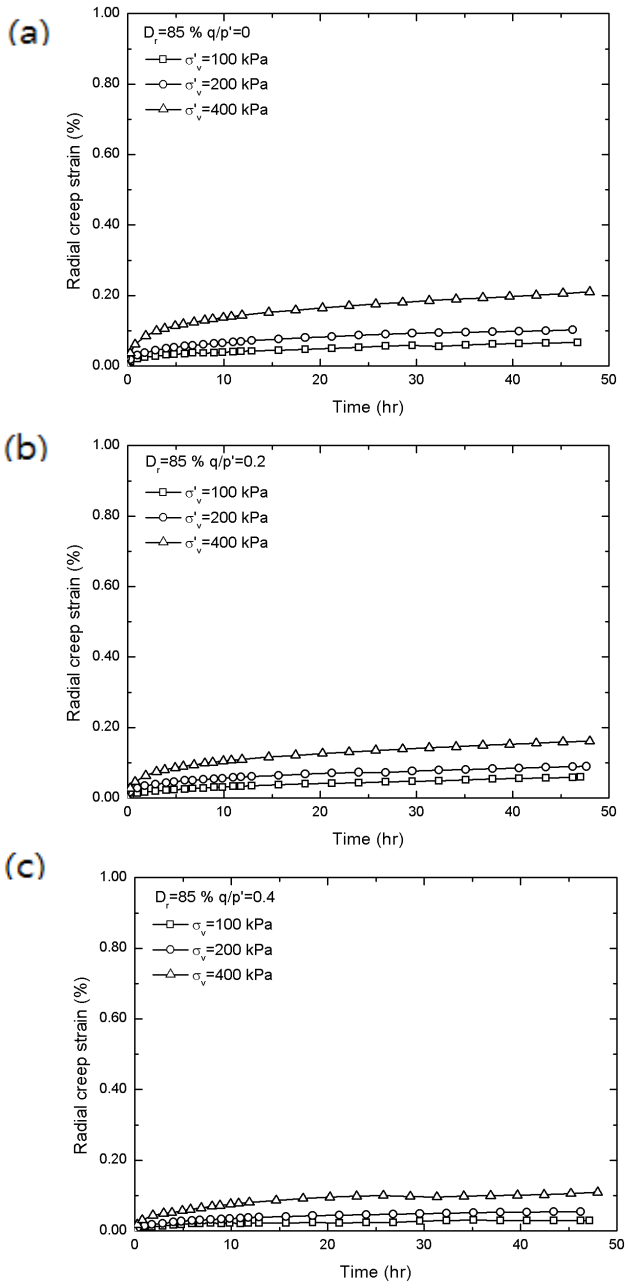

Figure 4.13 Radial creep strains for the specimens with D_r=85% of (a) q/p'=0, (b) q/p'=0.2, and (c) q/p'=0.4, respectively

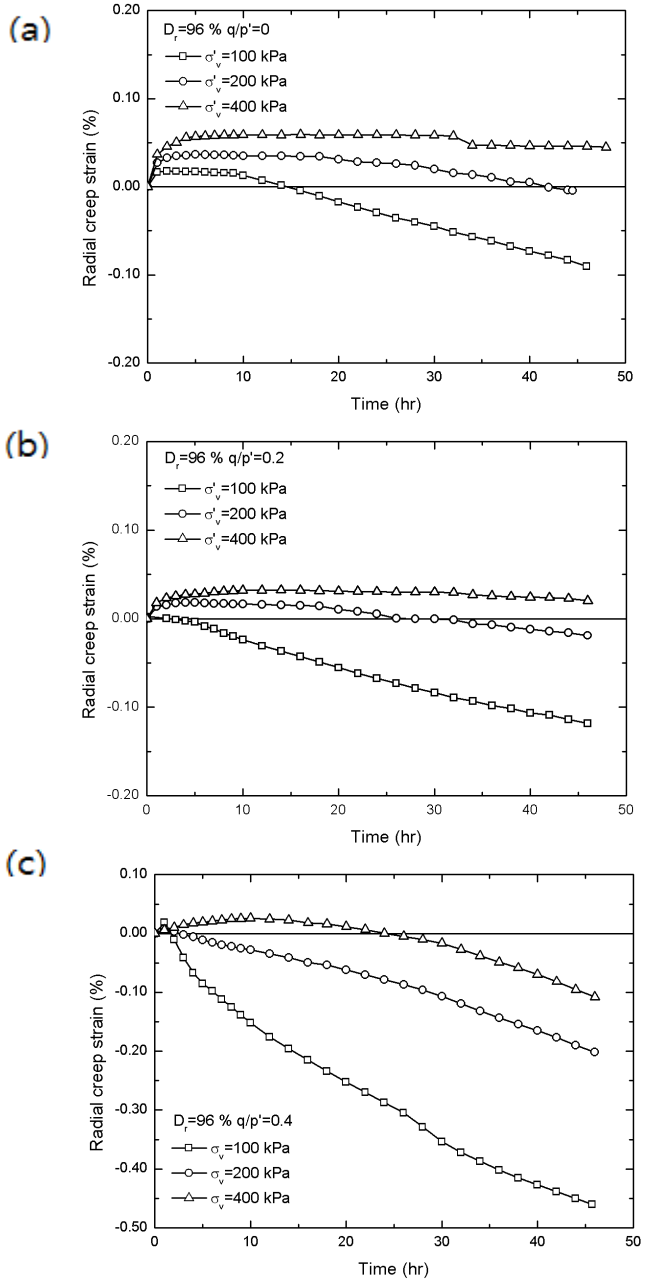

Figure 4.14 Radial creep strains for the specimens with D_r=96% of (a) q/p'=0, (b) q/p'=0.2, and (c) q/p'=0.4, respectively

Shear creep strain

Shear strains, ε_{sh} $(=2/3(\varepsilon_a-\varepsilon_r))$, are also calculated indirectly from axial strains and volumetric ones. Shear creep strains are also evaluated based on Figures 4.3~4.5.

Figures 4.15~4.17 demonstrate the developing shear creep strains with time of the specimens with the initial relative density of 73%, 85%, and 96%, respectively. As seen in Figures 4.15~4.16, the specimens with low and medium relative density show the negative shear strains under constant loading. As the stress ratio increases, the tendency of occurring shear creep strains moves toward an x-axis. In the isotropic consolidation condition, the negative shear creep strains were also described by the initial structures of samples due to heavy compaction, inducing the stiffer structures in the vertical direction than in the horizontal direction and resulting in larger creep strains in the horizontal direction than in the vertical direction. For this reason, it is considered that the amount of negative shear strains reduces as the radial stress decreases for the same vertical effective stress condition.

The specimens with very high relative density, however, show the complex shear creep behavior as the volumetric or radial response. At the beginning, larger contractive radial creep strains than axial creep strains led to initial negative shear strains. After certain time, shear creep strains began to increase as the dilative horizontal creep strains developed. The detailed development of strains (axial, radial, volumetric, and shear strains) during creep plotted against time are shown in Appendix A.3.

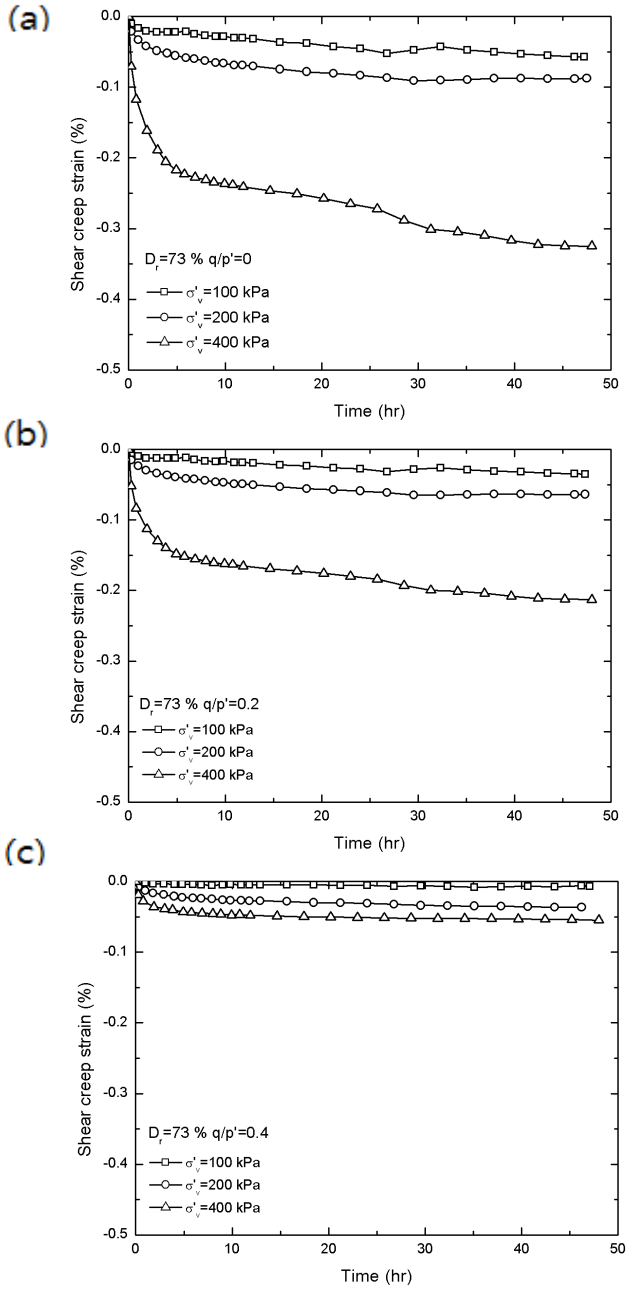

Figure 4.15 Shear creep strains for the specimens with D_r=73% of (a) q/p'=0, (b) q/p'=0.2, and (c) q/p'=0.4, respectively

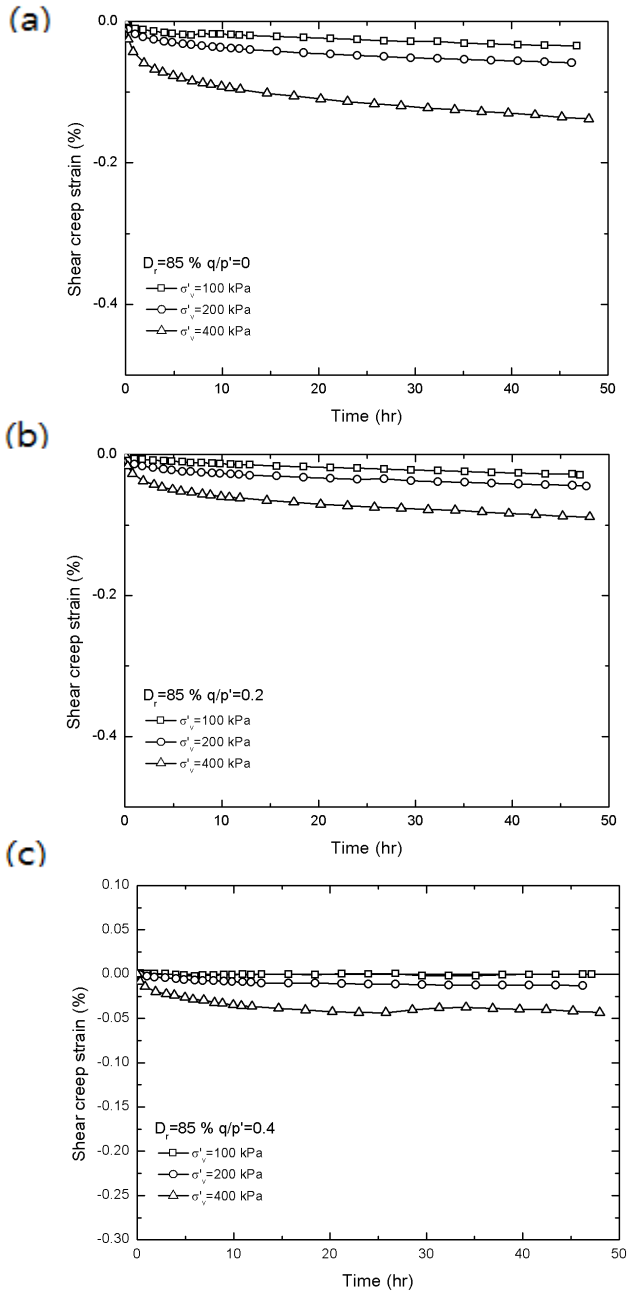

Figure 4.16 Shear creep strains for the specimens with D_r=85% of (a) q/p'=0, (b) q/p'=0.2, and (c) q/p'=0.4, respectively

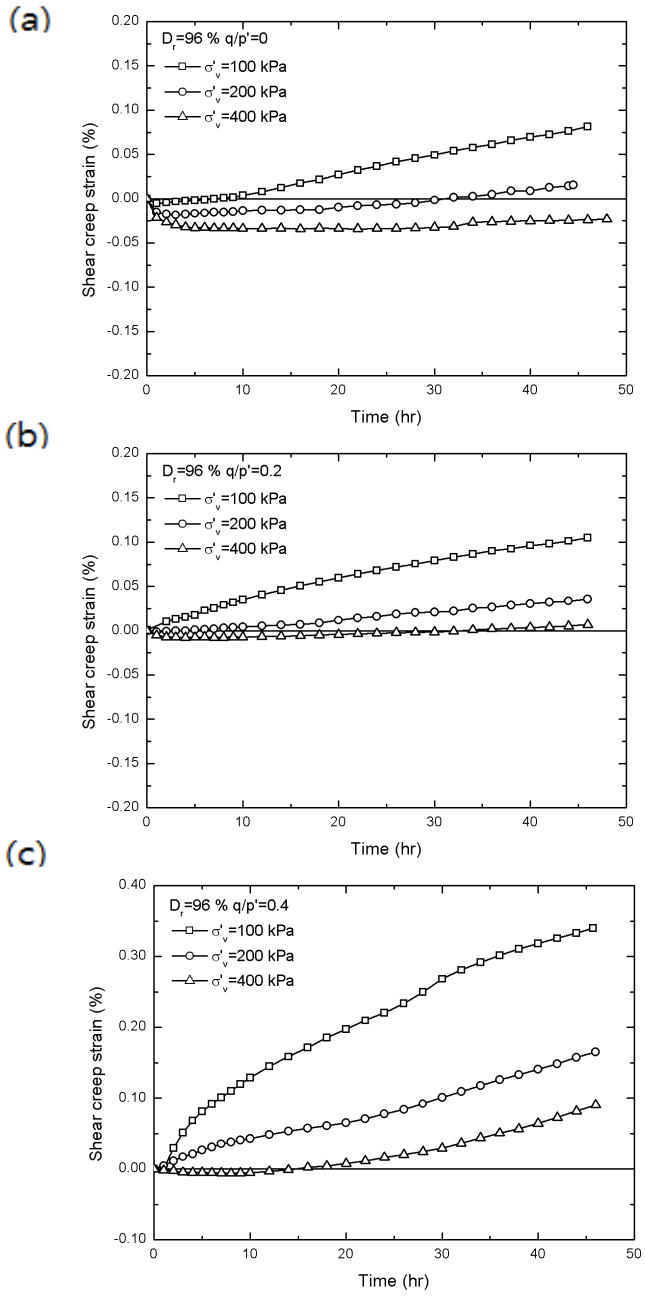

Figure 4.17 Shear creep strains for the specimens with D_r=96% of (a) q/p'=0, (b) q/p'=0.2, and (c) q/p'=0.4, respectively

4.2.4 Relative creep effect ($\varepsilon_{cr} / \varepsilon_{con}$)

Relative creep effect in axial strains

The axial strain developing during each consolidation stage and subsequent 40 hours of creep stage for the specimens of 73% initial relative density are shown in Figure 4.18. Table 4.1 summarizes the results. The validity of 40 hours of creep criteria is in Appendix A.5. For the specimens with the initial relative density of 73%, the axial creep strain increases as the vertical effective stress increases. The axial creep strain dramatically increases at 400kPa of vertical effective stress. The amount of consolidation drops slightly when the vertical effective stress increases from 100kPa to 200kPa and increases dramatically when the vertical effective stress increases from 200kPa to 400kPa.

Table 4.1 Axial strain during consolidation and subsequent 40 hours of creep for the specimens of 73% initial relative density

D_r= 73%	q/p'=0		q/p'=0.2		q/p'=0.4	
$\Delta\sigma'_v$	$\varepsilon_{con(a)}$ (%)	$\varepsilon_{cr(a)}$ (%)	$\varepsilon_{con(a)}$ (%)	$\varepsilon_{cr(a)}$ (%)	$\varepsilon_{con(a)}$ (%)	$\varepsilon_{cr(a)}$ (%)
30-100	0.161	0.025	0.188	0.031	0.215	0.036
100-200	0.143	0.038	0.151	0.042	0.159	0.046
200-400	0.377	0.177	0.395	0.198	0.412	0.234

(a)

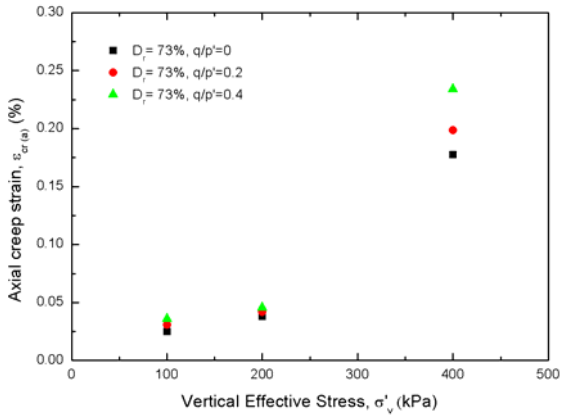

(b)

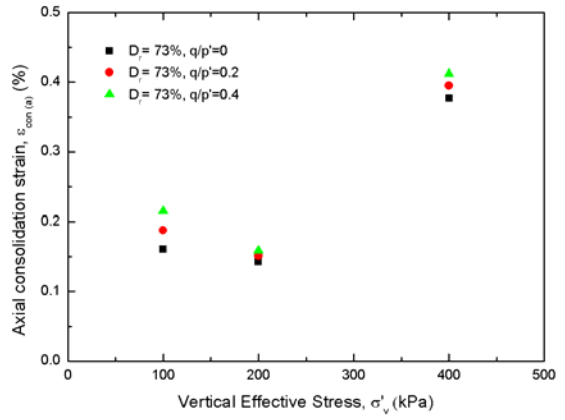

Figure 4.18 Developing (a) axial creep strain and (b) consolidation strain for the specimens of 73% initial relative density, respectively

Following Kuwano and Jardine (2002), the ratios of axial creep strains and consolidation strains, $\varepsilon_{cr(a)} / \varepsilon_{con(a)}$, representing relative creep effect for the specimens of initial relative density of 73% are plotted against vertical effective stress in Figure 4.19 and listed in Table 4.2. As can be seen in Figure

4.19, axial relative creep effect, $\varepsilon_{cr(a)} / \varepsilon_{con(a)}$, shows a clear increasing trend with the vertical effective stress for the specimens with 73% initial relative density. The axial relative creep effect is greater in the anisotropic consolidation (q/p'=0.2 and 0.4) conditions than that in the isotropic consolidation condition.

Table 4.2 Ratios of axial creep strains and consolidation strains for the specimens of 73% initial relative density

D_r= 73%	q/p'=0	q/p'=0.2	q/p'=0.4
$\Delta\sigma'_v$	$\varepsilon_{cr(a)} / \varepsilon_{con(a)}$	$\varepsilon_{cr(a)} / \varepsilon_{con(a)}$	$\varepsilon_{cr(a)} / \varepsilon_{con(a)}$
30-100	0.153	0.163	0.168
100-200	0.267	0.275	0.288
200-400	0.470	0.503	0.569

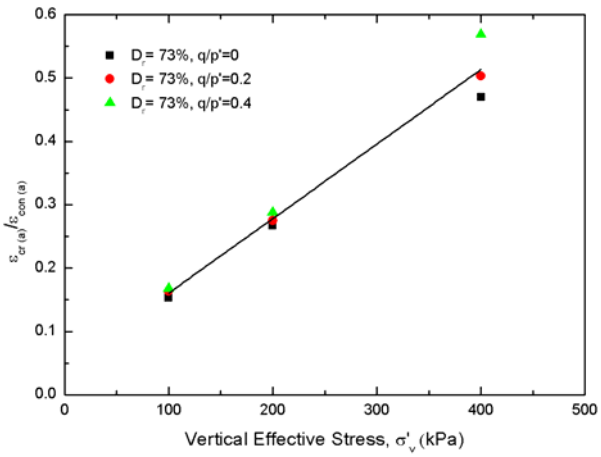

Figure 4.19 Ratios of axial creep strains and consolidation strains for the specimens of 73% initial relative density

The axial strain developing during each consolidation stage and subsequent 40 hours of creep stage for the specimens of 85% initial relative density are shown in Figure 4.20 and Table 4.3 summarizes the results. The specimens with initial relative density of 85% show different axial creep responses according to the stress ratio. In the case of isotropic consolidation, the axial creep strains of 85% initial relative density specimens decrease as the vertical effective stress increases as the results of the specimens with 96% initial relative density, whereas in the case of anisotropic consolidation, the axial creep strains of 85% initial relative density specimens increases with the vertical effective stress as the results of the specimens with 73% initial relative density. As shown in Figure 4.20 (b), the tendency of developing consolidation decreases as the vertical effective stress increases.

Table 4.3 Axial strain during consolidation and subsequent 40 hours of creep for the specimens of 85% initial relative density

D_r= 85%	q/p'=0		q/p'=0.2		q/p'=0.4	
$\Delta\sigma'_v$	$\varepsilon_{con(a)}$ (%)	$\varepsilon_{cr(a)}$ (%)	$\varepsilon_{con(a)}$ (%)	$\varepsilon_{cr(a)}$ (%)	$\varepsilon_{con(a)}$ (%)	$\varepsilon_{cr(a)}$ (%)
30-100	0.104	0.018	0.151	0.016	0.193	0.029
100-200	0.077	0.015	0.102	0.022	0.142	0.032
200-400	0.050	0.012	0.122	0.027	0.158	0.042

(a)

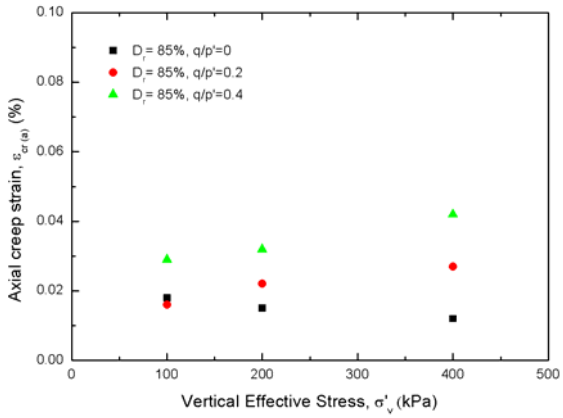

(b)

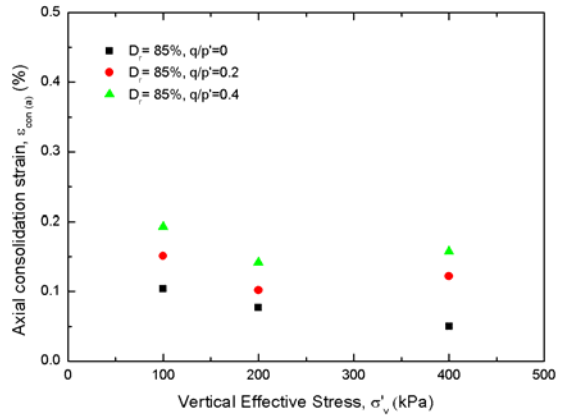

Figure 4.20 Developing (a) axial creep strain and (b) consolidation strain for the specimens of 85% initial relative density, respectively

The ratios of axial creep strains and consolidation strains, $\varepsilon_{cr(a)} / \varepsilon_{con(a)}$, representing relative creep effect for the specimens of initial relative density of 85% are shown in Figure 4.21 and listed in Table 4.4. While the relative creep effect of the specimens with medium density, $\varepsilon_{cr(a)} / \varepsilon_{con(a)}$, grows with the vertical effective stress like that of the specimens with low

density(D_r=73%), a rate of increase in relative creep effect in the medium dens sand (D_r=85%) is smaller than that in the loose sand (D_r=73%). It was also found that there's no clear correlation of the relative creep effect and the stress ratio in the medium dense specimens.

Table 4.4 Ratios of axial creep strains and consolidation strains for the specimens of 85% initial relative density

D_r= 85%	q/p'=0	q/p'=0.2	q/p'=0.4
$\Delta\sigma'_v$	$\varepsilon_{cr(a)} / \varepsilon_{con(a)}$	$\varepsilon_{cr(a)} / \varepsilon_{con(a)}$	$\varepsilon_{cr(a)} / \varepsilon_{con(a)}$
30-100	0.173	0.106	0.151
100-200	0.193	0.221	0.226
200-400	0.235	0.222	0.264

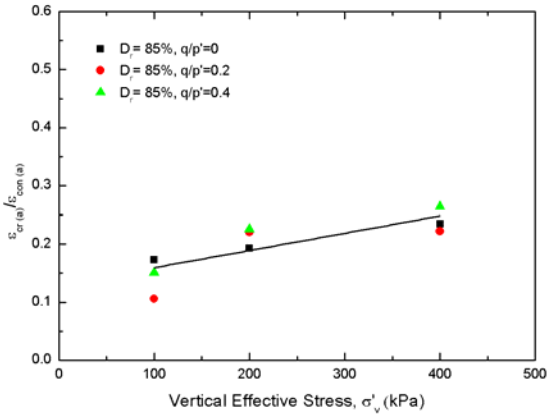

Figure 4.21 Ratios of axial creep strains and consolidation strains for the specimens of 85% initial relative density

The axial strains observed during each consolidation stage and subsequent 40 hours of creep stage for the specimens of 96% initial relative density are shown in Figure 4.22 and Table 4.5 lists the results. The axial creep strains of the specimens with initial relative density of 96% decrease as the vertical effective stress increases, possibly due to high effective stress inhibiting the particle rearrangement, one of the major mechanisms of creep, in the heavily packed structures. The axial consolidation also decreases as the vertical effective increases.

Table 4.5 Axial strain during consolidation and subsequent 40 hours of creep for the specimens of 96% initial relative density

D_r= 96%	q/p'=0		q/p'=0.2		q/p'=0.4	
$\Delta\sigma'_v$	$\varepsilon_{con(a)}$ (%)	$\varepsilon_{cr(a)}$ (%)	$\varepsilon_{con(a)}$ (%)	$\varepsilon_{cr(a)}$ (%)	$\varepsilon_{con(a)}$ (%)	$\varepsilon_{cr(a)}$ (%)
30-100	0.183	0.034	0.218	0.038	0.219	0.052
100-200	0.108	0.020	0.135	0.034	0.197	0.049
200-400	0.105	0.010	0.153	0.029	0.197	0.031

(a)

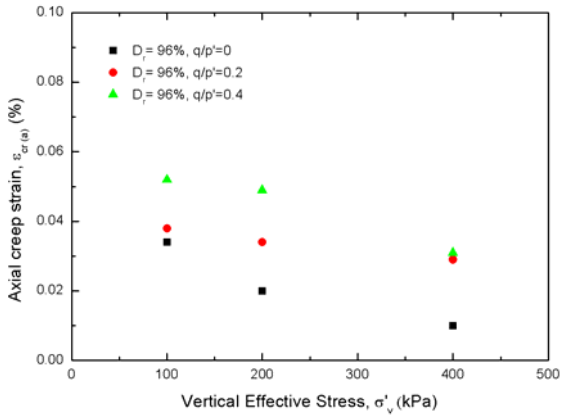

(b)

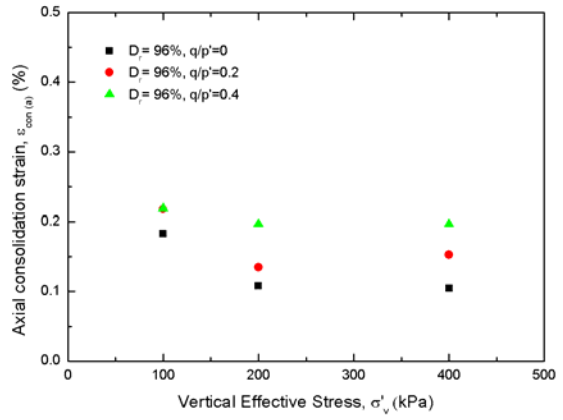

Figure 4.22 Developing (a) axial creep strain and (b) consolidation strain for the specimens of 96% initial relative density, respectively

The ratios of axial creep strains and consolidation strains, $\varepsilon_{cr(a)} / \varepsilon_{con(a)}$, representing relative creep effect for the specimens of initial relative density of 96% are shown in Figure 4.23 and listed in Table 4.6. As seen in Figure 4.23, the relative creep effect of the specimens with high relative density, contrast to the results of the specimens with low and medium relative density,

generally decreases as the vertical effective stress increases and especially is low at 400 kPa of vertical effective stress.

Contrary to the general notion that the consolidation and creep strain increases as the initial relative density decreases, the specimens with high relative density shows larger strains than the medium dense specimens. It is considered that the samples of 96% initial relative density prepared with relatively dense state having smaller particles due to heavy compaction result in larger strains.

From the test results, it is interesting to note that the developing strains during consolidation and creep highly depend on the initial relative density and stress condition.

Table 4.6 Ratios of axial creep strains and consolidation strains for the specimens of 96% initial relative density

D_r= 96%	q/p'=0	q/p'=0.2	q/p'=0.4
$\Delta\sigma'_v$	$\varepsilon_{cr(a)} / \varepsilon_{con(a)}$	$\varepsilon_{cr(a)} / \varepsilon_{con(a)}$	$\varepsilon_{cr(a)} / \varepsilon_{con(a)}$
30-100	0.185	0.175	0.239
100-200	0.183	0.254	0.250
200-400	0.094	0.192	0.160

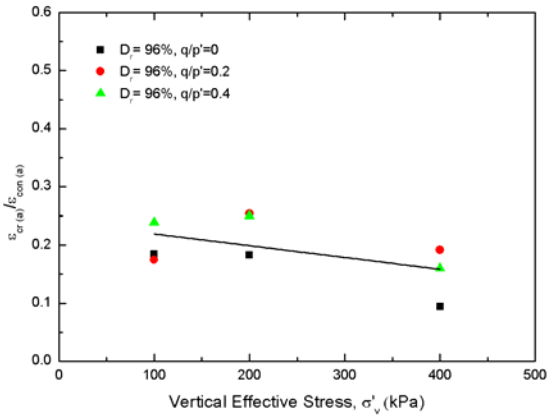

Figure 4.23 Ratios of axial creep strains and consolidation strains for the specimens of 96% initial relative density

Relative creep effect in volumetric strains

The volumetric strains developing during each consolidation stage and subsequent 40 hours of creep stage for the specimens of 73% initial relative density are shown in Figure 4.24 and Table 4.7 lists the results. The more volumetric creep strains with the specimens of initial relative density of 73% develop as the vertical effective stress increases. The tendency is similar to the results of axial creep strains. The volumetric creep strain dramatically increases at 400kPa of vertical effective stress. The amount of volumetric consolidation drops slightly when the vertical effective stress increases from 100kPa to 200kPa and increases sharply when the vertical effective stress increases from 200kPa to 400kPa.

Table 4.7 Volumetric strain during consolidation and subsequent 40 hours of creep for the specimens of 73% initial relative density

D_r= 73%	q/p'=0		q/p'=0.2		q/p'=0.4	
$\Delta\sigma'_v$	$\varepsilon_{con(v)}$ (%)	$\varepsilon_{cr(v)}$ (%)	$\varepsilon_{con(v)}$ (%)	$\varepsilon_{cr(v)}$ (%)	$\varepsilon_{con(v)}$ (%)	$\varepsilon_{cr(v)}$ (%)
30-100	1.007	0.231	0.817	0.187	0.626	0.128
100-200	0.919	0.376	0.759	0.316	0.600	0.183
200-400	3.134	1.482	2.541	1.219	1.948	0.862

(a)

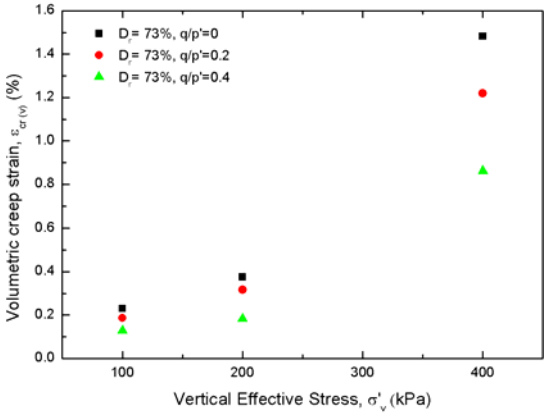

(b)

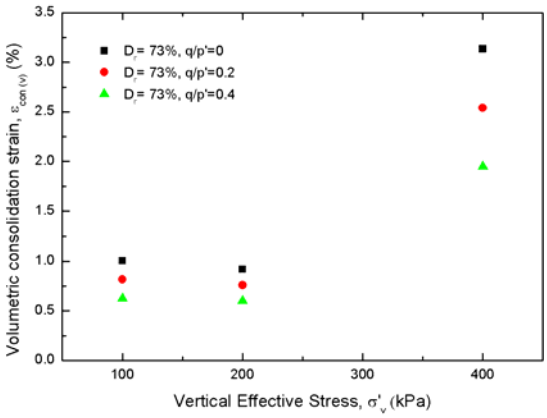

Figure 4.24 Developing (a) volumetric creep strain and (b) consolidation strain for the specimens of 73% initial relative density, respectively

As provided in the study of Kuwano and Jardine (2002), the ratios of volumetric creep strains and consolidation strains, $\varepsilon_{cr(v)} / \varepsilon_{con(v)}$, representing relative creep effect for the specimens of initial relative density of 73% are shown in Figure 4.25 and summarized in Table 4.8. The results showed that volumetric creep strains built up to 20~48% of the consolidation strains

within 40 hours of each loading stage for the specimens of initial relative density of 73%. The relative creep effect in volumetric strains, $\varepsilon_{cr(v)} / \varepsilon_{con(v)}$, increases as the vertical effective stress increases. The results indicated that the specimens with the stress ratio of 0.4 show the smallest relative creep effect.

Table 4.8 Ratios of volumetric creep strains and consolidation strains for the specimens of 73% initial relative density

D_r= 73%	q/p'=0	q/p'=0.2	q/p'=0.4
$\Delta\sigma'_v$	$\varepsilon_{cr(v)} / \varepsilon_{con(v)}$	$\varepsilon_{cr(v)} / \varepsilon_{con(v)}$	$\varepsilon_{cr(v)} / \varepsilon_{con(v)}$
30-100	0.230	0.229	0.205
100-200	0.409	0.416	0.306
200-400	0.473	0.480	0.442

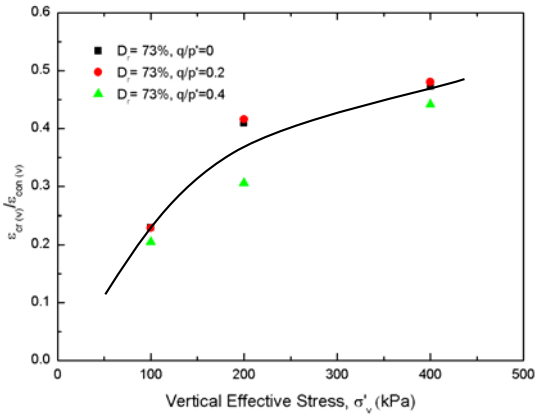

Figure 4.25 Ratios of volumetric creep strains and consolidation strains for the specimens of 73% initial relative density

The volumetric strains observed during each consolidation stage and subsequent 40 hours of creep stage for the specimens of 85% initial relative density are shown in Figure 4.26 and Table 4.9. The specimens with 85% initial relative density show marked increase in volumetric creep strains as the stress ratio decreases. It is considered that volumetric creep strains increases with the vertical effective stress prior to creep, due to the large stress to the specimens promoting the particle rearrangement or slippage under constant loading in the low and medium dense specimens. The amount of volumetric consolidation also increases as the vertical effective stress increases.

Table 4.9 Volumetric strain during consolidation and subsequent 40 hours of creep for the specimens of 85% initial relative density

D_r= 85%	q/p'=0		q/p'=0.2		q/p'=0.4	
$\Delta\sigma'_v$	$\varepsilon_{con(v)}$ (%)	$\varepsilon_{cr(v)}$ (%)	$\varepsilon_{con(v)}$ (%)	$\varepsilon_{cr(v)}$ (%)	$\varepsilon_{con(v)}$ (%)	$\varepsilon_{cr(v)}$ (%)
30-100	0.665	0.141	0.495	0.126	0.440	0.088
100-200	0.558	0.213	0.561	0.193	0.410	0.141
200-400	0.979	0.401	0.917	0.322	0.686	0.244

(a)

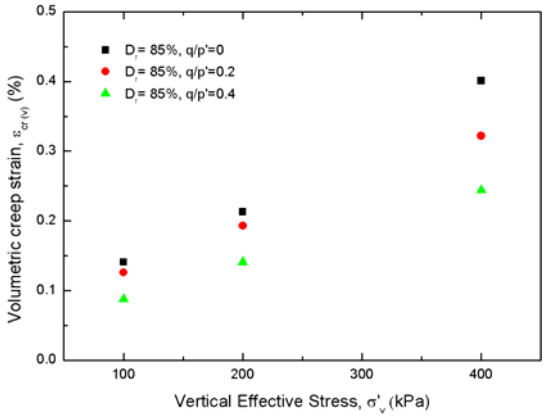

(b)

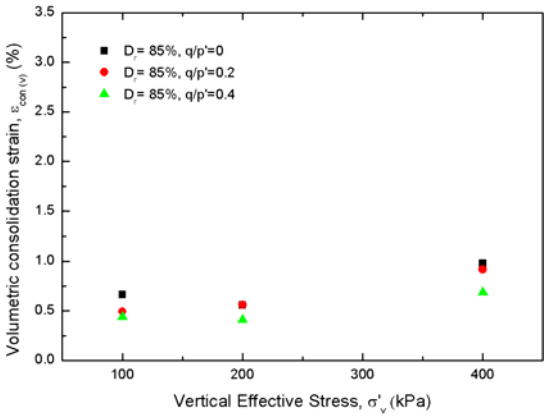

Figure 4.26 Developing (a) volumetric creep strain and (b) consolidation strain against vertical effective stress for the specimens of D_r= 85% , respectively

Table 4.10 and Figure 4.27 summarize the relative creep effect in volumetric strains, expressed as ratios of volumetric strains and consolidation strains, $\varepsilon_{cr(v)} / \varepsilon_{con(v)}$, for the specimens of 85% initial relative density. The results showed that volumetric creep strains built up to 20~41% of the

consolidation strains within 40 hours of each loading stage for the specimens of initial relative density of 85%. For the specimens with medium density, the relative creep effect in volumetric strains, $\varepsilon_{cr(v)} / \varepsilon_{con(v)}$, increases with the vertical effective stress, but the increase rate is slight.

Table 4.10 Ratios of volumetric creep strains and consolidation strains for the specimens of 85% initial relative density

D_r= 85%	q/p'=0	q/p'=0.2	q/p'=0.4
$\Delta\sigma'_v$	$\varepsilon_{cr(v)} / \varepsilon_{con(v)}$	$\varepsilon_{cr(v)} / \varepsilon_{con(v)}$	$\varepsilon_{cr(v)} / \varepsilon_{con(v)}$
30-100	0.211	0.254	0.201
100-200	0.382	0.343	0.344
200-400	0.410	0.352	0.356

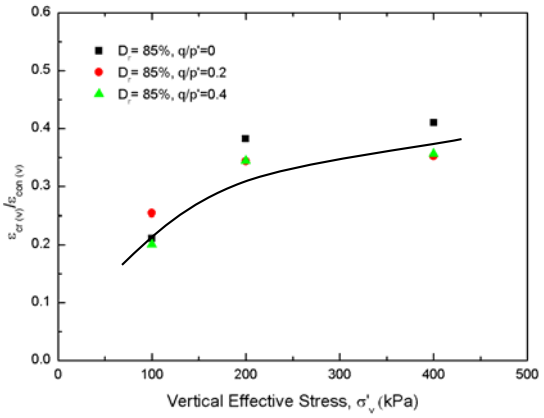

Figure 4.27 Ratios of volumetric creep strains and consolidation strains for the specimens of 85% initial relative density

Table 4.11 and Figure 4.28 indicate volumetric strains during consolidation and subsequent 40 hours of creep for the specimens of 96% initial relative density. Volumetric creep strains for the specimens with high relative density show dilative behavior at low mean normal effective stress level, but show contractive behavior at high mean normal effective stress level. As the stress ratio increases, dilative volumetric creep increases. The reason is that the conditions of low stress level and high stress ratio accelerate the unstable particle movement. The volumetric consolidations of the specimens with high density also generally increase as the vertical effective stress increases.

Table 4.11 Volumetric strain during consolidation and subsequent 40 hours of creep for the specimens of 96% initial relative density

D_r= 96%	q/p'=0		q/p'=0.2		q/p'=0.4	
$\Delta\sigma'_v$	$\varepsilon_{con(v)}$ (%)	$\varepsilon_{cr(v)}$ (%)	$\varepsilon_{con(v)}$ (%)	$\varepsilon_{cr(v)}$ (%)	$\varepsilon_{con(v)}$ (%)	$\varepsilon_{cr(v)}$ (%)
30-100	0.729	-0.155	0.637	-0.205	0.635	-0.919
100-200	0.563	0.005	0.511	-0.001	0.584	-0.350
200-400	0.819	0.101	0.607	0.075	0.799	-0.110

(a)

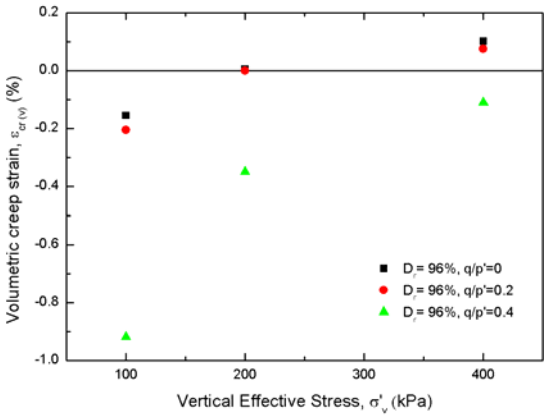

(b)

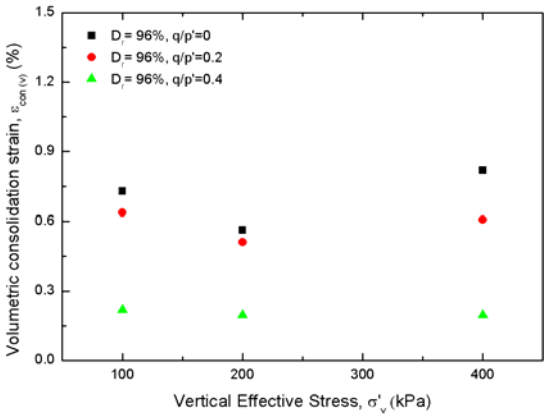

Figure 4.28 Developing (a) volumetric creep strain and (b) consolidation strain for the specimens of 96% initial relative density, respectively

Table 4.12 and Figure 4.20 show the relative creep effect in volumetric strains, expressed as ratios of volumetric strains and consolidation strains, $\varepsilon_{cr(v)} / \varepsilon_{con(v)}$, for the specimens of 96% initial relative density. The results showed that volumetric creep strains built up to -145~12% of the consolidation strains within 40 hours of each loading stage for the specimens

of initial relative density of 96%. The relative creep effect in volumetric strains for the specimens with initial relative density of 96% is greatest at 100 kPa vertical effective stress and 0.4 stress ratio condition due to significant dilative creep strains at low vertical effective stress and high stress ratio.

Table 4.12 Ratios of volumetric creep strains and consolidation strains for the specimens of 96% initial relative density

D_r= 96%	q/p'=0	q/p'=0.2	q/p'=0.4
$\Delta\sigma'_v$	$\varepsilon_{cr(v)} / \varepsilon_{con(v)}$	$\varepsilon_{cr(v)} / \varepsilon_{con(v)}$	$\varepsilon_{cr(v)} / \varepsilon_{con(v)}$
30-100	-0.213	-0.321	-1.449
100-200	0.008	-0.002	-0.600
200-400	0.123	0.124	-0.138

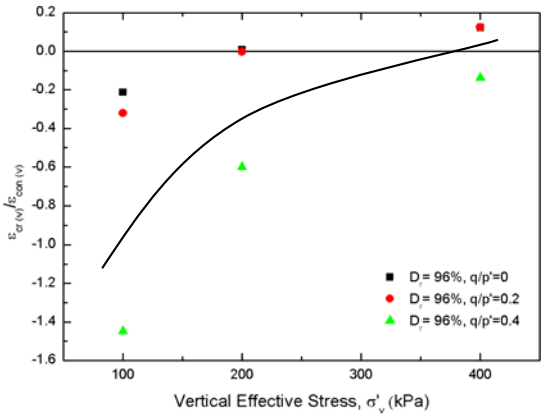

Figure 4.29 Ratios of volumetric creep strains and consolidation strains for the specimens of 96% initial relative density

Relative creep effect in radial strains

The radial strains developing during each consolidation stage and the following 40 hours of creep stage for the specimens of 73% initial relative density are shown in Figure 4.30 and Table 4.13. The more radial creep strains with the specimens of initial relative density of 73% develop as the vertical effective stress increases. The radial creep strain dramatically increases at 400kPa of vertical effective stress. As shown in Figure 4.30, the amount of radial consolidation drops slightly when the vertical effective stress increases from 100kPa to 200kPa and increases sharply when the vertical effective stress increases from 200kPa to 400kPa.

Table 4.13 Radial strain during consolidation and subsequent 40 hours of creep for the specimens of 73% initial relative density

D_r= 73%	q/p'=0		q/p'=0.2		q/p'=0.4	
$\Delta\sigma'_v$	$\varepsilon_{con(r)}$ (%)	$\varepsilon_{cr(r)}$ (%)	$\varepsilon_{con(r)}$ (%)	$\varepsilon_{cr(r)}$ (%)	$\varepsilon_{con(r)}$ (%)	$\varepsilon_{cr(r)}$ (%)
30-100	0.423	0.054	0.314	0.050	0.206	0.046
100-200	0.388	0.085	0.304	0.079	0.220	0.069
200-400	1.378	0.434	1.073	0.369	0.768	0.314

(a)

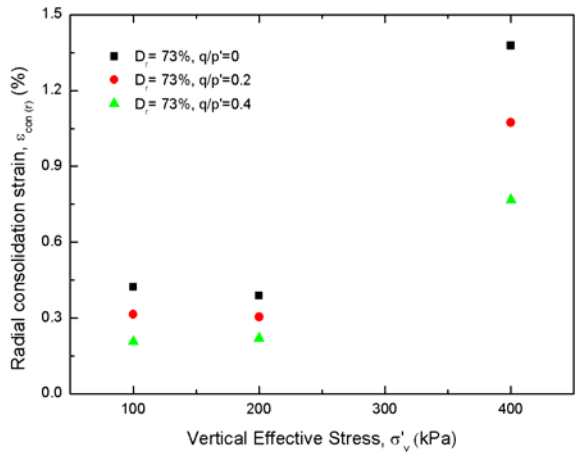

(b)

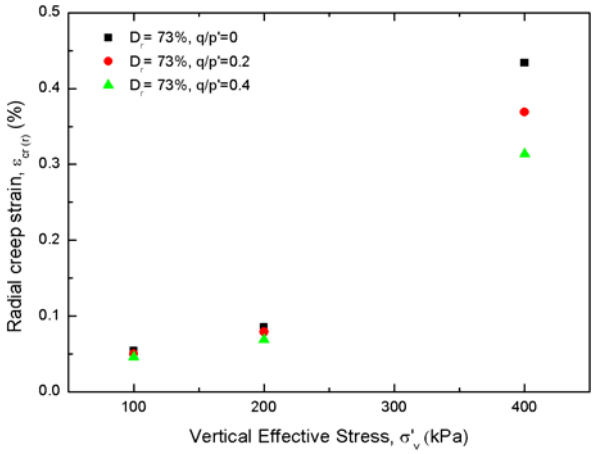

Figure 4.30 Developing (a) radial creep strain and (b) consolidation strain for the specimens of 73% initial relative density, respectively

Following the study of Kuwano and Jardine (2002), the ratios of radial creep strains and consolidation strains, $\varepsilon_{cr(r)} / \varepsilon_{con(r)}$, representing relative creep effect for the specimens of initial relative density of 73% are shown in

Figure 4.31 and summarized in Table 4.14. The results showed that radial creep strains built up to 12~41% of the consolidation strains within 40 hours of each loading stage for the specimens of initial relative density of 73%. The relative creep effect in radial strains, $\varepsilon_{cr(r)} / \varepsilon_{con(r)}$, increases as the vertical effective stress increases. The results indicated that the specimens with the stress ratio of 0.4 show the largest relative creep effect in the radial direction.

Table 4.14 Ratios of radial creep strains and consolidation strains for the specimens of 73% initial relative density

D_r= 73%	q/p'=0	q/p'=0.2	q/p'=0.4
$\Delta\sigma'_v$	$\varepsilon_{cr(r)} / \varepsilon_{con(r)}$	$\varepsilon_{cr(r)} / \varepsilon_{con(r)}$	$\varepsilon_{cr(r)} / \varepsilon_{con(r)}$
30-100	0.128	0.159	0.223
100-200	0.219	0.260	0.314
200-400	0.315	0.344	0.409

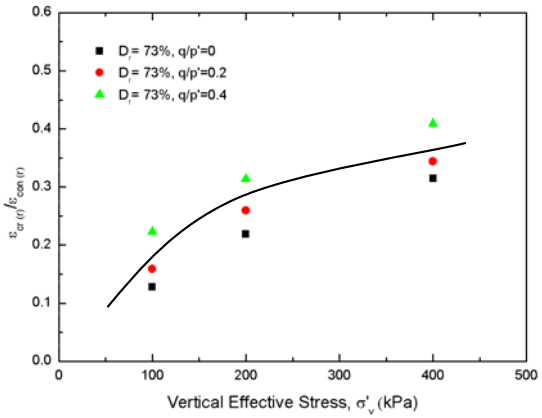

Figure 4.31 Ratios of radial creep strains and consolidation strains for the specimens of 73% initial relative density

The radial strains observed during each consolidation stage and subsequent 40 hours of creep stage for the specimens of 85% initial relative density are shown in Figure 4.32 and Table 4.15.

The specimens with 85% initial relative density show the increase in radial creep strains as the stress ratio decreases. It is considered that radial creep strains increases with the radial effective stress before creep, due to the large stress to the specimens promoting the particle rearrangement or slippage under constant loading in the radial direction. The amount of radial consolidation also increases as the vertical effective stress increases.

Table 4.15 Radial strain during consolidation and subsequent 40 hours of creep for the specimens of 85% initial relative density

D_r= 85%	q/p'=0		q/p'=0.2		q/p'=0.4	
$\Delta\sigma'_v$	$\varepsilon_{con(r)}$ (%)	$\varepsilon_{cr(r)}$ (%)	$\varepsilon_{con(r)}$ (%)	$\varepsilon_{cr(r)}$ (%)	$\varepsilon_{con(r)}$ (%)	$\varepsilon_{cr(r)}$ (%)
30-100	0.281	0.064	0.172	0.055	0.124	0.030
100-200	0.240	0.098	0.230	0.085	0.134	0.053
200-400	0.464	0.197	0.397	0.152	0.264	0.101

(a)

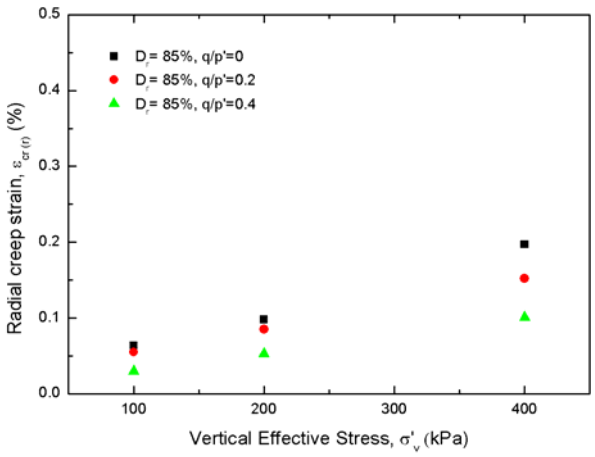

(b)

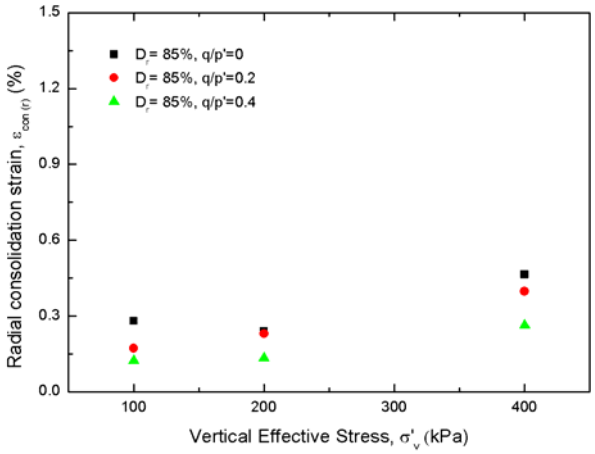

Figure 4.32 Developing (a) radial creep strain and (b) consolidation strain for the specimens of 85% initial relative density, respectively

The ratios of radial creep strains and consolidation strains, $\varepsilon_{cr(r)} / \varepsilon_{con(r)}$, representing relative creep effect for the specimens of initial relative density of 85% are shown in Figure 4.33 and summarized in Table 4.16. The results

showed that radial creep strains built up to 24~43% of the consolidation strains within 40 hours of each loading stage for the specimens of initial relative density of 85%. The relative creep effect in radial strains, $\varepsilon_{cr(r)} / \varepsilon_{con(r)}$, increases as the vertical effective stress increases.

Table 4.16 Ratios of radial creep strains and consolidation strains for the specimens of 85% initial relative density

D_r= 85%	q/p'=0	q/p'=0.2	q/p'=0.4
$\Delta\sigma'_v$	$\varepsilon_{cr(r)} / \varepsilon_{con(r)}$	$\varepsilon_{cr(r)} / \varepsilon_{con(r)}$	$\varepsilon_{cr(r)} / \varepsilon_{con(r)}$
30-100	0.228	0.320	0.242
100-200	0.408	0.370	0.396
200-400	0.425	0.383	0.383

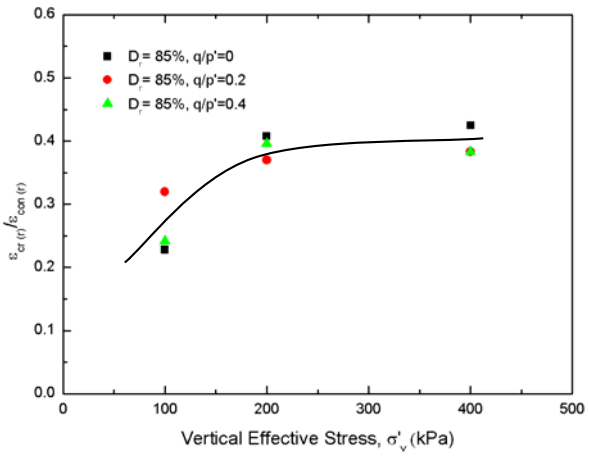

Figure 4.33 Ratios of radial creep strains and consolidation strains for the specimens of 85% initial relative density

The radial strains developing during each consolidation stage and subsequent 40 hours of creep stage for the specimens of 96% initial relative density are shown in Figure 4.34 and summarized in Table 4.17. Radial creep strains for the specimens with high relative density show dilative behavior at low mean normal effective stress level, but show contractive behavior at high mean normal effective stress level. As the stress ratio increases, dilative radial creep increases. The reason is that the conditions of low stress level and high stress ratio promote the unstable particle movement. However, there's no apparent tendency of the radial consolidations of the specimens for the high relative density with the stress conditions.

Table 4.17 Radial strain during consolidation and subsequent 40 hours of creep for the specimens of 96% initial relative density

D_r= 96%	q/p'=0		q/p'=0.2		q/p'=0.4	
$\Delta\sigma'_v$	$\varepsilon_{con(r)}$ (%)	$\varepsilon_{cr(r)}$ (%)	$\varepsilon_{con(r)}$ (%)	$\varepsilon_{cr(r)}$ (%)	$\varepsilon_{con(r)}$ (%)	$\varepsilon_{cr(r)}$ (%)
30-100	0.273	-0.073	0.210	-0.107	0.208	-0.427
100-200	0.228	0.005	0.188	-0.012	0.193	-0.165
200-400	0.357	0.046	0.227	0.024	0.301	-0.069

(a)

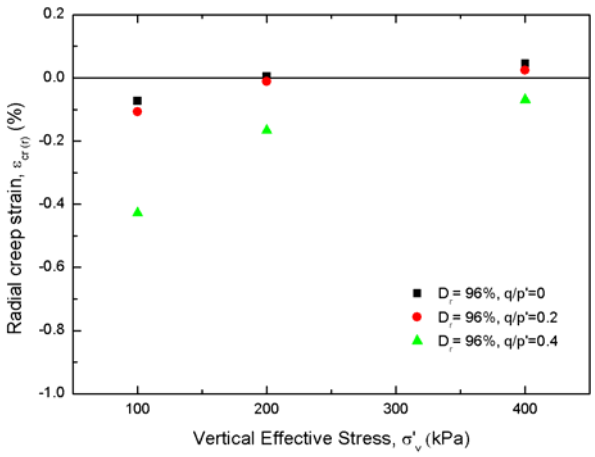

(b)

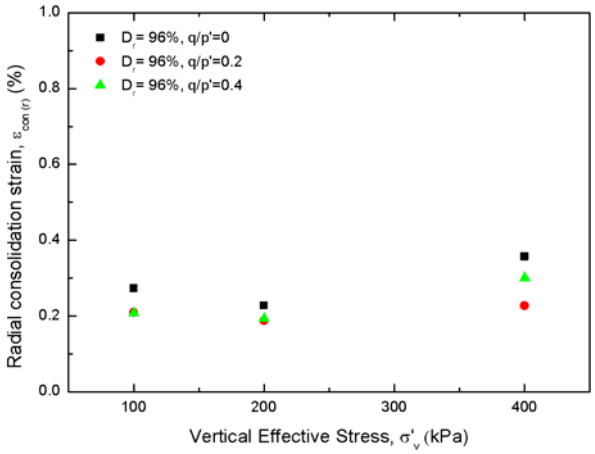

Figure 4.34 Developing (a) radial creep strain and (b) consolidation strain for the specimens of 96% initial relative density, respectively

The ratios of radial creep strains and consolidation strains, $\varepsilon_{cr(r)} / \varepsilon_{con(r)}$, representing relative creep effect for the specimens of initial relative density of 96% are shown in Figure 4.35 and summarized in Table

4.18. The relative creep effect in radial strains, $\varepsilon_{cr(r)} / \varepsilon_{con(r)}$, increases as the vertical effective stress increases. The results indicated that the specimens with the stress ratio of 0.4 show the smallest relative creep effect.

Table 4.18 Ratios of radial creep strains and consolidation strains for the specimens of 96% initial relative density

D_r= 96%	q/p'=0	q/p'=0.2	q/p'=0.4
$\Delta\sigma'_v$	$\varepsilon_{cr(r)} / \varepsilon_{con(r)}$	$\varepsilon_{cr(r)} / \varepsilon_{con(r)}$	$\varepsilon_{cr(r)} / \varepsilon_{con(r)}$
30-100	-0.267	-0.510	-2.053
100-200	0.022	-0.064	-0.855
200-400	0.129	0.106	-0.229

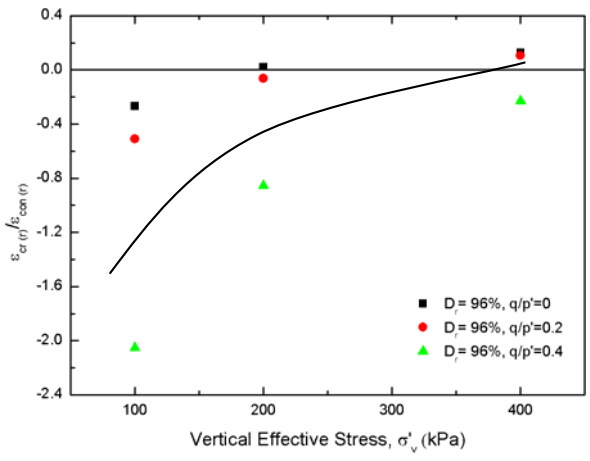

Figure 4.35 Ratios of radial creep strains and consolidation strains for the specimens of 96% initial relative density

Relative creep effect in shear strains

The shear strains developing during each consolidation stage and the following 40 hours of creep stage for the specimens of 73% initial relative density are shown in Figure 4.36 and Table 4.19. The larger negative shear creep strains with the specimens of initial relative density of 73% develop as the vertical effective stress increases. The negative shear creep strain dramatically increases at 400kPa of vertical effective stress. The amount of negative shear consolidation drops slightly when the vertical effective stress increases from 100kPa to 200kPa and increases sharply when the vertical effective stress increases from 200kPa to 400kPa.

Table 4.19 Shear strain during consolidation and subsequent 40 hours of creep for the specimens of 73% initial relative density

D_r= 73%	q/p'=0		q/p'=0.2		q/p'=0.4	
$\Delta\sigma'_v$	$\varepsilon_{con(sh)}$ (%)	$\varepsilon_{cr(sh)}$ (%)	$\varepsilon_{con(sh)}$ (%)	$\varepsilon_{cr(sh)}$ (%)	$\varepsilon_{con(sh)}$ (%)	$\varepsilon_{cr(sh)}$ (%)
30-100	-0.175	-0.016	-0.084	-0.013	0.006	-0.007
100-200	-0.163	-0.025	-0.102	-0.034	-0.041	-0.036
200-400	-0.667	-0.171	-0.452	-0.114	-0.237	-0.053

(a)

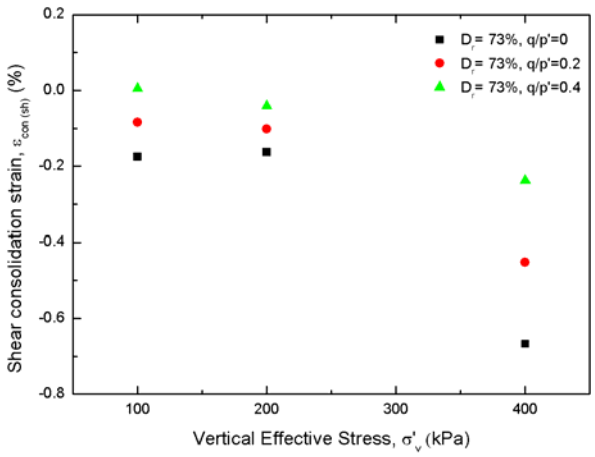

(b)

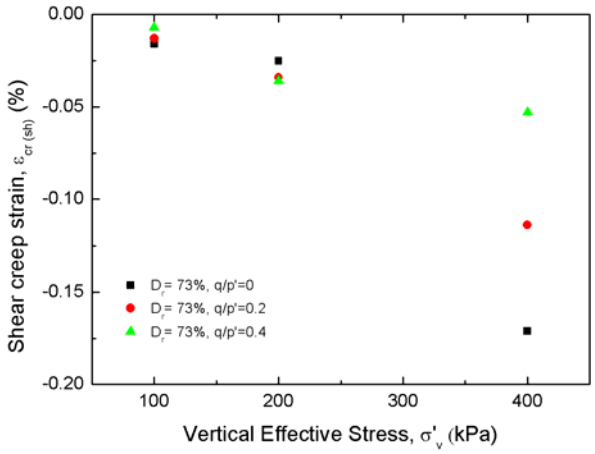

Figure 4.36 Developing (a) shear creep strain and (b) consolidation strain for the specimens of 73% initial relative density, respectively

Following the study of Kuwano and Jardine (2002), the ratios of shear creep strains and consolidation strains, $\varepsilon_{cr(sh)} / \varepsilon_{con(sh)}$, representing relative creep effect for the specimens of initial relative density of 73% are shown in

Figure 4.37 and summarized in Table 4.20. However, there's no tendency between the relative creep effect in shear strains and the stress conditions.

Table 4.20 Ratios of shear creep strains and consolidation strains for the specimens of 73% initial relative density

D_r= 73%	q/p'=0	q/p'=0.2	q/p'=0.4
$\Delta\sigma'_v$	$\varepsilon_{cr(sh)} / \varepsilon_{con(sh)}$	$\varepsilon_{cr(sh)} / \varepsilon_{con(sh)}$	$\varepsilon_{cr(sh)} / \varepsilon_{con(sh)}$
30-100	0.091	0.155	-1.167
100-200	0.153	0.333	0.878
200-400	0.256	0.252	0.224

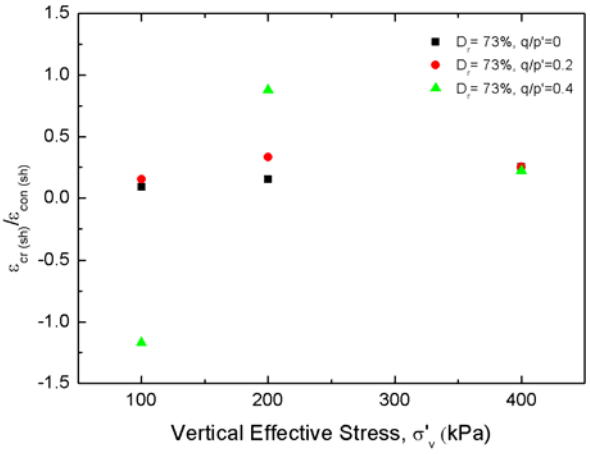

Figure 4.37 Ratios of shear creep strains and consolidation strains for the specimens of 73% initial relative density

The shear strains observed during each consolidation stage and subsequent 40 hours of creep stage for the specimens of 85% initial relative density are shown in Figure 4.38 and Table 4.21. The specimens with 85% initial relative density show the increase in negative shear creep strains as the stress ratio decreases and the vertical effective stress increases. The amount of negative shear consolidation also increases as the stress ratio decreases and the vertical effective stress increases.

Table 4.21 Shear strain during consolidation and subsequent 40 hours of creep for the specimens of 85% initial relative density

D_r= 85%	q/p'=0		q/p'=0.2		q/p'=0.4	
$\Delta\sigma'_v$	$\varepsilon_{con(sh)}$ (%)	$\varepsilon_{cr(sh)}$ (%)	$\varepsilon_{con(sh)}$ (%)	$\varepsilon_{cr(sh)}$ (%)	$\varepsilon_{con(sh)}$ (%)	$\varepsilon_{cr(sh)}$ (%)
30-100	-0.118	-0.032	-0.015	-0.026	0.046	0.000
100-200	-0.109	-0.056	-0.085	-0.042	0.005	-0.013
200-400	-0.276	-0.129	-0.183	-0.083	-0.071	-0.040

(a)

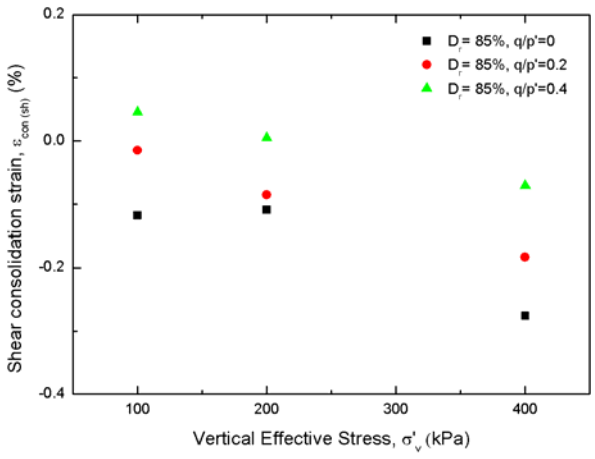

(b)

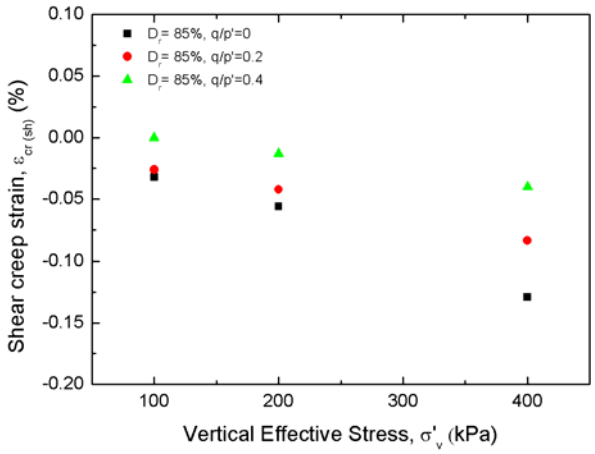

Figure 4.38 Developing (a) shear creep strain and (b) consolidation strain for the specimens of 85% initial relative density, respectively

The ratios of shear creep strains and consolidation strains, $\varepsilon_{cr(sh)} / \varepsilon_{con(sh)}$, representing relative creep effect for the specimens of initial relative density of 85% are shown in Figure 4.39 and summarized in Table

4.22. There's no tendency between the relative creep effect in shear strains and the stress conditions as in the specimens with 73% relative density.

Table 4.22 Ratios of shear creep strains and consolidation strains for the specimens of 85% initial relative density

D_r= 85%	q/p'=0	q/p'=0.2	q/p'=0.4
$\Delta\sigma'_v$	$\varepsilon_{cr(sh)} / \varepsilon_{con(sh)}$	$\varepsilon_{cr(sh)} / \varepsilon_{con(sh)}$	$\varepsilon_{cr(sh)} / \varepsilon_{con(sh)}$
30-100	0.271	1.733	0.000
100-200	0.514	0.494	-2.600
200-400	0.467	0.454	0.563

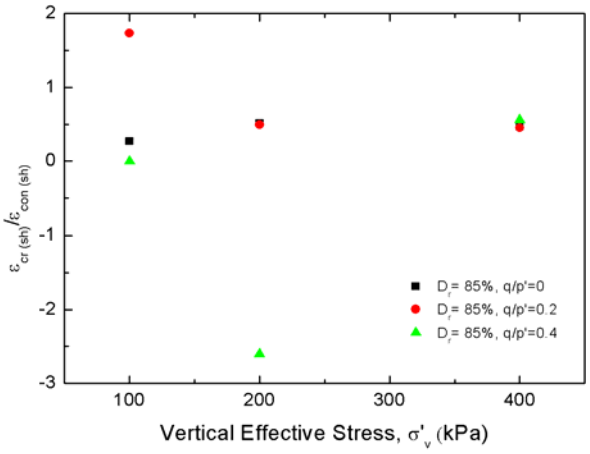

Figure 4.39 Ratios of shear creep strains and consolidation strains for the specimens of 85% initial relative density

The shear strains developing during each consolidation stage and subsequent 40 hours of creep stage for the specimens of 96% initial relative density are shown in Figure 4.40 and summarized in Table 4.23. The high positive shear creep strains for the specimens with high relative density at the low vertical effective stress levels. As the stress ratio increases, positive shear creep increases. The larger negative shear consolidation strains were observed in the high stress level than in the low stress level.

Table 4.23 Shear strain during consolidation and subsequent 40 hours of creep for the specimens of 96% initial relative density

D_r= 96%	q/p'=0		q/p'=0.2		q/p'=0.4	
$\Delta\sigma'_v$	$\varepsilon_{con(sh)}$ (%)	$\varepsilon_{cr(sh)}$ (%)	$\varepsilon_{con(sh)}$ (%)	$\varepsilon_{cr(sh)}$ (%)	$\varepsilon_{con(sh)}$ (%)	$\varepsilon_{cr(sh)}$ (%)
30-100	-0.060	0.070	0.005	0.096	0.008	0.318
100-200	-0.080	0.009	-0.035	0.030	0.003	0.140
200-400	-0.168	-0.025	-0.050	0.004	-0.070	0.064

(a)

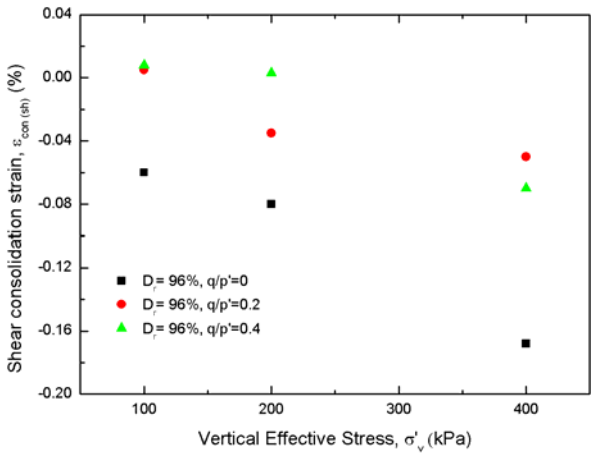

(b)

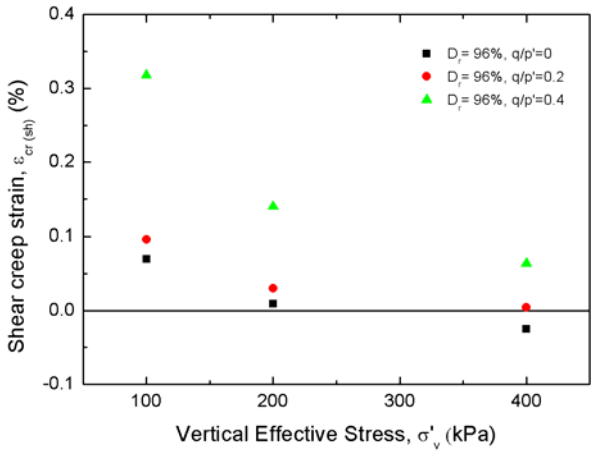

Figure 4.40 Developing (a) shear creep strain and (b) consolidation strain for the specimens of 96% initial relative density, respectively

The ratios of shear creep strains and consolidation strains, $\varepsilon_{cr(sh)} / \varepsilon_{con(sh)}$, representing relative creep effect for the specimens of initial relative density of 96% are shown in Figure 4.41 and summarized in Table 4.24. There's no

tendency between the relative creep effect in shear strains and the stress conditions as in the specimens with 73% relative density.

Table 4.24 Ratios of shear creep strains and consolidation strains for the specimens of 96% initial relative density

D_r= 96%	q/p'=0	q/p'=0.2	q/p'=0.4
$\Delta\sigma'_v$	$\varepsilon_{cr(sh)} / \varepsilon_{con(sh)}$	$\varepsilon_{cr(sh)} / \varepsilon_{con(sh)}$	$\varepsilon_{cr(sh)} / \varepsilon_{con(sh)}$
30-100	-1.167	19.200	39.750
100-200	-0.113	-0.857	46.667
200-400	0.149	-0.080	-0.914

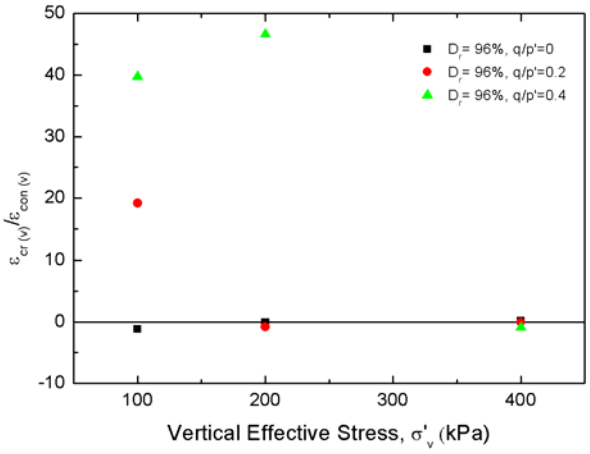

Figure 4.41 Ratios of shear creep strains and consolidation strains for the specimens of 96% initial relative density

4.3 State-dependent volumetric creep behavior

4.3.1 Introduction

A series of triaxial creep tests were performed to investigate the time-dependent deformation behavior of weathered residual soil in Korea. The previous chapter presents the results of creep strain for various test conditions. Also, the occurring creep strains were plotted on the basis of 40 hours, because the creep strain converged to 95% of the total creep strain.

Herein, based on the experimental observations, state-dependent volumetric creep behavior is presented. Experimental results to investigate effects of relative density and stress conditions on subsequent creep behavior showed that volumetric creep strains of weathered residual soil in Korea highly depend on the initial relative density and stress conditions. In drained creep test conditions at a given effective stress level, relatively loose samples, which have an initially high void ratio, contract when they undergo creep whereas relatively dense samples, which have an initially low void ratio, expand when they undergo creep. The contractive creep strains in the loose specimens increase as the mean normal effective stress increases. However, the dilative creep strains in the dense specimens decrease as the mean normal effective stress increase.

In this chapter, state-dependent volumetric creep behavior for Korean weathered residual soil based on the experimental observation was examined.

This chapter consists of following two parts:

(1) Volumetric creep strain at a given mean normal effective stress (p') on the basis of 40 hours, and

(2) State-dependent volumetric creep behavior of Korean weathered residual soil.

4.3.2 Volumetric creep strain at a given mean normal effective stress

Volumetric creep strain at a given mean normal effective stress (p') on the basis of 40 hours was plotted in Figures 4.42~4.44. Volumetric creep strain highly depends on the initial relative densities.

In drained creep test conditions at a given effective stress level, relatively loose samples (73% and 85% initial relative densities), which have an initially high void ratio, contract when they creep while relatively dense samples (96% initial relative density), which have an initially low void ratio, expand when they creep. In the case of 73% and 85% initial relative densities, the volumetric contractive creep strain increases, as the mean normal effective stress increases. On the other hand, in the case of 96% initial relative density, the more expansive creep strain is observed at the low mean normal effective stress and at the high stress ratio.

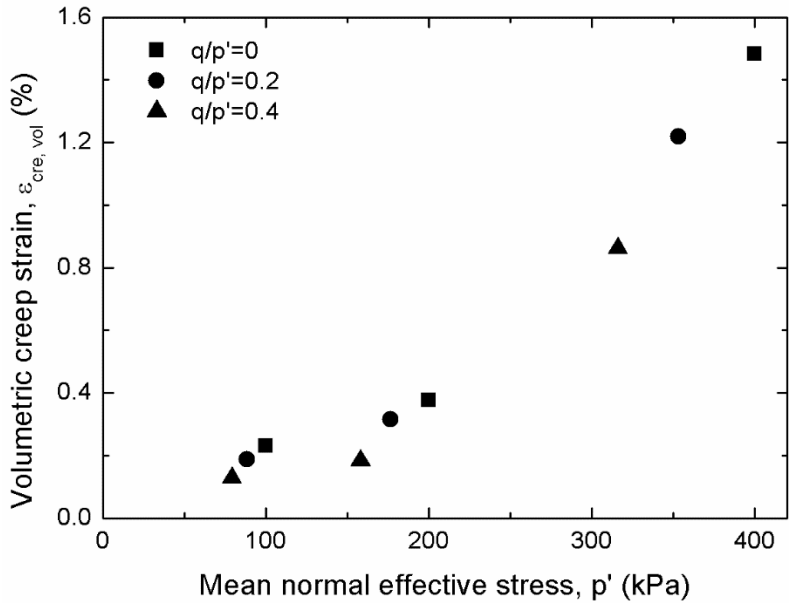

Figure 4.42 Volumetric creep strain on the basis of 40 hours, D_r=73%

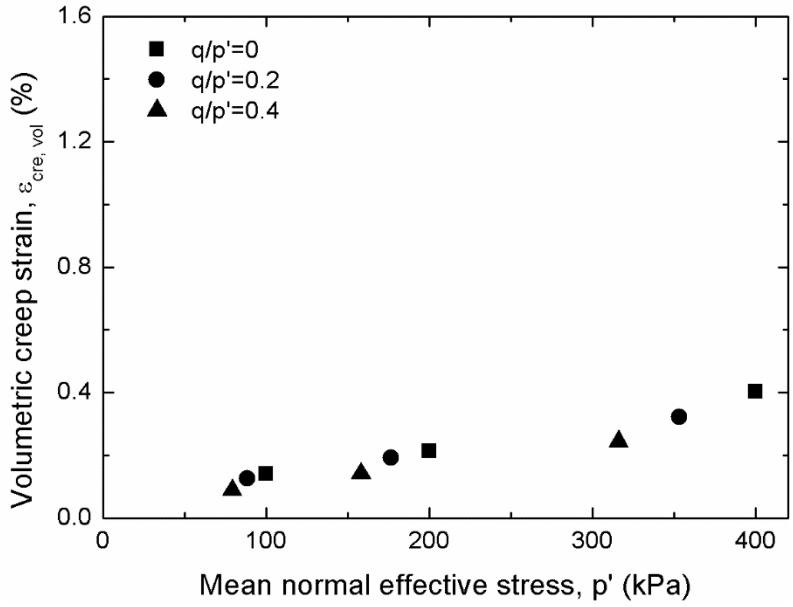

Figure 4.43 Volumetric creep strain on the basis of 40 hours, D_r=85%

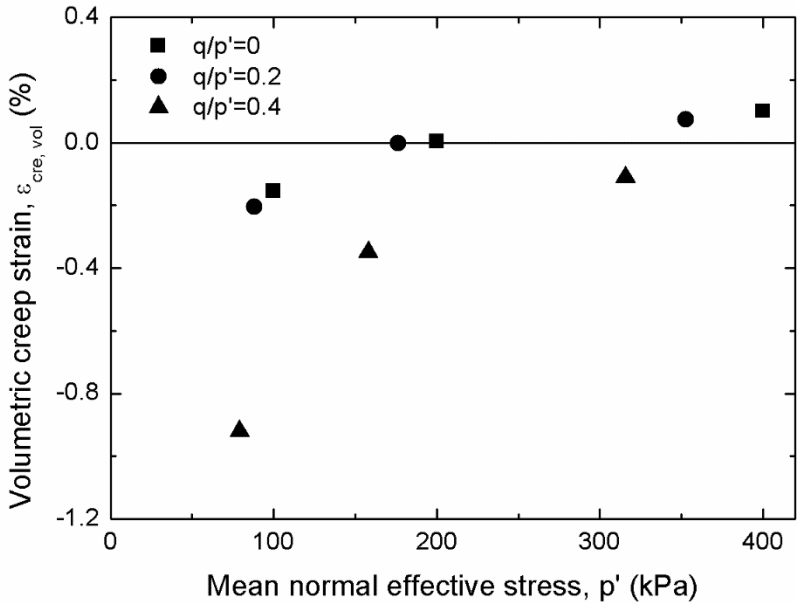

Figure 4.44 Volumetric creep strain on the basis of 40 hours, D_r=96%

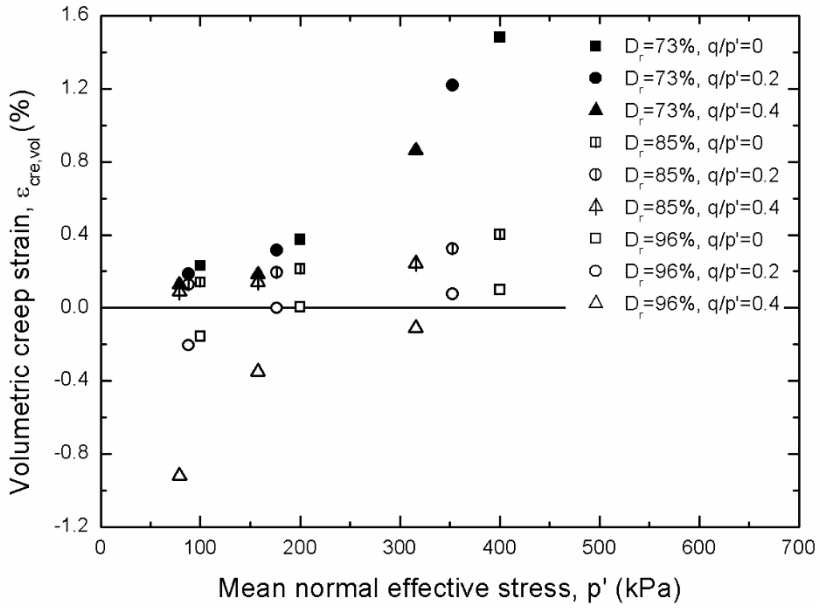

Figure 4.45 Volumetric creep strain on the basis of 40 hours

Figure 4.45 shows the volumetric creep strain for all the test conditions. The results show contrast behaviors between the responses of the initially loose samples and the initially dense samples. Initially loose samples crept more at high mean normal effective stress. Initially dense samples of weathered residual soils show the expansive creep strain at low stress levels. Initially dense samples of weathered residual soils show the contractive creep strain at high stress levels.

4.3.3 State-dependent volumetric creep behavior of weathered residual soil in Korea

The volumetric creep behavior shows contrast responses between the initially loose specimens and the initially dense specimens. Surprisingly, this contrast volumetric creep behavior shows the very similar trend with the volumetric behavior of granular materials during shearing at critical state. It was observed that not only during shearing but also during creep, the volumetric contraction is observed in the loose specimens and this contractive strains increases with the mean normal effective stress, while, dilative volumetric response is observed in the dense specimens and this dilative strains decreases as the mean normal effective stress increases.

In this study, paying attention to the point that the granular materials tend to reach the same void ratio when the specimen is shearing and this behavior is expressed as a unique critical state line (Rosceo et al. 1958), it is considered that volumetric creep responses can be expressed as a certain relationships in the e-p' plane. However, it is hard for the specimens to reach a specific void ratio when the specimens undergo creep unlike shearing because the volumetric creep deformations are much smaller than the consolidation or shearing deformations. Thus, it is considered that the state where the change of a void ratio due to creep becomes zero might exist between the contractive volumetric creep behavior of the specimens with low density and the dilative creep behavior of the contrast volumetric creep behavior of the specimens with high density at a given stress state. Therefore, the void ratio where the

change of void ratio due to creep become zero, called as creep-free state, was investigated to express overall volume change during creep rather than find the converged void ratio at a given stress level.

To investigate the creep-free state for Korean weathered residual soil, the variation of void ratio during creep was estimated. Tables 4.25~4.27 summarize the changes of void ratio during creep (for 40 hours). The changes of void ratio during creep were plotted with initial relative densities at a given mean normal effective stress (in Figures 4.46~4.48). Then, the relative density where the changes of void ratio become zero can be obtained with the regression lines of data. The void ratio where the changes of void ratio becomes zero also can be calculated. The increase of stress level reduces the void ratio before creep. Consequently, creep-free void ratio decreases as the mean normal effective stress increases.

Table 4.25 Summary of the changes of void ratio during 40 hours of creep for the specimens subjected to the stress ratio of 0

P' (kPa)	Δe (D_r=73%)	Δe (D_r=85%)	Δe (D_r=96%)	D_r where Δe =0	e where Δe =0
100	0.00459	0.002634	-0.00283	89.38%	0.698
200	0.006854	0.003753	0.000191	97.23%	0.618
400	0.027594	0.008022	0.00166	98.96%	0.600

Table 4.26 Summary of the changes of void ratio 40 hours of creep for the specimens subjected to the stress ratio of 0.2

P' (kPa)	Δe (D_r=73%)	Δe (D_r=85%)	Δe (D_r=96%)	D_r where Δe =0	e where Δe =0
86.5	0.003512	0.002355	-0.00334	87.46%	0.717
176.1	0.00551	0.003435	9.58E-05	96.05%	0.630
352.6	0.021984	0.006554	0.001298	98.74%	0.602

Table 4.27 Summary of the changes of void ratio 40 hours of creep for the specimens subjected to the stress ratio of 0.4

P' (kPa)	Δe (D_r=73%)	Δe (D_r=85%)	Δe (D_r=96%)	D_r where Δe =0	e where Δe =0
77.1	0.002437	0.001575	-0.015	79.68%	0.797
156.2	0.004166	0.002573	-0.00504	86.11%	0.731
315.2	0.016374	0.005167	-0.00348	91.67%	0.674

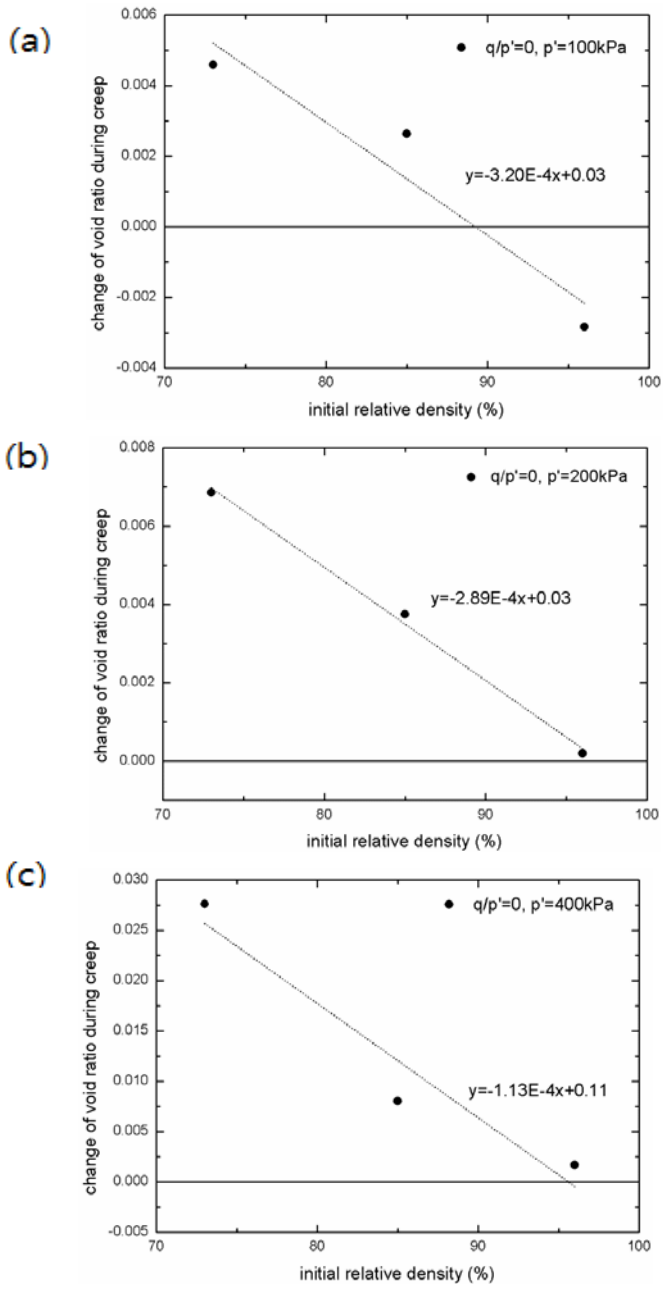

Figure 4.46 Change of e during isotropic creep (q/p'=0) for the specimens of (a) p'=100, (b) p'=200, and (c) p'=400 kPa, respectively

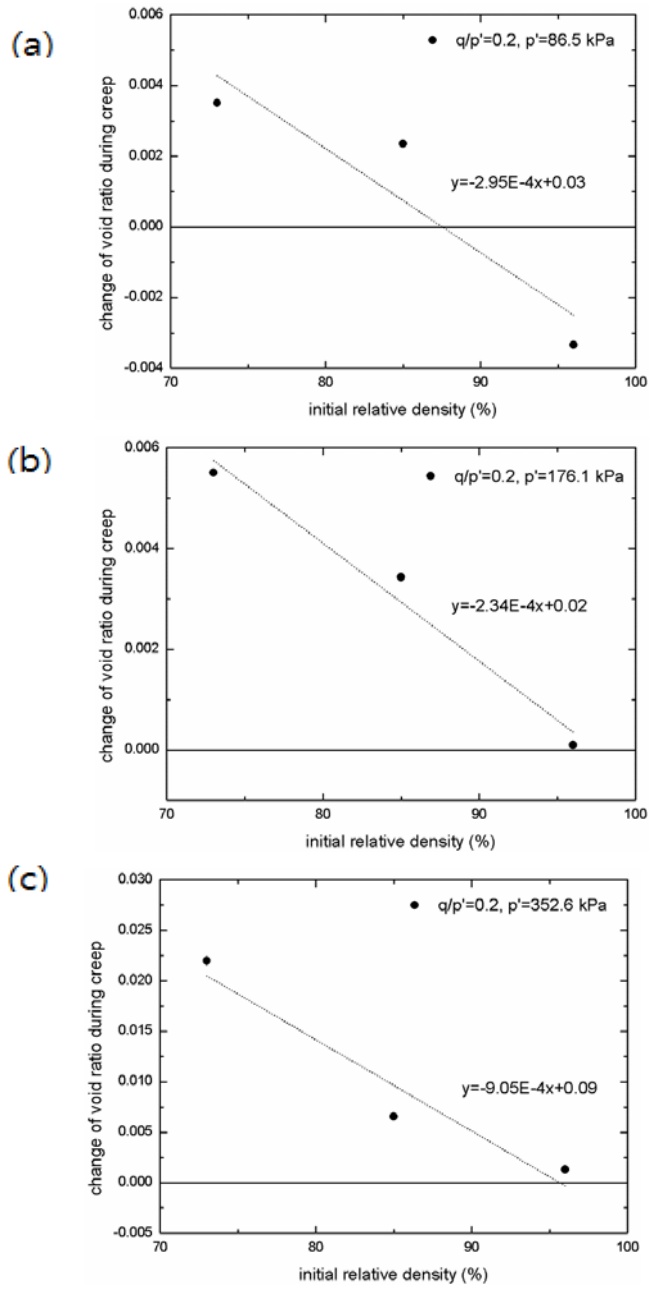

Figure 4.47 Change of e during anisotropic creep (q/p'=0.2) for the specimens of (a) p'=100, (b) p'=200, and (c) p'=400 kPa, respectively

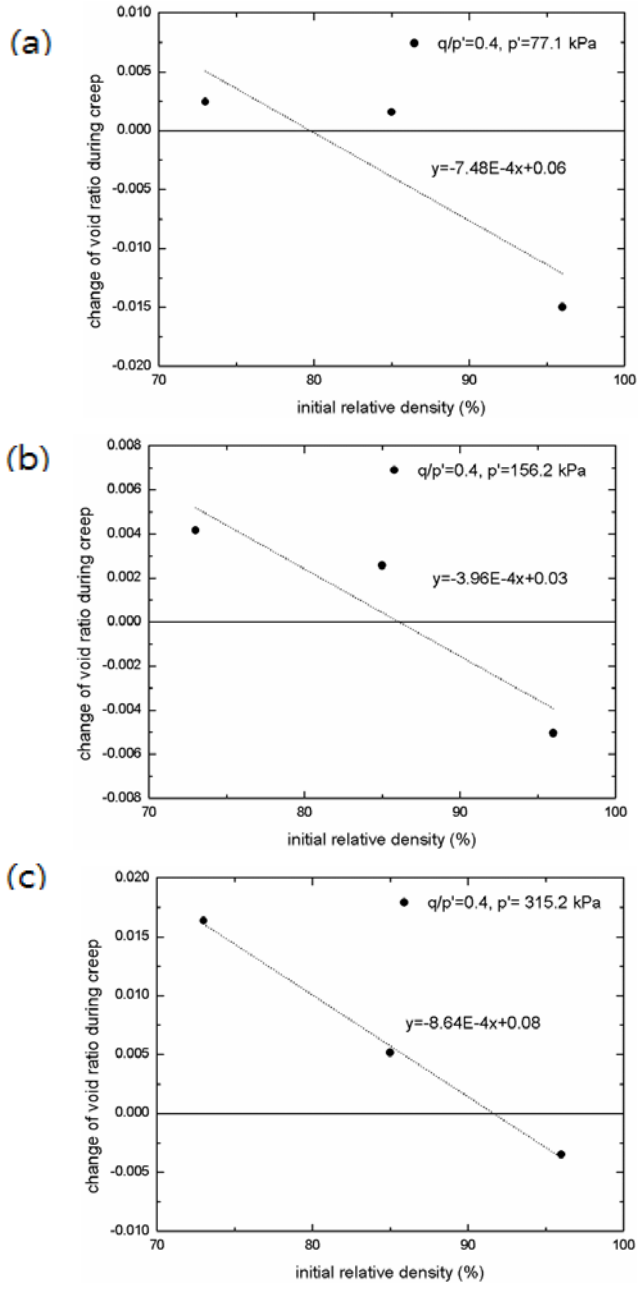

Figure 4.48 Change of e during anisotropic creep (q/p'=0.4) for the specimens of (a) p'=100, (b) p'=200, and (c) p'=400 kPa, respectively

Figure 4.49 shows the creep-free void ratio with the mean normal effective stress. Interestingly, the relationship between the creep-free void ratio and the mean normal effective stress shows a similar tendency as the relationship between general critical void ratio and the mean normal effective stress during shearing. In common with the general critical state concept, the creep-free void ratio decreases as the mean normal effective stress increases. The creep-free state for Korean weathered residual soil is stress level dependent as the general critical state. As a result, creep-free void ratio and the mean normal effective stress can be expressed by a regression line roughly. With the additional experimental studies, drawing the zone of creep-free void ratio might be possible.

The results of stress ratio of 0 and 0.2 can be expressed as just one curve. However, the results of stress ratio of 0.4 are slightly different from those of stress ratio of 0 and 0.2. The initial structure of specimen in the vertical direction is stiffer than that in the horizontal direction. In the case of 0.4 stress ratio, when the vertical effective stress is 100 kPa, the horizontal effective stress is 68.4 kPa (K value=0.684). In the loose specimens of 0.4 stress ratio, smaller contractive volumetric creep strain is generated because of lower p'. On the other hand, the very dense specimens of stress ratio of 0.4, expansive volumetric creep strains are stimulated in the horizontal direction. That is, void ratio without volume change is inclined to locate in the smaller relative density (the larger void ratio) because of the smaller contractive creep strain (in 73% initial relative density) and the larger dilative creep strain (in 96% initial relative density). This tendency will be intensified as the stress ratio

increases.

The chart of creep-free void ratio provides information which can control the deformation due to creep to minimize.

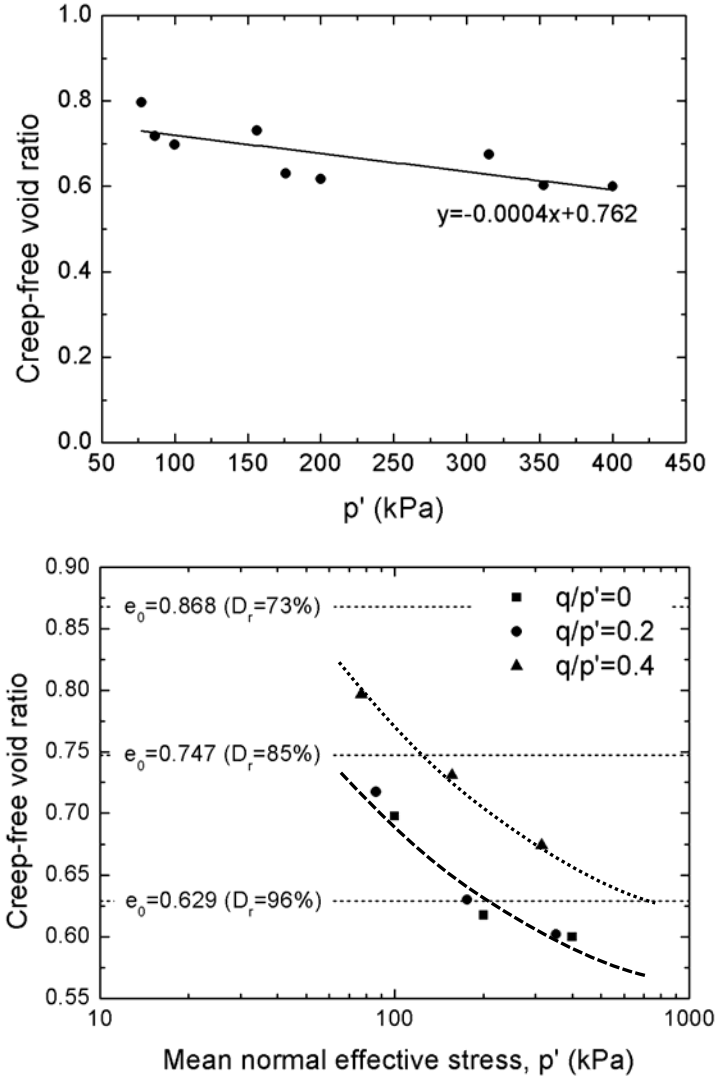

Figure 4.49 Creep-free void ratio

4.4 Summary

4.4.1 Creep strains of triaxial creep tests

The objective of this study is to investigate the creep behavior of weathered residual soil in Korea. To illustrate the field conditions, various sample conditions with different relative densities and shear conditions with different confining stresses were considered. Based on the results and analyses of the data, the following conclusions are drawn related to the effect of various testing conditions on the creep behavior of weathered residual soil in Korea.

(1) The creep behavior of weathered residual soils highly depends on the initial relative density, current stress state, and stress ratio.
(2) For the specimens with low and medium initial relative density, contractive volumetric creep strains were observed while dilative volumetric creep strains developed for the specimens with high initial relative density.
(3) High stress conditions stimulate the particle rearrangement or sliding under constant loading conditions, resulting in more contractive creep strains for the specimens with low and medium relative density.
(4) Contrast to the specimens with low and medium relative density, the high stress condition inhibits the particle rearrangement or sliding, resulting in dilative creep strains behavior in the specimens with high relative density. That is because the structure of high density

soil reaches the limit state in contraction, and then it shows expansion. The low p' and high q/p' conditions promote dilative behavior during creep.

4.4.2 State-dependent volumetric creep behavior

Based on the experimental observations, the concept of state-dependent volumetric creep behavior is proposed. In drained creep test conditions at a given effective stress level, relatively loose samples, which have an initially high void ratio, contract when they undergo creep whereas relatively dense samples, which have an initially low void ratio, expand when they undergo creep. Therefore, it is considered that the state which the change of a void ratio due to creep become zero might exist.

The creep-free void ratio was defined as the state which the change of a void ratio due to creep becomes zero. As a result, interestingly, the creep-free void ratio decreases when the mean normal effective stress increases as the general critical state concept. With the additional experimental studies, drawing the zone of the creep-free void ratio might be possible. This approach is expected to shed much light on our understanding of the overall creep behavior of granular materials and to provide information with which to ensure minimized creep deformation.

Chapter 5. Experimental Results and Analysis: Elastic Shear Stiffness Characteristics

5.1 Introduction

The anisotropy of soil in stiffness is also an important factor in various problems relating to ground deformations. Previous researchers such as Ochiai and Lade (1983) and Kirkgard and Lade (1991 and 1993) experimentally investigated the influence of the initial fabric anisotropy on the failure of soils.

To measure the shear wave velocities in the different directions, two pairs of locally designed and manufactured bender elements were used. Shear wave velocities in two different horizontal directions were measured via two pairs of bender elements during creep. A single-pulse sinusoidal input signal of 10-volt amplitude was shot for each measurement using bender elements.

The main topics of chapter 5 are:

(1) Stiffness obtained from the overall stress-strain curve
(2) Stiffness degradation curve
(3) Variations in the elastic shear stiffness during creep
(4) Quantifying the time-dependent increase in the elastic shear stiffness
(5) Stiffness anisotropy

5.2 Stiffness obtained from the overall stress-strain curve

The relationships between the axial stress and the axial strain during consolidation and creep for the specimens applied to the stress ratio of 0, 0.2, and 0.4 are already described in Chapter 4.2.1. The slope of the stress-strain curve prior to creep stage is quite different from that after the creep stage, as shown in Figure 5.1. To quantitatively evaluate this difference, the Young's moduli, E_1 and E_2 that measure the slopes in two different portions of the stress-strain curve as illustrated in Figure 5.1, were used. The slopes were determined using the data ranging less than 0.005% axial strains. Figure 5.2 compares E_1 and E_2 for the different conditions of stresses and initial densities.

As expected, E_2 are notably higher than E_1 for every condition. Contrary to the general notion that a specimen with higher initial relative density exhibits stiffer response than others, the values of E_1 and E_2 for the specimens with the medium initial density of 85% exhibit higher stiffness than others. The secant modulus, E, however, depends on the stress. To evaluate only the creep effect on the stiffness, the values of E are normalized by σ'_v as in Figure 5.3. Figure 5.3 shows the normalized E_1 and E_2 for the different conditions. Normalized E_2 are still remarkably higher than E_1 for every condition reflecting the creep effect on the stiffness of weathered residual soil obviously.

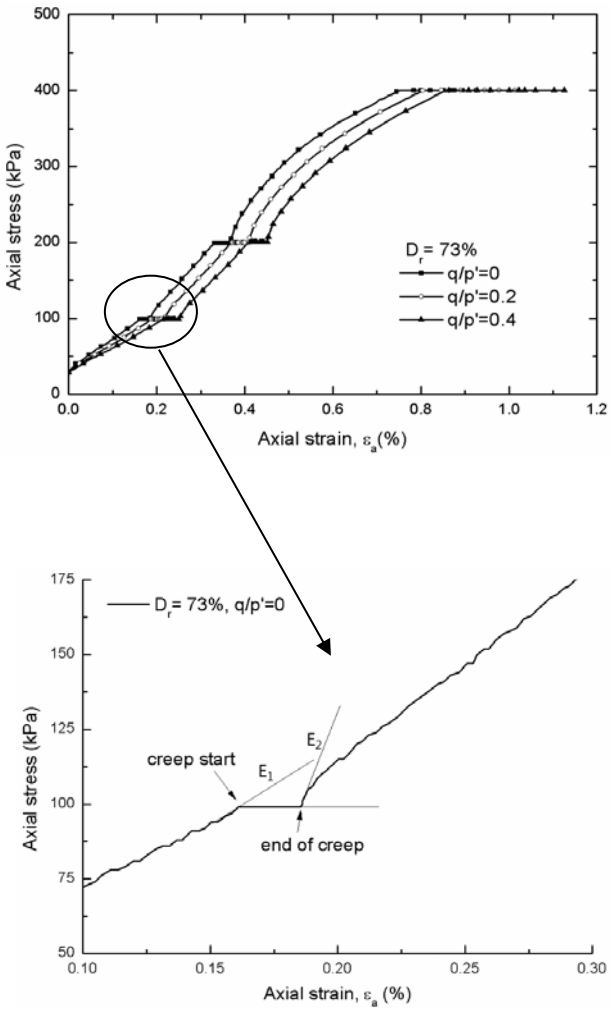

Figure 5.1 Young's moduli, E_1 and E_2, measuring the slopes of the curve before and after the creep stage

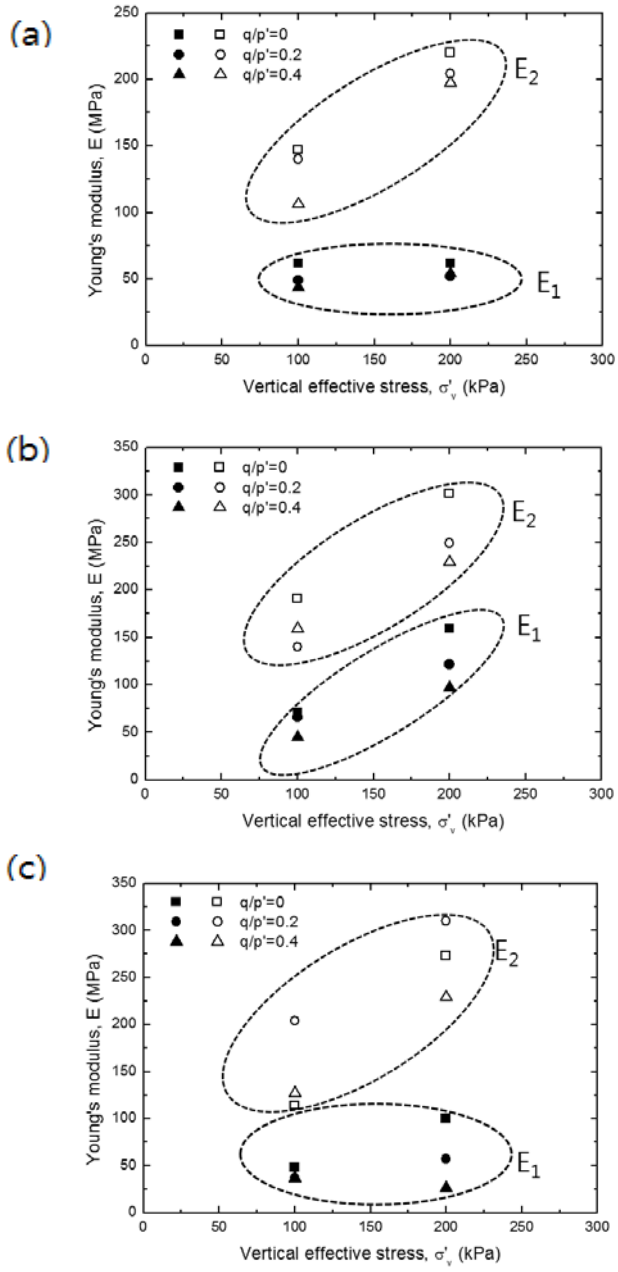

Figure 5.2 E_1 and E_2 of initial relative density of (a) 73%, (b) 85%, and (c) 96%, respectively

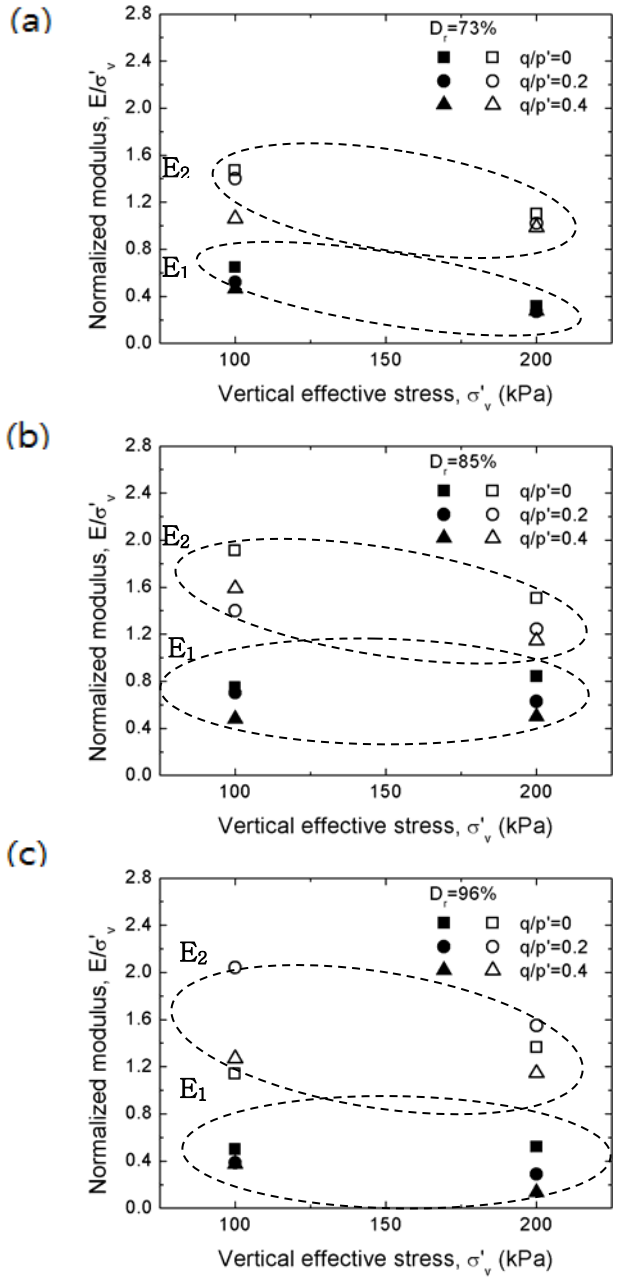

Figure 5.3 Normalized E_1 and E_2 of initial relative density of (a) 73%, (b) 85%, and (c) 96%, respectively

5.3 Stiffness degradation curve

Recently, the small strain stiffness and strain dependent stiffness have been used for the advanced deformation analysis in geotechnical engineering with finite element method. In this section, the nonlinear behavior of weathered residual soil is demonstrated.

There are two different methods to estimate the stiffness in the triaxial tests. One is the measurement using the local LVDTs in triaxial testing. The other is the measurement using bender elements, resonant column tests or cyclic triaxial tests. In this study, stiffness degradation curve was estimated by local LVDTs and compared with the initial stiffness obtained from bender element test results. The elastic stiffness is calculated using the elastic shear moduli obtained from bender element test results. The elastic stiffness can be calculated using the expression:

$$E' = 2G_{BE} \times (1+\nu) \tag{5.1}$$

In this study, poisson's ratio is assumed to be 0.4 for the relatively dense specimens. The stress-strain curves were interpreted in terms of E, taken to the secant to the curve, and the continuous values of E were plotted against axial strains. Figures 5.4~6 show the stiffness degradation curves with bender element test results for the specimens of initial relative density of 73%, 85%, and 96%, respectively. As can be seen in Figures 5.4~6, initial stiffness obtained from bender elements is generally consistent with the secant modulus of stress-strain curve. The stiffness degradation curves are located in the upper part as the confining stress increases. This results can be used for the deformation prediction modeling in the geotechnical design. However, to figure out the effect of aging on the degradation curves owing to the stiffness depending on the stress level, further study will be needed. The additional stiffness degradation curves are shown in Appendix A.6.

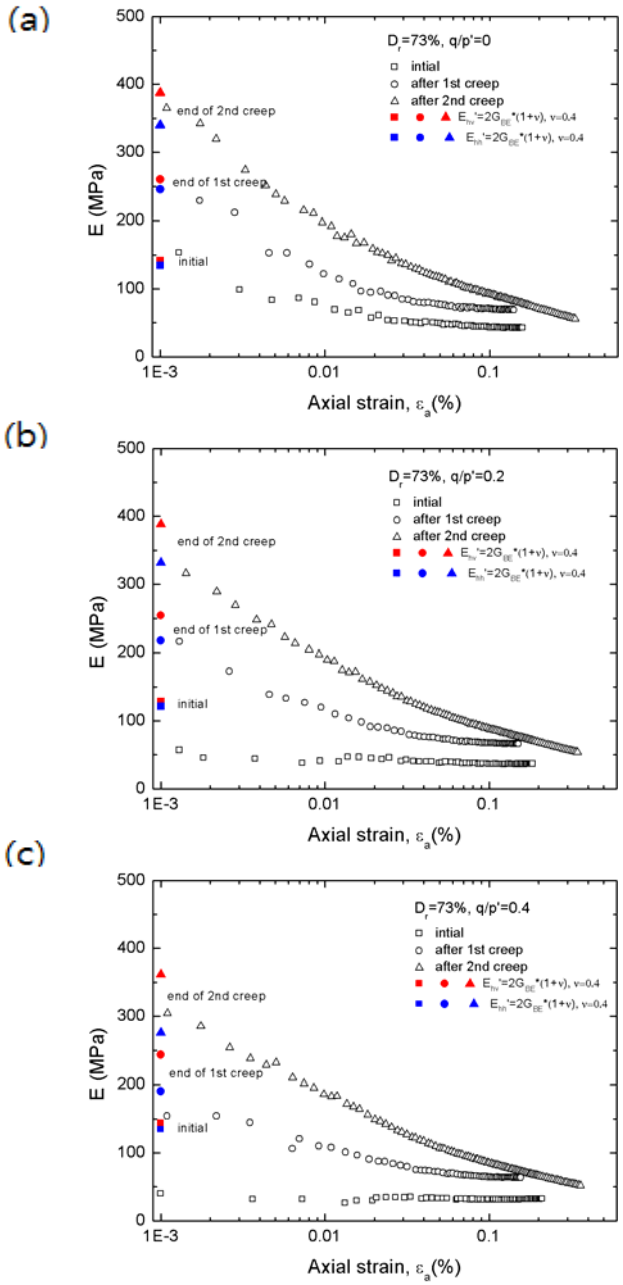

Figure 5.4 Stiffness degradation curves with bender element test results for the specimens of D_r=73% (a) q/p'=0, (b) q/p'=0.2, and (c) q/p'=0.4

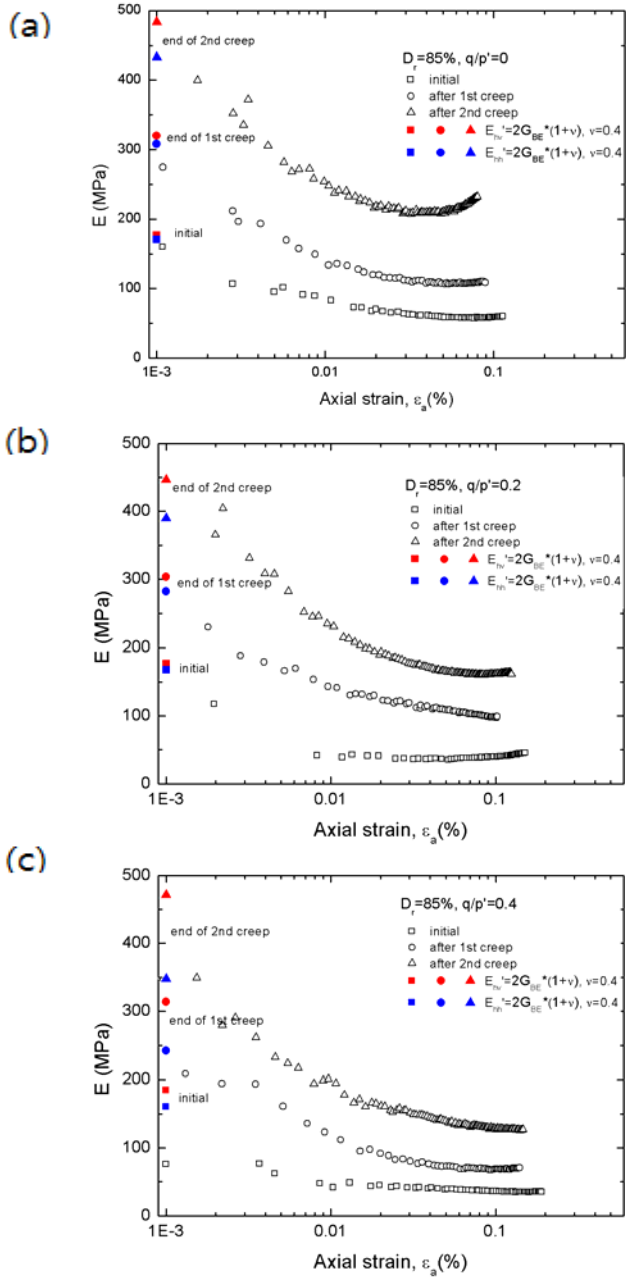

Figure 5.5 Stiffness degradation curves with bender element test results for the specimens of D_r=85%, (a) q/p'=0, (b) q/p'=0.2, and (c) q/p'=0.4,

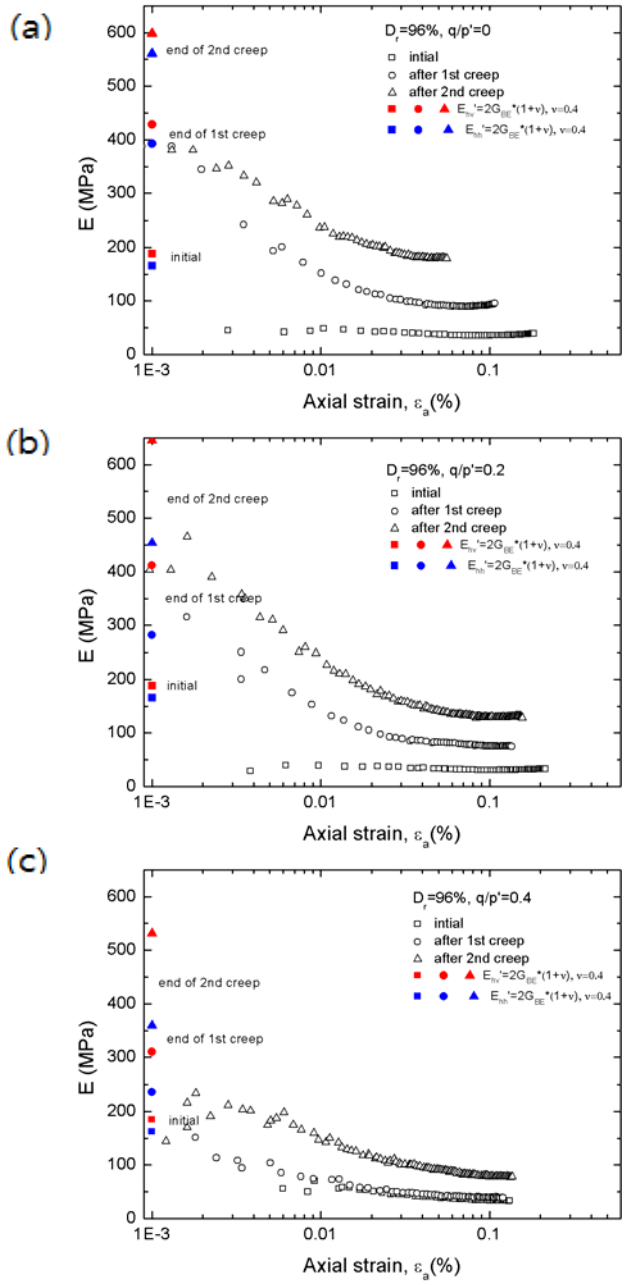

Figure 5.6 Stiffness degradation curves with bender element test results for the specimens of D_r=96%, (a) q/p'=0, (b) q/p'=0.2, and (c) q/p'=0.4

5.4 Variations in the elastic shear stiffness during creep

Gains in the elastic shear moduli during creep were evaluated via bi-directional bender element tests. Figures 5.7~5.15 compare the variations in elastic shear moduli and strains plotted against the time for creep. It was found that the development of strains during creep depends on the initial relative densities. As described in Chapter 4, the specimens with low density developed larger compressive axial strains during creep than the specimens with the medium initial density (Figures 5.7~5.12). As can be seen in Figures 5.13~5.15, it is of interest that the radial strains of the specimen with a high initial density, however, became negative, thus resulting in the dilative volume increase during creep.

Following Mesri et al. (1990) and Schmertmann (1991), the creep in granular soils has been frequently explained by particle rearrangement or slippage in particle contacts that could result in compressive creep strains and thus make the specimen with low initial density stable. In case of the specimens with high density, however, the arrangement of particles is already likely too stable to be compressed during creep. Reminding Taylor (1948)'s simple model illustrating the dilatancy in the dense granular soil with interlocked particles, one can rationally expect the volume increase during creep in the specimen with high initial density as the cases shown in Figures 5.13~5.15.

The creep deformation accompanies the gains in the elastic shear moduli or aging in the stiffness. As also shown in Figures 5.7~5.15, two elastic shear

moduli, G_{hv} and G_{hh}, measured by a pair of bender elements generally increase during creep. However, there is an exception in the G_{hh} of the specimen with high initial density that ceases to increase immediately after its initial increase during the creep stage. This exception may be related to the exceptional dilative radial strains observed in the same specimens during creep. In other words, in the low and medium density specimens, the contractive creep strains occur because the structure tends to be more stable.

The contact between particles increases as the creep strain develops, and this is reflected in the elastic shear stiffness. On the other hand, in the specimens with high initial relative density, applying constant external stresses, the soil cannot be compressed any more. Subsequently, the dilative creep strains generate unstable states and the original structure collapses, which results in unstable contact of particles. With losing contact of particles, the possibility of reduction in stiffness increases during aging. Variations in the elastic shear stiffness during aging shows relatively unstable tendency as in Figures 5.13~5.15.

Figures 5.16~5.24 present the aging rate of stiffness and creep strains with time in logarithm scales. As can be seen in Figures 5.16~5.21, the aging rate both in the horizontal and vertical direction in stiffness of the specimen increases as the compressive creep strains develop. Moreover, the aging rate is higher in the vertical direction than in the horizontal direction. This tendency of aging rate contributes to the evolution of anisotropy during creep. The evolution of anisotropy will be discussed in the later section. However, for the specimens of very high density as in Figures 5.22~5.24, it is hard to find out

the tendency of aging rate. This might be because of the unstable dilative creep strains in the horizontal direction.

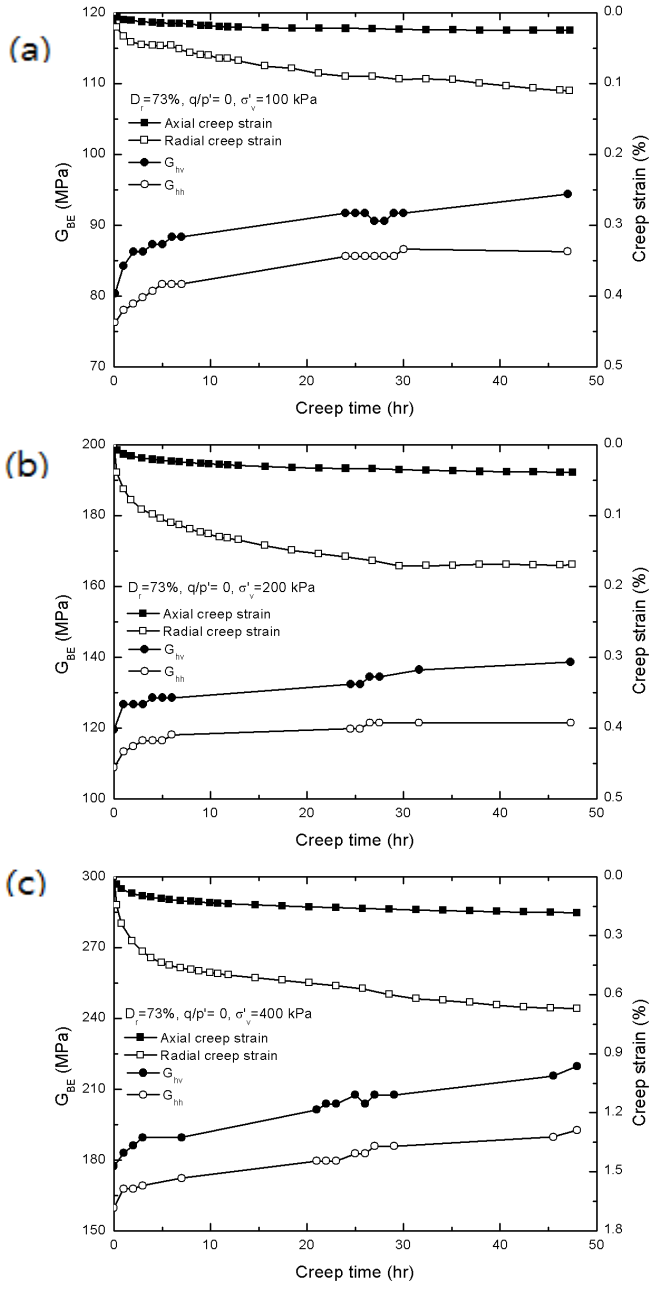

Figure 5.7 Elastic shear stiffness during creep of the specimens with D_r=73%, q/p'=0 (a) σ'_v = 100, (b) σ'_v = 200, and (c) σ'_v = 400 kPa

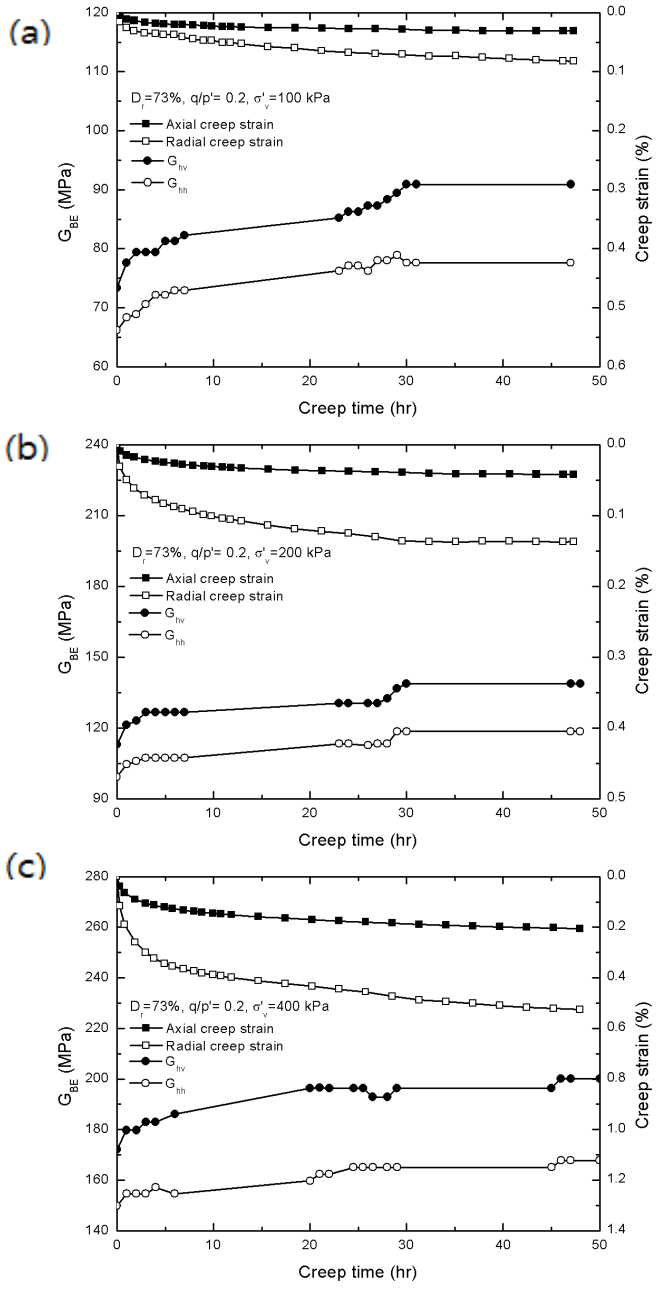

Figure 5.8 Elastic shear stiffness during creep of the specimens with D_r=73%, q/p'=0.2 (a) σ'_v = 100, (b) σ'_v = 200, and (c) σ'_v = 400 kPa

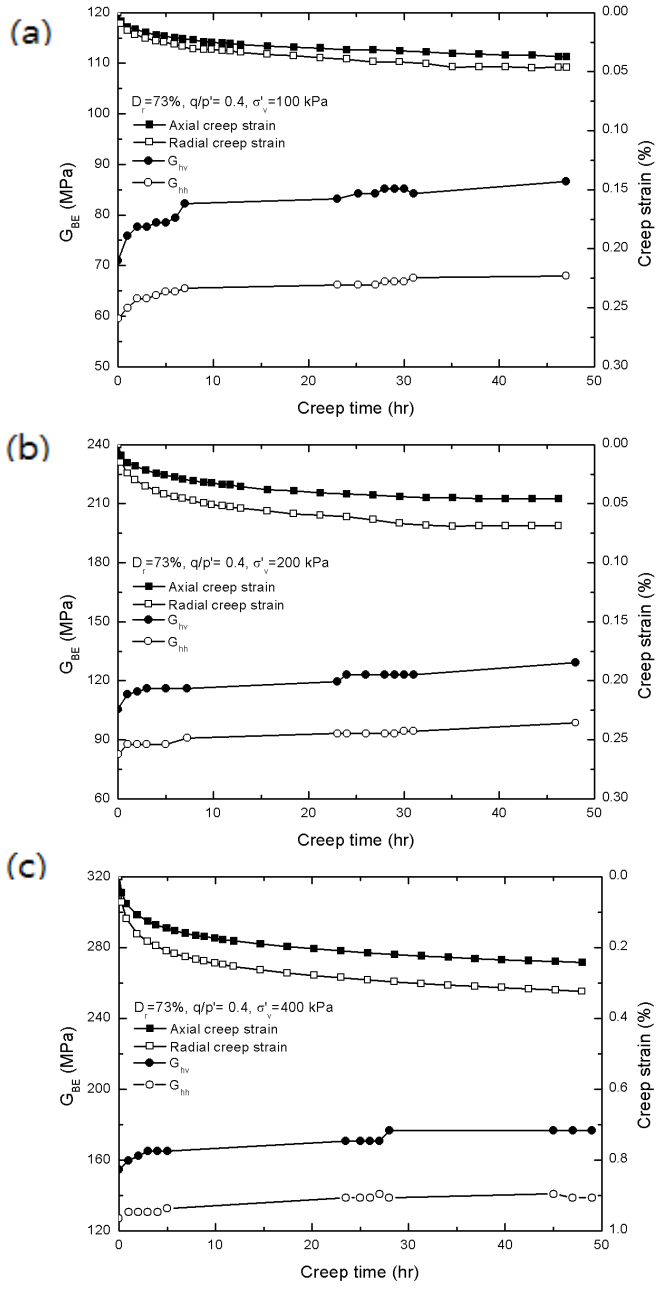

Figure 5.9 Elastic shear stiffness during creep of the specimens with D_r=73%, q/p'=0.4 (a) σ'_v = 100, (b) σ'_v = 200, and (c) σ'_v = 400 kPa

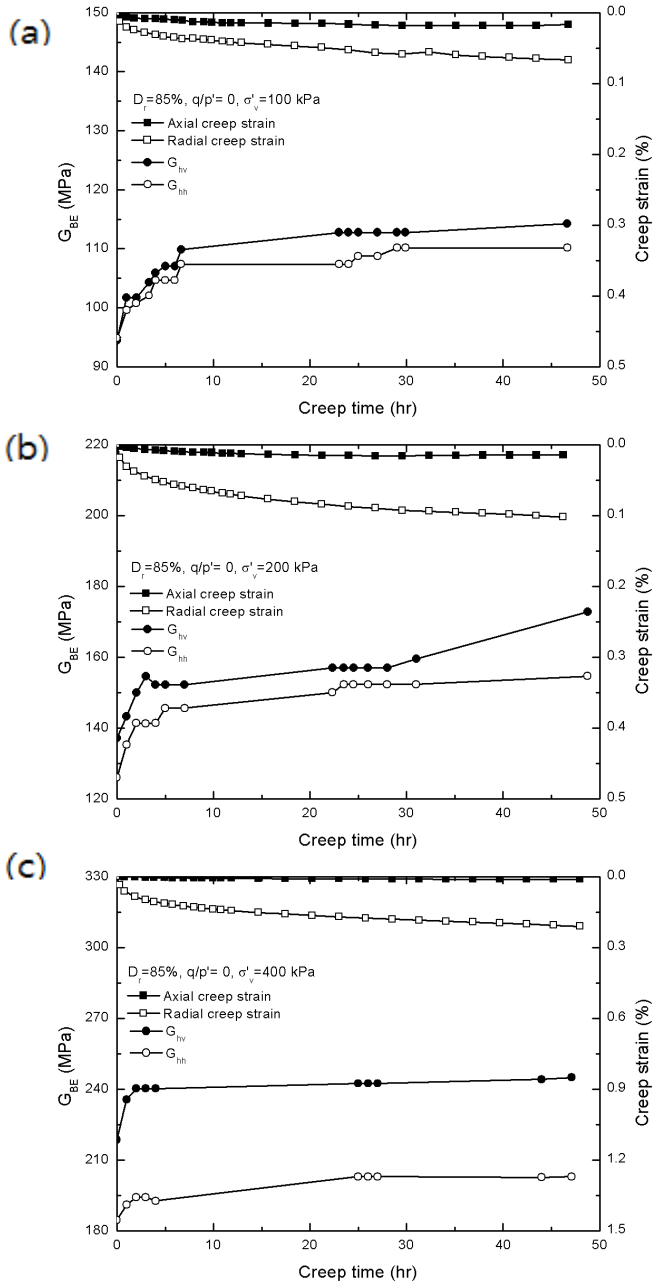

Figure 5.10 Elastic shear stiffness during creep of the specimens with D_r=85%, q/p'=0 (a) σ'_v = 100, (b) σ'_v = 200, and (c) σ'_v = 400 kPa

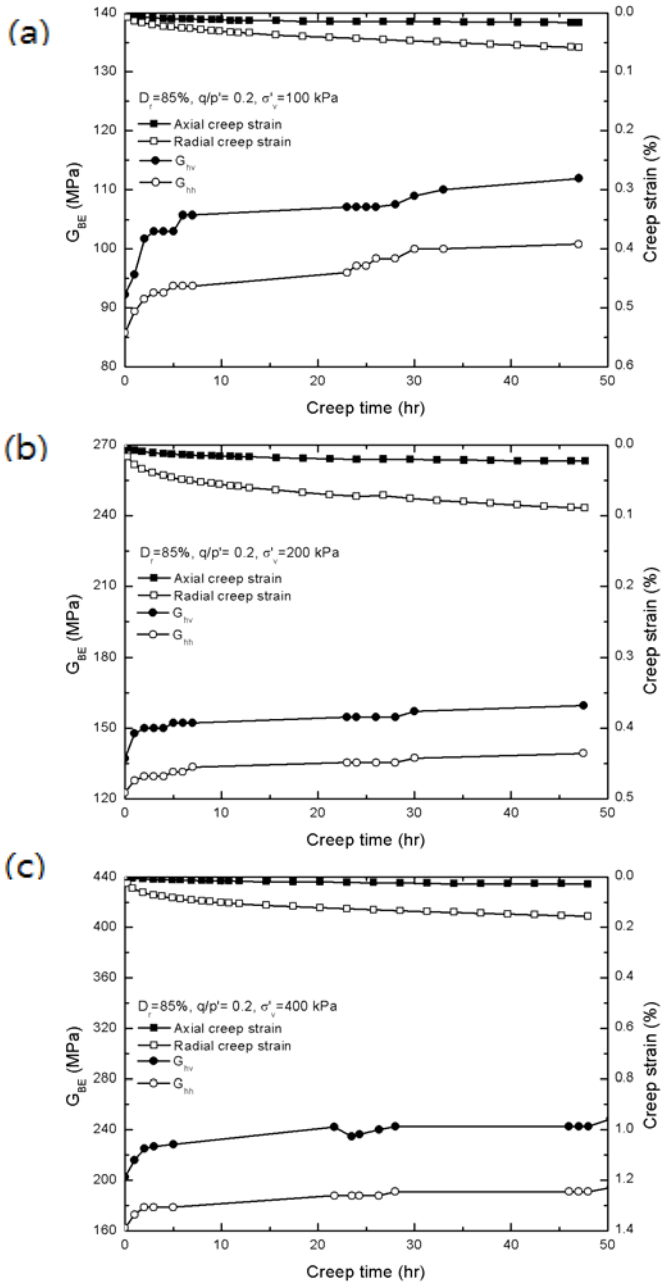

Figure 5.11 Elastic shear stiffness during creep of the specimens with D_r=85%, q/p'=0.2 (a) σ'_v = 100, (b) σ'_v = 200, and (c) σ'_v = 400 kPa

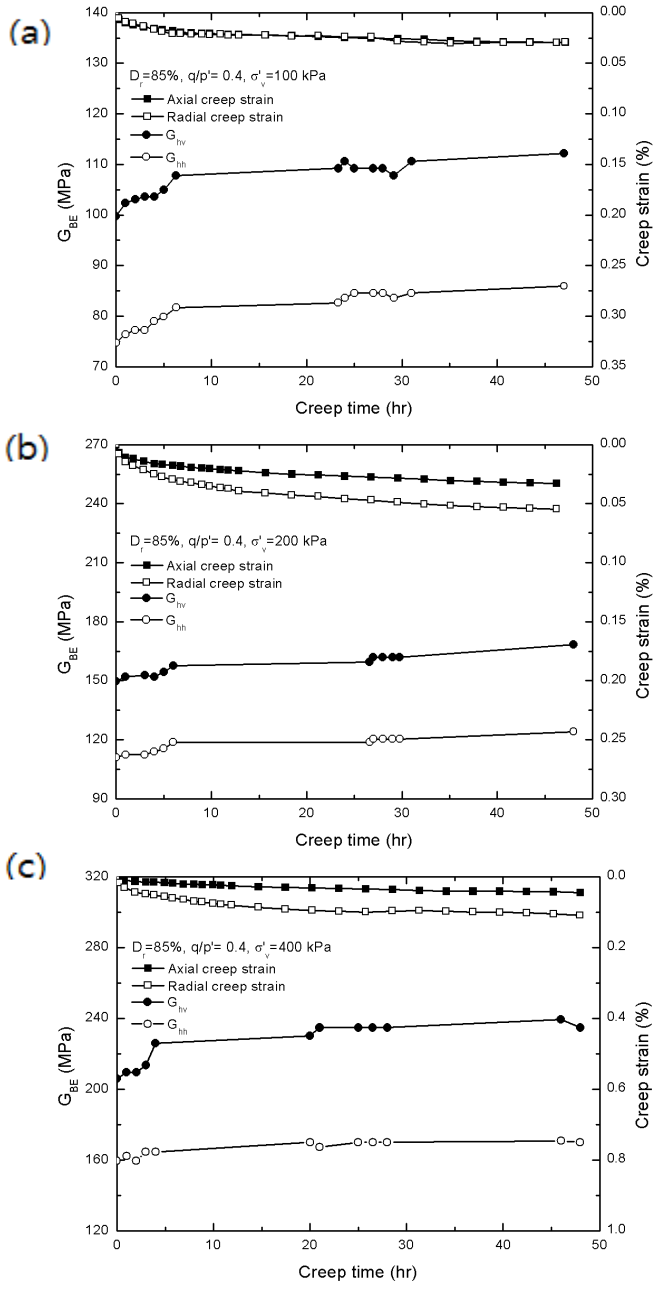

Figure 5.12 Elastic shear stiffness during creep of the specimens with D_r=85%, q/p'=0.4 (a) σ'_v = 100, (b) σ'_v = 200, and (c) σ'_v = 400 kPa

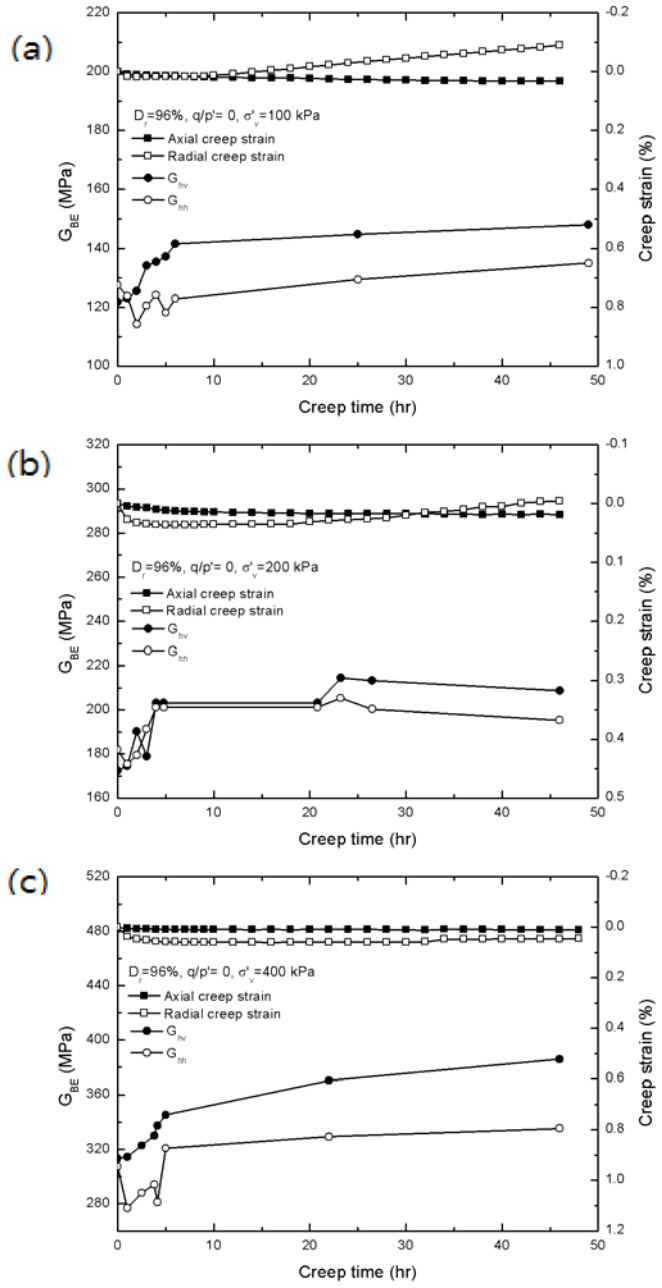

Figure 5.13 Elastic shear stiffness during creep of the specimens with D_r=96%, q/p'=0 (a) σ'_v = 100, (b) σ'_v = 200, and (c) σ'_v = 400 kPa

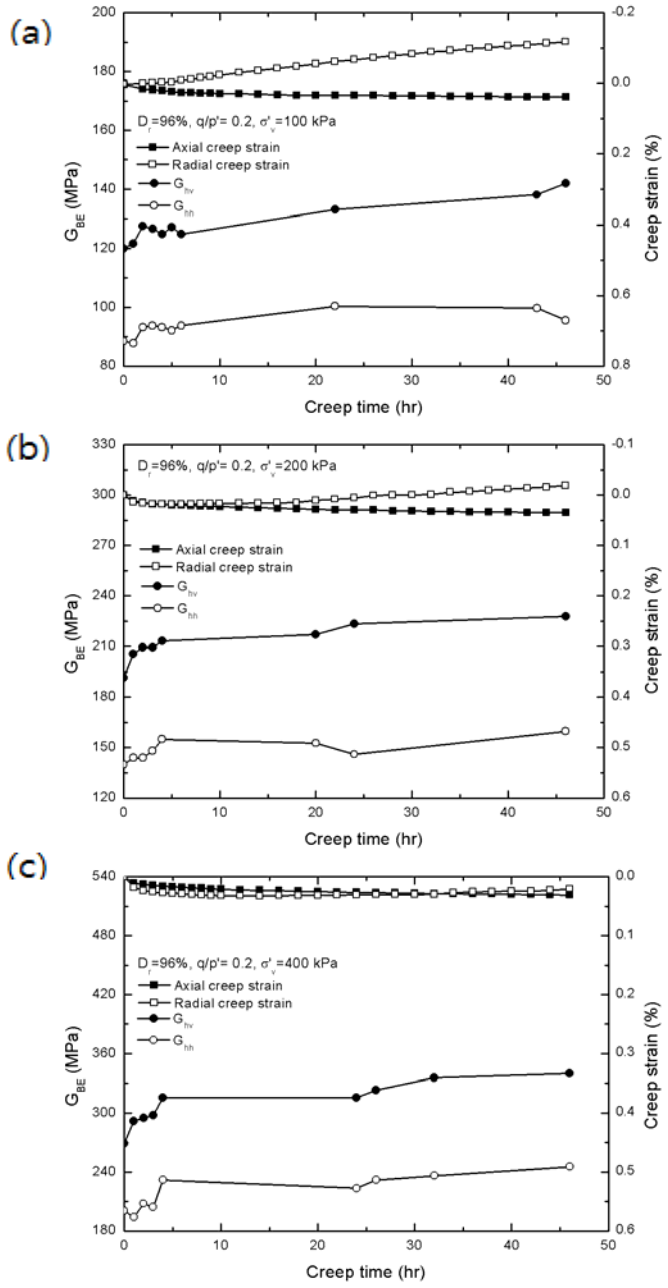

Figure 5.14 Elastic shear stiffness during creep of the specimens with D_r=96%, q/p'=0.2 (a) σ'_v = 100, (b) σ'_v = 200, and (c) σ'_v = 400 kPa

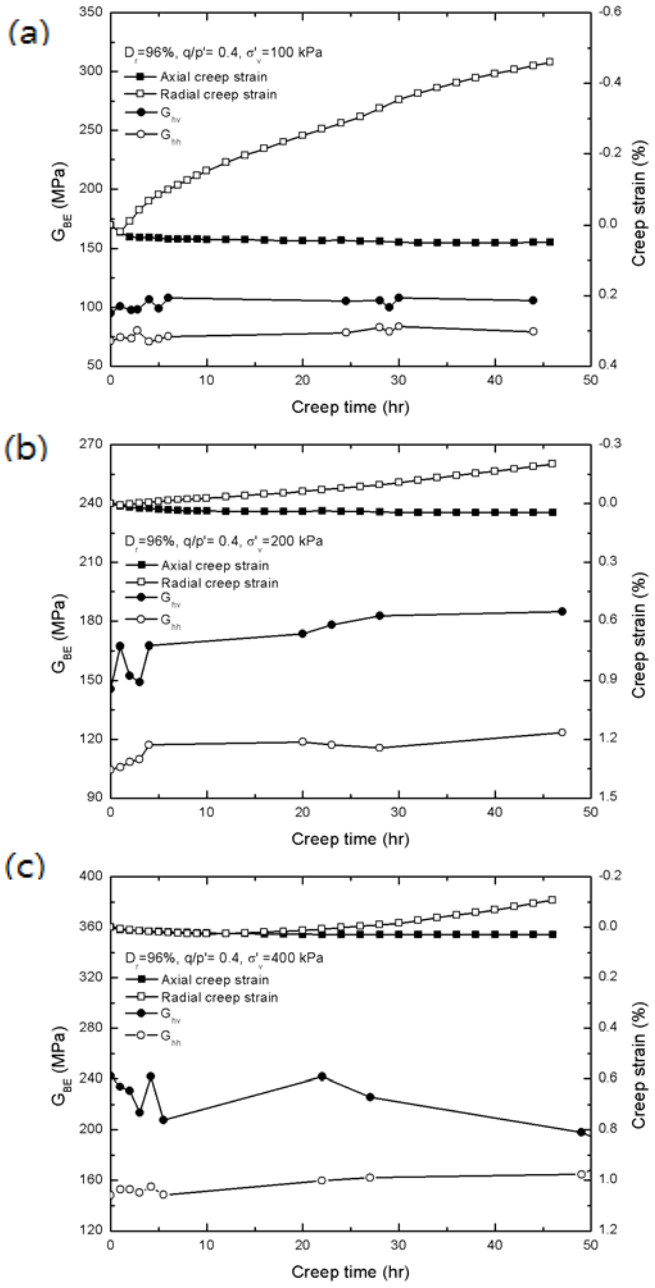

Figure 5.15 Elastic shear stiffness during creep of the specimens with D_r=96%, q/p'=0.4 (a) σ'_v = 100, (b) σ'_v = 200, and (c) σ'_v = 400 kPa

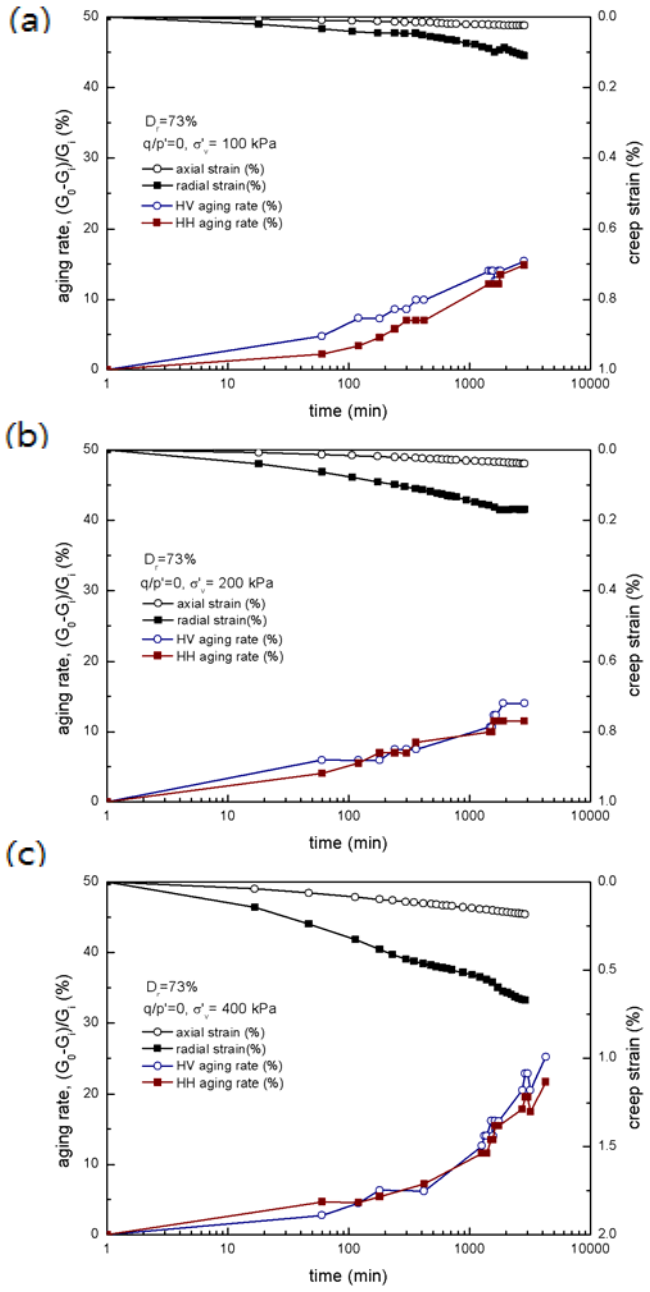

Figure 5.16 Aging rate and creep strain of the specimens with D_r=73%, q/p'=0

(a) σ'_v = 100, (b) σ'_v = 200, and (c) σ'_v = 400 kPa

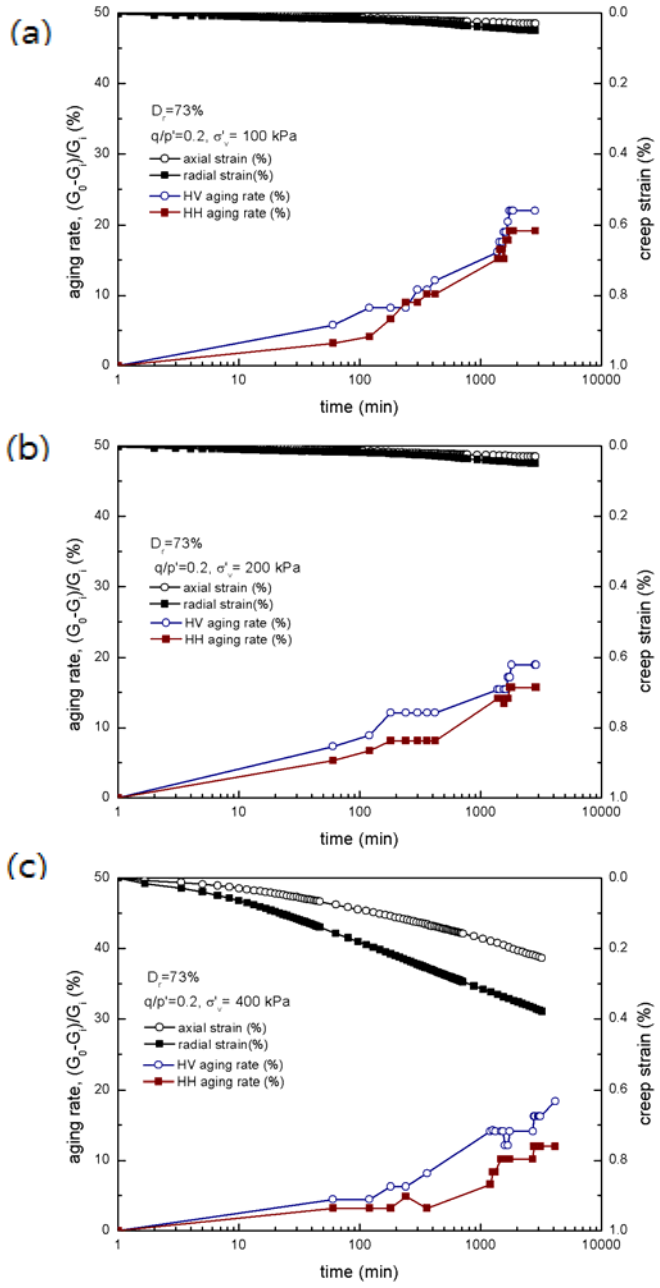

Figure 5.17 Aging rate and creep strain of the specimens with D_r=73%, q/p'=0.2 (a) σ'_v = 100, (b) σ'_v = 200, and (c) σ'_v = 400 kPa

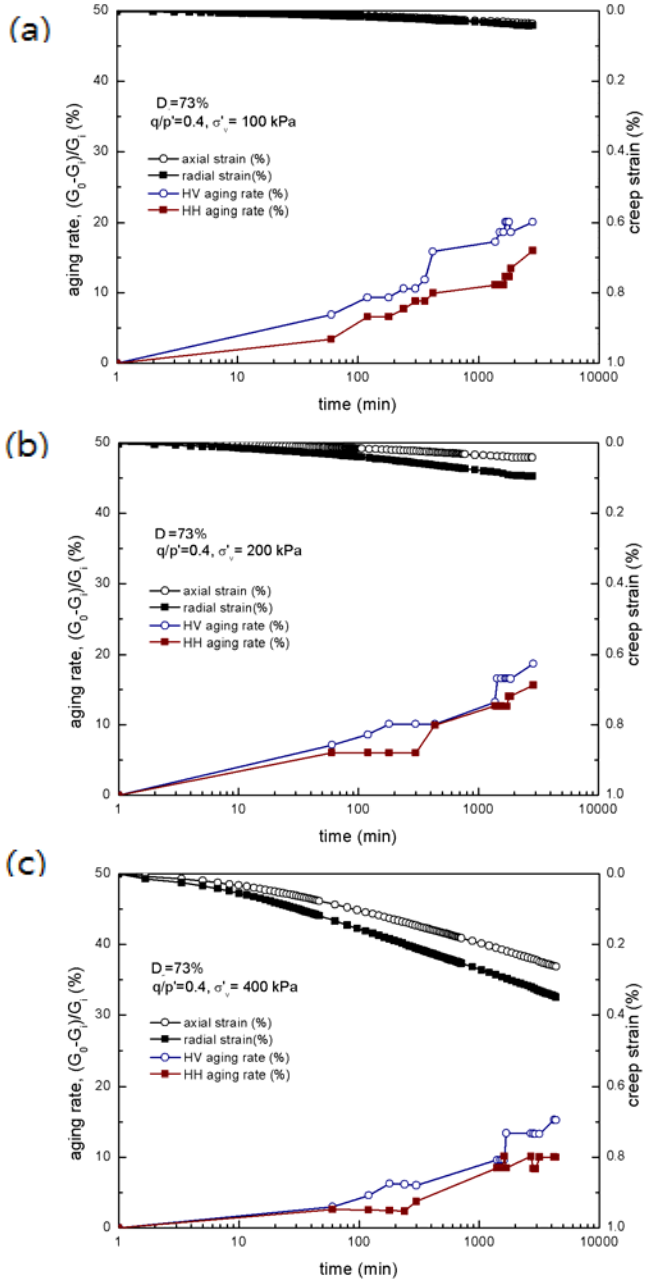

Figure 5.18 Aging rate and creep strain of the specimens with D_r=73%, q/p'=0.4 (a) σ'_v = 100, (b) σ'_v = 200, and (c) σ'_v = 400 kPa

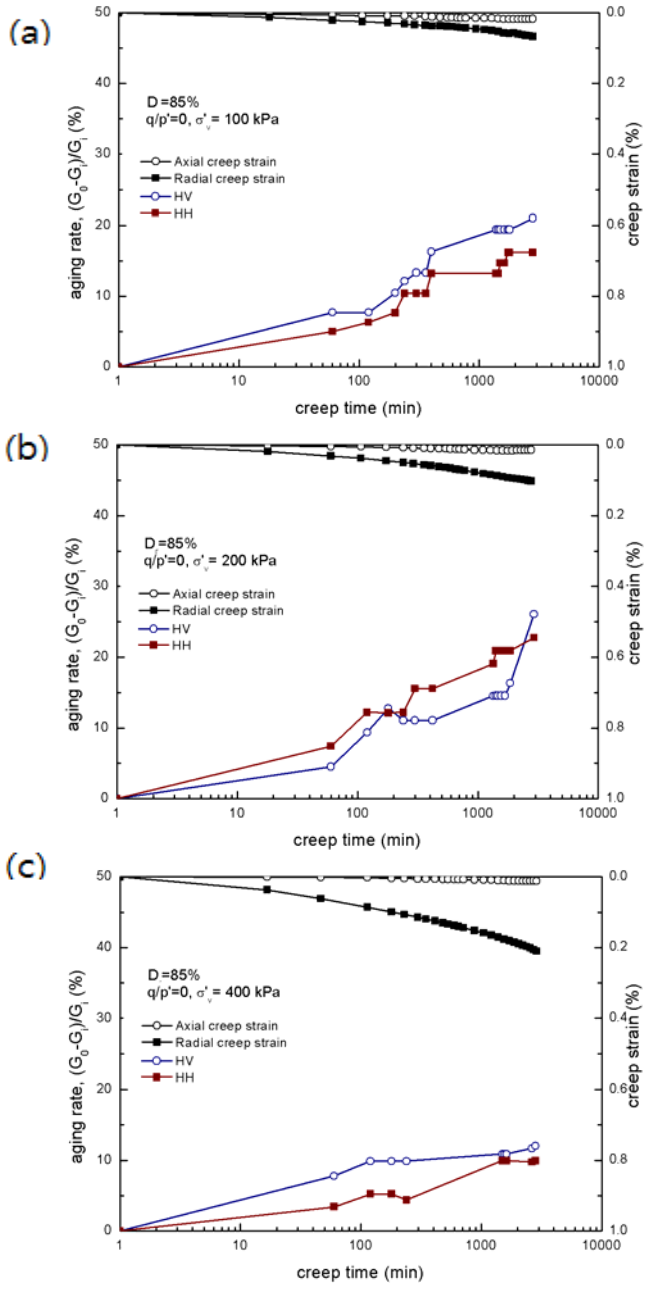

Figure 5.19 Aging rate and creep strain of the specimens with D_r=85%, q/p'=0

(a) σ'_v = 100, (b) σ'_v = 200, and (c) σ'_v = 400 kPa

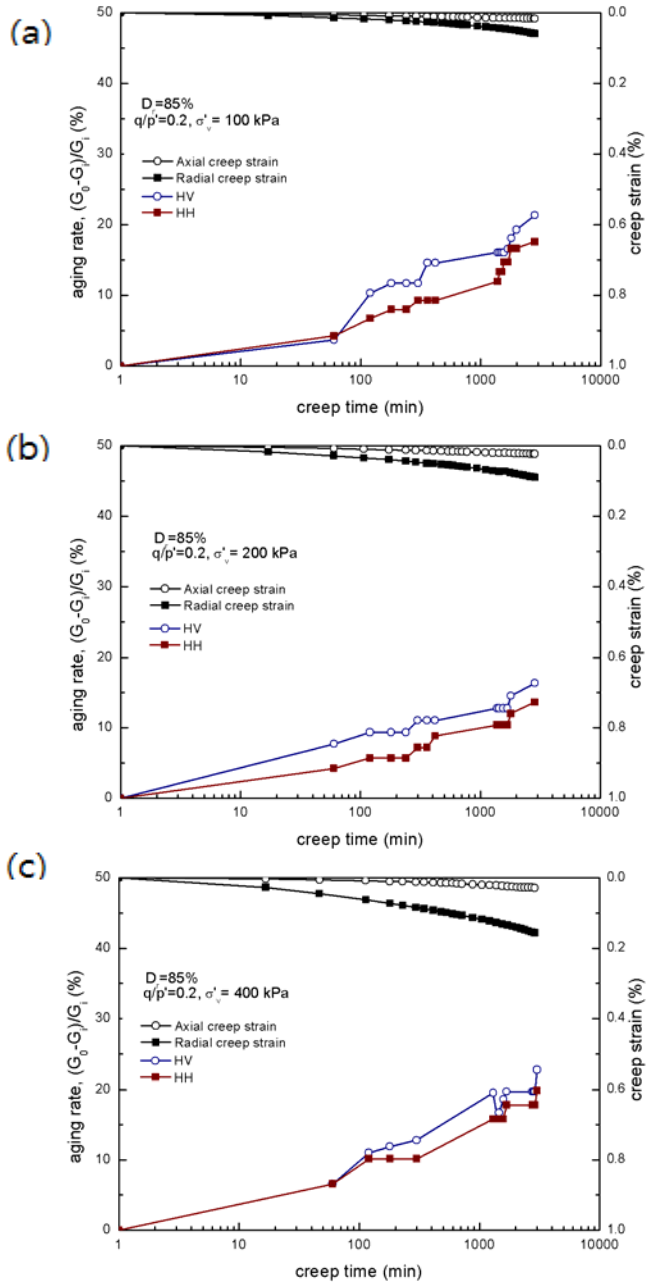

Figure 5.20 Aging rate and creep strain of the specimens with D_r=85%, q/p'=0.2 (a) σ'_v = 100, (b) σ'_v = 200, and (c) σ'_v = 400 kPa

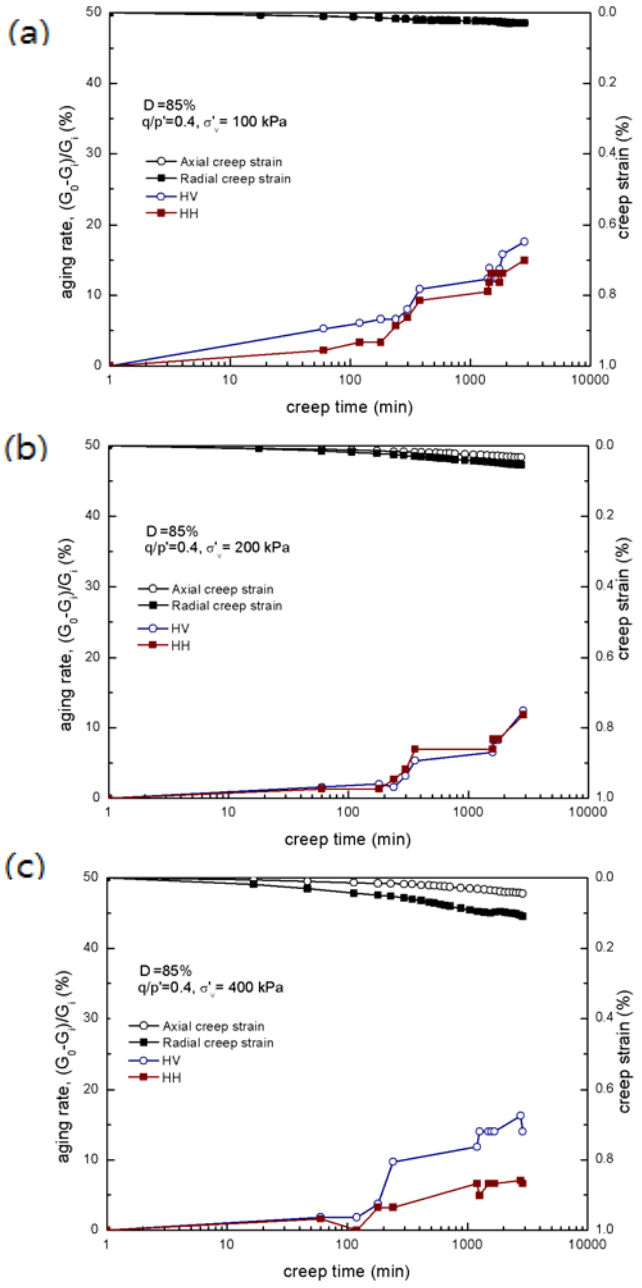

Figure 5.21 Aging rate and creep strain of the specimens with D_r=85%, q/p'=0.4 (a) σ'_v = 100, (b) σ'_v = 200, and (c) σ'_v = 400 kPa

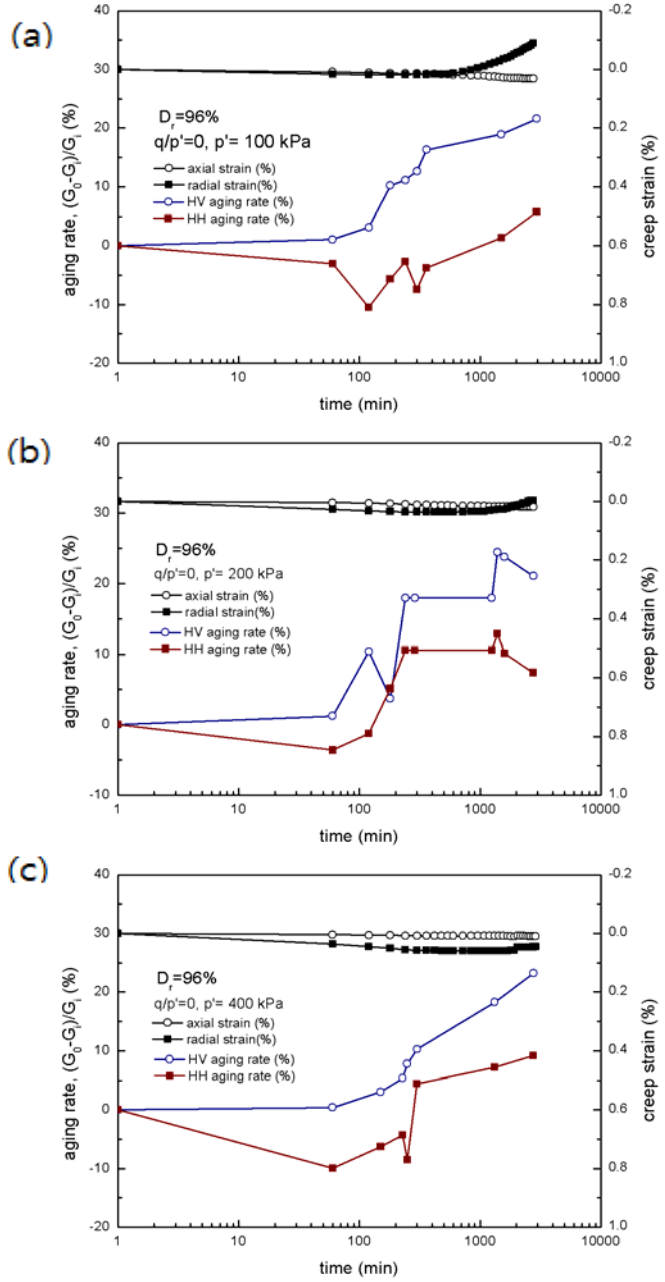

Figure 5.22 Aging rate and creep strain of the specimens with D_r=96%, q/p'=0

(a) σ'_v = 100, (b) σ'_v = 200, and (c) σ'_v = 400 kPa

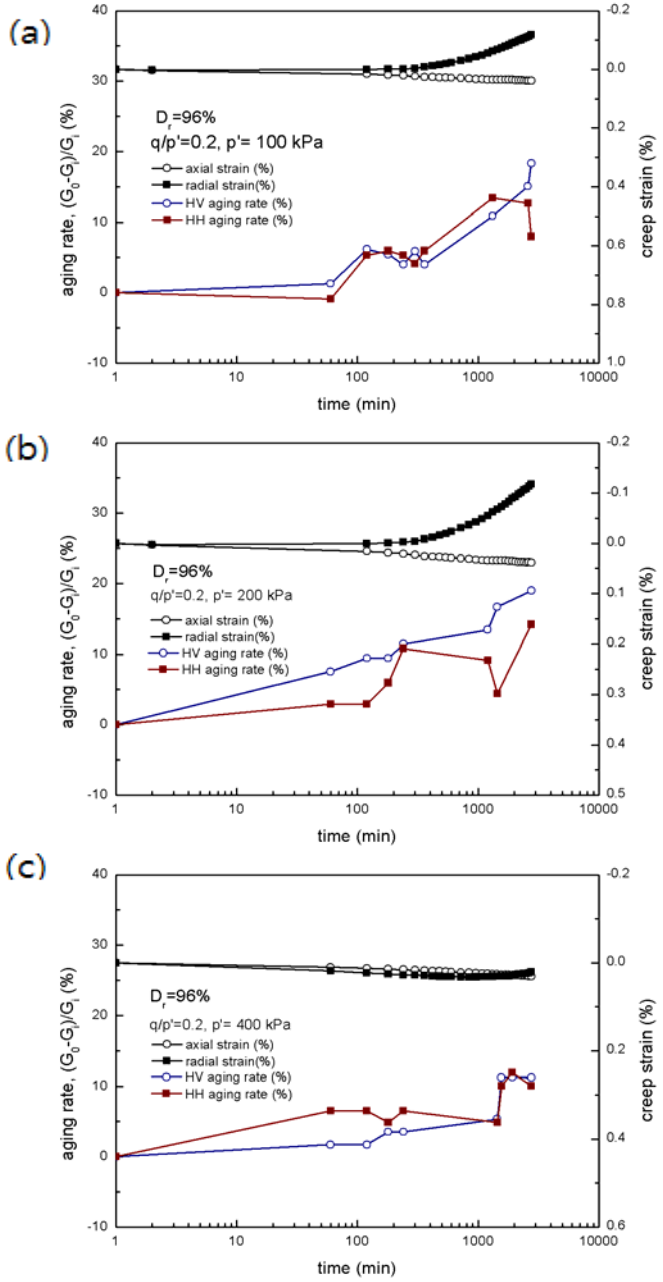

Figure 5.23 Aging rate and creep strain of the specimens with D_r=96%, q/p'=0.2 (a) σ'_v = 100, (b) σ'_v = 200, and (c) σ'_v = 400 kPa

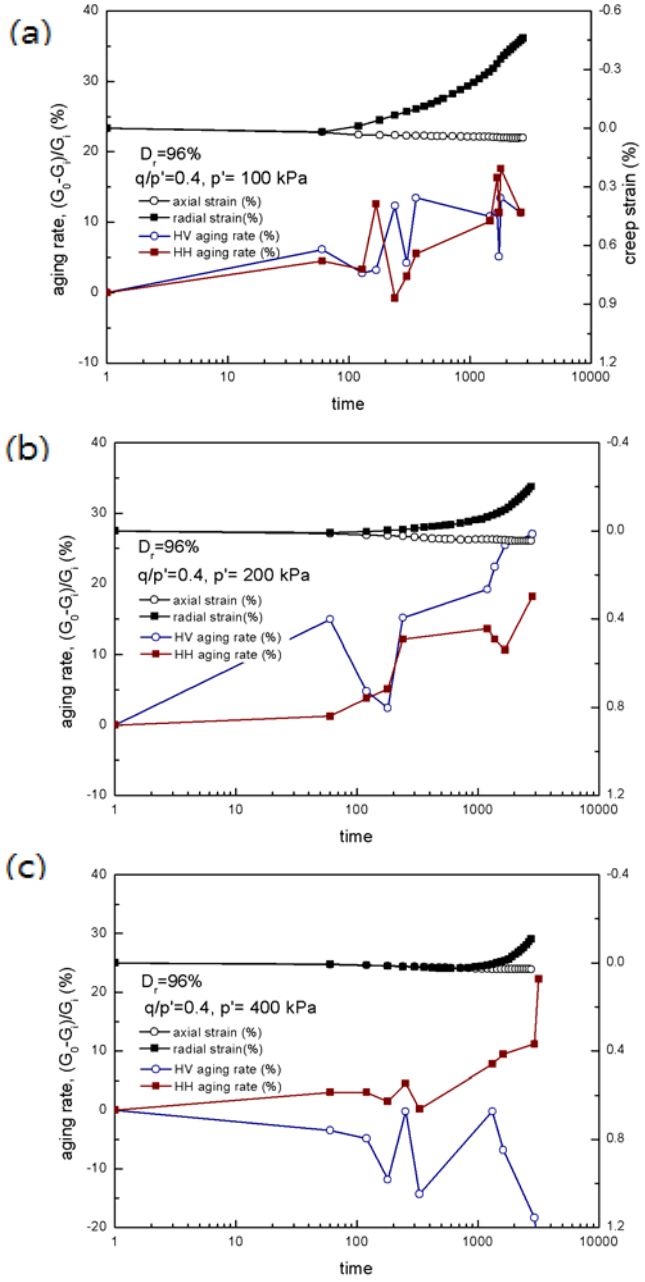

Figure 5.24 Aging rate and creep strain of the specimens with D_r=96%, q/p'=0.4 (a) σ'_v = 100, (b) σ'_v = 200, and (c) σ'_v = 400 kPa

5.5 Quantifying the time-dependent increase in the elastic shear stiffness

Anderson and Stokoe (1978) proposed the following relationships to quantify the time-dependent increase in the elastic shear stiffness given as:

$$I_G = \frac{\Delta G}{\log(t_2 / t_1)} \tag{5.2}$$

$$N_G = \frac{I_G}{G_{1000}} \tag{5.3}$$

where I_G is the coefficient of shear modulus increase with time, t_1 is a reference time, t_2 is specific time of interest, ΔG is the gain in the elastic shear modulus during a period from t_1 to t_2, G_{1000} is the elastic shear modulus measured at 1000 minutes since t_1 under the constant confining pressure, and N_G is the normalized shear modulus increase with time. Values of N_G for clays are reported to have a range of 0.05 ~ 0.25. According to Mesri et al. (1990), N_G for sands varies from 0.01 to 0.03. Figure 5.25 shows values of N_G for various soils including weathered residual soil in Korea. Based on the data shown in Figures 5.7~5.15, the value of N_G for the material used in this study ranges from 0.02 to 0.11. It was found that the values of N_G for weathered residual soil are irrelevant to any stress conditions.

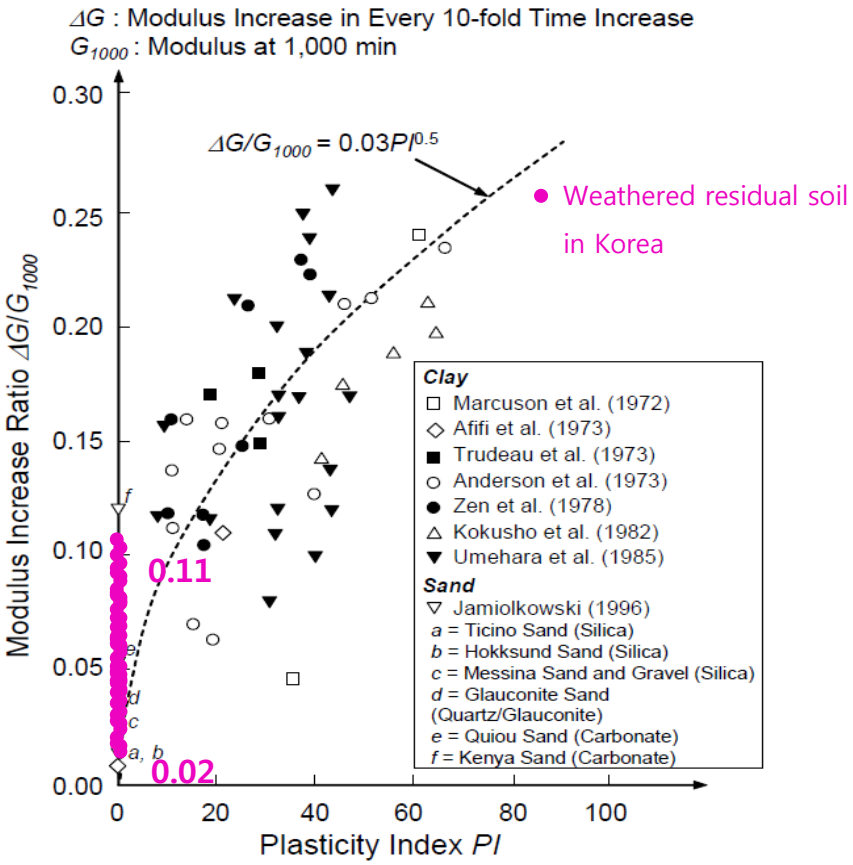

Figure 5.25 Values of N_G for various soils

5.6 Stiffness anisotropy

5.6.1 Introduction

Stiffness anisotropy is one of the important factors in various problems relating to ground deformation. Previous researchers such as Ochiai and Lade (1983) and Kirkgard and Lade (1991 and 1993) experimentally investigated the influence of initial fabric anisotropy on the failure of soils. Despite its significance in geotechnical engineering, the effect of creep on the characteristics of the stiffness anisotropy of weathered residual soil in Korea has not been fully investigated yet. Therefore, a series of triaxial tests of weathered residual soil in Korea with different relative density and shearing conditions were performed. To study the effect of creep on the stiffness anisotropy, the directional shear wave velocities were measured via bi-directional bender element tests. Herein, the stiffness anisotropy were evaluated by the ratio of G_{hv} and G_{hh}.

5.6.2 Effect of stress ratio on stiffness anisotropy

Firstly, the influences of stress conditions on stiffness anisotropy of weathered residual soils were examined. Figure 5.26 represents the stiffness anisotropy defined by the ratio of G_{hv} to G_{hh} for the different initial relative densities. As can be seen in Figure 5.26, under a given relative density, the stiffness anisotropy estimated by the slope of the fitted line increases as the stress ratio, q/p', increases. This means that the high value of the axial stress for the high q/p' value results in faster increase in G_{hv} that measures the elastic shear modulus in the axial direction of the specimen than in the horizontal direction. Subsequently, it can be inferred that the increase of the elastic stiffness is more sensitive to the direction of the major principal stress (axial stress) than that of the minor principal stress (radial stress) during creep.

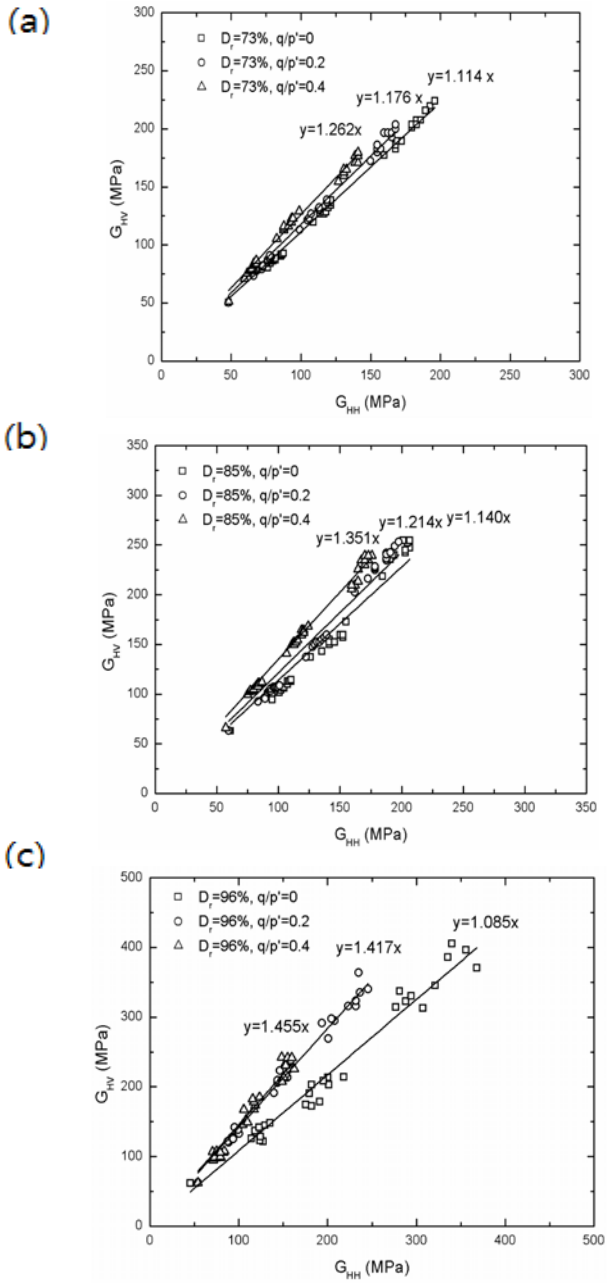

Figure 5.26 Influneces of stress ratio on the results of G_{hv} against G_{hh} (a) D_r= 73%, (b) D_r=85%, and (c) D_r=96%, respectively

5.6.3 Effect of creep on stiffness anisotropy

Recently, relatively abundant researches on effects of effective stresses on stiffness anisotropy have been reported. However, relatively little research on variations in the stiffness anisotropy under constant loading has been conducted. The variations of stiffness anisotropy under constant loading could be a key design factor in the geotechnical engineering. Therefore, it is important to investigate the effect of creep on stiffness anisotropy.

Figure 5.27 shows the change in the stiffness anisotropy before and after 48-hour lasting creep stage. As shown in Figure 5.27, an arrow connects starting and ending values of the stiffness anisotropy at a given stress condition during creep. At an initial confining pressure of 30 kPa, G_{hv} is consistently greater than G_{hh}, possibly due to the effect of the compaction for preparing relatively dense samples used in this study. Figure 5.27 shows that as the initial relative density increases, the increase in the stiffness anisotropy during creep becomes pronounced.

In general, the stiffness anisotropy, G_{hv}/G_{hh}, increases during creep. Together with the preference of the increase in the elastic shear stiffness to the major principal stress direction, variations in the stiffness anisotropy can also be explained by the patterns of straining during creep. It is also interesting that the elastic stiffness decreases during creep at the high stress ratio for the specimen with high density which exhibits the radial dilative strains during creep. As already described in Chapter 4, the creep strain develops more in the horizontal direction than in the vertical. One might

describe that in the horizontal direction the soil deforms radially rather than it alters the internal structure, changing the horizontal elastic stiffness during creep.

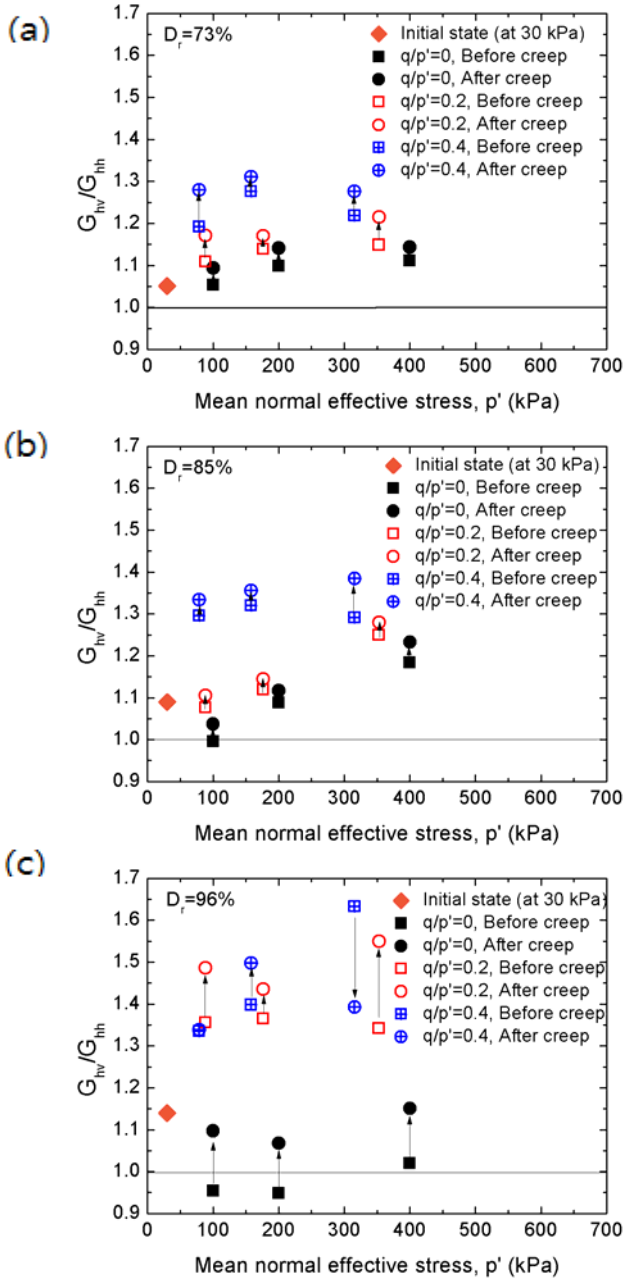

Figure 5.27 Stiffness anisotropy (a) D_r= 73%, (b) D_r=85%, and (c) D_r=96% of samples before creep and after 48-hour lasting creep stage

5.7 Summary

5.7.1 Stiffness obtained from the overall stress-strain curve

Before investigating the stiffness anisotropic evolution during creep, effects of creep on stiffness obtained from the overall stress-strain curve were quantitatively evaluated. In comparison with the slopes of the stress-strain curve before and after the creep stages, the increase in stiffness was clearly detected due to creep for every condition. Also, the normalized stiffness after creep, the slopes which were normalized with the vertical effective stress to remove the stress effect, is higher than that prior to creep. The results showed the effect of creep on the stiffness obtained from overall stress-strain curves obviously.

5.7.2 Stiffness degradation curve

Stiffness degradation curves were examined with the elastic stiffness obtained from the bender element tests. As a result, initial stiffness obtained from bender elements is consistent with the secant modulus of stress-strain curve. Given small strain stiffness and strain dependent stiffness can be used for the advanced deformation analysis in geotechnical engineering with finite element method. Although stiffness degradation curves were obtained for each end of creep stage, further study will be needed to investigate the effect of aging on the degradation curves.

5.7.3 Variations in the elastic shear stiffness during creep

Stiffness gains of weathered residual soil in Korea resulting from creep were illustrated in the previous chapter. 'How does the directional stiffness vary under constant loading?', however, still remains a question. In order to investigate the directional stiffness during creep, bi-directional bender element tests were performed. The results show that continuous change in stiffness during creep is closely related to the patterns in creep deformation. In the case of specimens with the low and medium relative density, compressive creep strain developed and elastic shear moduli (G_{hv} and G_{hh}) generally increase during creep. There was an exception in the G_{hh} of the specimen with the high initial relative density which may relate to the exceptional dilative radial creep strains.

5.7.4 Quantifying the time-dependent increase in the elastic shear stiffness

To quantify the time-dependent increase in the elastic shear stiffness, the equations proposed by Anderson and Stokoe (1978) were used. The value of N_G for the material used in this study ranges from 0.02 to 0.11.

5.7.5 Stiffness anisotropy

Continuous change in the stiffness anisotropy during creep was closely related to the patterns in creep deformation. The specimens with the low

density generated larger compressive axial strains during creep than those with the medium initial density. However, the negative radial strains of the specimens with the high initial density occurred the dilative volume increase during creep. The increase of the elastic stiffness is more sensitive to the direction of the major principal stress (axial stress) than that of the minor principal stress (radial stress) during creep. In the horizontal direction the soil deforms radially rather than it alters the internal structure, and it changes the horizontal elastic stiffness during creep.

Chapter 6. Creep Parameters of Weathered Soil for Numerical Modeling

6.1 Introduction

The purpose of this study is providing the creep parameters based on the triaxial experimental results (Chapter 4) to predict the creep deformations in the actual geotechnical problems. Owing to the creep deformation characteristics highly depending on the initial relative density, the equations modeling the creep deformations were suggested separately.

Based on the empirical curve fitting, optimal creep deformation curves expressed by the stress ratio, the mean normal effective stress, and the time were obtained. Herein, the creep parameters were suggested only for the specimens with monotonic contractive volumetric creep strains. That is because the volumetric response of specimens with the high initial relative density is too complicated to be expressed. For the comparative study, the creep parameters from one-dimensional compression tests were also obtained.

The significance of this research is that providing the creep parameters for the numerical modelling predictions and applying test results directly to construction designs are possible.

The main topics of chapter 6 are as follows:

(1) Theoretical background and

(2) Creep parameters.

6.2 Theoretical background

General stress-strain time function

In order to predict the creep deformations in the field based on the experimental results, it is important to decide the creep model describing the original creep curve.

Generally, the creep strain rate following the power law can be expressed by:

$$\dot{\varepsilon} = Ae^{\alpha D}\left(\frac{t_1}{t}\right)^m \tag{6.1}$$

Where A and m are the creep parameters, α and D are the term of stress conditions, and t_1 is a reference time. A general relationship between strain and time is obtained by integration of Eq. (6.2). Two equations are obtained depending on the value of m.

$$\varepsilon = \varepsilon_1 + \frac{A}{1-m}e^{\alpha D}\left(t^{1-m} - 1\right) \qquad \text{when} \quad m \neq 1 \tag{6.2}$$

$$\varepsilon = \varepsilon_1 + Ae^{\alpha D}\ln t \qquad \text{when} \quad m = 1 \tag{6.3}$$

In this study, a similar equation to the Eq. (6.2) was used as follows in order to illustrate the original creep curves:

$$\varepsilon_{cr} = A * \exp(f(\eta, p'))t^m \tag{6.4}$$

Where A and m are the creep parameters and η is the stress ratio. The advantages of this equation (Eq. 6.4) are simple, basic, and popular formula to obtain the creep parameters.

6.3 Creep parameters

6.3.1 Triaxial test results

Peacock diagram of creep of weathered residual soil

The peacock diagram was firstly constructed by William Hubert Peacock in 1967. With the peacock diagram, the behavior of sand at any void ratio after consolidation and at any confining pressure can be predicted.

In this study, this approach was similarly applied to predict the creep behavior at a given confining pressure. As described in Chapter 4, based on the experimental observations, the existence of creep-free state was proposed. Combining the concept of the creep-free state with volumetric creep strains in a single three-dimensional graph, the peacock diagram for creep of weathered residual soil could be obtained as shown in Figure 6.1. As the stress ratio (q/p') increases from 0 or 0.2 to 0.4, the creep-free surface also moves toward outside of the e-p' plane as in Figure 6.1. This diagram will help understand the relationship between volumetric creep strains and mean normal effective stresses for various values of initial void ratios.

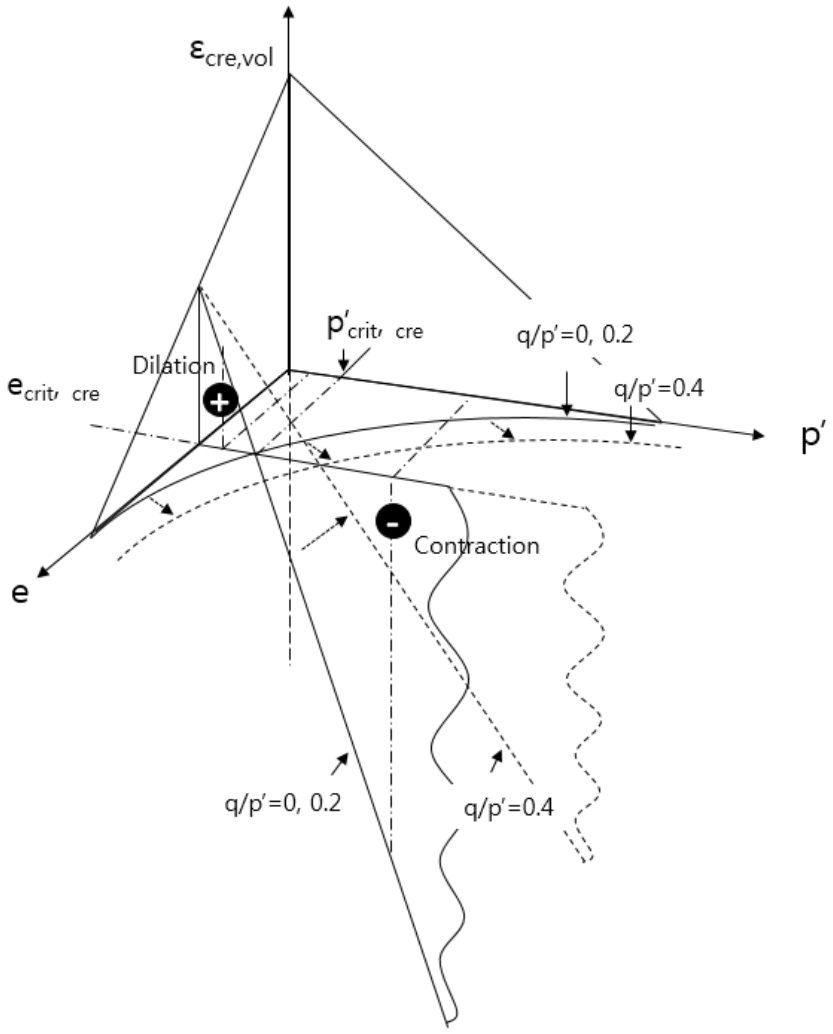

Figure 6.1 Peacock diagram for creep of weathered residual soil in Korea

Creep parameters for volumetric strain

For the specimens showing monotonic contractive volumetric creep strains, i.e., for the specimens with 73% and 85% initial relative density, the volumetric creep strains are expressed as $\varepsilon_{vol} = Cf(p', q/p', ...)t^m$.

Figure 6.2 shows the diagram of creep for the specimens with 73% initial relative density. With this diagram, the volumetric creep deformation can be predicted after 40 hours of creep at any stress conditions. The suggested parameters are available in this range.

For the specimens with relative density of 73%, the volumetric creep parameters A and m, obtained from the best fit lines shown in Figure 6.3 are summarized in Table 6.1. However, with 2 variable parameters, it is hard to find out the relationships between the constant A, and the stress conditions. Herein, to obtain the relationships between the creep parameter A, and stress conditions, the value of m was fixed as the average value of m.

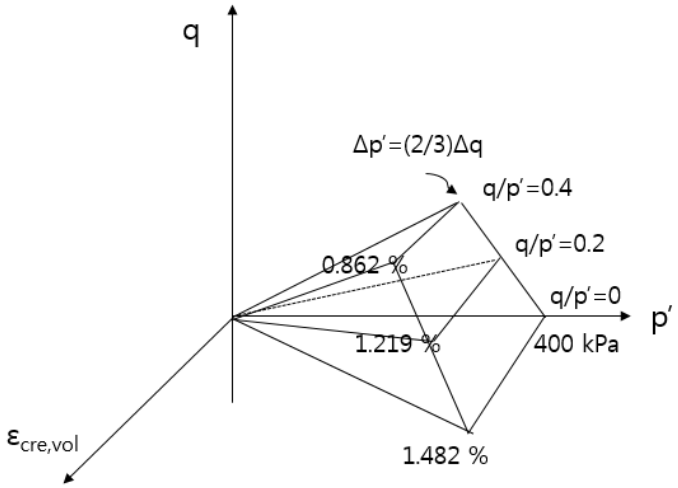

Figure 6.2 Diagram of volumetric creep for the specimens with 73% initial relative density

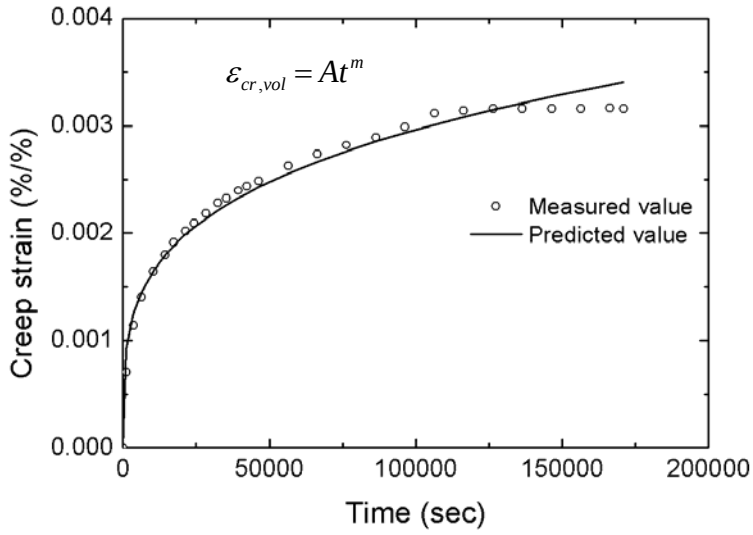

Figure 6.3 Prediction of volumetric creep strain

Table 6.1 Volumetric creep parameters (a) A and (b) m, for the specimens with initial relative density of 73%

(a)

q/p' \ $\sigma'_v(kPa)$	100	200	400
q/p'=0	4.50E-05	2.24E-04	1.02E-03
q/p'=0.2	4.49E-05	1.75E-04	8.69E-04
q/p'=0.4	4.53E-05	9.33E-05	6.46E-04

(b)

q/p' \ $\sigma'_v(kPa)$	100	200	400
q/p'=0	0.331	0.240	0.225
q/p'=0.2	0.314	0.245	0.223
q/p'=0.4	0.281	0.252	0.219

The averaged value of m for the specimens with 73% initial relative density is 0.259. Applying the averaged value of m, the new volumetric creep parameter A', can be obtained for the every stress condition as listed in Table 6.2. The relationships between the new creep parameter A', and the mean normal effective stress are plotted in Figure 6.4.

Table 6.2 New volumetric creep parameters A', of the specimens with initial relative density of 73%

$\sigma'_v\,(kPa)$ / q/p'	100	200	400
q/p'=0	1.03E-04	1.81E-04	6.94E-04
q/p'=0.2	8.39E-05	1.50E-04	5.75E-04
q/p'=0.4	5.83E-05	8.64E-05	4.12E-04

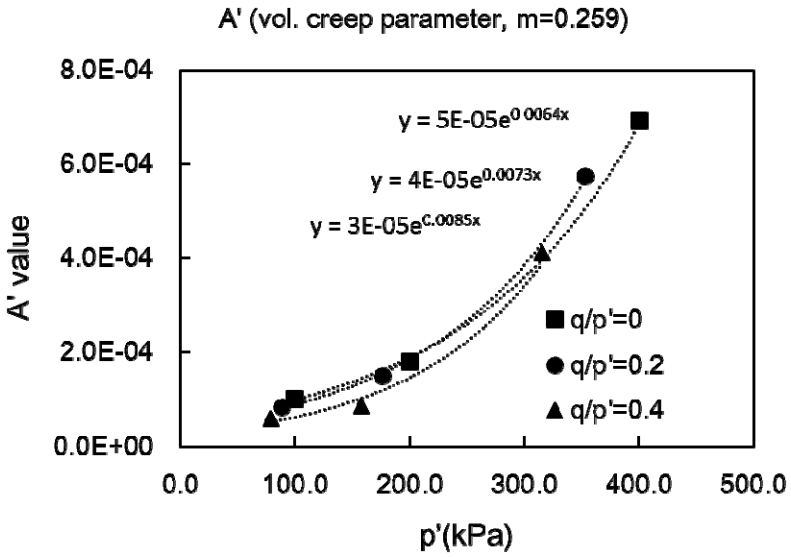

Figure 6.4 Relationships between the creep parameter (A') and p' for the specimens with D_r=73%

Based on the results of regression as in Figure 6.4, the volumetric creep strain for the specimens of initial relative density of 73% can be expressed as the following equation:

$$\varepsilon_{vol} = (5\times10^{-5})(1-\eta)\exp((0.0064+0.0045\eta)\times p')\times t^{0.259} \qquad (6.1)$$

where, $\eta = q / p'$ and t=time in sec.

Figures 6.5~6.7 compare the predicted volumetric creep deformations with the measured experimental data as described in Chapter 4. It can be concluded that the proposed creep model, Eq. 6.1, is well predicting the original creep curve of 73% of the initial relative density of weathered residual soil.

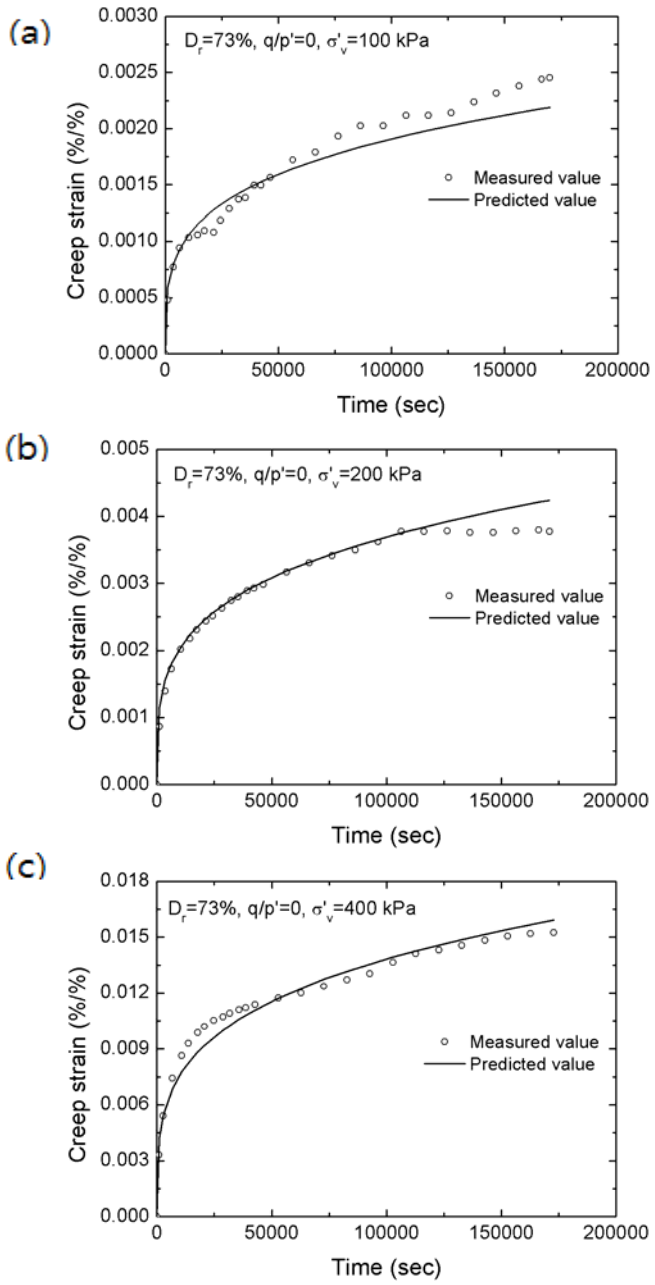

Figure 6.5 Comparison of predicted and measured volumetric creep strain of the specimens with D_r=73% and q/p'=0

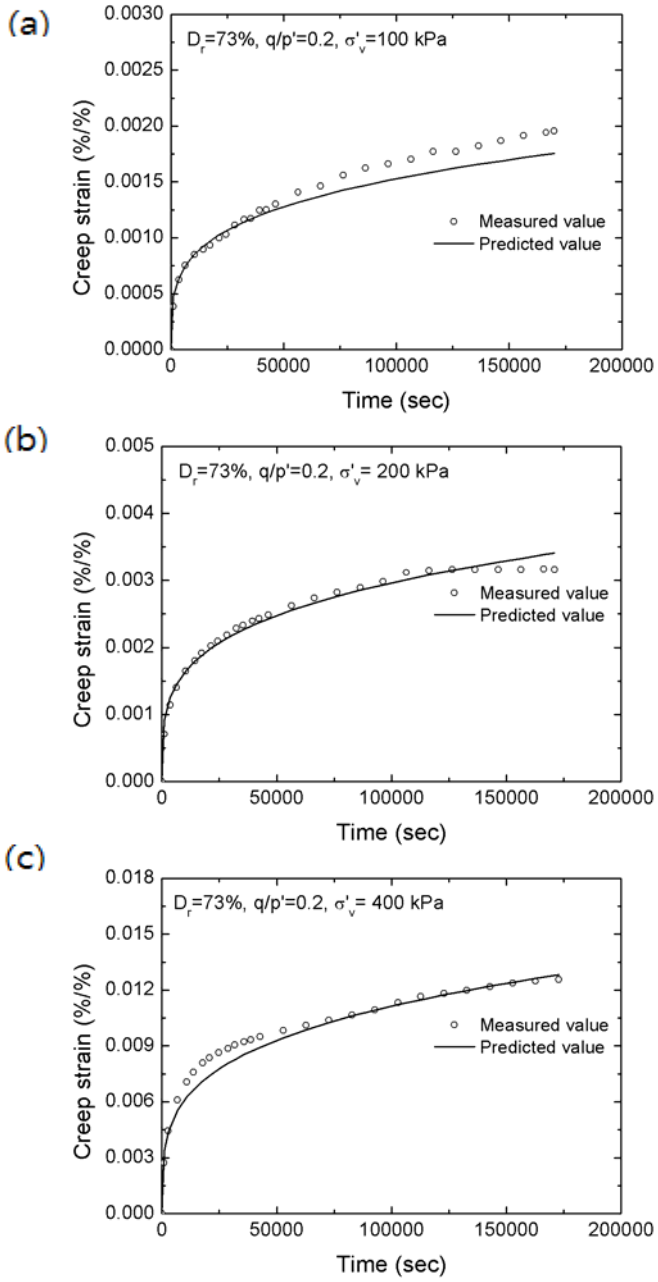

Figure 6.6 Comparison of predicted and measured volumetric creep strain of the specimens with D_r=73% and q/p'=0.2

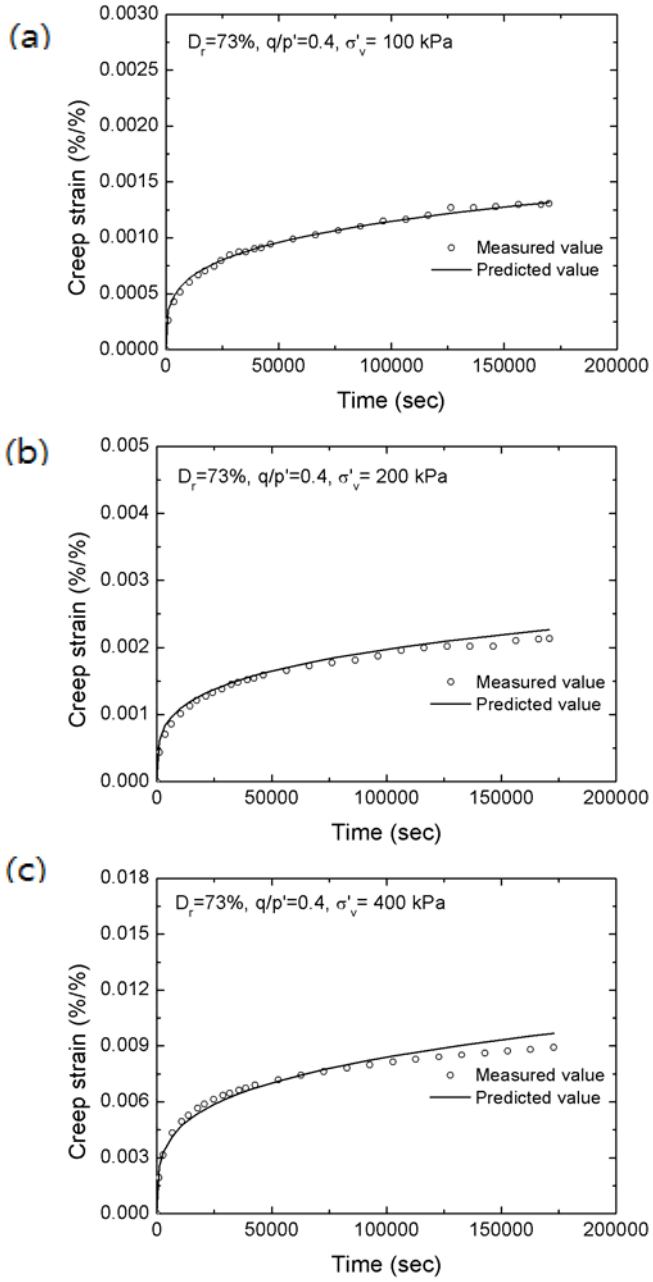

Figure 6.7 Comparison of predicted and measured volumetric creep strain of the specimens with D_r=73% and q/p'=0.4

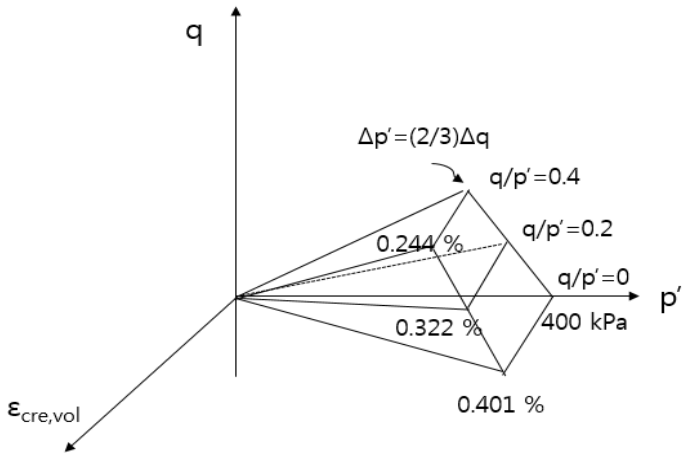

Figure 6.8 Diagram of volumetric creep for the specimens with 85% initial relative density

Figure 6.8 shows the diagram of creep for the specimens with 85% initial relative density. With this diagram, the volumetric creep deformation can be predicted after 40 hours of creep at any stress conditions. The volumetric creep parameters of the specimens of initial relative density of 85% were obtained in the same way as the specimens with relative density of 73%. First, for the specimens with relative density of 85%, the volumetric creep parameters A and m, obtained from the best fit lines shown in Figure 6.3 are listed in Table 6.3. As mentioned earlier, however, with 2 variable parameters, it is hard to find out the relationships between the constant, A, and the stress conditions. Herein, to obtain the relationships between the creep parameter A, and stress conditions, the value of m was fixed as the average value of m.

Table 6.3 Volumetric creep parameters (a) A and (b) m, for the specimens with initial relative density of 85%

(a)

$\sigma'_v\,(kPa)$ / q/p'	100	200	400
q/p'=0	3.50E-05	6.96E-05	1.46E-04
q/p'=0.2	4.49E-05	1.75E-04	8.69E-04
q/p'=0.4	3.93E-05	3.47E-05	9.56E-05

(b)

$\sigma'_v\,(kPa)$ / q/p'	100	200	400
q/p'=0	0.310	0.290	0.279
q/p'=0.2	0.285	0.301	0.278
q/p'=0.4	0.261	0.312	0.276

The averaged value of m for the specimens with 85% initial relative density is 0.280. Applying the averaged value of m, the new volumetric creep parameter A', can be obtained regarding the every stress condition as listed in Table 6.4. The relationships between the new creep parameter A', and the mean normal effective stress are plotted in Figure 6.9.

Table 6.4 New volumetric creep parameters A', of the specimens with initial relative density of 85%

$\sigma'_v\,(kPa)$ / q/p'	100	200	400
q/p'=0	4.98E-05	7.88E-05	1.47E-04
q/p'=0.2	4.09E-05	6.47E-05	1.20E-04
q/p'=0.4	3.20E-05	5.07E-05	9.22E-05

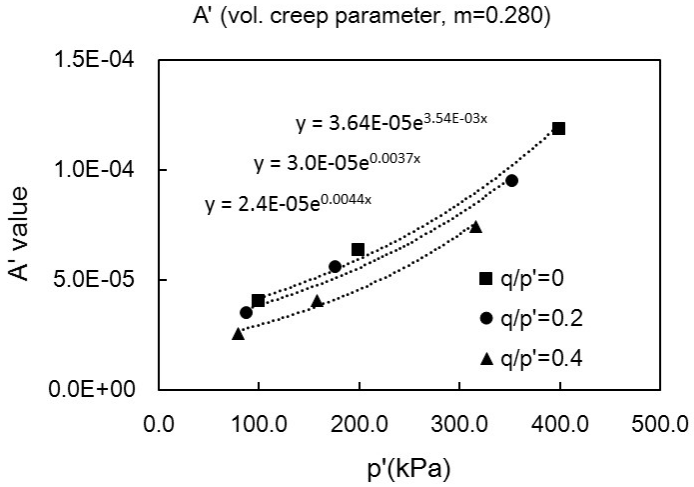

Figure 6.9 Relationships between the creep parameter (A') and p' for the specimens with D_r=85%

Based on the results of regression as in Figure 6.9, the volumetric creep strain for the specimens of initial relative density of 85% can be expressed as the following equation:

$$\varepsilon_{vol} = (3\times10^{-5})(1.2-\eta)\exp((0.0035+0.0025\eta)\times p')\times t^{0.280} \qquad (6.2)$$

where, $\eta = q / p'$ and t=time in sec.

Figures 6.10~6.12 compare the predicted volumetric creep deformations with the measured experimental data as described in Chapter 4. It can be concluded that the proposed creep model, Eq. 6.2, is well predicting the original creep curve of 85% of the initial relative density of weathered residual soil. The limitation of this study is that the provided creep parameters can be applied only for the contractive creep case. To estimate the overall creep behavior (both contractive creep and expansion creep behavior) with the numerical modeling, a further extended modeling is needed.

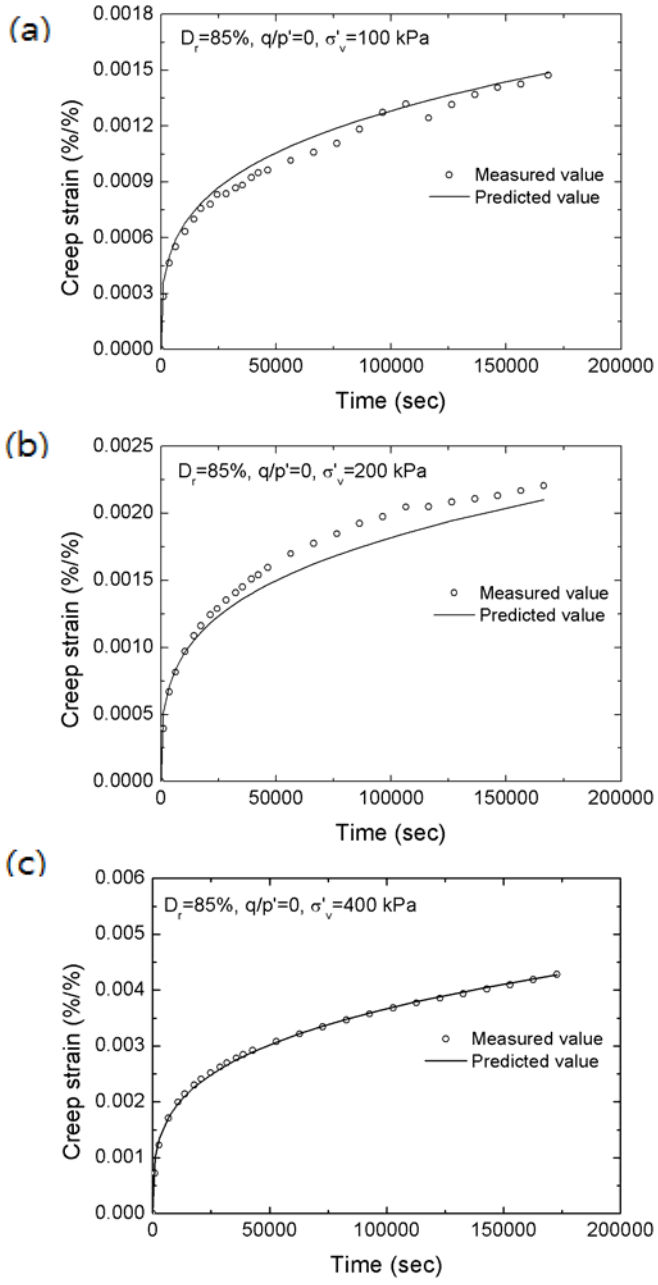

Figure 6.10 Comparison of predicted and measured volumetric creep strain of the specimens with D_r=85% and q/p'=0

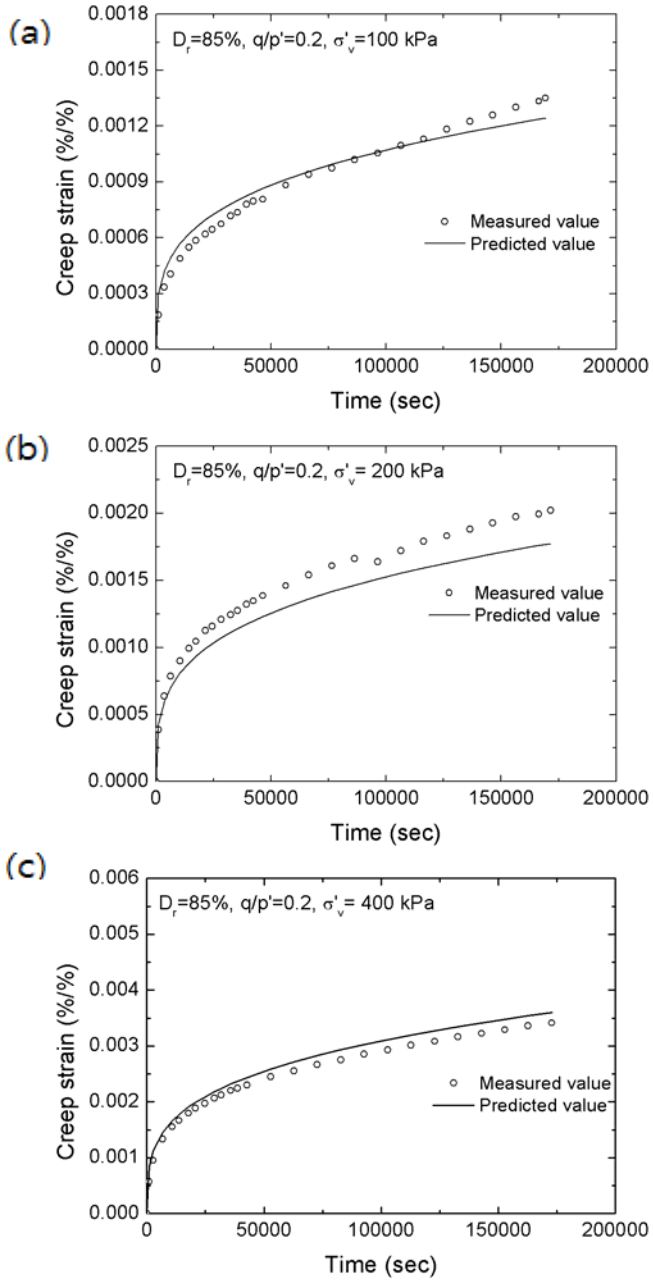

Figure 6.11 Comparison of predicted and measured volumetric creep strain of the specimens with D_r=85% and q/p'=0.2

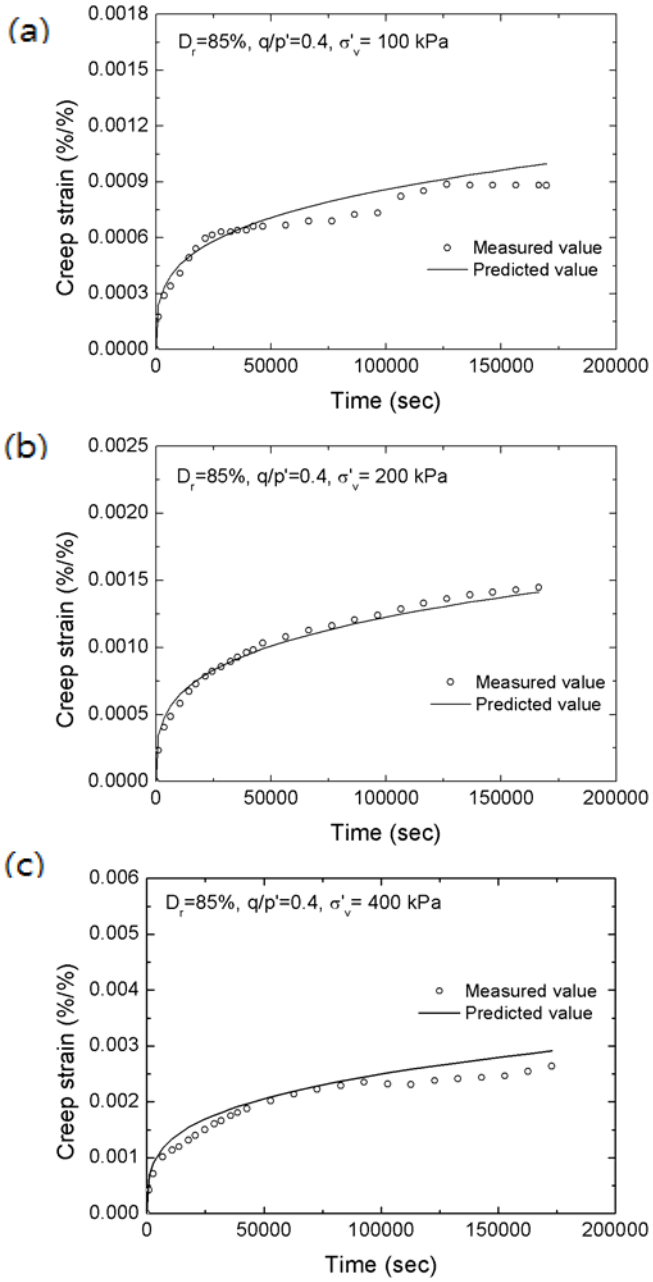

Figure 6.12 Comparison of predicted and measured volumetric creep strain of the specimens with D_r=85% and q/p'=0.4

Creep parameters for shear strain

For the numerical analysis predicting creep deformations, the information of deviator deformation is concurrently necessary with the volumetric deformations. Therefore, for the specimens showing monotonic negative shear creep strains, i.e., the specimens with D_r= 73% and 85%, the shear creep strains are expressed as $\varepsilon_{sh} = -Cf(p', q/p', ...)t^m$.

Figure 6.13 shows the diagram of shear creep for the specimens with 73% initial relative density. With this diagram, the shear creep deformation can be predicted after 40 hours of creep at any stress conditions. The suggested parameters are available in this range.

For the specimens with relative density of 73%, the shear creep parameters A and m, obtained from the best fit lines shown in Figure 6.14 are summarized in Table 6.5. As mentioned earlier, with 2 variable parameters, it is hard to find out the relationships between the constant A, and the stress conditions. Herein, to obtain the relationships between the creep parameter A, and stress conditions, the value of m was fixed as the average value of m.

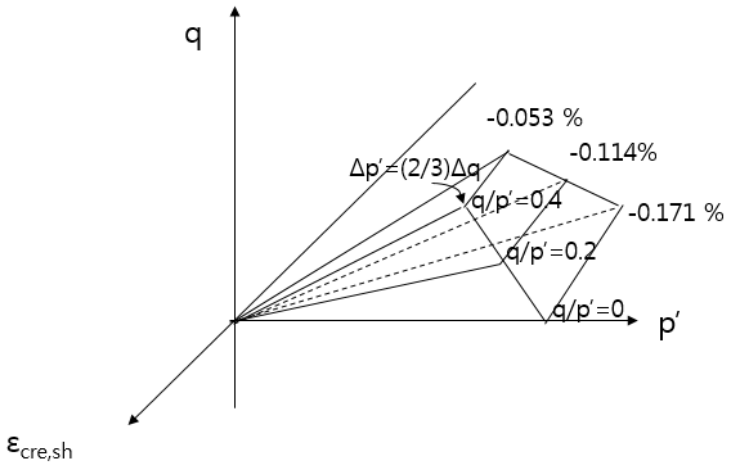

Figure 6.13 Diagram of shear creep for the specimens with 73% initial relative density

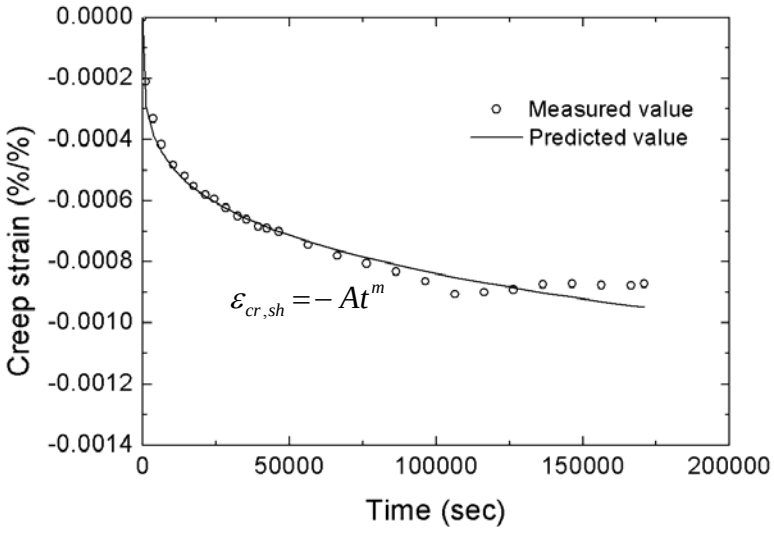

Figure 6.14 Prediction of shear strain

Table 6.5 Shear creep parameters (a) A and (b) m, for the specimens with initial relative density of 73%

(a)

q/p' \ $\sigma'_v(kPa)$	100	200	400
q/p'=0	-5.16E-06	-5.73E-05	-2.28E-04
q/p'=0.2	-2.55E-06	-3.60E-05	-1.96E-04
q/p'=0.4	-1.31E-06	-1.97E-05	-1.08E-04

(b)

q/p' \ $\sigma'_v(kPa)$	100	200	400
q/p'=0	0.389	0.233	0.221
q/p'=0.2	0.406	0.241	0.199
q/p'=0.4	0.333	0.244	0.136

The averaged value of m for the shear creep strains of specimens with 73% initial relative density is 0.267. Applying the averaged value of m, the new shear creep parameter A', can be obtained for the every stress condition as listed in Table 6.6. The relationships between the new creep parameter A', and the mean normal effective stress are plotted in Figure 6.15.

Table 6.6 New shear creep parameters A', of the specimens with initial relative density of 73%

$\sigma'_v(kPa)$ / q/p'	100	200	400
q/p'=0	-2.07E-05	-3.60E-05	-1.35E-04
q/p'=0.2	-1.25E-05	-2.78E-05	-9.02E-05
q/p'=0.4	-2.81E-06	-1.52E-05	-2.45E-05

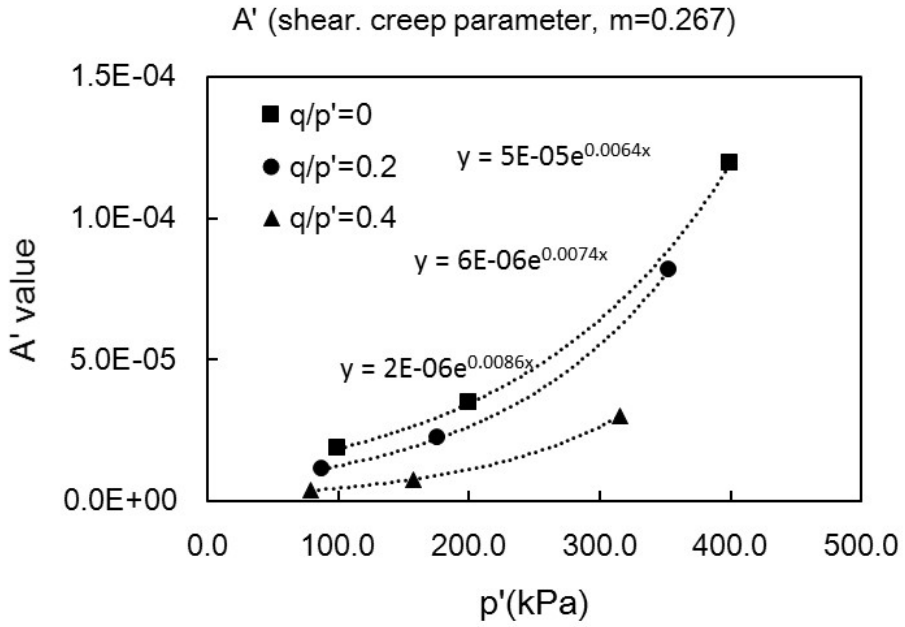

Figure 6.15 Relationships between the shear creep parameter (A') and p' for the specimens with D_r=73%

Based on the results of regression as in Figure 6.15, the shear creep strain for the specimens of initial relative density of 73% can be expressed as the following equation:

$$\varepsilon_{sh} = -(1\times10^{-5})(1-2\eta)\exp((0.0062+0.006\eta)\times p')\times t^{0.267} \qquad (6.3)$$

where, $\eta = q/p'$ t=time in sec.

Figures 6.16~6.18 compare the predicted shear creep deformations with the measured experimental data as described in Chapter 4. It can be concluded that the proposed creep model, Eq. 6.3, is relatively well predicting the original shear creep curve of 73% initial relative density of weathered residual soil except for the case of 0.2 stress ratio with 200 kPa vertical effective stress.

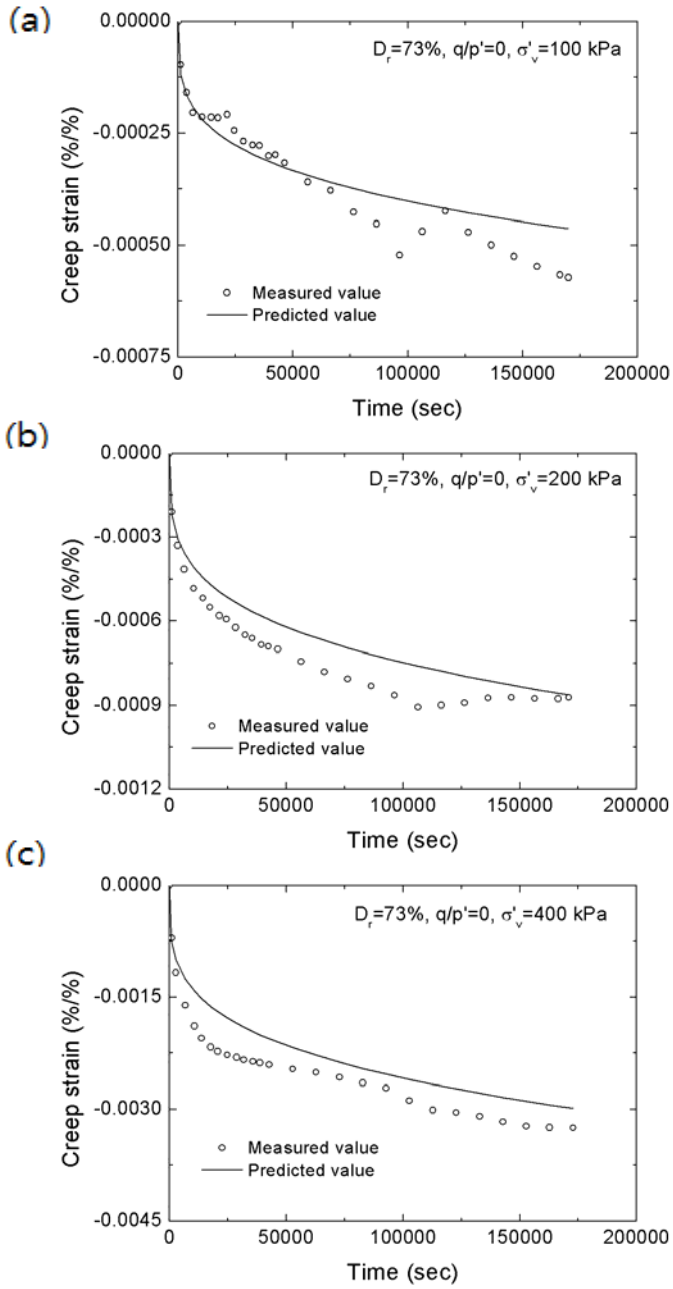

Figure 6.16 Comparison of predicted and measured shear creep strain of the specimens with D_r=73% and q/p'=0

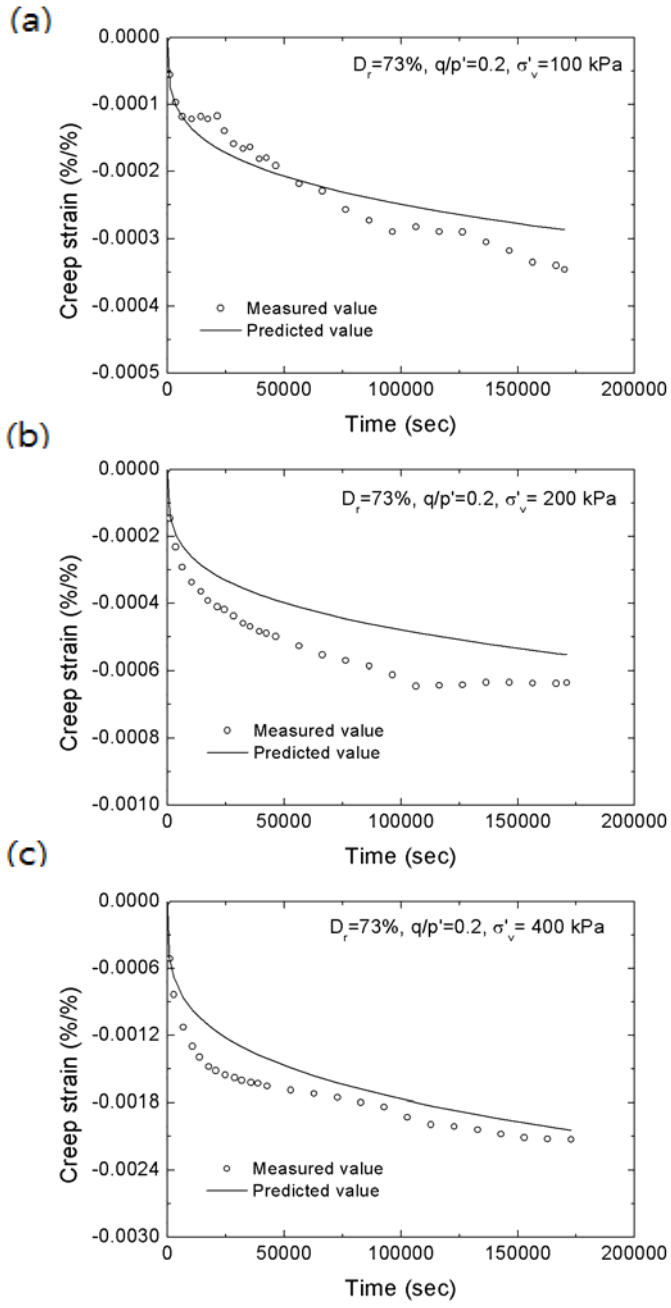

Figure 6.17 Comparison of predicted and measured shear creep strain of the specimens with D_r=73% and q/p'=0.2

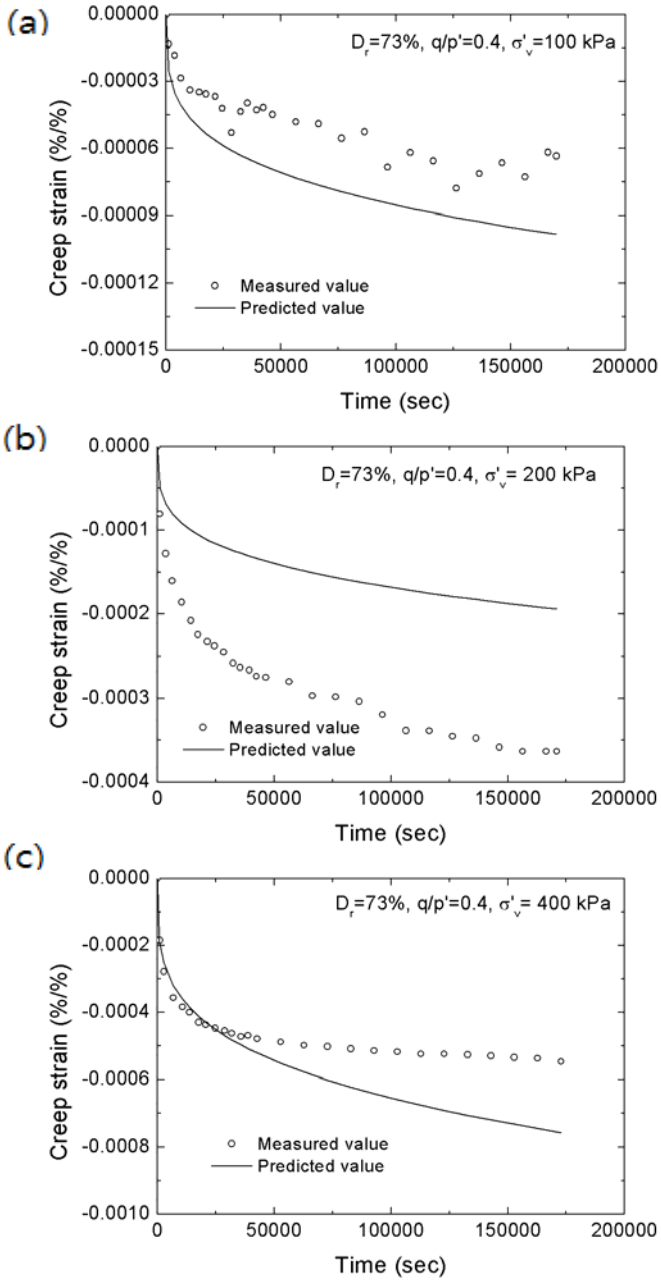

Figure 6.18 Comparison of predicted and measured shear creep strain of the specimens with D_r=73% and q/p'=0.4

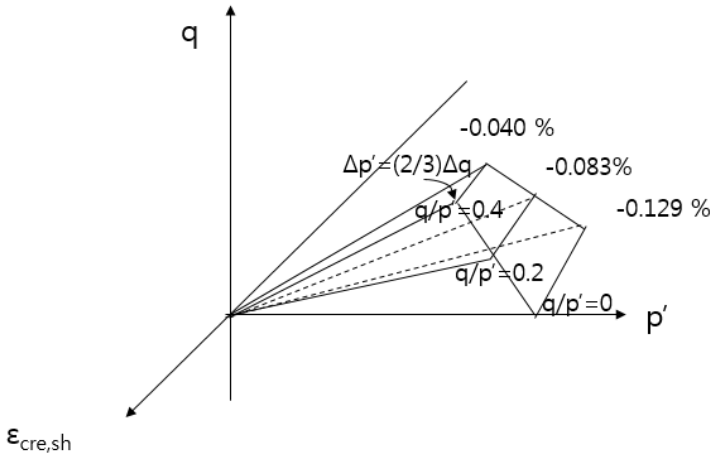

Figure 6.19 Diagram of shear creep for the specimens with 85% initial relative density

Figure 6.19 describes the shear creep diagram for the specimens with 85% initial relative density. With this diagram, the shear creep deformation can be predicted after 40 hours of creep at any stress conditions. For the specimens with relative density of 85%, the shear creep parameters A and m, obtained from the best fit lines as shown in Figure 6.14 are listed in Table 6.7. As mentioned earlier, to find out the relationships between the constant A, and the stress conditions, the average value of m was obtained as 0.329 for the shear creep strains of the specimens with initial relative density of 85%.

Table 6.7 Shear creep parameters (a) A and (b) m, for the specimens with initial relative density of 85%

(a)

$\sigma'_v(kPa)$ / q/p'	100	200	400
q/p'=0	4.50E-05	2.24E-04	1.02E-03
q/p'=0.2	4.49E-05	1.75E-04	8.69E-04
q/p'=0.4	4.53E-05	9.33E-05	6.46E-04

(b)

$\sigma'_v(kPa)$ / q/p'	100	200	400
q/p'=0	0.331	0.240	0.225
q/p'=0.2	0.314	0.245	0.223
q/p'=0.4	0.281	0.252	0.219

Applying the fixed value of m as 0.329, the new shear creep parameters A', can be taken as summarized in Table 6.8. The relationships between the new shear creep parameter A', and the mean normal effective stress are plotted in Figure 6.20.

Table 6.8 New shear creep parameters A', of the specimens with initial relative density of 85%

$\sigma'_v(kPa)$ / q/p'	100	200	400
q/p'=0	-6.23E-06	-1.14E-05	-2.71E-05
q/p'=0.2	-3.17E-06	-6.98E-06	-1.82E-05
q/p'=0.4	-1.20E-07	-2.60E-06	-9.18E-06

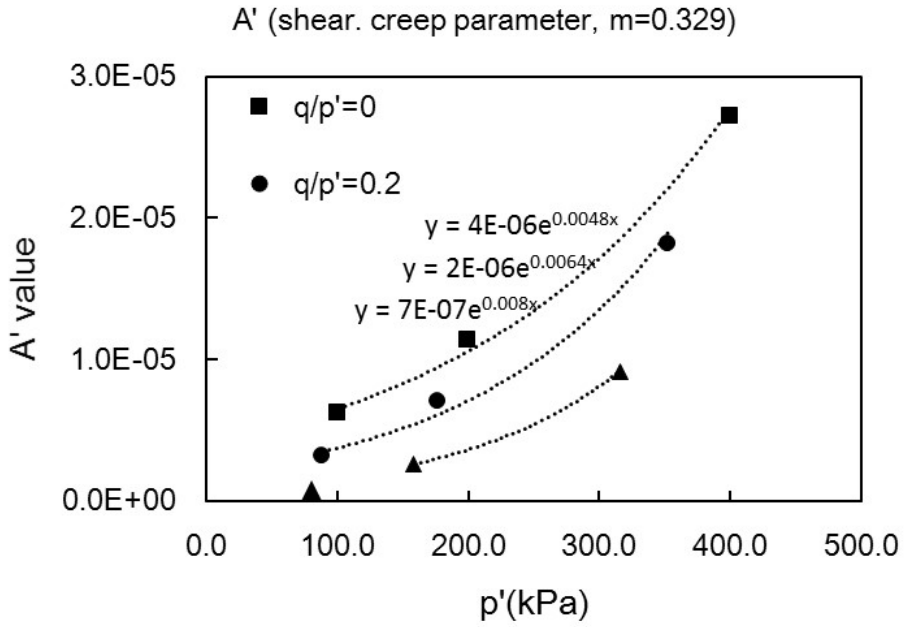

Figure 6.20 Relationships between the shear creep parameter (A') and p' for the specimens with D_r=85%

Based on the regression lines for the relationships between the new shear creep parameter A', and the mean normal effective stress, the shear creep strain for the specimens of initial relative density of 85% can be expressed as the following equation:

$$\varepsilon_{sh} = -(4\times10^{-6})(1-2\eta)\exp((0.0048+0.008\eta)\times p')\times t^{0.329} \qquad (6.4)$$

where, $\eta = q / p'$ and t=time in sec.

Figures 6.21~6.23 represent comparisons of the predicted shear creep deformations and the measured experimental data. It can be concluded that the proposed shear creep model, Eq. 6.4, is generally well predicting the original shear creep curve of 85% initial relative density of weathered residual soil except for the case of 0.4 stress ratio with 100kPa vertical effective stress.

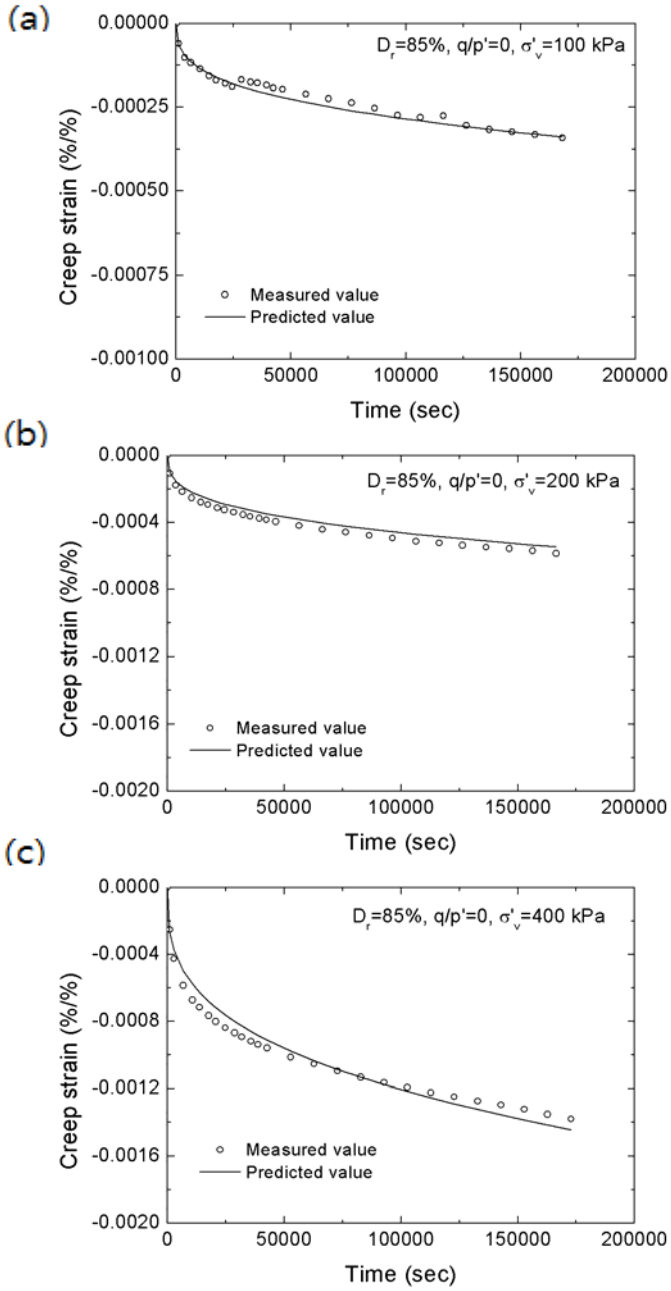

Figure 6.21 Comparison of predicted and measured shear creep strain of the specimens with D_r=85% and q/p'=0

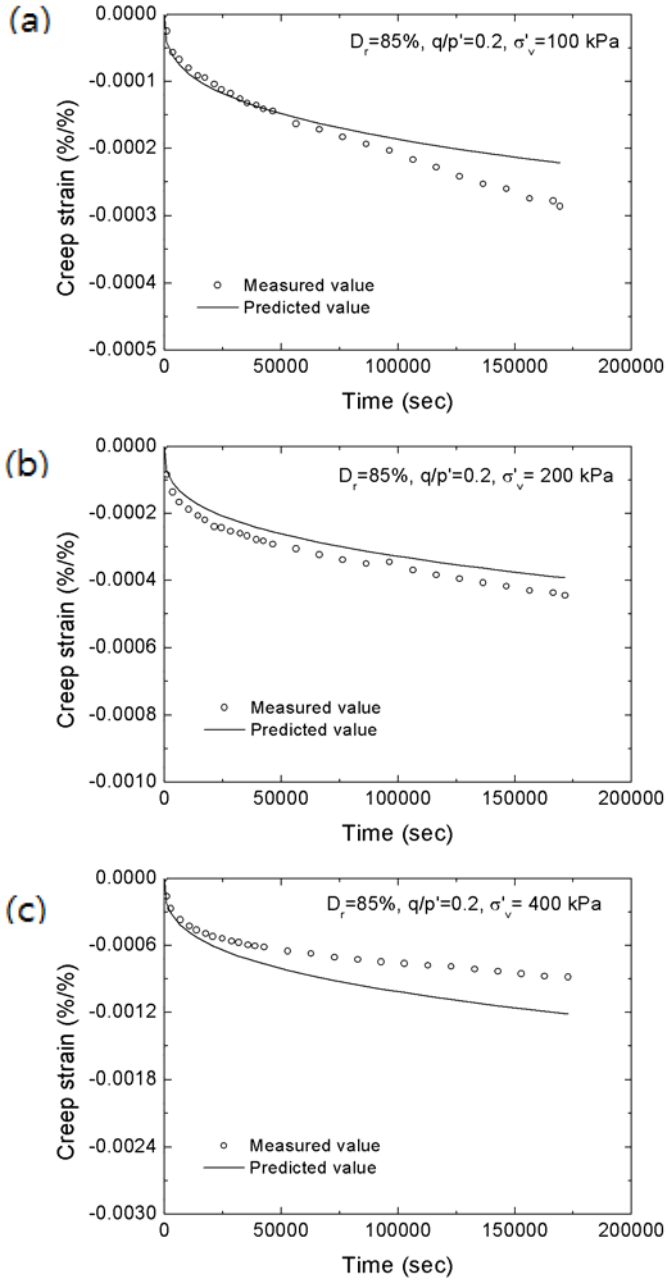

Figure 6.22 Comparison of predicted and measured shear creep strain of the specimens with D_r=85% and q/p'=0.2

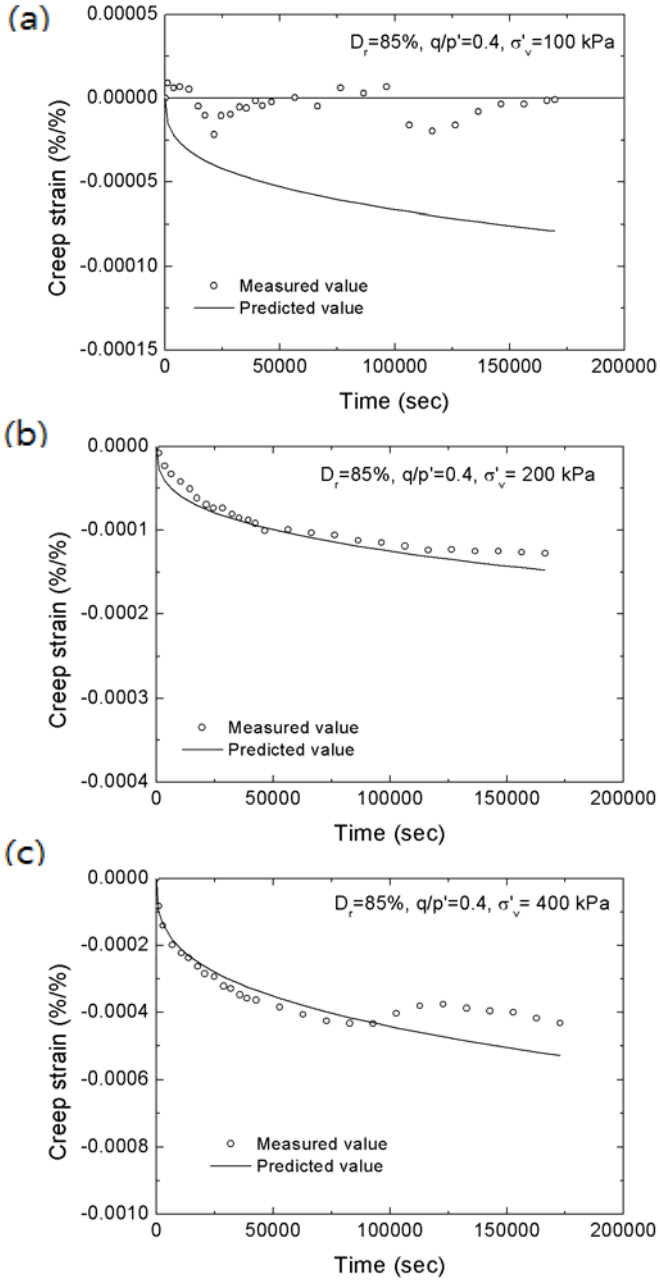

Figure 6.23 Comparison of predicted and measured shear creep strain of the specimens with D_r=85% and q/p'=0.4

6.3.2 One-dimensional compression test results

A series of one-dimensional compression creep tests were performed to investigate the time-dependent deformation behavior of weathered residual soil in Korea under lateral confined conditions. In the one-dimensional creep tests, Jumunjin sand was also used in comparison with weathered residual soil. The specimens of Jumunjin sand was prepared to have the same void ratio with the specimens of weathered soil of 96% initial relative density. Comparing the results of Jumunjin sand with the results of weathered residual soil, the effect of grain size distribution, fine contents, or material shapes on creep behavior could be recognized. Total 4 sets of one-dimensional compression creep tests were conducted. Test conditions are summarized in Table 6.9. The specimens with different initial relative density were tested at vertical effective stress form 10 to 640 kPa using double loading method. Each loading step of one-dimensional creep tests lasted until the vertical deformation developed less than 0.005mm/day. Duration of each loading step is about 6~8 days. It is assumed that the stress ratio is about K_0 conditions due to the laterally confined conditions.

Table 6.9 Test conditions for one-dimensional creep tests

No.	Soil type	Initial relative density (%)	Initial water contents (%)	Initial void ratio
1	Weathered soil (passing # 20 sieve)	73	15	0.868
2		85	15	0.747
3		96	15	0.631
4	Jumunjin sand	90	15	0.636

Specifying the time origin of the creep phase

In order to specify the time origin of the creep phase from the total settlement, the total strain of each loading step against time graphs were plotted in double logarithm scales as in Figure 6.24. As shown in Figure 6.24, taking the linear line in the graph, the reference strain and reference time can be obtained. That is, a reference strain is assumed to be an elastic strain. To estimate the validity of this method, constrained modulus (oedometric modulus, E_{oed}) can be evaluated with the reference strains. An approximate range of values of oedometric modulus of deformation E_{oed} for individual soils and a typical stress range are listed in Table 6.10. In this study, the odeometric modulus of weathered residual soil ranged from 9 to 15 MPa and these results can be acceptable.

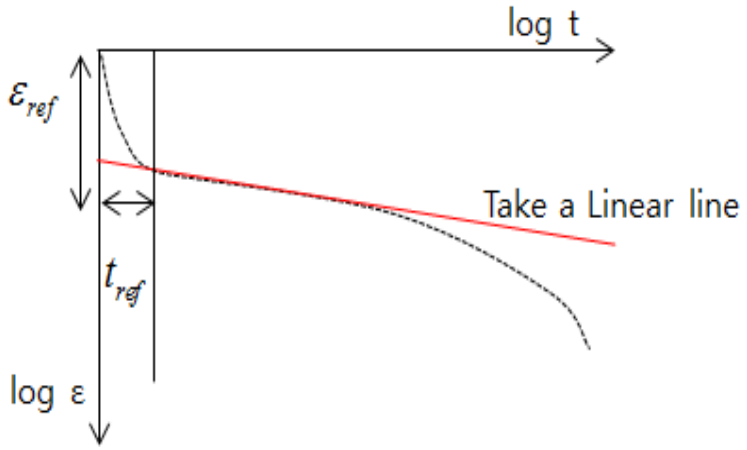

Figure 6.24 Specifing the time origin of the creep phase in the one-dimensional creep tests

Table 6.10 Approximate range of values of oedometric modulus of deformation E_{oed} for individual soils and typical stress range

Soil type	E_{oed} [MPa]
Gravels	60-600
Medium dense sand to Dense sand	7-130
Clay	2-30

Creep parameters of one-dimensional creep tests

Based on Figure 6.24, the reference time was obtained for each test condition. The reference time was 100 sec regardless of soil types or stress conditions. Table 6.11 shows the elastic strain corresponding to the reference time for each loading steps and various soil types.

Table 6.11 Elastic strain of each loading steps for various soil conditions

Pressure (kPa)	Δpressure (kPa)	Weathered soil D_r=73% ($\varepsilon_{w\,ref}$)	Weathered soil D_r=85% ($\varepsilon_{w\,ref}$)	Weathered soil D_r=96% ($\varepsilon_{w\,ref}$)	Jumunjin Sand D_r=90% ($\varepsilon_{j\,ref}$)
20	10	0.002	0.0013	0.00215	
40	20	0.00325	0.0018	0.0022	0.00185
80	40	0.00565	0.0025	0.0033	0.00235
160	80	0.00505	0.00325	0.0039	0.00295
320	160	0.00545	0.0051	0.0048	0.00345
640	320	0.00685	0.00725	0.00617	

After specifying the time origin of the creep phase in the one-dimensional creep tests, only for the creep deformations, curve fitting method was used to find out the creep parameters.

For the specimens of the one-dimensional creep tests, the creep

parameters A and m, obtained from the best fit lines as shown in Figure 6.25 are listed in Table 6.12.

Table 6.12 Creep parameters A and m, for one-dimensional compression tests

D_r (%)		Vertical Effective Stress (kPa)					
		20	40	80	160	320	640
73	A	1.32.E-4	4.42E-5	1.04E-5	3.57E-5	6.61E-5	9.31E-5
	m	0.247	0.353	0.479	0.386	0.344	0.327
85	A	4.70E-5	1.58E-5	2.19E-5	3.09E-5	2.28E-5	1.49E-4
	m	0.333	0.438	0.402	0.368	0.352	0.264
96	A	2.04E-6	2.70E-5	3.16E-5	1.72E-5	1.61E-5	8.49E-5
	m	0.576	0.381	0.312	0.416	0.379	0.282

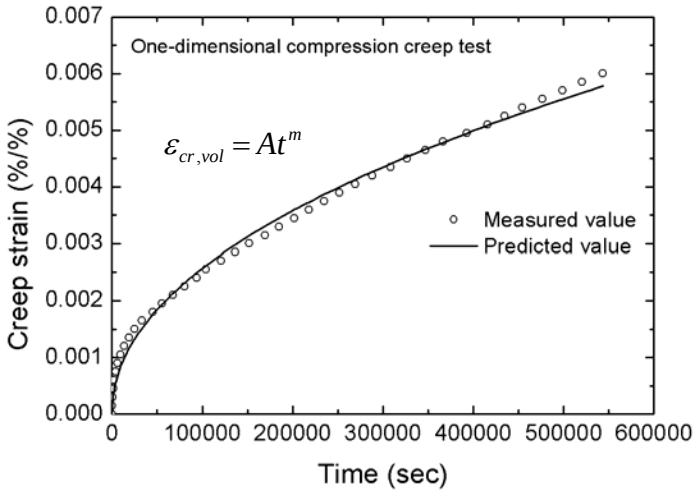

Figure 6.25 Prediction of creep strains of one-dimensional creep tests

To find out the relationships between the constant, A, and the stress conditions, the average value of m was obtained as 0.384, 0.346, and 0.347 for the creep strains of the specimens of weathered residual soil in Korea with initial relative density of 73%, 85%, and 96%, respectively. For the fixed m, obtained new creep parameter A', is listed in Table 6.13.

Table 6.13 New creep parameters A', of weathered soil for the different relative density

Confining pressure (kPa)	D_r=73% A' (m=0.384)	D_r=85% A' (m=0.346)	D_r=96% A' (m=0.347)
40		4.98E-05	
80	3.40E-05	4.35E-05	4.02E-05
160	3.67E-05	4.05E-05	4.27E-05
320	4.01E-05	2.45E-05	2.42E-05
640	4.39E-05	5.05E-05	3.91E-05

In order to investigate the effect of grain size distribution, fine contents, or material shapes on creep behavior, the specimens of Jumunjin sand were prepared to have the same void ratio with the specimens of weathered soil of 96% initial relative density. The initial relative density of this Jumunjin sand is about 90%.

In the same way as the obtaining creep parameters of weathered residual soil, new creep parameters A', for Jumunjin sand were obtained as in Table 6.14. The average value of m for Jumunjin sand is 0.25.

Table 6.14 New creep parameters A', of the Jumunjin sand for 90% relative density

Confining pressure (kPa)	D_r =90% A' (m=0.25)
40	9.19 E-05
80	1.34 E-04
160	1.20 E-04
320	1.79E-04

Whereas the converging rate of creep strains of Jumunjin sand is faster than that of weathered residual soil, the creep strains of weathered residual soil generally increase with time. In other words, the creep strains of uniformly graded soil are smaller than that of well graded soil for the same period. It can be concluded that fine contents influence the creep behaviors. The amount of creep strains increases as the fine contents increases. This is also associated with the evaluated value of m as 0.25 for Jumunjin sand and as 0.346~0.384 for weathered residual soil. In the case of the specimens of initial relative density of 73%, the new creep parameter A', increases as the vertical effective stress. In the case of the specimens of initial relative density of 85% and 96%, the new creep parameter A', decreases until the vertical effective stress reaches 320 kPa and increases at 640 kPa vertical effective stress.

Comparison one-dimensional creep parameters with triaxial creep parameters

Using different testing apparatus, triaxial and one-dimensional consolidation, creep deformations were obtained and the creep parameters were estimated for the specimens of the same initial relative densities.

Comparing the creep parameters obtained from triaxial creep tests with those obtained from one-dimensional creep tests, some discrepancies are exists. The average creep parameter m, of oedometer tests is in the range of 0.346~0.384 whereas that of triaxial creep tests is in the range of 0.259~0.280. The new parameter A', of oedometer tests is also different from that of triaxial creep tests. The parameter m of oedometer creep tests is lower than that of the triaxial creep test. That is because the stress conditions of oedometer tests are quite different from the triaxial creep tests. Contrary to the triaxial testing apparatus, the one-dimensional consolidation apparatus is laterally restrained. Thus, the specimens in the oedometer cell are pressed in horizontal direction rather than dilative horizontally. Michalowski and Nadukuru (2012) also pointed out that horizontal stress increases under one-dimensional strain conditions. Another possible reason is the smaller specimen size of oedometer creep tests than that of triaxial creep tests. The creep strains of granular materials might be too small to obtain the creep parameters by 2 cm height of oedometer specimen.

6.4 Summary

The creep parameters for numerical modelling were obtained based on the experimental results in this chapter. Before we evaluate the creep parameters, the peacock diagram of creep deformations, which idealizes the relationships among the creep deformations, void ratio, and the mean normal effective stress, was proposed. Then, the basic, simple, and one of the widely used equations, $\varepsilon_{cr} = At^m$, was used to model the creep strains. For the triaxial creep test results, the creep parameters were evaluated in terms of volumetric and shear creep strains. Also, the creep equations expressed as the stress ratio and mean normal effective stress were proposed. For the one-dimensional creep test, laterally restrained, the creep parameters were evaluated in terms of volumetric (=axial) creep strains. In the one-dimensional creep tests, to investigate the effect of the grain size distribution, fine contents, or particle shapes on creep behavior the specimens of Jumunjin sand were also prepared.

As a result, following conclusions can be drawn:

1) The proposed creep model using the basic parameters A and m, is well predicting the original volumetric and shear creep curve for the specimens with initial relative density of 73% and 85% which showed monotonic contractive volumetric responses.
2) The average volumetric creep parameter m is 0.259 and 0.280 for

the specimens with the initial relative density of 73% and 85%, respectively. For the specimens with the initial relative density of 73%, the new volumetric creep parameter (A'), applying the average m, is in the range of $5.83\times10^{-5} \sim 6.94\times10^{-4}$ depending on the stress conditions. For the specimens with the initial relative density of 85%, the new volumetric creep parameter (A') is in the range of $3.20\times10^{-5} \sim 1.47\times10^{-4}$ depending on the stress conditions.

3) The average shear creep parameter m is 0.267 and 0.329 for the specimens with initial relative density of 73% and 85%, respectively. For the specimens with initial relative density of 73%, the new shear creep parameter A' is in the range of $-2.81\times10^{-6} \sim -1.35\times10^{-4}$ depending on the stress conditions. For the specimens with initial relative density of 85%, the new shear creep parameter m is in the range of $-1.20\times10^{-7} \sim -2.71\times10^{-5}$ depending on the stress conditions.

4) As a result of the one-dimensional compression creep tests comparing the creep behavior of weathered residual soil and that of Jumunjin sand, it can be concluded that the fine contents influence the creep behaviors. The amount of creep strains increases as the fine contents increase.

5) Although the creep tests were conducted for the same initial void ratio conditions in the two different testing apparatuses, the different creep parameters were obtained. This might be because of differences in stress conditions or the size of the specimens.

6) The limitation of this study is that the provided creep parameter can be applied only for the contractive creep case. To estimate the overall creep behavior (both contractive creep and expansion creep behavior) with the numerical modeling, a further extended modeling is needed.

Chapter 7. Conclusions and Recommendations

The main objectives of this research are to evaluate and investigate creep behavior and to investigate variations in the elastic shear stiffness during creep of weathered residual soil in Korea. In order to achieve these goals, a series of stress path creep tests were designed such that the effects of various sample conditions and with different relative densities and shear conditions with different confining pressures on the time-dependent behaviors of weathered residual soil could be characterized. The principal conclusions and recommendations are given below.

7.1 Non-linear deformations during creep

The results describe the deformation behaviors of weathered residual soil in Korea. A series of triaxial creep tests were conducted to investigate the creep deformation overall. First, the overall stress-strain behavior is briefly introduced. Secondly, the procedures specifying the time origin of the creep phase are examined, after which the creep strains in terms of axial, radial, volumetric, and shear deformations are evaluated. Based on the volumetric creep responses, the concept of state-dependent volumetric creep behavior is also suggested. For the deformation characteristics during creep, the following conclusions can be drawn:

7.1.1 Creep strains of triaxial compression tests

(1) For specimens with low and medium initial relative densities, contractive volumetric creep strains were observed, whereas dilative volumetric creep strains developed for specimens with high initial relative density.

(2) High stress conditions stimulate particle rearrangement or sliding under constant loading conditions, resulting in more contractive creep strains for specimens with low and medium relative densities.

(3) In contrast to specimens with low and medium relative densities, a high stress condition inhibits particle rearrangement or sliding, resulting in dilative creep strain behavior in specimens with high relative densities. This occurs because the structure of high density soil reaches a limit during contraction, after which it expands. The low p' and high q/p' conditions promote dilative behavior during creep.

7.1.2 State-dependent volumetric creep behavior

Based on the experimental observations that relatively loose samples, which have an initially high void ratio, contract when they undergo creep whereas relatively dense samples, which have an initially low void ratio, expand when they undergo creep at a given effective stress level, the concept of state-dependent volumetric creep behavior was proposed. The creep-free state refers to a state in which the change of the void ratio due to creep becomes

zero. The characteristics of state-dependent volumetric creep behavior are given below.

(1) The contrast in the volumetric creep behavior for specimens with various densities is an analogous to the volumetric response under shearing.
(2) The creep-free void ratio decreases when the mean normal effective stress increases as a general critical state concept.

The concept of state-dependent volumetric creep behavior is also expected to shed much light on our understanding of the overall creep behavior of granular materials and to provide the information with which to ensure minimized creep deformations.

Additional studies are recommended to supplement this research.

(1) In further studies, a series of triaxial creep tests for relatively high stress ratios (higher than 0.4) are recommended. With this additional study, the completion of state-dependent volumetric creep behavior would be possible.
(2) A study of critical states of weathered residual soil type is necessary. Details pertaining to the relationships between the creep behavior and the general critical state could thus be obtained. Moreover, this additional research would provide a better understanding of the

overall deformation behavior of weathered residual soil.

7.2 Elastic shear moduli during creep

In order to investigate variations in the elastic shear stiffness during creep, the elastic shear stiffness were estimated via bi-directional bender element tests under various conditions with different initial relative densities, stress ratios, and effective stresses. Initially, the stiffness after creep is compared with the stiffness before creep as obtained from the overall stress-strain curves. Secondly, variations in the elastic shear stiffness during creep over time are presented. The time-dependent increase in the elastic shear stiffness in each case is then quantified using existing equations. Finally, the evolution of the stiffness anisotropy is investigated. Conclusions are summarized below.

7.2.1 Stiffness obtained from the overall stress-strain curve

Before investigating the evolution in the anisotropic stiffness during creep, the effects of creep on the stiffness as obtained from the overall stress-strain curve were quantitatively evaluated. In comparison with the slopes of the stress-strain curve before and after the creep stages, an increase in the stiffness was clearly detected due to creep for every condition. Moreover, the normalized stiffness after creep, i.e., the slopes which were normalized with the vertical effective stress to remove the stress effect, is higher than that

prior to creep. These results clearly showed the effect of creep on the stiffness as obtained from the overall stress-strain curves.

7.2.2 Stiffness degradation curve

Stiffness degradation curves were examined with the elastic stiffness results obtained from the bender element tests. It was found that the initial stiffness obtained from the bender elements is consistent with the secant modulus of the stress-strain curve. The determined small-strain stiffness and strain dependent stiffness can be used for advanced deformation analyses in geotechnical engineering with the finite element method.

7.2.3 Variations in the elastic shear stiffness during creep

In order to investigate the directional stiffness during creep, bi-directional bender element tests were performed. The results show that a continuous change in the stiffness during creep is closely related to the patterns which arise during creep deformation. For specimens with low and medium relative densities, compressive creep strain developed and the elastic shear moduli (G_{hv} and G_{hh}) generally increased during creep. There was an exception of the G_{hh} value of the specimen with a high initial relative density, which may be related to exceptional dilative radial creep strains.

7.2.4 Quantifying the time-dependent increase in the elastic shear stiffness

To quantify the time-dependent increase in the elastic shear stiffness, the equations proposed by Anderson and Stokoe (1978) were used. The value of N_G for the material used in this study ranges from 0.02 to 0.11.

7.2.5 Stiffness anisotropy

The continuous change in the stiffness anisotropy during creep was found to be closely related to the patterns which arose during creep deformation. Specimens with low density levels generated larger compressive axial strains during creep as compared to those with medium initial densities. However, the negative radial strains of the specimens with high initial density caused a dilative volume increase during creep. The increase in the elastic stiffness is more sensitive to the direction of the major principal stress (axial stress) than that of the minor principal stress (radial stress) during creep. In the horizontal direction, soil deforms radially rather than undergoing a change in its internal structure, and this changes the horizontal elastic stiffness during creep.

The significance of this research is to promote a better understanding of anisotropy evolution during creep. Therefore, with an estimation of the anisotropy, more precise predictions of deformation may be possible under a constant stress state (i.e., after construction).

7.3 Creep parameters of weathered residual soil for numerical modeling

Based on these experimental results, creep parameters were suggested for numerical modeling to predict creep deformation. Optimal creep deformation curves expressed by the stress ratio, the mean normal effective stress, and time were obtained.

1) The proposed creep model using the basic parameters A and m is suitable for predicting the original volumetric and shear creep curves of specimens with initial relative densities of 73% and 85%, which show monotonic contractive volumetric responses.
2) The average volumetric creep parameter m is 0.259 and 0.280 for specimens with an initial relative density of 73% and 85%, respectively. For the specimens with the initial relative density of 73%, the new volumetric creep parameter (A'), applying the average m, is in the range of $5.83\times10^{-5} \sim 6.94\times10^{-4}$ depending on the stress conditions. For the specimens with the initial relative density of 85%, the new volumetric creep parameter (A') is in the range of $3.20\times10^{-5} \sim 1.47\times10^{-4}$ depending on the stress conditions.
3) The average shear creep parameter m is 0.267 and 0.329 for the specimens with an initial relative density of 73% and 85%, respectively. For the specimens with initial relative density of 73%, the new shear creep parameter A' is in the range of

$-2.81\times10^{-6} \sim -1.35\times10^{-4}$ depending on the stress conditions. For the specimens with initial relative density of 85%, the new shear creep parameter m is in the range of $-1.20\times10^{-7} \sim -2.71\times10^{-5}$ depending on the stress conditions.

The significance of this research is that it provides creep parameters for the numerical modeling of deformation predictions over time.

Further research is recommended to supplement this research. It is necessary to verify the creep equations based on the field measurement data to secure the feasibility of the proposed creep parameters.

References

Anderson, D., and Stokoe, K. (1978). "Shear modulus: a time-dependent soil property", *Dynamic Geotechnical Testing, ASTM STP, 654*, 66-90.

Axelsson, G. (2002). "A conceptual model of pile set-up for driven piles in non-cohesive soil", *Geotechnical Special Publication, 1*, 64-79.

Baldi, G., Hight, D. W., and Thomas, G. E. (1988). "A reevaluation of conventional triaxial test methods", *Advanced triaxial testing of soil and rock, ASTM STP, 977*, 219-263.

Baxter, C. D., and Mitchell, J. K. (2004). "Experimental study on the aging of sands", *Journal of Geotechnical and Geoenvironmental Engineering, 130*(10), 1051-1062.

Been, K., and Jefferies, M. G. (1985). "A state parameter for sands", *Geotechnique, 35*(2), 99-112.

Bellotti, R., Jamiolkowski, M., Presti, D. L., and O'neill, D. (1996). "Anisotropy of small strain stiffness in Ticino sand", *Geotechnique*, 46(1), 115-131.

Bowman, E. T., and Soga, K. (2003). "Creep, aging and microstructural change in dense granular materials", *Soils and Foundations, 43*(4), 107-117.

Bowman, E. T., and Soga, K. (2005). "Mechanisms of setup of displacement piles in sand: laboratory creep tests", *Canadian Geotechnical Journal, 42*(5), 1391-1407.

Chang, C. S., Sundaram, S. S., and Misra, A. (1989). "Initial moduli of particulated mass with frictional contacts", *International Journal for Numerical and Analytical Methods in Geomechanics*, 13(6), 629-644.

Charlie, W., Jacobs, P. J., and Doehring, D. (1992a). "Blast-induced liquefaction of an alluvial sand deposit", *Geotechnical Testing Journal, 15*(1).

Charlie, W. A., Rwebyogo, M. F., and Doehring, D. O. (1992b). "Time-dependent cone penetration resistance due to blasting", *Journal of Geotechnical Engineering, 118*(8), 1200-1215.

Chow, F., Jardine, R., Brucy, F., and Nauroy, J. (1998). "Effects of time on capacity of pipe piles in dense marine sand", *Journal of Geotechnical and Geoenvironmental Engineering, 124*(3), 254-264.

Coop, M., Jovičić, V., and Simić, M. (1996). "Objective criteria for determining G_{max} from bender element tests", *Geotechnique*(46), 357-362.

Daramola, O. (1980). "Effect of consolidation age on stiffness of sand", *Geotechnique, 30*(2), 213-216.

Dowding, C. H., and Hryciw, R. D. (1986). "A laboratory study of blast

densification of saturated sand", *Journal of Geotechnical Engineering, 112*(2), 187-199.

Gao, Y. and Wang, Y. (2011). "Aging Effects on Fabric-induced, Small-Strain, Stiffness Anisotropy in Sand", *Proceedings of the Fifth International Symposium on Deformation Characteristics of Geomaterials*, IS-Seoul 2011, 1-3 September 2011, Seoul, Korea.

Howie, J., Shozen, T., and Vaid, Y. (2002). "Effect of aging on stiffness of very loose sand", *Canadian Geotechnical Journal, 39*(1), 149-156.

Joshi, R., Achari, G., Kaniraj, S. R., and Wijeweera, H. (1995). "Effect of aging on the penetration resistance of sands", *Canadian Geotechnical Journal, 32*(5), 767-782.

Jovicic, V., and Coop, M. (1998). "The measurement of stiffness anisotropy in clays with bender element tests in the triaxial apparatus", *ASTM Geotechnical Testing Journal*, 21(1), 3-10.

Karimpour, H., and Lade, P. V. (2013). "Creep behavior in Virginia Beach sand", *Canadian Geotechnical Journal, 50*(11), 1159-1178.

Kirkgard, M., and Lade, P. (1991). "Anisotropy of normally consolidated San Francisco bay mud", *Geotechnical Testing Journal, 14*(3).

Kirkgard, M., and Lade, P. V. (1993). "Anisotropic three-dimensional behavior of a normally consolidated clay", *Canadian Geotechnical Journal,*

30(5), 848-858.

Kuhn, M. R. (1999). “Structured deformation in granular materials”, *Mechanics of Materials, 31*(6), 407-429.

Kuwano, R., and Jardine, R. J. (2002). “On measuring creep behaviour in granular materials through triaxial testing”, *Canadian Geotechnical Journal, 39*(5), 1061-1074.

Lade, P. V., and Liu, C.-T. (1998). “Experimental study of drained creep behavior of sand”, *Journal of Engineering Mechanics, 124*(8), 912-920.

Lee, J.-S., and Santamarina, J. C. (2005). “Bender elements: performance and signal interpretation”, *Journal of Geotechnical and Geoenvironmental Engineering, 131*(9), 1063-1070.

Leung, C., Lee, F., and Yet, N. (1997). “The role of particle breakage in pile creep in sand”, *Canadian Geotechnical Journal, 33*(6), 888-898.

Mejia, C., Vaid, Y., and Negussey, D. (1988). "Time dependnet behavior of sand", *International Conference on Rheology and Soil Mechanic*s, 12-16.

Mesri, G., Feng, T., and Benak, J. (1990). "Postdensification penetration resistance of clean sands", *Journal of Geotechnical Engineering, 116*(7), 1095-1115.

Michalowski, R. L., and Nadukuru, S. S. (2012). "Static fatigue, time effects, and delayed increase in penetration resistance after dynamic

compaction of sands", *Journal of Geotechnical and Geoenvironmental Engineering, 138*(5), 564-574.

Mitchell, J. K., and Solymar, Z. V. (1984). "Time-dependent strength gain in freshly deposited or densified sand", *Journal of Geotechnical Engineering, 110*(11), 1559-1576.

Mitchell, J. K., and Soga, K. (2005). *Fundamentals of soil behavior*, 3rd Ed., Wiley, New York

Murayama, S., Michihiro, K., and Sakagami, T. (1984). "Creep characteristics of sand", *Soils and Foundations, 24*(5).

Myrayama, S. (1983). "Formulation of stress-strain-time behavior of soils under deviatoric stress condition", *Soils and Foundations, 23*(2), 43-57.

Ochiai, H., and Lade, P. V. (1983). "Three-dimensional behavior of sand with anisotropic fabric", *Journal of Geotechnical Engineering, 109*(10), 1313-1328.

Oda, M., Nemat-Nasser, S., and Konishi, J. (1985). "Stress-induced anisotropy in granular masses", *Soils and Foundations, 25*(3), 85-97.

Peacock, W. H. (1967). "*Liquefaction of Saturated Sands Under Cyclic Loading Simple Shear Conditions",* University of California, Berkeley.

Rimoy, S. P., and Jardine, R. J. (2011). "*On strain accumulation in a silica sand under creep and low level cyclic loading", Proceedings of the Fifth*

International Symposium on Deformation Characteristics of Geomaterials, IS-Seoul 2011, 1-3 September 2011, Seoul, Korea.

Roscoe, K. H., Schofield, A., and Wroth, C. (1958). "On the yielding of soils", *Geotechnique, 8*(1), 22-53.

Santamarina, J. C., Klein, A., and Fam, M. A. (2001). “Soils and waves: Particulate materials behavior, characterization and process monitoring”, *Journal of Soils and Sediments*, 1(2), 130-130.

Schmertmann, J. (1986). "Suggested method for performing the flat dilatometer test", *Geotechnical Testing Journal, 9*(2), 93-101.

Schmertmann, J. H. (1991). "The mechanical aging of soils", *Journal of Geotechnical Engineering, 117*(9), 1288-1330.

Tavenas, F., and Audy, R. (1972). "Limitations of the driving formulas for predicting the bearing capacities of piles in sand", *Canadian Geotechnical Journal, 9*(1), 47-62.

Taylor, D. W. (1948). "Fundamentals of soil mechanics", *Soil Science, 66*(2), 161.

Thomann, T. G., and Hryciw, R. D. (1992). "Stiffness and strength changes in cohesionless soils due to disturbance", *Canadian Geotechnical Journal, 29*(5), 853-861.

Troncoso, J., and Garcés, E. (2000). "Aging effects in the shear modulus of

soils", *Soil Dynamics and Earthquake Engineering, 19*(8), 595-601.

Wang, Y.-H., and Tsui, K.-Y. (2009). "Experimental characterization of dynamic property changes in aged sands", *Journal of Geotechnical and Geoenvironmental Engineering, 135*(2), 259-270.

Wang, Y., and Mok, C. (2008). “Mechanisms of small-strain shear-modulus anisotropy in soils”, *Journal of Geotechnical and Geoenvironmental Engineering*, 134(10), 1516-1530.

Wang, Y.-H., Xu, D., and Tsui, K. Y. (2008). "Discrete element modeling of contact creep and aging in sand", *Journal of Geotechnical and Geoenvironmental Engineering, 134*(9), 1407-1411.

Wang, Y., and Gao, Y. (2013). "Mechanisms of aging-induced modulus changes in sand with inherent fabric anisotropy", *Journal of Geotechnical and Geoenvironmental Engineering, 139*(9), 1590-1603.

Yamamuro, J. A., and Lade, P. V. (1993). "Effects of strain rate on instability of granular soils", *Geotechnical Testing Journal, 16*, 304-304.

Yamashita, S., Hori, T., and Suzuki, T. (2003). “Effects of fabric anisotropy and stress condition on small strain stiffness of sands”, *Deformation Characteristics of Geomaterials*, 1, 187-194.

York, D. L., Brusey, W. G., Clémente, F. M., and Law, S. K. (1994). "Setup and relaxation in glacial sand”, *Journal of Geotechnical Engineering,*

120(9), 1498-1513.

Appendices

A.1 Stiffness anisotropy

The value of G_{vh} can be estimated by the measurements of local LVDTs as in the Figure A.1. The Figure A.1 shows the stiffness degradation curves obtained from local LVDTs with the stiffness (E_v) obtained from the bender element tests. To compare the stiffness of the LVDTs and that of bender element tests, the poisson's ratio should be assumed. In this study, the poisson's ratio of the specimens is assumed to be 0~0.4. As a result, the values of E_v (E_{vh}) obtained from local LVDTs are similar to the values of E_{hv} obtained from bender element tests.

Figure A.2 shows the evolution of G_{vh} and the G_{hv} during creep and aging rates of the Toyoura sand. According to Gao and Wang (2011), the value of G_{vh} and the G_{hv} are almost same and the aging rates of G_{vh} and the G_{hv} are similar not only for the specimens of uniform Toyoura sand but also for the specimens of containing different contents of fines. In addition, previous researchers such as Chang et al. (1989), Bellotti et al. (1996) Jovicic and Coop (1998), Santamarina et al. (2001), Yamashita et al. (2003), Mitchell and Soga (2005), Wang and Mok (2008) reported that the ratio of G_{hv} to G_{vh} is almost equal to 1. Therefore, it is considered that this study to investigate the stiffness anisotropy of weathered residual soil in Korea with bi-directional bender element tests might be moderate.

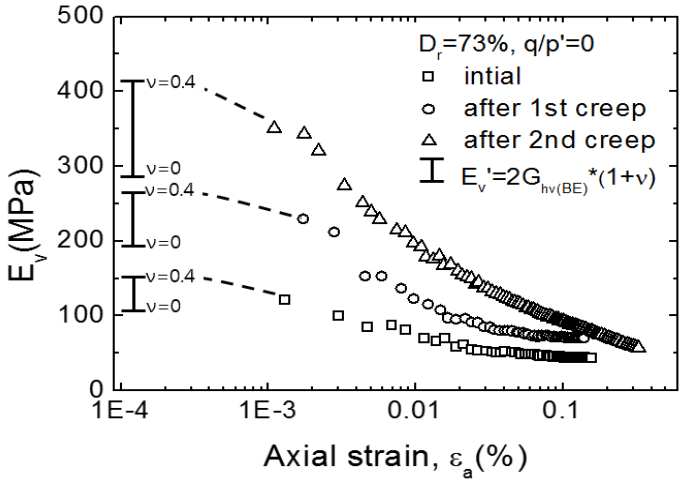

Figure A.1 Stiffness degradation curves with the bender element test results

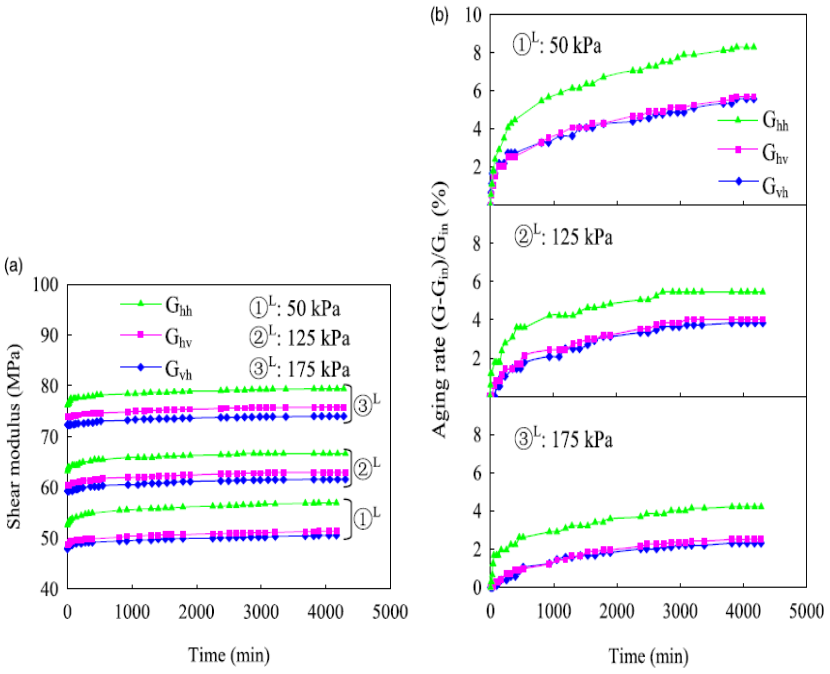

Figure A.2 (a) Evolution of small-strain shear moduli and (b) associated aging rates (Gao and Wang, 2011)

A.2 Changes of relative density due to consolidation or creep

The relative density changes continuously during consolidation or creep. Thus, in this study, the term of 'the initial relative density' was used to express the initial condition of the specimens. Table A.1~A.3 summarize the change of the relative density during consolidation or creep.

Table A.1 Changes of relative density during consolidation or creep (D_r=73%)

D_r=73		σ'_v=100 kPa		σ'_v=200 kPa		σ'_v=400 kPa	
q/p'	initial	con	creep	con	creep	con	creep
0	72.7	74.5	75.0	76.7	77.4	83.2	85.9
0.2	72.7	74.2	74.5	75.9	76.5	81.2	83.4
0.4	72.7	73.8	74.1	75.2	75.6	79.2	80.8

Table A.2 Changes of relative density during consolidation or creep (D_r=85%)

D_r=85		σ'_v=100 kPa		σ'_v=200 kPa		σ'_v=400 kPa	
q/p'	initial	con	creep	con	creep	con	creep
0	84.5	85.6	85.9	86.9	87.2	88.9	89.7
0.2	84.5	85.3	85.6	86.5	86.9	88.5	89.1
0.4	84.5	85.2	85.4	86.1	86.4	87.6	88.1

Table A.3 Changes of relative density during consolidation or creep (D_r=96%)

D_r=96		σ'_v=100 kPa		σ'_v=200 kPa		σ'_v=400 kPa	
q/p'	initial	con	creep	con	creep	con	creep
0	95.9	97.0	96.7	97.6	97.6	98.9	99.1
0.2	95.9	96.8	96.5	97.3	97.3	98.3	98.4
0.4	95.9	96.8	95.4	96.3	95.8	97.9	97.6

A.3 Strain development during Creep

The development of strains (axial, radial, volumetric, and shear strains) during creep were plotted against time in the same plane. Figure A.3~A.11 show the development of strains for 40 hours of creep depending on the initial relative densities and the stress conditions. Also, Table A.4~A.6 summarize the development of axial creep strains within 3 hours, 40 hours, and their ratios, respectively. Table A.7~A.9 list the development of volumetric creep strains within 3 hours, 40 hours, and their ratios, respectively.

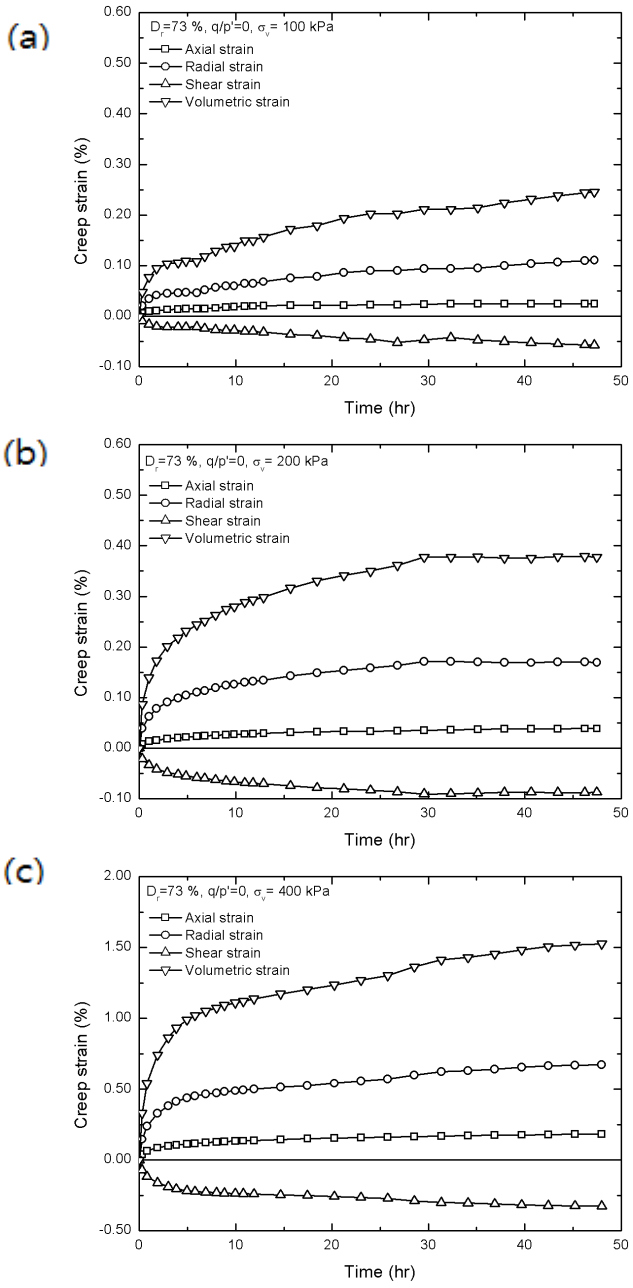

Figure A.3 Development of creep strains for the specimens of D_r=73%, q/p'=0, (a) σ'_v=100 kPa, (a) σ'_v=200 kPa, and (c) σ'_v=400 kPa, respectively

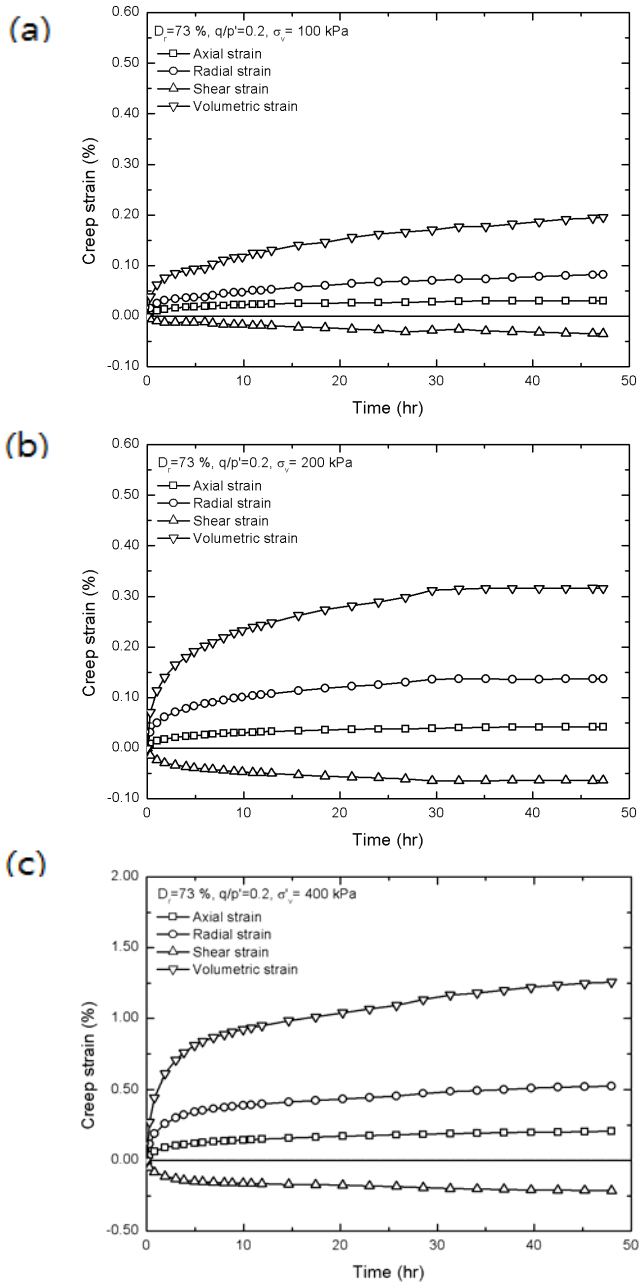

Figure A.4 Development of creep strains for the specimens of D_r=73%, q/p'=0.2, (a) σ'_v=100 kPa, (a) σ'_v=200 kPa, and (c) σ'_v=400 kPa, respectively

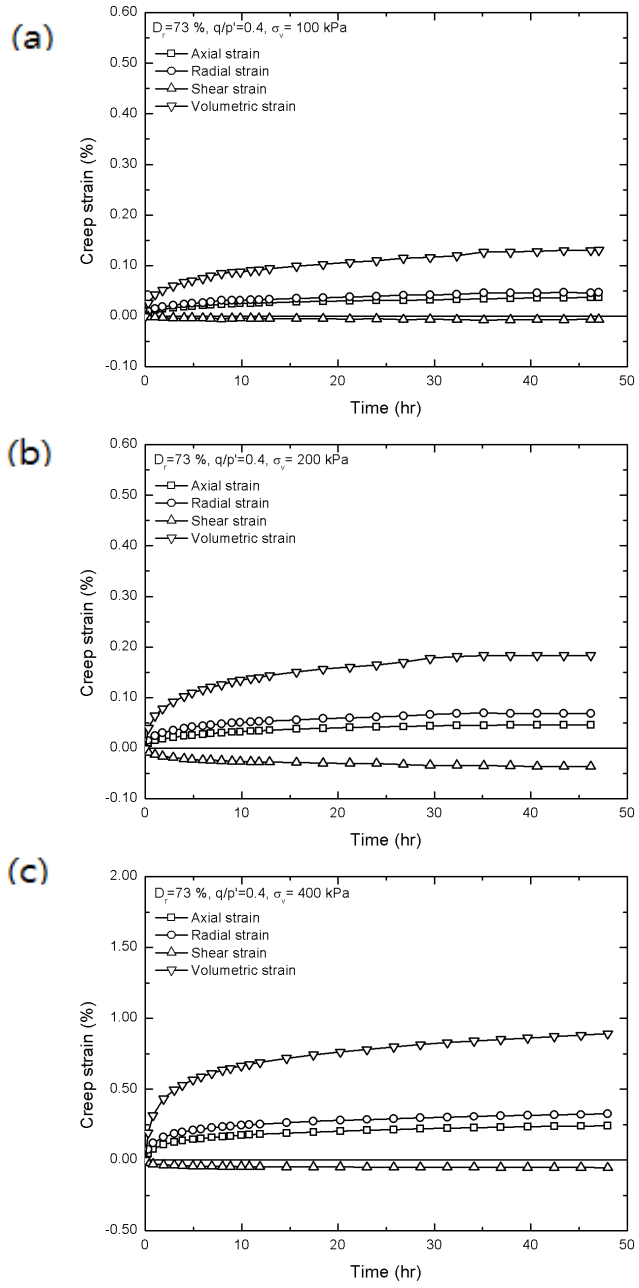

Figure A.5 Development of creep strains for the specimens of D_r=73%, q/p'=0.4, (a) σ'_v=100 kPa, (a) σ'_v=200 kPa, and (c) σ'_v=400 kPa, respectively

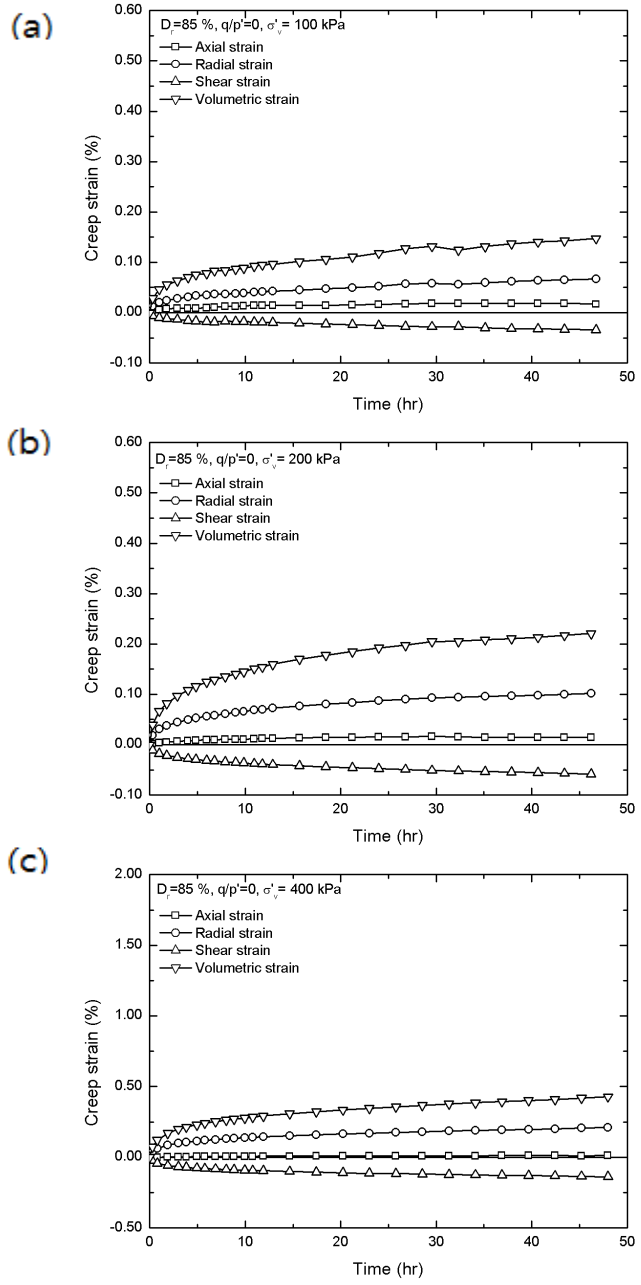

Figure A.6 Development of creep strains for the specimens of D_r=85%, q/p'=0, (a) σ'_v=100 kPa, (a) σ'_v=200 kPa, and (c) σ'_v=400 kPa, respectively

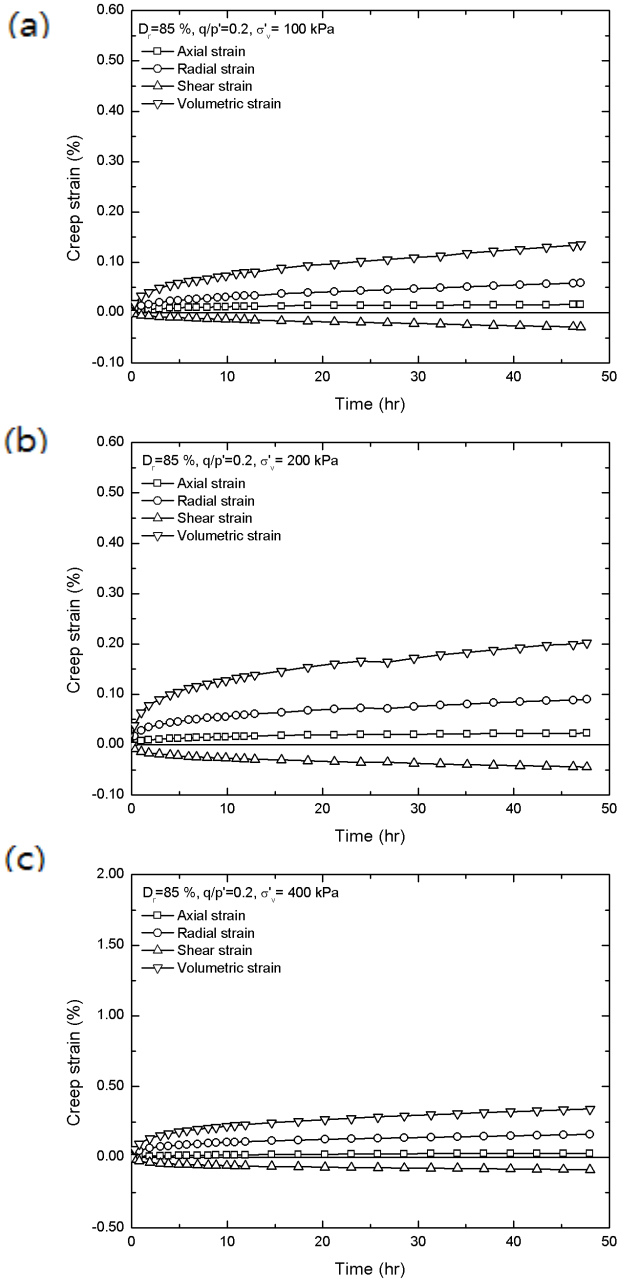

Figure A.7 Development of creep strains for the specimens of D_r=85%, q/p'=0.2, (a) σ'_v=100 kPa, (a) σ'_v=200 kPa, and (c) σ'_v=400 kPa, respectively

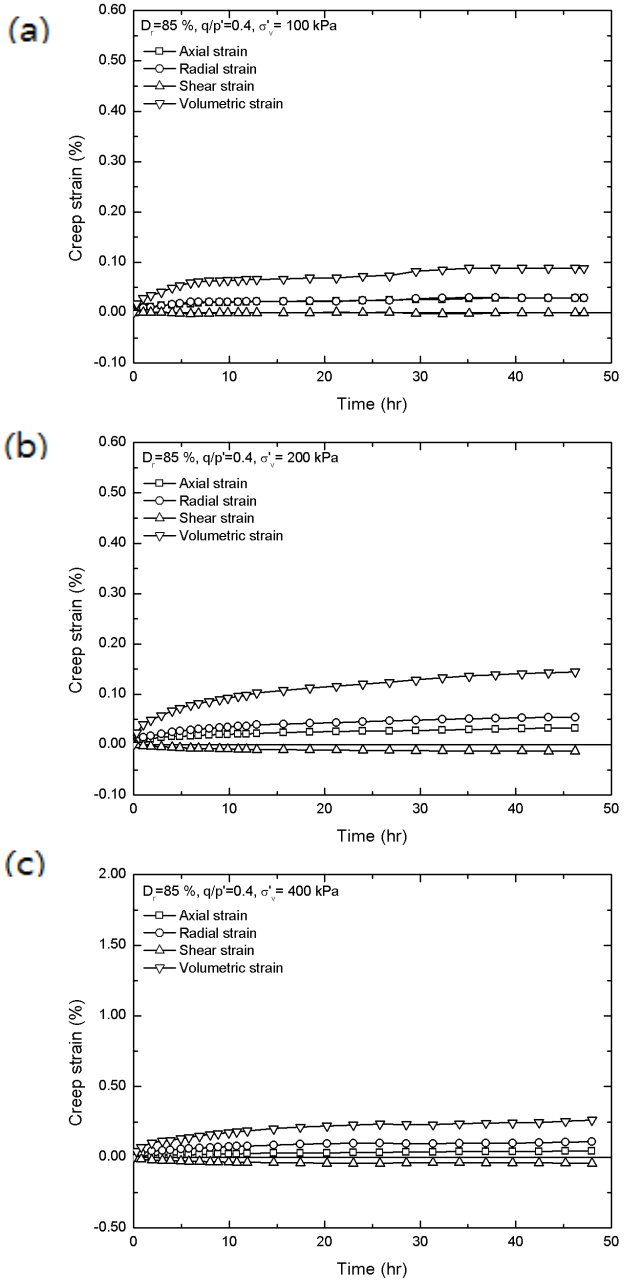

Figure A.8 Development of creep strains for the specimens of D_r=85%, q/p'=0.4, (a) σ'_v=100 kPa, (a) σ'_v=200 kPa, and (c) σ'_v=400 kPa, respectively

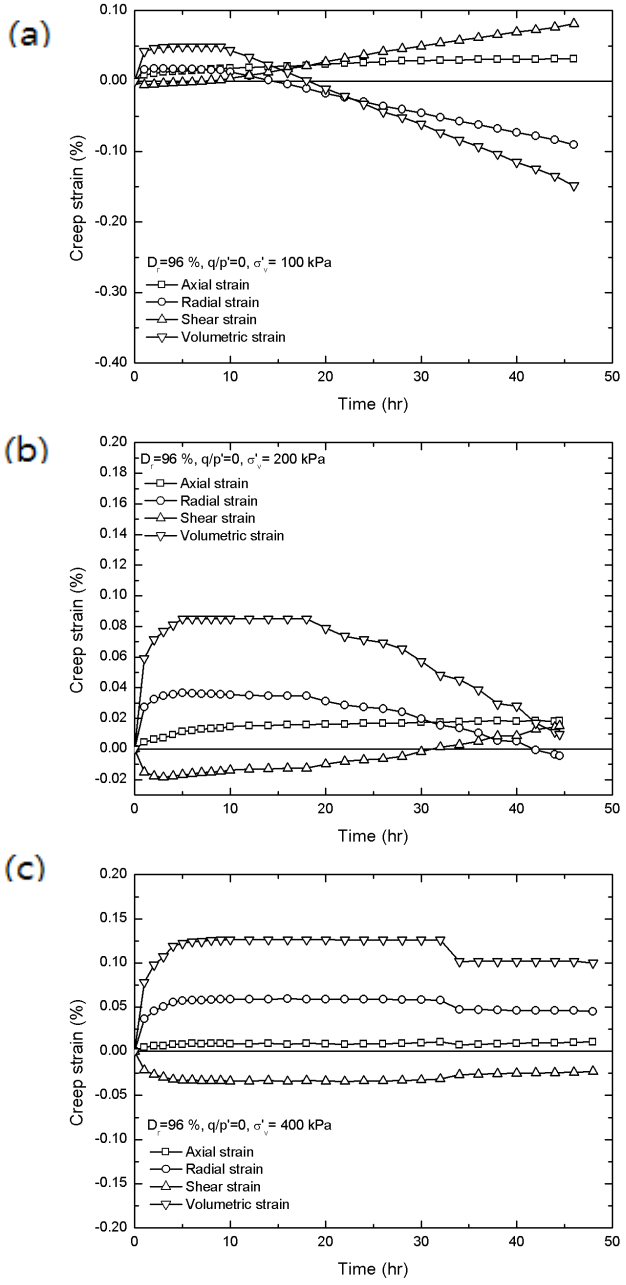

Figure A.9 Development of creep strains for the specimens of D_r=96%, q/p'=0, (a) σ'_v=100 kPa, (a) σ'_v=200 kPa, and (c) σ'_v=400 kPa, respectively

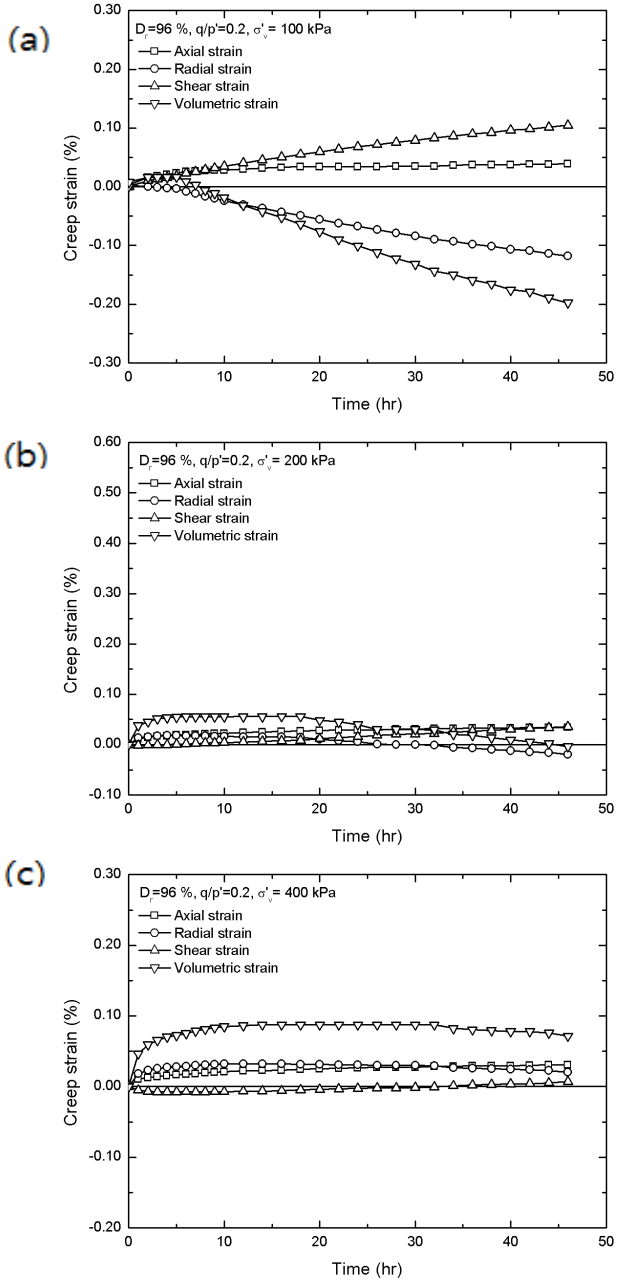

Figure A.10 Development of creep strains for the specimens of D_r=96%, q/p'=0.2, (a) σ'_v=100 kPa, (a) σ'_v=200 kPa, and (c) σ'_v=400 kPa, respectively

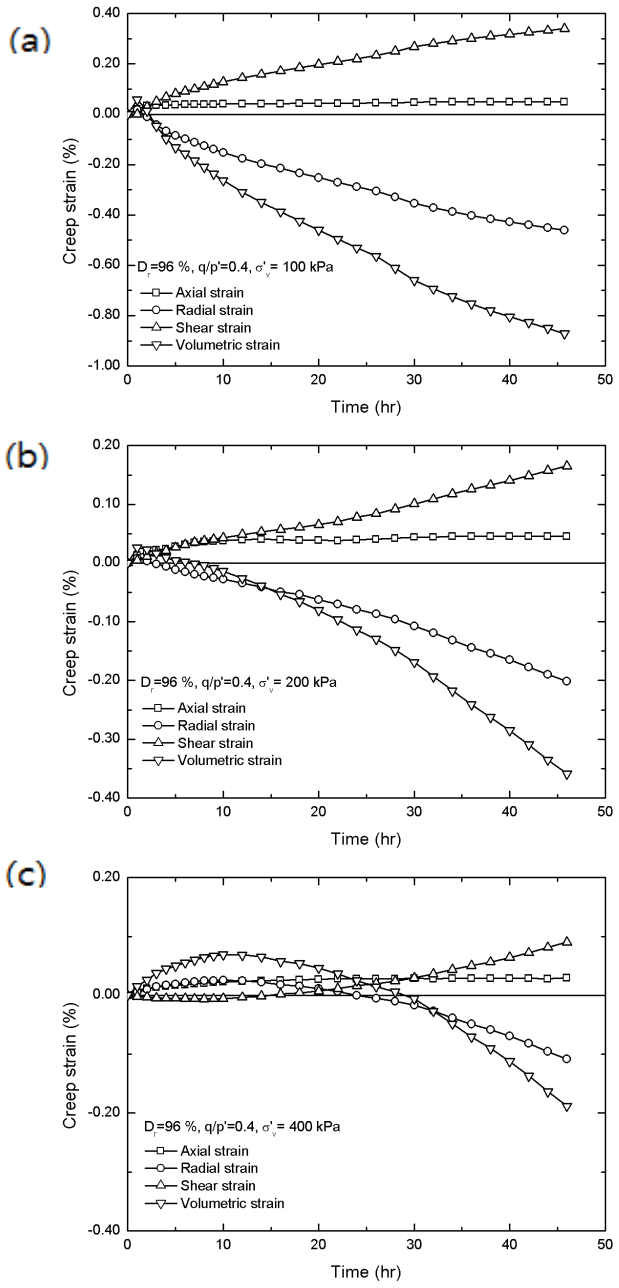

Figure A.11 Development of creep strains for the specimens of D_r=96%, q/p'=0.4, (a) σ'_v=100 kPa, (a) σ'_v=200 kPa, and (c) σ'_v=400 kPa, respectively

Table A.4 Summary of the development of axial creep strains within 3 hours, 40 hours, and their ratios, respectively (D_r= 73%)

D_r= 73%	q/p'=0			q/p'=0.2			q/p'=0.4		
$\Delta\sigma'_v$	3hr	40hr	ratio	3hr	40hr	ratio	3hr	40hr	ratio
30-100	0.013	0.025	52.4	0.016	0.031	52.1	0.017	0.036	46.1
100-200	0.019	0.038	49.5	0.021	0.042	50.5	0.022	0.046	47.2
200-400	0.099	0.177	55.8	0.105	0.198	53.2	0.126	0.234	54.0

Table A.5 Summary of the development of axial creep strains within 3 hours, 40 hours, and their ratios, respectively (D_r= 85%)

D_r= 85%	q/p'=0			q/p'=0.2			q/p'=0.4		
$\Delta\sigma'_v$	3hr	40hr	ratio	3hr	40hr	ratio	3hr	40hr	ratio
30-100	0.008	0.018	46.6	0.008	0.016	51.8	0.014	0.029	49.0
100-200	0.007	0.015	43.7	0.010	0.020	53.4	0.012	0.032	37.5
200-400	0.004	0.012	34.7	0.010	0.027	37.4	0.016	0.042	37.4

Table A.6 Summary of the development of axial creep strains within 3 hours, 40 hours, and their ratios, respectively (D_r= 96%)

D_r= 96%	q/p'=0			q/p'=0.2			q/p'=0.4		
$\Delta\sigma'_v$	3hr	40hr	ratio	3hr	40hr	ratio	3hr	40hr	ratio
30-100	0.013	0.034	37.1	0.019	0.038	48.9	0.036	0.052	68.3
100-200	0.007	0.020	36.0	0.017	0.034	50.0	0.023	0.049	46.3
200-400	0.006	0.010	62.0	0.014	0.029	49.7	0.014	0.031	43.9

Table A.7 Summary of the development of volumetric creep strains within 3 hours, 40 hours, and their ratios, respectively (D_r= 73%)

D_r= 73%	q/p'=0			q/p'=0.2			q/p'=0.4		
$\Delta\sigma'_v$	3hr	40hr	ratio	3hr	40hr	ratio	3hr	40hr	ratio
30-100	0.104	0.231	44.9	0.085	0.187	45.5	0.060	0.128	46.9
100-200	0.201	0.376	53.6	0.165	0.316	52.1	0.092	0.183	50.3
200-400	0.863	1.482	58.2	0.706	1.219	57.9	0.494	0.862	57.4

Table A.8 Summary of the development of volumetric creep strains within 3 hours, 40 hours, and their ratios, respectively (D_r= 85%)

D_r= 85%	q/p'=0			q/p'=0.2			q/p'=0.4		
$\Delta\sigma'_v$	3hr	40hr	ratio	3hr	40hr	ratio	3hr	40hr	ratio
30-100	0.063	0.141	45.0	0.049	0.126	38.8	0.041	0.088	46.6
100-200	0.097	0.213	45.5	0.090	0.193	46.6	0.058	0.141	41.2
200-400	0.200	0.401	49.8	0.155	0.322	48.2	0.114	0.244	46.7

Table A.9 Summary of the development of volumetric creep strains within 3 hours, 40 hours, and their ratios, respectively (D_r= 96%)

D_r= 96%	q/p'=0			q/p'=0.2			q/p'=0.4		
$\Delta\sigma'_v$	3hr	40hr	ratio	3hr	40hr	ratio	3hr	40hr	ratio
30-100	0.048	-0.155	-30.8	0.016	-0.205	-8.0	-0.047	-0.919	5.1
100-200	0.077	0.005	1536.4	0.052	-0.001	-5190.0	0.016	-0.35	-4.7
200-400	0.107	0.101	106.1	0.066	0.075	87.4	0.038	-0.11	-34.1

A.4 Creep rate of weathered residual soil in Korea

To compare the creep rate of weathered residual soil in Korea to that of other materials in the literatures, volumetric creep strain rate was plotted against time as in Figure A.12~A.13. As a result, the creep rate of weathered residual soil is lower than that of clay and higher than that of clean sand. The creep rate increases with the increase in the vertical effective stress and the decrease in the stress ratio and the initial relative density.

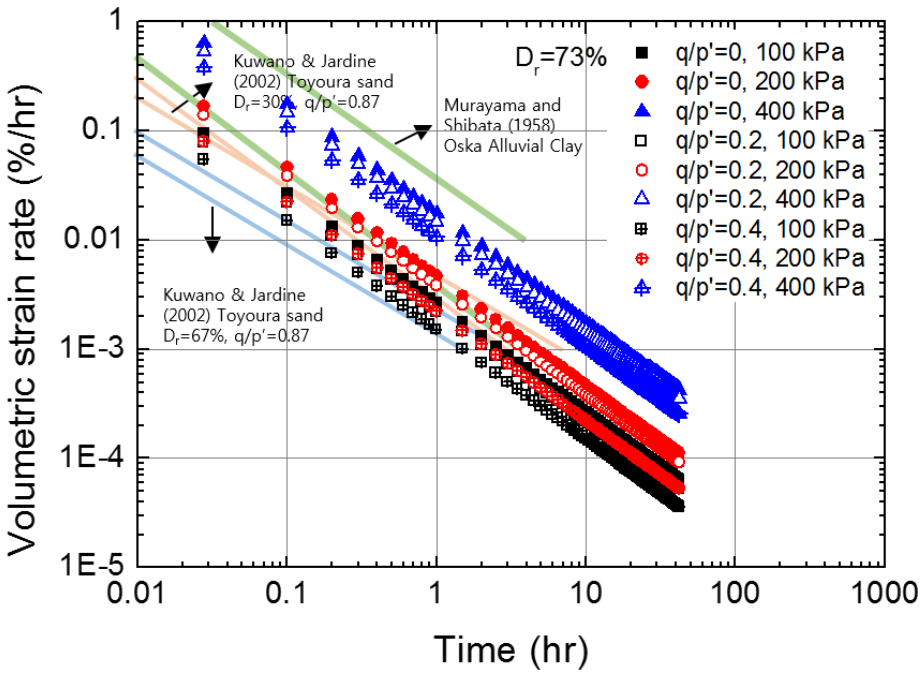

Figure A.12 Volumetric strain rate of D_r=73%

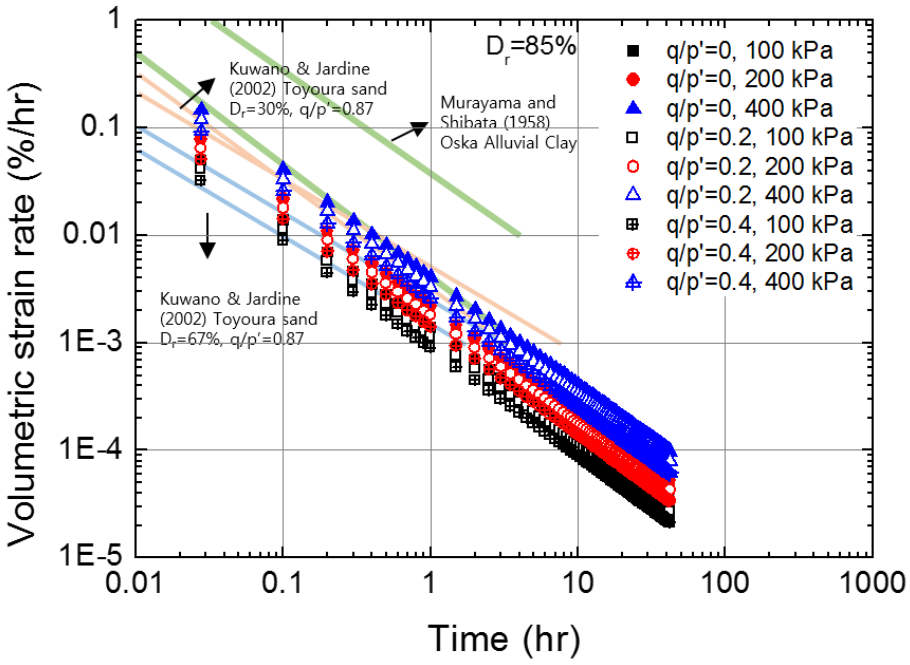

Figure A.13 Volumetric strain rate of D_r=85%

A.5 Validity of 40 hours of creep criteria

As mentioned in Chapter 2.5, primary creep and secondary creep are the areas of engineering interest. Figure A.14 shows the general creep behavior and the axial creep strain of weathered residual soil obtained from this research. As in Figure A.14, creep behaviors of weathered residual soil can be classified as 1 or 2. Weathered residual soil has nearly decreasing or constant rate with time. The 40 hours criteria analyzing the creep behavior is long enough to obtain the tendency of converging creep behavior. Therefore, it is reasonable that the creep behavior is analyzed on the basis of 40 hours. Also, the creep deformations developed after 40 hour point would be predictable using the suggested creep parameters.

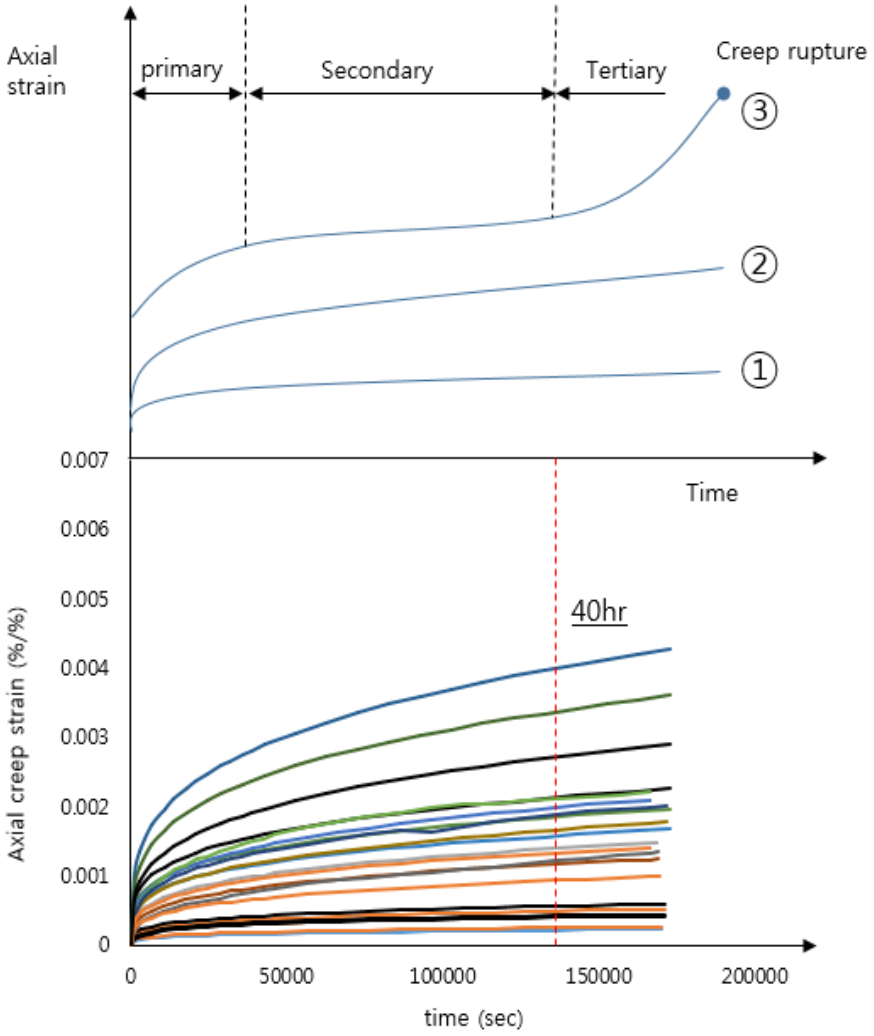

Figure A.14 Validity of 40 hours of creep criteria

A.6 Stiffness degradation curves of weathered residual soil in Korea

Figure A.15~A.20 show the stress-strain curves interpreted in terms of E or K*, taken to the secant to the curves of axial or volumetric stress-strain. The continuous values of E and K* were plotted against axial or volumetric strains.

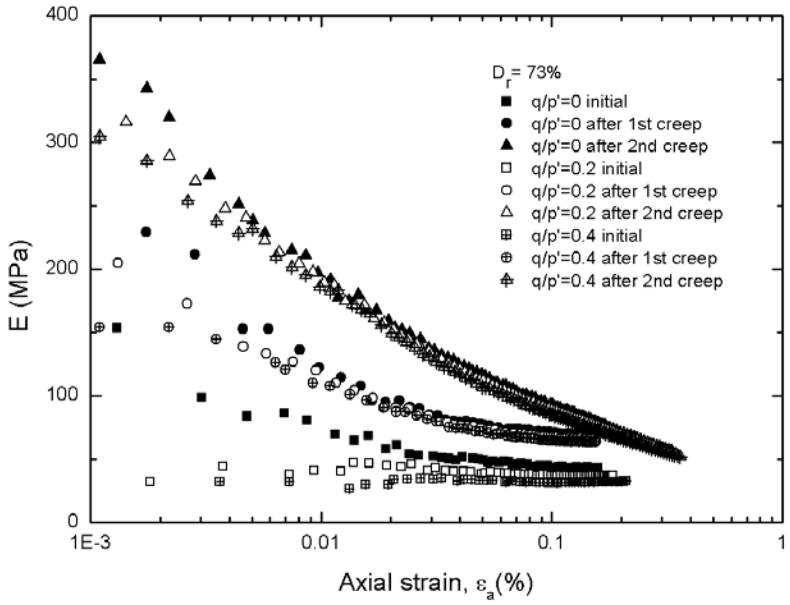

Figure A.15 Stiffness (E) degradation curves of the specimens of D_r=73%

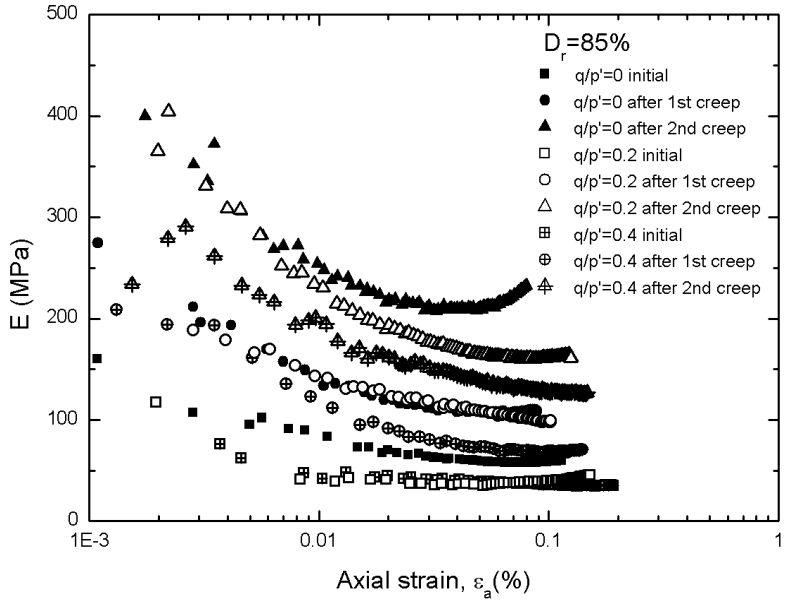

Figure A.16 Stiffness (E) degradation curves of the specimens of D_r=85%

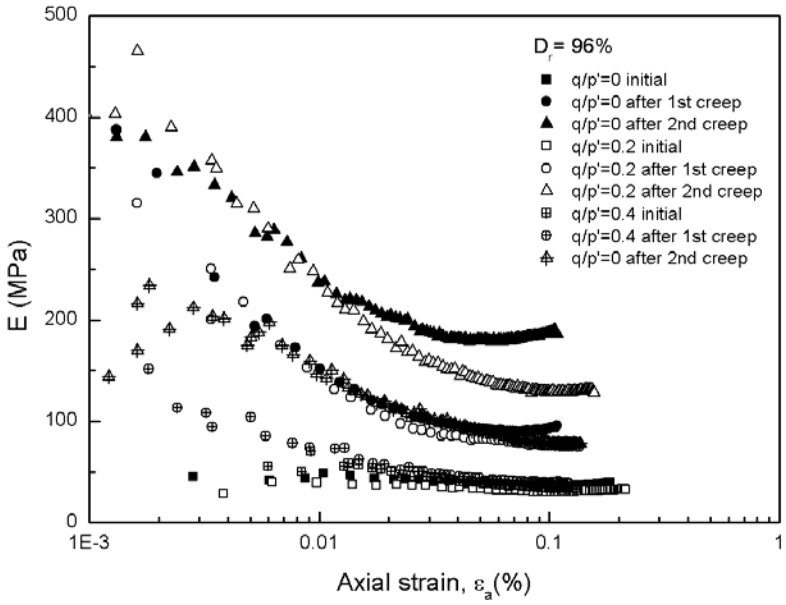

Figure A.17 Stiffness (E) degradation curves of the specimens of D_r=96%

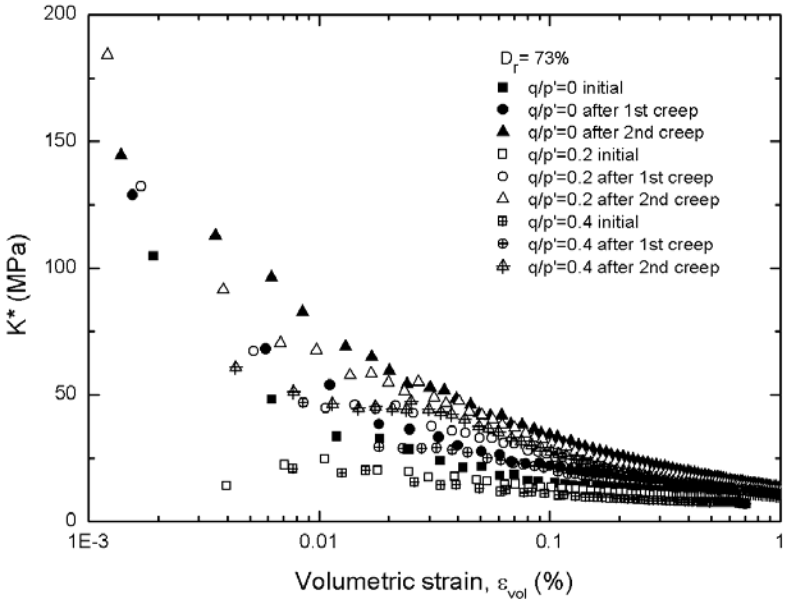

Figure A.18 Stiffness (K*) degradation curves of the specimens of D_r=73%

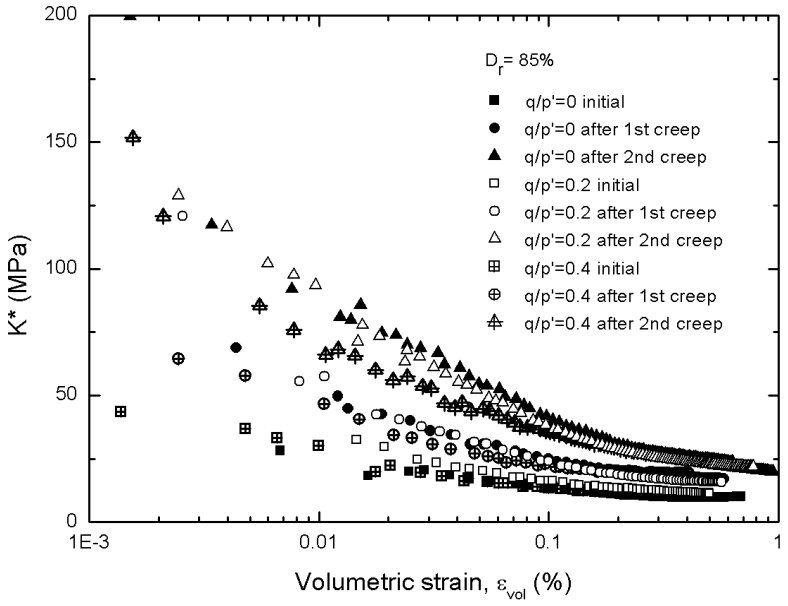

Figure A.19 Stiffness (K*) degradation curves of the specimens of D_r=85%

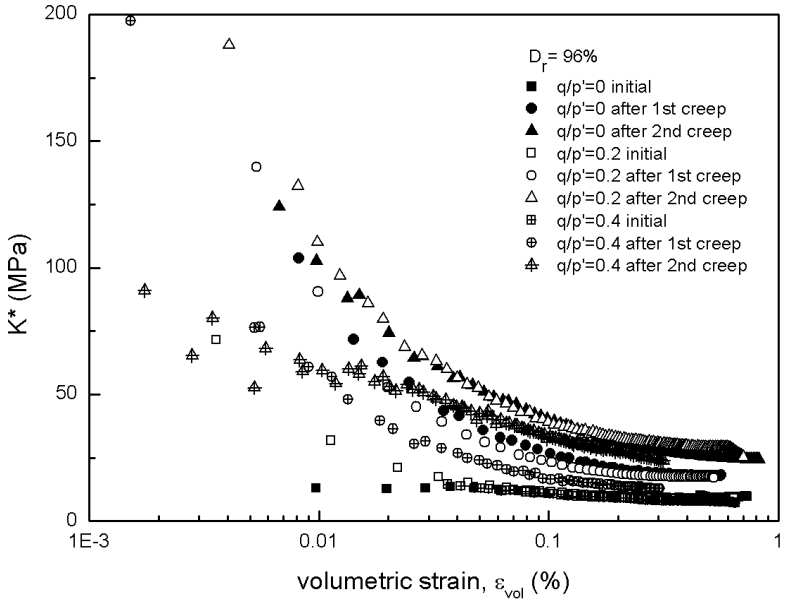

Figure A.20 Stiffness (K*) degradation curves of the specimens of D_r=96%

초 록

모든 흙의 공학적 특성은 시간에 따라 변화한다. 특히, 흙의 시간의존적인 특성은 지반 위의 구조물이나, 교각 및 교대, 옹벽구조물, 사면 등에 영향을 미치고, 이로 인한 과도한 변형은 구조물의 사용성에 문제를 일으킬 수 있다. 그러나 현재 국내 건설산업의 설계분야에서 이러한 시간의존적인 변형을 간과하는 것이 대부분이어서 건설 후 예기치 못한 지반이나 구조물의 변형이 발생하고, 심하게는 파괴에 이르는 등 현장에서 다양한 문제가 발생하고 있다. 이처럼 실제 발생하는 지반공학적 문제를 해결하기 위해서는 변형 거동을 보다 정밀하고 종합적으로 예측하고 평가하여 실제 설계에 반영하는 것이 중요하다.

일반적으로 흙의 시간 의존적인 거동은 점성토에서 주로 일어나는 현상으로 인식되어 왔으나, 최근 점성토뿐만 아니라 사질토에서도 시간이 지남에 따라 일정한 하중 하에서 지속적인 변형, 강성 또는 강도증가가 일어나는 현상이 현장시험 등을 통해 관찰되면서 사질토의 시간의존적인 거동에 관한 연구가 점차 늘고 있다. Mitchell과 Solymar(1984), Thomann과 Hryciw(1992), Ng(1998) 등은 콘 관입 시험결과를 통한 사질토의 강도와 강성의 증가를 측정하였으며, York(1994), Chow(1998), Jardine과 Standing(1999), Axelsson(2000) 등은 사질토 지반에 근입된 말뚝의 setup 효과를 확인함으로써 사질토의 시간에 따른 강도증가 효과를 확인한 바 있다. 근래에는 Kuwano 와 Jardine (2002), Bowman 과 Soga (2003),

Wang 등 (2008), 그리고 Wang 과 Gao (2013)은 사질토의 크리프와 이로 인한 강성증가를 실험적으로 제시한바 있으며, 그 결과로부터 사질토의 시간의존적인 거동을 결코 무시할 수 없는 현상임을 강조하였다.

한편, 세립분이 일부 포함되어 실트질 모래로 구분되는 풍화토는 국내에서 광범위하게 분포하고 있을 뿐만 아니라, 건설현장에서 건설재료로 다양하게 사용됨에도 불구하고, 그 장기거동에 관한 연구는 미미한 실정이다. 시간 의존적인 거동은 재료 특성, 구속압 뿐만 아니라 상대밀도에도 크게 영향을 받는다. 특히, 실제 현장에서는 풍화토를 다양한 다짐도로 활용하고 있으며, 이는 결국 상대밀도와 관련이 있다. 따라서 풍화토의 장기거동을 보다 명확히 파악하기 위해서는 상대밀도의 영향을 분석하는 것이 매우 중요하다.

본 연구에서는 풍화토의 시간의존적인 특성을 크게 두 가지 주제로 나누어 실험하고 분석하였다. 첫번째로 다양한 상대밀도의 풍화토를 등방 압밀과 이방 압밀 조건으로 각각 세가지 유효 연직압 (100, 200, 400 kPa) 하에서 48시간 동안 크리프 시험을 실시하여, 압밀 응력비와 구속압에 따른 풍화토의 연직 변형률, 횡방향 변형률, 부피 변형률, 그리고 전단변형률의 관점에서 크리프 거동을 분석하였다. 또한, 표준압밀 시험기를 이용하여 크리프에 의한 변형을 평가하였고, 삼축 시험 결과와 함께 비교하였다. 이로부터 화강풍화토의 시간의존적인 거동을 종합적으로 분석하고 나아가 수치해석에 사용할 수 있는 파라미터를 제시하여 실제 설계에 반영할 수 있도록 하였다.

두 번째로는 다양한 실험 조건 (상대밀도, 응력비, 압밀압 등)의 크리프 동안 직교하는두 방향의 벤더엘리먼트 시험을 일정한 간격으로 실시하여, 방향별 전단탄성계수의 변화를 고찰함으로써 크리프로 인한 에이징 효과에 대하여 분석하였다. 이로부터 크리프 동안 흙의 구조 변화를 유추할 수 있으며, 크리프 변형과 흙의 강성의 관계도 파악할 수 있다. 아울러 크리프 동안 국내 화강풍화토의 이방성의 변화에 대하여 분석하였다. 본 연구로부터 얻어진 화강풍화토의 시간의존적 거동을 실제 설계에 적용한다면, 지반과 구조물 간의 변형을 보다 정확하고 정밀하게 예측이 가능하고, 실제 문제가 발생했을 때 효과적으로 제어가 가능할 것으로 기대된다.

주요어: 크리프, 에이징, 삼축시험, 화강풍화토, 사질토, 시간의존적 거동, 이방성

학 번: 2010-30238